AD-775 649

THEORETICAL STUDIES OF HIGH-POWER INFRARED WINDOW MATERIALS

Marshall S. Sparks, et al

Xonics, Incorporated

Prepared for:

Advanced Research Projects Agency
Defense Supply Service

6 December 1973

Unclassified

Security Classification

AD 775649

DOCUMENT CONTROL DATA - R & D

(Security classification of title, body of abstract and indexing annotation must be entered when the overall report is classified)

1 ORIGINATING ACTIVITY (Corporate author)

Xonics, Incorporated
6837 Hayvenhurst Avenue
Van Nuys, California 91406

2a. REPORT SECURITY CLASSIFICATION

Unclassified

2b. GROUP

N/A

3 REPORT TITLE

THEORETICAL STUDIES OF HIGH-POWER INFRARED WINDOW MATERIALS

4 DESCRIPTIVE NOTES (Type of report and inclusive dates)

Second Technical Report, 30 June 1973 through 6 December 1973

5 AUTHOR(S) (First name, middle initial, last name)

Marshall S. Sparks, C. J. Duthler

6 REPORT DATE	7a. TOTAL NO. OF PAGES	7b. NO. OF REFS
6 December 1973	260 263	184

8a. CONTRACT OR GRANT NO	9a. ORIGINATOR'S REPORT NUMBER(S)
DAHC15-73-C-0127	
b. PROJECT NO.	
c.	9b. OTHER REPORT NO(S) (Any other numbers that may be assigned this report)
d.	ARPA Order No 1969, Amendment No. 1

10 DISTRIBUTION STATEMENT

This document may be further distributed by any holder only with specific prior approval of the Defense Supply Service - Washington, D. C.

11 SUPPLEMENTARY NOTES	12. SPONSORING MILITARY ACTIVITY
Sponsored by Advanced Research Projects Agency	Defense Supply Service - Washington Room 1D245, The Pentagon Washington, D.C. 20310

13. ABSTRACT

Theory indicates that concentrations of less than 0.1 ppm of NO_2^-, HCO_3^-, SO_4^{2-}, and CrO_4^{2-}, which are molecular ions that substitute for the halide ion, yield an absorption coefficient $\beta > 10^{-4}\,cm^{-1}$ at 10.6 μm. Predicted temperature dependences are given. Divalent ions added to strengthen alkali halides should not give rise to measurable ($\beta \approx 10^{-4}\,cm^{-1}$) absorption, with two possible exceptions. The known result of no correlation between Pb^{2+} concentration and β is shown to be the result expected. The U center is the only known impurity in alkali halides with localized vibrational mode sufficiently close to 10.6 μm to cause noticeable absorption. Absorption in the far high-frequency wings of various impurity-absorption resonances should be important. Molecular and macroscopic surface absorption, electronic states in the bandgap in both semiconductor and alkali-halide crystals, and absorption by electrical carriers and electronic absorption are potentially important. Electronic levels with small spacing have already been observed to give rise to IR absorption. Material failure from absorption by macroscopic inclusions, electrical breakdown of dirty air, stimulated scattering processes, and electron avalanche breakdown occur at typical breakdown intensities as low as 10^6, 10^7, 10^8, and $10^{10}\,W/cm^2$, respectively. Parametric instabilities of phonons, self focusing, multiphoton absorption, and electrostrictive defocusing are shown to have higher breakdown intensities. An explanation of laser-damage cone-shaped surface pits in terms of absorption by inclusions is proposed. Parametric instabilities of phonons are predicted to be observable at the Reststrahl resonance and in Raman scattering. Values of the total power θ that a window can transmit under specified conditions are calculated for use as figures of merit for window materials. For continuous operation, large-diameter $D > D_{EF}$ windows should be face cooled, but small-diameter windows may be edge cooled, and θ often decreases as the diameter D increases. For pulsed operation, θ

DD FORM 1 NOV 65 1473

Unclassified

Security Classification

14 KEY WORDS	LINK A		LINK B		LINK C	
	ROLE	WT	ROLE	WT	ROLE	WT
infrared absorption						
alkali halides						
diamond						
extrinsic absorption						
molecular ion impurities						
NO_2^-, HCO_3^-, SO_4^{2-}, and CrO_4^{2-}						
U center						
inclusions						
parametric instability of phonons						
surface damage						
figure of merit						
multiphonon absorption						
selection rule						
nonlinear infrared absorption						

ABSTRACT (Continued)

increases as D increases. For pulsed operation and for $D > D_{EF}$ in cw operation, θ is independent of thermal conductivity K, while for $D < D_{EF}$ in cw operation, $\theta \propto K$. Typically, $D_{EF} \sim 7$-100 cm. The alkaline-earth fluorides have the greatest figures of merit for large-diameter windows in the 2-6 μm range; for small-diameter windows, Si, BaF_2, and GaAs have the greatest values of θ. For continuous operation at 10.6 μm with bulk absorption, a diamond window with D = 1 cm has the greatest value of the existing materials and values of D (1-100 cm) considered. A new derivation of the multiphonon absorption coefficient yields $\beta \sim \exp(-\omega\tau)$ directly, rather than as a sum on n (number of phonons), and provides a prescription for estimating the range of ω over which the nearly exponential behavior extends. A proposed quasiselection rule is useful in explaining several multiphonon absorption results including the small number of two-phonon peaks observed in NaCl-structure crystals. The classical theory of absorption developed in the previous report is extended to incorporate the effects of a nonlinear dipole moment. Ultraviolet-induced infrared absorption and low-intensity inelastic scattering are shown to be negligible, and higher-order multiphonon-absorption vertex corrections are calculated.

THEORETICAL STUDIES OF HIGH-POWER INFRARED WINDOW MATERIALS

M. Sparks, Principal Investigator, 213 / 787-7380
C. J. Duthler, Principal Scientist, 213 / 787-7380

Xonics, Incorporated
Van Nuys, California 91406

Second Technical Report
6 December 1973

Contract No. DAHC15-73-C-0127
Effective Date of Contract: 7 December 1972
Contract Expiration Date: 6 December 1974

Prepared for
Defense Supply Service - Washington, D.C.

Sponsored by Advanced Research Projects Agency
ARPA Order No. 1969, Amendment No. 1; Program Code No. 3D10

This research was supported by the Advanced Research Projects Agency of the Department of Defense and was monitored by the Defense Supply Service-Washington, D.C. under Contract No. DAHC15-73-C-0127. The views and conclusions contained in this document are those of the authors and should not be interpreted as necessarily representing the official policies, either expressed or implied, of the Advanced Research Projects Agency or the U. S. Government.

TABLE OF CONTENTS

TABLE OF CONTENTS (Cont'd)

TABLE OF CONTENTS (Cont'd)

LIST OF ILLUSTRATIONS

LIST OF ILLUSTRATIONS (Cont'd)

PREFACE

This Second Technical Report describes the work performed on Contract DAHC15-73-C-0127 on Theoretical Studies of High-Power Infrared Window Materials during the period from June 30, 1973 through December 6, 1973. The work on the present contract is a continuation of that of the previous Contract DAHC15-72-C-0129.

The following investigators contributed to this report:

Mr. H. C. Chow, research associate

Dr. C. J. Duthler, principal research scientist

Dr. A. M. Karo, consultant, Lawrence Livermore Laboratory, Livermore, California

Dr. A. A. Maradudin, consultant, University of California, Irvine, California

Dr. D. L. Mills, consultant, University of California, Irvine, California

Dr. L. J. Sham, consultant, University of California, San Diego, California

Dr. M. Sparks, principal investigator

The material in this report constitutes the final results on the subjects covered. Previously reported results are not repeated in the present report. However, the list of publications and summary of results in Sec. N include all publications and results of this and the previous contract. The brief overviews in the Introduction (Sec. A) and in the general sections B on Extrinsic Absorption Processes and D on Very High-Intensity Effects also mention previous work.

As of the present date, the emphasis of the program will be on ultraviolet materials.

SUMMARY

This summary covers the material presented in the present report only. An overview of the complete program is given in Sec. A, and the list of publications and outline of results in Sec. N cover the previous investigations as well as those of the present report.

Extrinsic Absorption. It is proposed that an important class of impurities limiting infrared transmission in alkali-halide laser-window materials are molecular-ion impurities that substitute for the halide ion in these crystals. Evidence is found from a survey of the experimental literature that concentrations of less than 0.1 ppm of NO_2^-, HCO_3^-, SO_4^{2-}, and CrO_4^{2-} will yield an absorption coefficient β greater than $10^{-4}\,cm^{-1}$ at 10.6 μm. Predicted temperature dependences of impurity-limited β (10.6 μm) are: $T^{1.6}$, temperature independent, and decreasing β with increasing temperature depending on the particular ionic impurity.

A theoretical analysis suggests that divalent ions added to alkali halides to strengthen them should not give rise to measurable ($\beta \approx 10^{-4}\,cm^{-1}$) absorption. Two possible exceptions, which are believed to be unlikely in general, are that a divalent ion could activate another impurity or that the added ions could have electronic levels that are very closely spaced. The negative experimental result of no correlation between Pb^{2+} concentration and 10.6 μm absorption in alkali halides is shown to be the result expected.

The U center is the only known impurity in alkali halides that has a localized vibrational mode sufficiently close to 10.6 μm to cause noticeable absorption. Absorption in the far high-frequency wing ($\omega >> \omega_{res}$) of the impurity-absorption

resonance, in addition to absorption near resonance, may be important, in contrast to previous beliefs. The high-frequency side of the resonance is the more important region because the intrinsic absorption increases rapidly with decreasing frequency, thus obscuring the low-frequency wing. Gap-mode and resonance-mode absorption are shown theoretically to be negligible at 10.6 μm. Impurity-induced infrared activity of phonon modes is estimated to be negligible.

Analyses and estimates indicated that surface absorption can give rise to an equivalent absorption coefficient of $\beta > 10^{-4}\ cm^{-1}$. Molecular absorption and inclusion absorption are two important sources of surface absorption. Electronic states in the band gap in both semiconductor and alkali-halide crystals are potentially important absorption centers. Absorption by pure surface vibrational modes is believed to be negligible.

Absorption by electrical carriers and electronic absorption is important. Electronic levels with small spacing have already been observed to give rise to infrared absorption (near 2 μm for Cr in zincblende-structure crystals). Shallow levels that can be emptied thermally can give rise to absorption with β decreasing with increasing temperature. Electronic absorption across the gap is negligible at 10.6 μm. Stress-induced multiphonon absorption was shown theoretically to be negligible.

Very High-Intensity Effects. In a general discussion of nonlinear and other very high-intensity effects, it is pointed out that material failure from absorption by macroscopic inclusions, electrical breakdown of dirty air, stimulated scattering processes, and electron avalanche breakdown occur at typical breakdown intensities as low as 10^6, 10^7, 10^8, and $10^{10}\ W/cm^2$, respectively. Parametric instabilities of phonons, self focusing, multiphoton absorption, and electrostrictive defocusing are shown to have higher breakdown intensities.

An explanation of laser-damage cone-shaped surface pits is proposed. An anisotropic, quasistatic stress distribution is found in the material surrounding an absorbing inclusion of a radius a centered a distance d below the surface of a transparent host. Maximum tensile stress greater than the pressure at the inclusion-host interface occurs at the angle $\theta_m = \cos^{-1}(a/d)$ from the line joining the inclusion center to the surface, resulting in cone-shaped fracture.

Nonlinear infrared absorption from parametric instabilities of phonons is considered in detail, and is shown to be negligible in the low-absorption region of exponential frequency dependence of the optical absorption coefficient β. However, it is observable at the Reststrahl resonance and in Raman scattering. At low intensity, the transmission T curve is independent of intensity, as usual, but at high intensity, the $T(\omega)$ curve broadens and the transmission at resonance increases. The time constant for the approach to the steady state is important since the steady state is not attained in short laser pulses in important cases in which long-lived phonons give rise to low steady-state threshold intensities for anomalous absorption. The threshold for the parametric instability is quite sharp when considered as a function of the amplitude of the fundamental phonon, but smooth when considered as a function of the incident laser intensity. In contrast to a previously accepted result, even crystals, such as NaCl, having a center of inversion could have anomalously low thresholds since the threshold is controlled by the phonon (in the pair) having the longer lifetime. Chain instabilities and enhanced relaxation from mutual interaction of excited pair phonons are negligible for the phonon instabilities, in contrast to previous results for plasmas and parallel pumping in ferromagnetic resonance, respectively. The method of calculation, using Boson occupation numbers rather

than mode amplitudes, has the simplicity and power to allow us to obtain more information about parametric instabilities, including effects above the threshold, than has been possible previously.

High-Power 2-6 μm and 10.6 μm Window-Material Figures of Merit with Edge Cooling and Surface Absorption Included. Values of the total power θ that a window can transmit under specified conditions are calculated for use as figures of merit for window materials. New features of the figures of merit are: consideration of edge as well as face cooling, treatment of surface as well as bulk absorption, use of θ rather than intensity as the figure of merit, effects of improving materials and calculation for 3.8 and 5.25 μm as well as 10.6 μm. New results include the following: For continuous operation, large-diameter windows should be face cooled, but small-diameter windows may be edge cooled, and θ often decreases as the diameter D increases. For pulsed operation, θ increases as D increases, as intuitively expected. Values of the diameter D_{EF}, above which face cooling should be used, are surprisingly large, ranging between 7 and 100 cm, typically. For pulsed operation and for $D > D_{EF}$ in cw operation, θ is independent of thermal conductivity K, while for $D < D_{EF}$ in cw operation, $\theta \propto K$. For small-diameter windows, the high temperature at the center of the window may limit the value of θ and the theoretical thickness may be unreasonably small.

The alkaline-earth fluorides have the greatest figures of merit for large-diameter windows in the 2-6 μm range, with $\theta = 76$ MW for a one-second pulse on a ten-centimeter-diameter window of BaF_2 at 3.8 μm with a bulk absorption coefficient of 10^{-4} cm^{-1}. For small-diameter windows (1 cm-diameter), Si, BaF_2, and GaAs have the greatest values of $\theta = 1.8$, 0.94, and 0.76 MW, respectively, for cw or 1 sec pulse duration at 3.8 μm. For continuous operation at 10.6 μm

with bulk absorption, a diamond window with D = 1 cm has the greatest value ($\mathcal{P}$ = 0.57 MW) of the existing materials and values of D considered. If the materials are improved (absorption coefficient β reduced for ZnSe, strength σ increased for KCl, and both improvements for CdTe and KBr), 1 cm-diameter windows of ZnSe, KCl, KBr, and CdTe will transmit 0.74, 0.58, 0.51, and 0.24 MW, respectively. For one-second pulse operation, a 100 cm-diameter window of KCl transmits 67 MW for σ = 330 psi or 260 MW for σ improved to 5,000 psi.

Explicit Exponential Frequency Dependence of Multiphonon Infrared Absorption. The nearly exponential frequency dependence of the infrared absorption coefficient β observed by Rupphrecht, Deutsch, and others has been explained previously by evaluating the individual n-phonon contributions to β, summing the results, and noting that the sum was nearly exponential over a fairly wide range of frequencies. A new derivation of the multiphonon absorption coefficient yields $\beta \sim \exp(-\omega\tau)$ directly, rather than as a sum on n, and provides a prescription for estimating the range of ω over which the nearly exponential behavior extends.

Quasiselection Rule for Infrared Absorption by NaCl-Structure Crystals. A selection rule forbids splitting of a Reststrahl phonon into two phonons on the same branch. We propose that the interaction (summation or difference) of a Reststrahl phonon with two acoustical or two optical phonons is much weaker than the interaction with one acoustical and one optical phonon. This quasiselection rule is useful in explaining several multiphonon absorption results including the small number of two-phonon peaks observed in NaCl-structure crystals.

The Absorption Coefficient of Alkali Halides in the Multiphonon Regime: Effects of Nonlinear Dipole Moments. The theory of the absorption coefficient for a model of alkali halide crystals in the multiphonon regime developed in the previous report is extended to incorporate the effects of a nonlinear dipole moment. The resulting expression for the absorption coefficient is evaluated for several different interatomic potential functions and choices for the nonlinear dipole moment. We suggest that the relative sign of the contributions to the absorption coefficient from crystalline anharmonicity and the nonlinear variation of the electric dipole moment with interatomic separation could be such that these contributions interfere constructively in the alkali halides.

Vertex Corrections for Multiphonon Absorption. In the previous technical report, vertex-correction factors Λ_n were calculated for all processes through $n = 6$, where n is the number of final phonons created in the absorption process. In numerical calculations in progress, the value of Λ_n was needed. Thus, this seventh-order vertex is calculated.

Negligible effects. There are many effects in addition to those considered in the present and previous reports that give rise to infrared absorption, but whose strengths are too small to be observable. Simple order-of-magnitude calculations indicate that ultraviolet-induced infrared absorption and low-intensity inelastic scattering including Raman, Brillouin, and ionic Raman and Brillouin scattering, in addition to several processes already mentioned, fall into this category.

A. INTRODUCTION

The emphasis to date on the present contract and on a previous contract (DAHC15-72-C-0129) has been on theoretical studies of high-power infrared-window materials. Since the remainder of the program will emphasize studies on ultraviolet materials, a very brief overview of the infrared results is given. A summary of results of the complete program is given in outline form in Sec. N.

The motivation for the program on theoretical studies of high-power infrared window materials was the availability of high-power infrared lasers for current Department of Defense programs and the realization that lack of transparent materials for windows may limit the usefulness of many laser systems. As higher powers and shorter pulse lengths become available, the problem of obtaining materials with acceptably low absorption will become even more serious. At the beginning of the program, values of the optical absorption coefficient β of candidate window materials were needed in order to evaluate the potential performance of the materials. There had been no previous calculations of the numerical values of β in the highly transparent regions for materials of interest (such as KBr and ZnSe at 10.6μm), and the available corresponding experimental values were of questionable efficacy since they were believed to be extrinsic (i.e., caused by imperfections that can be removed in principle).

The paucity of experimental and theoretical information on the values of β was one of the most pressing problems in the Department of Defense high-power window programs. It was especially important to know if the values of β were intrinsic or extrinsic and to have reliable estimates of the intrinsic value of β before undertaking imperfection-identification and sample-purification programs since

there were many candidate materials and these expensive programs should be undertaken only if there were a good chance of reducing β to the required value. Thus an objective of the program was to determine if the current experimental values were intrinsic or extrinsic and to obtain reliable estimates of the intrinsic and extrinsic values of β for materials of interest. It was not known if any reduction in the value of β could be obtained until this former information was available. Furthermore, the frequency and temperature of β for the extrinsic processes should be invaluable to materials-improvement programs in identifying sources of extrinsic absorption.

In order to define the problem in greater detail, consider the schematic illustration of the frequency and temperature dependence of β shown in Fig. A1. There is a region of very small intrinsic absorption bounded by the fundamental lattice peak and the electronic absorption edge. At sufficiently small values of intrinsic absorption, β is expected to be dominated by extrinsic processes, as marked on the figure. In the study of the values of β, the primary interest is first in the value at 10.6μm and second in the 2-6μm range. It was pointed out in the first quarterly report of the previous contract[1] that the values of β over large ranges of values of ω and T are extremely useful in determining if an experimental value of β at, say, 10.6μm is intrinsic or extrinsic and in estimating the intrinsic value of β at 10.6μm. Thus, the calculations included values of ω between the fundamental lattice absorption edge and the electronic edge and values of temperature between liquid helium and the melting point of the material.

The value of β required for a given application varies greatly. Required values for high-power systems are as low as 10^{-4} cm^{-1}, possibly lower. Most of the previous theoretical work had been concerned with derivations of formal expressions

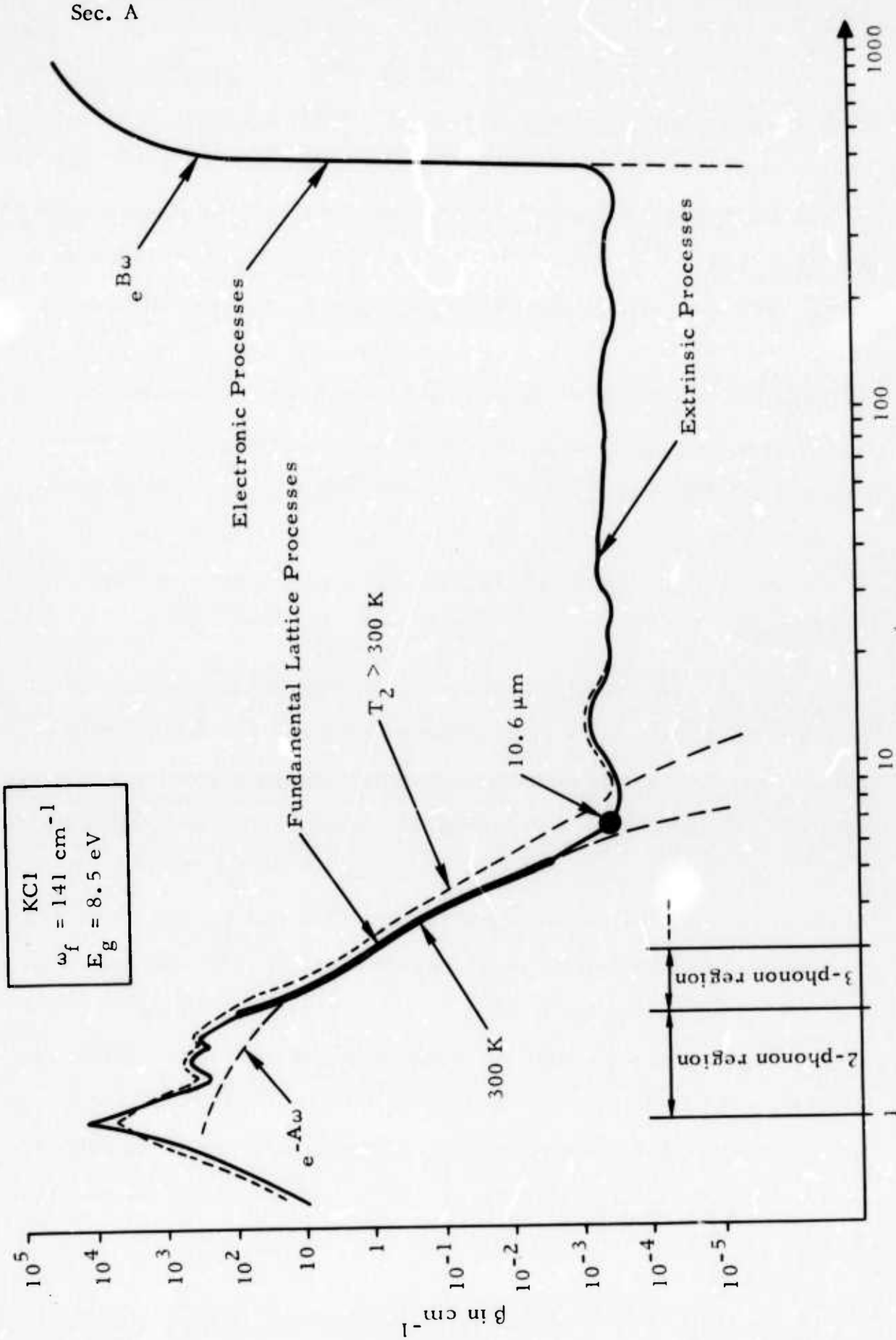

Fig. A1. Absorption in KCl. The heavy curve and the point at 10.6 μm are plots of Raytheon results. The rest of the curve is a schematic illustration of the extrinsic region and the electronic absorption edge.

for β, or, equivalently, the imaginary part of the dielectric constant. Very little consideration had been given to the calculation of the numerical values of β, and all such calculations had been for frequencies near the fundamental resonance where β is large ($\beta >> 1\,\mathrm{cm}^{-1}$). There are a number of reasons why there had been no previous calculations for the numerical values of β in the range of frequencies where $\beta << 1\,\mathrm{cm}^{-1}$. First, the need for this information has become pressing only within the last few years as higher-power lasers have become available. Second, previous interest was in obtaining information about the phonon dispersion relations, and this information was obtained without the knowledge of the absolute magnitude of β. Finally, the calculations are not trivial. Straightforward computer calculations of β in the n-phonon region for large n surely would yield paltry results.

In the intervening twenty-four months there has been considerable theoretical and experimental progress. We have explained quantitatively the nearly exponential frequency dependence of the optical absorption frequency β observed by Rupprecht[2] and by Deutsch[3] and the substantial deviations from the expected temperature dependence observed by Harrington and Hass.[4] The calculations are based on a reasonable model of the lattice with the Born-Mayer interaction potential. They include the dispersion relations of the phonons, and the approximations made were shown to be reasonable. The Raytheon measurements of $\beta(\omega)$ and our theoretical prediction that there should be no drastic deviations from the extrapolations of the measured $\beta(\omega)$ have settled the question of whether the values of β measured at $10.6\,\mu\mathrm{m}$ are intrinsic or extrinsic for most materials of interest and have afforded estimates of the intrinsic values. With the exception of KCl, the estimated

intrinsic values of $\beta_{10.6}$ for candidate 10.6 μm window materials are well below the lowest measured values. The most interesting problems in the theory of intrinsic multiphonon absorption now appear to be solved.

The emphasis then shifted to extrinsic absorption and to nonlinear and other very high-power effects. The results are discussed in Secs. B and C and Secs. D and E, respectively.

A number of practical effects such as thermally and pressure-induced optical distortion, edge and face cooling, engineering solutions to the window problem, tabulations of $\beta(\omega)$ results, and guidelines for selecting materials were considered. (See the list of publications in Sec. N.) Finally, new figures of merit for window materials are considered in Secs. G and H.

The following will be included in the next technical report: stimulated Raman scattering, higher-order dipole moments, U-center absorption, and results of numerical evaluation of multiphonon absorption.

REFERENCES

1. M. Sparks and T. Azzarelli, "Theoretical Studies of High-Power Infrared Window Materials," Xonics, Inc. Quarterly Technical Progress Report No. 1, Contract DAHC15-72-C-0129, March (1972).
2. G. Rupprecht, Phys. Rev. Lett. 12, 580 (1964).
3. F. A. Horrigan and T. F. Deutsch, "Research in Optical Materials and Structures for High-Power Lasers," Raytheon Research Division, Final Technical Report, Contract DAAH01-70-C-1251, September (1971).
4. J. A. Harrington and M. Hass, Phys. Rev. Lett. 31, 710 (1973).

B. EXTRINSIC ABSORPTION

A theoretical analysis suggests that divalent ions added to alkali halides to strengthen them should not give rise to measurable ($\beta \approx 10^{-4}\,cm^{-1}$) absorption. Two possible exceptions, which are believed to be unlikely in general, are that a divalent ion could activate another impurity or that the added ions could have electronic levels that are very closely spaced. The negative experimental result of no correlation between Pb^{2+} concentration and 10.6 μm absorption in alkali halides is shown to be the result expected.

The U center is the only known impurity in alkali halides that has a localized vibrational mode sufficiently close to 10.6 μm to cause noticeable absorption. Absorption in the far high-frequency wing ($\omega >> \omega_{res}$) of the impurity-absorption resonance, in addition to absorption near resonance, may be important, in contrast to previous beliefs. The high-frequency side of the resonance is the more important region because the intrinsic absorption increases rapidly with decreasing frequency, thus obscuring the low-frequency wing. Gap-mode and resonance-mode absorption are shown theoretically to be negligible at 10.6 μm. Impurity-induced infrared activity of phonon modes is estimated to be negligible.

Analyses and estimates indicated that surface absorption can give rise to an equivalent absorption coefficient of $\beta > 10^{-4}\,cm^{-1}$. Molecular absorption and inclusion absorption are two important sources of surface absorption. Electronic states in the band gap in both semiconductor and alkali-halide crystals are potentially important absorption centers. Absorption by pure surface vibrational modes is believed to be negligible.

Absorption by electrical carriers and electronic absorption is important. Electronic levels with small spacing have already been observed to give rise to infrared absorption (near 2 μm for Cr in zincblende-structure crystals). Shallow levels that can be emptied thermally can give rise to absorption with β decreasing with increasing temperature. Electronic absorption across the gap is negligible at 10.6 μm. Stress-induced multiphonon absorption was shown theoretically to be negligible.

I. Introduction

As discussed in Sec. A, it appears likely that the most interesting problems of intrinsic absorption have been solved. This is not the case for extrinsic absorption, although we have made considerable progress recently. The obvious central problem of imperfection absorption is that unwanted imperfections can cause unacceptably large absorption. In addition to unwanted imperfections, impurity ions may be introduced into crystals intentionally in order to compensate semiconductor materials or to strengthen alkali halides.

Before discussing specific impurity absorption processes, it is again emphasized that experimental studies of the frequency and temperature dependence of β, especially on intentionally doped samples, would be extremely useful in helping to understand impurity absorption. The present investigation suggests that interesting dopants for the alkali halides are U centers, NO_2^-, HCO_3^-, SO_4^{2-}, and CrO_4^{2-}. Studies of β in the far wings, particularly on the high-frequency side of resonance, of the impurity lines for specific impurities would be particularly useful.

II. Classification

Before considering specific absorption mechanisms, it is useful to classify extrinsic-absorption mechanisms as follows:

Point imperfections include molecules in anion sites and possibly other sites, isolated impurity ions, self and impurity interstitial ions, vacancies, and various "centers" such as U centers. A small cluster of the above, such as impurity-ion pairs or a vacancy plus a neighboring impurity ion, will be considered as a point defect in the spirit of radiation damage studies.

Extended imperfections include clean and contaminated grain boundaries, voids, second phases, inclusions, dislocations, stresses, and regions of deviation from stoichiometry (with possible variations throughout the sample).

Surface effects include effects of molecules and ions on or near the surface, surface contamination from solvents, dirt, etc., pits and scratches, electronic surface modes, surface free-carrier absorption, and vibrational or electronic "pure" surface states (resulting from the discontinuity at a perfect surface).

Electrical-carrier absorption includes free-carrier absorption, interband transitions of holes or electrons, and electron or hole transitions involving levels in the electronic band gap.

A given imperfection can have: vibrational effects, in which the absorption involves the motion of nuclei; electronic effects, in which the absorption involves transitions between electronic levels of the impurity, roughly speaking; or electrical-carrier effects, in which the imperfections contribute the current-carrying electrons or holes. Some processes, such as Raman scattering, involve both vibrational and electronic effects.

III. Macroscopic Inclusions

Macroscopic inclusions are extended imperfections such as voids, second-phase inclusions, contaminated grain boundaries, and regions of deviation from stoichiometry. It was shown in the previous report[1] that these imperfections can be very important in increasing the value of β and in causing material failure.

IV. Molecules in Anion Sites

This subject is discussed in detail in Sec. C, where it is shown that impurity concentrations as low as parts per billion can give rise to $\beta \sim 10^{-4}\ \mathrm{cm}^{-1}$.

V. Vibrational Absorption by Point Imperfections

Three types of vibrational impurity modes are well known: localized modes, having $\omega > \omega_{max}$, where ω_{max} is the greatest of the phonon frequencies, and resonance and gap modes having $\omega < \omega_{max}$. Light, weakly bound impurities tend to give rise to localized modes, while heavy, tightly bound ones tend to give rise to resonance and gap modes. Order-of-magnitude estimates show clearly that the latter two types give negligibly small contributions to β for $\omega >> \omega_{max}$ and normal impurity concentrations, the reason being that the impurity absorption is basically weaker than, and just as far off resonance as, the fundamental resonance.

In alkali halides, the U center (H^- in anion site) is the only imperfection known to have localized-mode resonance frequencies ω_r well above ω_{max}. The resonance frequencies of the U center in KCl and KBr are 502 and 446 cm^{-1}, respectively, for example. The importance of absorption in the high-frequency wing of the absorption line and the magnitude of the absorption are discussed in Sec. VI.

Imperfections can render phonon modes other than the fundamental mode infrared active and can give rise to an increase in the value of the relaxation frequency of the fundamental resonance, thus increasing the value of β. Crude arguments and order-of-magnitude estimates indicate that these effects are negligible when $\omega >> \omega_{max}$ for point imperfections, voids, second phases and inclusions of nonabsorbing materials, clean grain boundaries, and clean surface pits and scratches. For example, the normal modes in the presence of vibrational imperfections are admixtures of ordinary phonons. Many of these normal modes are infrared active because they contain admixtures of the fundamental-phonon mode. Thus, in a sense, the fundamental mode is spread out among the new normal modes. This could cause measurable effects for $\omega < \omega_{max}$. However, for $\omega >> \omega_{max}$, it should make little difference whether the phonon modes are admixed or not.

VI. Absorption in the Far Wings of Extrinsic Lines

At the beginning of the program it was expected that localized-mode absorption β_{loc} would be important only if ω_r were within a few line widths of the operating frequency. The same argument would have applied to the molecular absorption considered in Sec. C. It now appears that extrinsic absorption β_{ext} may be important at frequencies many line widths $\Delta\omega$ above ω_r. The simple reason seems to have been overlooked previously. That is, even though β_{ext} decreases rapidly as $|\omega - \omega_r| / \Delta\omega$ increases, the intrinsic multiphonon contribution β_{int} also decreases rapidly, as seen in Fig. B1. Thus, it is possible that β_{ext} could be greater than β_{int} for all $\omega > \omega_r$. Notice in passing that

the value of $\beta_{loc} = 7.5\,cm^{-1}$ at resonance from Fig. B1 implies a cross section $\sigma_{loc} \cong 7.5\ cm^{-1} / 10^{22}$ (ions/cm^3)(10^{-4} impurity concentration) $\cong 10^{-17}\ cm^2$ at resonance. This agrees with the fundamental resonance value of $\sigma_f \cong 10^5\ cm^{-1} / (10^{22}\ ions/cm^3) = 10^{-17}\ cm^2$.

In Fig. B1 the slope (on the log scale) in the far wings of the U-center absorption is assumed to be equal to the intrinsic slope. In determining the effect of β_{ext} for $\omega >> \omega_r$, it is obviously important to know if the slope of β_{ext} is greater or less than that of β_{int}. A theoretical formulation has been developed and is being applied to specific cases to determine the slope of $\log \beta_{ext}$. It should be emphasized that measurements of $\beta_{loc}(\omega)$ for $\omega >> \omega_r$ for samples with known concentrations of imperfections would be extremely important in impurity-absorption studies.

Until more experimental results are available, reliable estimates of β_{ext} at 10.6 μm cannot be made. In the absence of this information, it is interesting to notice that the equal-slope-extrapolation of Fig. B1 (for 100 ppm U centers) indicates that $\beta_{loc} = \beta_{int}$ at 10.6 μm in KCl for ~10 ppm U-center concentration.

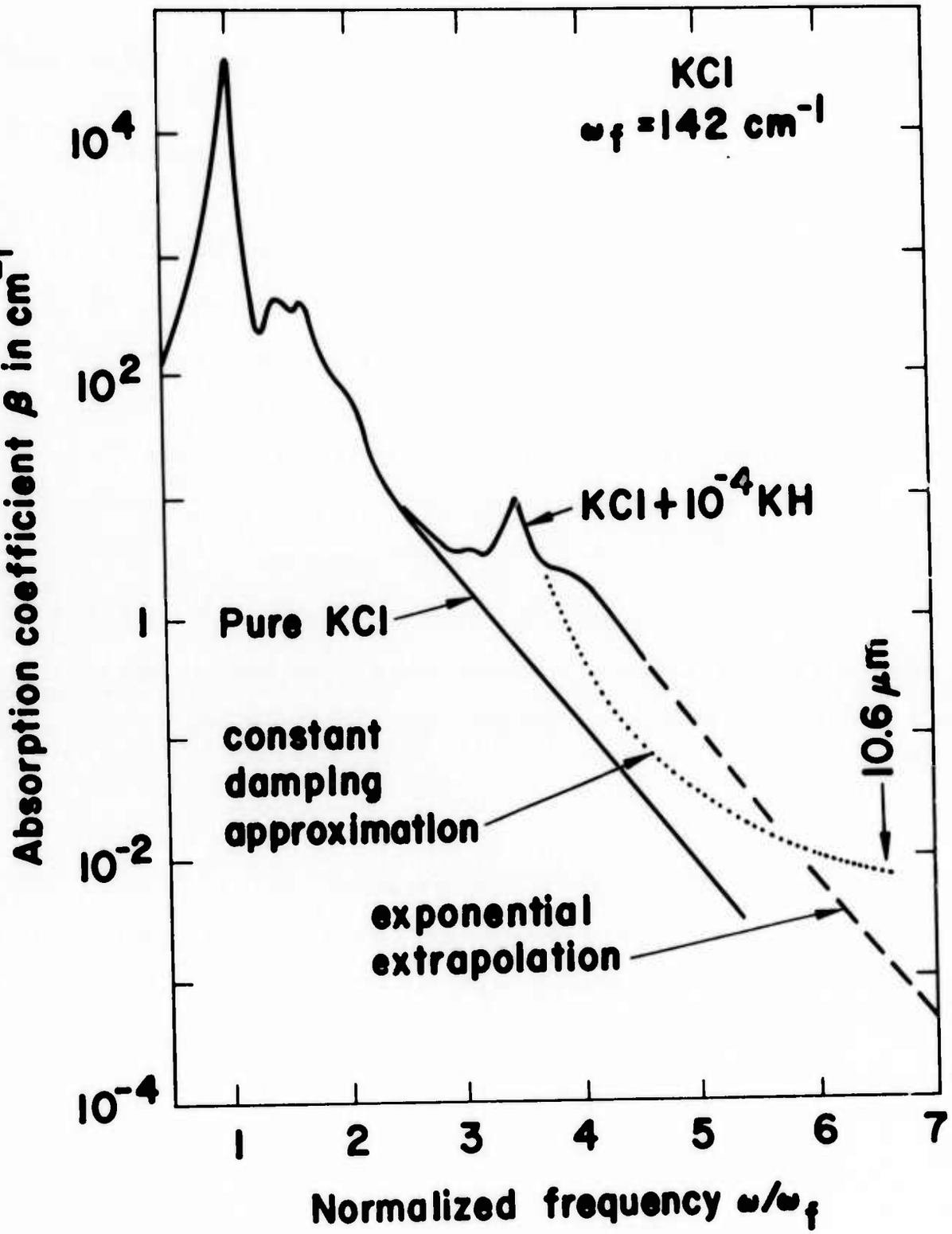

Fig. B1. Schematic illustration of the added absorption from U centers in KC1, illustrating the greater importance of the high-frequency wing.

VII. Absorption from Surface Effects

It has been shown[2] that impurity ions, atoms, or molecules on sample surfaces can give rise to absorption of the order of 0.1 percent per surface, which is equivalent to a bulk absorption coefficient of $\beta = 2 \times 10^{-3}$ cm^{-1} for a one-centimeter-thick sample (with two absorbing surfaces). That such large effects are plausible can be seen by an order-of-magnitude argument. For a 5 A-thick surface layer of material having a value of $\beta = 10^{5}$ cm^{-1} at resonance, $\beta \ell_{su} \cong 5 \times 10^{-3}$, or 0.5 percent absorption per surface. For a one-centimeter-thick sample with absorption on both surfaces, this is equivalent to a bulk absorption of $\beta = 10^{-2}$ cm^{-1}. Thus, this layer could give rise to an equivalent bulk absorption of $\beta = 10^{-4}$ cm^{-1} rather far from the resonance.

Molecular absorption (see Sec. C) and macroscopic inclusions[3,4] such as embedded polishing compounds are two of the most likely sources of surface absorption. Absorption by electronic surface states is discussed in Sec. VIII.

The opinion obtained from the current literature and from discussions with workers in the field is that vibrational "pure" modes will not give rise to absorption as large as 0.1 percent per surface for materials of interest at ~2-10 μm, but it is not certain that this is the case. This problem is interesting, and it should be easy to obtain an estimate of β. However, the problem was not addressed under the present contract as it was anticipated that the results would be negative and have far less impact than the other results which were obtained.

VIII. Electrical-Carrier and Electronic Absorption

Free-carrier absorption is sufficiently well understood that no additional study was necessary. The conditions required to avoid free-carrier absorption and measurement of "near λ^2" dependence of β and measurement of electrical conductivity as methods of detecting free-carrier absorption were discussed in the previous technical reports.

Electronic transitions across the band gap surely do not give rise to observable absorption at 10.6 or 3.8 μm in the alkali halides or wide-band gap semiconductors of interest since the absorption edge near $\omega_g = E_g/\hbar$ (in the ultraviolet or visible region) is too far from ω. As discussed in Sec. D, 42 photons typically are required to conserve energy. Furthermore, there is no evidence of β increasing with ω, as would be expected for this electronic absorption.

On the other hand, electronic absorption associated with smaller-energy electronic transitions can be important. At impurity concentrations so low that the usual free-carrier absorption is not detectable, transitions of holes between two different valence bands can give rise to broad absorption bands that can be strong ($\beta = 0.3\,\mathrm{cm}^{-1}$ in one case, for example) in the 2-6 μm region.[5] The interpretation of such absorption given by Kahn[6] apparently has been overlooked in recent literature. Transitions of electrons between different regions of the conduction band where the densities of states are high also should give rise to observable values of β. For example, the two conduction-band levels responsible for Gunn-Hilsum-Ridley oscillations in GaAs are separated by 0.36 eV, which corresponds to 2900 cm^{-1}, or 3.4 μm.

Electronic transitions between "crystal-field" levels separated by infrared energies can give rise to infrared absorption. For example, Vallin, Slack, Roberts, and Hughes[7] have shown that Cr^{2+} ions in zincblende-structure crystals give rise to absorption bands near 2 μm (crystal-field-split levels) and probably others near 20 μm (Jahn-Taller-split ground-state levels).

Electronic levels in the band gap generally can give rise to absorption. Such levels can arise from impurities or from surface states. Levels near the conduction band that are sufficiently shallow can be emptied thermally. This gives rise to absorption that decreases as the temperature increases.[8]

Finally, the bending of the bands at the surface of semiconductors could give rise to absorption. This effect was not investigated in view of its expected low probability of high-impact results.

IX. Stress-Induced 10.6 μm Absorption

It has been observed that KCl crystals with internal stresses have an absorption coefficient which is twice as great as the value observed when the same crystals were annealed ($\beta_{10.6\,\mu m} = 6 \times 10^{-4}$ cm^{-1}, annealed).[9] The following crude calculation shows that the stress-induced absorption most likely is not due to changes in the intrinsic multiphonon absorption, but instead arises from changes in the extrinsic contribution to β. For example, molecular anion impurities (see Sec. C) are likely to be stress sensitive. The fact that the value of β for the annealed sample is an order of magnitude greater than the extrapolated intrinsic value supports the suggestion of a strain-dependent extrinsic contribution to β.

Phonon frequencies are known to be temperature and stress dependent. To estimate the effect of stress on the intrinsic multiphonon absorption, the usual

exponential dependence of β on frequency is retained and changes in β are assumed to result from changes in ω_f, the fundamental Reststrahl frequency of the crystal. In the unstressed crystal, $\omega(\text{laser}) = 6.6\,\omega_f$. The stressed crystal will have compressed regions and stretched regions. Thus, ω_f and ω/ω_f vary throughout the crystal. Due to the exponential dependence of β on ω/ω_f, those regions having $\omega(\text{laser}) > 6.6\,\omega_f$ will result in a negligible decrease in β.

The pressure dependence of ω_f in KCl is derived from the estimated temperature dependence of ω_f ($d\omega_f/dT \approx 4 \times 10^{-2}\ \text{cm}^{-1}/\text{K}$)[10] by assuming that the change in frequency is a result of changes in volume producted by either temperature or pressure:

$$\frac{d\omega_f}{dP} = \frac{d\omega_f}{dT}\,\frac{dT}{dV}\,\frac{dV}{dP} \tag{1}$$

where

$$dT/dV = 1/3\alpha V \tag{2}$$

and

$$dV/dP = V/B \quad . \tag{3}$$

In (1)-(3), T is the temperature, V is the crystal volume, P is the local pressure (or stress), α is the linear thermal expansion coefficient, and B is the bulk modulus. Volume changes, hence frequency changes, are much less sensitive to pressure than to temperature. Using $\alpha = 3.93 \times 10^{-5}\ \text{K}^{-1}$ and $B = 1.78 \times 10^{11}\ \text{dynes/cm}^2$, (2) and (3) indicate that a 1 K temperature change is equivalent to a 300 psi pressure change.

Substitution of (2) and (3) into (1) yields

$$\frac{d\omega_f}{dP} = \frac{1}{3\alpha B} \frac{d\omega_f}{dT} = 1.3 \times 10^{-4} \text{ cm}^{-1}/\text{psi} \ . \tag{4}$$

Since $d(\log \beta)/d(\omega/\omega_f) \cong 1$, in order for β to change by a factor of 2, ω/ω_f must change by 0.3. With $\omega = 6\,\omega_f$ and $\omega_f = 142 \text{ cm}^{-1}$, the change in ω_f is 7.1 cm^{-1}, which according to (4) requires a pressure change of 5×10^4 psi. This is an underestimate since the stress must be averaged over the volume of the crystal. When the stressed samples are viewed in a polariscope, a shift of approximately one fringe of visible light is observed between regions of high and low stress.[9] Using the stress-optic coefficient and assuming that differences in the principal stresses are comparable to the magnitude of the stresses, the stresses in the crystal are estimated to be of the order of 10^2 psi, which is much smaller than the above value of 5×10^4 psi estimated to produce the observed change in β.

A similar analysis starting from the potential

$$\Phi = E\, e^{-r/e} - e^2/r \tag{5}$$

yields the same result. In this case the frequency changes are calculated from $d^3\Phi/dr_0^3$ and $d^4\Phi/dr_0^4$, where r_0 is the equilibrium lattice constant.

REFERENCES

1. M. Sparks, "Theoretical Studies of High-Power Infrared Window Materials," Xonics, Inc. First Technical Report, Contract No. DAHC15-73-C-0127, June (1973).
2. T. F. Deutsch and R. I. Rudko, "Research in Optical Materials and Structures for High-Power Lasers," Raytheon Research Division Final Technical Report, Contract No. DAAH01-72-C-0194, January (1973).
3. M. Sparks and C. J. Duthler, J. Appl. Phys. 44, 3038 (1973).
4. C. J. Duthler, "Explanation of Laser-Damage Cone-Shaped Surface Pits," Appl. Phys. Lett., in press.
5. F. A. Horrigan and T. F. Deutsch, "Research in Optical Materials and Structures for High-Power Lasers," Raytheon Research Division, Final Technical Report, Contract No. DAAH01-70-C-1251, September (1971).
6. A. H. Kahn, Phys. Rev. 97, 1647 (1955).
7. J. T. Vallin, G. A. Slack, S. Roberts, and A. E. Hughes, Phys. Rev. B2, 4313 (1970).
8. I. V. Skryabinskii and Yu. I. Ukhanov, Sov. Phys. - Solid State 14, 3041 (1973).
9. R. C. Pastor and M. Braunstein, "Advanced Mode Control and High-Power Optics Technology," Hughes Research Laboratories Technical Report No. AFWL-TR-72-152, Vol. II, July (1973).
10. M. Sparks and L. J. Sham, Phys. Rev. Lett. 31, 714 (1973).

C. EXTRINSIC ABSORPTION IN 10.6 μm LASER WINDOW MATERIALS DUE TO MOLECULAR-ION IMPURITIES

C. J. Duthler

Xonics, Incorporated, Van Nuys, California 91406

It is proposed that an important class of impurities limiting infrared transmission in alkali-halide laser window materials is molecular-ion impurities which substitute for the halide ion in these crystals. Evidence is found from a survey of the experimental literature that concentrations of less than 0.1 ppm of NO_2^-, HCO_3^-, SO_4^{2-}, and CrO_4^{2-} will yield an absorption coefficient $\beta > 10^{-4}\ cm^{-1}$ (current value of interest) at 10.6 μm. Predicted temperature dependences of impurity limited β(10.6 μm) are: $T^{1.6}$, nearly temperature independent, and decreasing β with increasing temperature depending on the particular ionic impurity.

I. INTRODUCTION

Recently there has been considerable interest in reducing the absorption coefficient β of transparent materials used in high-power CO_2 laser systems. Laser windows can fail catastrophically by fracturing due to inhomogeneous internal stresses, or less dramatically due to thermal defocusing of the beam[1] which result from heating by absorbed radiation.

Among the most promising materials for use with high-power 10.6 μm wavelength CO_2 lasers are the alkali halides, in particular KCl and KBr. The mechanism for intrinsic infrared absorption in these materials is due to multiphonon absorption with the fundamental Reststrahl frequency ν_ℓ of these crystals being 6 to 8 times smaller than the CO_2 laser frequency of 943 cm^{-1}. It has been established experimentally[2] and theoretically[3] that for $\nu > \nu_\ell$, the intrinsic multiphonon absorption coefficient β_{int} decreases nearly exponentially with increasing frequency. Extrapolation of the measured low-frequency intrinsic absorption coefficients yields $\beta_{int} = 8 \times 10^{-5}\ cm^{-1}$ for KCl and $\beta_{int} = 5 \times 10^{-7}$ for KBr at 10.6 μm. However, absorption in even the best presently available materials is impurity dominated with $\beta > 10^{-4}\ cm^{-1}$ at the CO_2 laser frequency.

The purposes of the present paper are to present evidence that an important class of infrared absorbing impurities are polyatomic molecular anion impurities which substitute for the halide ions in the crystal lattices and to identify those ionic impurities that absorb most strongly at 10.6 μm (943 cm^{-1}). The influence of absorbing inclusions on the bulk absorption coefficient and the failure of materials containing inclusions have been considered in previous publications.[4,5]

Nominally pure commercial crystals are commonly observed to contain molecular anion impurities such as the metaborate ion[6,7] (BO_2^-) and the carbonate ion[6] (CO_3^{2-}) using conventional absorption spectroscopy. The hydroxyl ion (OH^-) is especially difficult to remove from alkali halides during purification,[8] but should yield little 10.6 μm absorption. These anion impurities along with divalent metal cation impurities[8,9] are most likely still present in small concentrations in specially purified laser window materials and less than one part per million of certain anions can result in the presently observed extrinsic absorption.

Molecular cation impurities are less likely to be found in alkali-halide crystals due to the small size of the alklai ions which they replace, although NH_4^+ in KCl has been studied.[10] Monatomic impurities can also absorb infrared radiation either through local modes of vibration or by activating phonons other than the fundamental Reststrahl phonon.[11] However, absorption due to monatomic impurities at 943 cm^{-1} is expected to be negligible because phonon and local mode frequencies are generally much smaller than 943 cm^{-1} with the local mode of H^- in KCl (U center) at 500 cm^{-1} having the highest frequency of this group. Absorption due to electronic transitions of impurities is not considered in this paper.[12]

II. IMPURITY SPECTRA

The infrared absorption spectrum of a crystal containing substitional molecular anion impurities typically consists of a number of sharp lines corresponding to the infrared active internal vibration modes of the polyatomic molecular ion. Generally the internal vibrations of the impurity ions are only slightly affected by the host crystal: There are small shifts in frequency and increases in the line width which depend on the particular host. Due to a lowering of the symmetry of the ion when it interacts with the host, infrared inactive modes may become weakly absorbing and degenerate modes may be split into several components. In fact, the technique of alklai-halide matrix isolation has been used extensively to isolate and concentrate these ions for study by infrared absorption spectroscopy.

The probability of the laser frequency being exactly coincident with the peak of an impurity absorption line is extremely small, with the laser line usually falling in the wings of the absorption line. In order to estimate the absorption coefficient β at $\nu = 943\ \mathrm{cm}^{-1}$ due to an absorption line centered at frequency ν_0, a Lorentzian line shape

$$\beta(\nu) = (\text{const.})\ \frac{\Delta\nu}{(\nu - \nu_0)^2 + (\Delta\nu/2)^2} \tag{1}$$

is assumed, where $\Delta\nu$ is the full width at half maximum. With 0.1% impurity concentration, the absorption coefficient at the center of an allowed transition $\beta(\nu_0)$ typically ranges from $10^2\ \mathrm{cm}^{-1}$ to $10^3\ \mathrm{cm}^{-1}$ with $\Delta\nu$ ranging from $4\ \mathrm{cm}^{-1}$ to $50\ \mathrm{cm}^{-1}$, depending on the particular molecular species and host.

Although experimentally observed line shapes near resonance are described quite accurately by (1) using a constant relaxation frequency $\Delta\nu$,[13-16] it is used for extrapolation to the wings with certain reservations. Widths of the fundamental absorption lines of matrix isolated molecular impurities are in general a result of weak coupling between the internal molecular vibrations and the lattice vibrations of the host crystal.[17] With $|\nu - \nu_0| < \nu_m$, where ν_m is the maximum phonon frequency (210 cm^{-1} for KCl), there will be structure in $\Delta\nu$, hence in $\beta(\nu)$, reflecting the one-phonon density of states and phonon selection rules. This will be important for extrapolation of narrow lines ($\Delta\nu \lesssim 10\ cm^{-1}$), since the measured line width in this case samples only a small part of the phonon spectrum.

For extrapolation far from the line center $|\nu - \nu_0| > \nu_m$, $\Delta\nu$ is expected to decrease with increasing $|\nu - \nu_0|$ resulting in a more rapid decrease in β than is predicted by (1). In this region it is likely that β will decrease exponentially with increasing $|\nu - \nu_0|$ in analogy with intrinsic multiphonon absorption.[3] Nevertheless, judicious use of (1) together with measured impurity line strengths and line widths from the experimental literature is felt to be reliable for order-of-magnitude estimates of $\beta(943\ cm^{-1})$.

Fundamental absorption lines of molecular ion impurities are often accompanied by other nearby lines which may not be resolved at room temperature and may be confused with the fundamental line width. In the case of small ions such as OH^- and NO_2^- the additional lines arise from rotational and local translational motions of the ions.[17-23] (Recall that for a freely rotating diatomic molecule, the angular momentum selection rule requires that the vibrational transition be a doublet.) The fundamental absorption lines of large polyatomic ions are often accompanied by nearby "hot" bands from transitions originating from low energy excited states, and by isotope lines.[7,24]

Measured absorption frequencies of several molecular-ion impurities that have been isolated in KCl crystals are listed in the first two columns of Table I.[25-50] The third column presents an estimated impurity concentration in parts per million for each ion required to produce $\beta = 10^{-4}\,\mathrm{cm}^{-1}$ at the frequency 943 cm^{-1}. These estimates were obtained by extrapolating the measured absorption lines using an assumed Lorentzian line shape with measured line widths where they were available. Details of the spectra can be found in the original literature references which are listed in the fourth column.

Isolated diatomic ions typically have fundamental absorption frequencies that are far removed from 943 cm^{-1}. As a result, impurities such as OH^- that are commonly observed in alkali halides should have little effect on absorption at 943 cm^{-1} in spite of the large line width of typically 50 cm^{-1} at room temperature. Using $\beta(\nu_0) \cong 1\ \mathrm{cm}^{-1}$ and $\Delta\nu = 50\ \mathrm{cm}^{-1}$ in (1) for 1000 ppm, OH^- in KCl yields $\beta(943\ \mathrm{cm}^{-1}) \cong 10^{-4}\,\mathrm{cm}^{-1}$.[22]

The polyatomic impurities NO_2^-, HCO_3^-, SO_4^{2-}, and CrO_4^{2-} yield $\beta(943\ \mathrm{cm}^{-1}) > 10^{-4}\,\mathrm{cm}^{-1}$ at concentrations less than 0.1 ppm. These impurities, if present in alkali-halide laser windows, will result in a severe limitation in the laser transmission.

In the case of NO_2^- in KCl at room temperature, the absorption lines are relatively broad with the strongest absorption line occurring at $\nu_3 = 1290\ \mathrm{cm}^{-1}$ with a weaker (by a factor of 10^{-4}) absorption line at $\nu_2 = 805\ \mathrm{cm}^{-1}$. With $\Delta\nu = 38\ \mathrm{cm}^{-1}$ for both lines, extrapolation using the Lorentzian line shape in (1) indicates that the principal absorption at 943 cm^{-1} comes from ν_3. For 0.1% impurity concentration, $\beta(1290\,\mathrm{cm}^{-1}) = 10^{3}\,\mathrm{cm}^{-1}$, which results in $\beta(943\ \mathrm{cm}^{-1}) = 3\ \mathrm{cm}^{-1}$ at this concentration, or $\beta(943\,\mathrm{cm}^{-1}) = 10^{-4}\,\mathrm{cm}^{-1}$ with 0.03 ppm NO_2^- in KCl.

Table I. Experimentally observed absorption frequencies of several impurity ions in KCl crystals and the estimated impurity concentration to produce $\beta = 10^{-4}\,cm^{-1}$ at the CO_2 laser frequency.

Ion	Frequencies (cm^{-1})	Conc. (ppm) for $\beta(943\,cm^{-1}) = 10^{-4}\,cm^{-1}$	References
H^-	500	> 10	11
OH^-	3640	> 100	22, 23, 25, 26, 27
SH^-	2590	> 100	28
CN^-	2089	100	20, 21
BO_2^-	590, 1972	10 - 100	6, 29, 30
CO_2^-	1696	10 - 100	31
N_3^-	642, 2049	100	32
NCO^-	629, 1232, 2169	10	15, 14, 24, 7, 33
NO_2^-	805, 1290, 1329	0.1	19, 13, 34, 18, 35
NO_3^-	842, 1062, 1396	10	16, 17, 13, 34, 18, 36, 37, 9
CO_3^{2-} a	680-720, 883, 886, 1058, 1064, 1378, 1416, 1488, 1518	10	6, 38, 9, 39
BO_3^{3-}	736, 949(w), 1222	1-10	40
SeO_3^{3-}	broad 738-850	1-10	41
HCO_3^-	589, 672, 713, 840, 971, 1218, 1346, 1701, 3339	0.01	42
BH_4^-	1142, 2321	10	43, 29
SO_4^{2-} a	630, 978, 1083, 1149, 1188	0.03	44, 45, 46, 9
CrO_4^{2-} a	862, 890, 930, 941	< 0.1	47, 48, 49, 46
SeO_4^{2-} a	834, 860, 909, 923	< 0.1	41
MnO_4^{2-} a	899, 909, 914, 925	< 0.1	50
NH_4^{2+}	1405, 3100	10	10

a. Exact frequencies and intensities very dependent on presence of compensating M^{2+}.

With HCO_3^- the principal absorption at 943 cm^{-1} is from the $\nu_5 = 971\,cm^{-1}$ fundamental. Estimating from published absorption curves that $\beta(971\,cm^{-1}) = 10^3$ cm^{-1} and $\Delta\nu = 4\ cm^{-1}$ with 0.1% concentration, (1) yields $\beta(943\,cm^{-1}) = 5\ cm^{-1}$. Including additional contributions from $\nu_3 = 1346\ cm^{-1}$ and $\nu_4 = 1218\ cm^{-1}$ which have $\Delta\nu \cong 20\ cm^{-1}$ results in $\beta(943\ cm^{-1}) = 10^{-4}$ with a concentration of 0.01 ppm.

The polyvalent ions listed in Table I each have several absorption lines near 943 cm^{-1}. In order to preserve the charge neutrality of the crystal, divalent impurity anions must be accompanied by compensating anion vacancies, or as is frequently observed, by a divalent cation impurity (such as Mg^{2+}, Ca^{2+}, Ba^{2+}, Pb^{2+}, or Sr^{2+}) which are usually located at neighboring lattice sites. In heavily doped crystals, the solubility of the divalent anions is enhanced by simultaneous doping with divalent cations. The exact absorption frequencies and relative line strengths of the anions are dependent on the particular accompanying cation, especially in the case of CO_3^{2-} which is strongly perturbed with different metal ions.

The group of divalent ions SO_4^{2-}, CrO_4^{2-}, SeO_4^{2-}, MoO_4^{2-}, and WO_4^{2-} have similar spectra with the strong ν_3 fundamental of these ions falling very near to $943\,cm^{-1}$. Due to their large size, MoO_4^{2-} and WO_4^{2-} are reported to be insoluble in KCl and KBr.[51] Depending on the particular perturbing cation impurity, the normally threefold degenerate ν_3 fundamental of SO_4^{2-} is split into three strongly absorbing components from 1050 cm^{-1} to 1200 cm^{-1} each with $\Delta\nu \cong 15\ cm^{-1}$. The otherwise forbidden ν_1 fundamental becomes weakly absorbing in the crystal with frequencies from 975 cm^{-1} to 980 cm^{-1} and with $\Delta\nu \cong 15\ cm^{-1}$. Additional absorption lines due to the ν_4 and ν_2 fundamentals are observed near 600 cm^{-1} and 500 cm^{-1}, respectively. The components of the ν_3 fundamental of CrO_4^{2-} are even closer to the laser line than SO_4^{2-} with frequencies in this case varying from 880 cm^{-1} to 950 cm^{-1}.

III. TEMPERATURE DEPENDENCE

Absorption frequencies and line widths of matrix isolated ions are observed to be temperature dependent, which can result in temperature dependent absorption at 943 cm^{-1}. In the case of ions which have broad absorption lines resulting from coupling to the lattice phonons and which have ionic fundamentals within the approximate range from 50 cm^{-1} to 300 cm^{-1} of 943 cm^{-1}, the temperature dependence can be simply predicted. With $| \nu - \nu_0 | >> (\Delta\nu/2)$, Equation (1) can be written

$$\beta(\nu = 943\ cm^{-1}) = (const.)\,(\Delta\nu)/(\nu - \nu_0)^2 \quad . \tag{2}$$

Above 100 K, the line widths $\Delta\nu$ of the nitrite[13] (NO_2^-), nitrate[13] (NO_3^-), cyanate[14] (NCO^-) and hydroxyl[22] (OH^-) ions are observed to vary as T^n with $n \cong 1.6$, and will dominate the small temperature dependent changes in ν_0 in (2). As a result, $\beta(943\,cm^{-1})$ will vary as $T^{1.6}$, especially in the important case of NO_2^-, where the approximations are fairly well satisfied. For OH^-, the use of the Lorentzian line shape is not justified and the absorption at 943 cm^{-1} due to this ion if seen at all should have a stronger temperature dependence, with $n > 1.6$, in analogy with intrinsic multiphonon absorption.[52]

With the ions SO_4^{2-}, CrO_4^{2-}, and HCO_3^-, the laser frequency is near many relatively narrow lines and the temperature dependence of the absorption is more difficult to predict. Published spectra of these ions taken at different temperatures show small increases in line width and small shifts in frequency. In these cases changes in ν_0 can be nearly as important as changes in $\Delta\nu$, and it is not clear that the observed line widths are entirely due to phonon coupling. That is, part of the absorption in the wings which contributes at 943 cm^{-1} could be due to hot bands,

and in the case of divalent ions to differing perturbing impurities accompanying the molecular ion. As a result, the 943 cm^{-1} absorption of crystals containing these ions is expected to be less temperature dependent than crystals containing smaller, monovalent ions. It is interesting to note that Figures 2 and 3 of Dem'yanenko et al[48] indicate that with CrO_4^{2-} in KCl, the 943 cm^{-1} absorption could even decrease with increasing temperature.

IV. DISCUSSION

Table I lists only those absorbing impurities which have been isolated and studied in KCl crystals and serves to illustrate the importance of substitutional molecular anion impurities on laser transmission at 943 cm^{-1}. In addition to these, there must be other ionic impurities that have been overlooked in this survey along with still others that remain to be studied in alkali-halide crystals. One such possible ion is SiO_4^{4-} which is observed to have strong absorption near 1000 cm^{-1} in several glasses.[53]

In addition to the substitutional ionic impurities, there are other possible molecular impurities that will limit laser transmission at 943 cm^{-1}. Neutral molecules such as H_2O or CO_2 can exist at interstitial sites in the bulk of the crystal or condensed on the surface.[54-56] Organic molecules condensed on crystal surfaces are another possibility.[57]

There has been little experimental work done on the effects of impurities on absorption in materials used for high-power laser components. Further studies of impurity-induced absorption at 943 cm^{-1} are needed to more firmly establish the relationship between the absorption in the wings and the fundamental absorption at the line centers. The temperature dependence of $\beta(943\ cm^{-1})$ found in intentionally doped crystals can possibly be used as a guide in identifying unknown impurities in other crystals.

A study of Pb doped KCl found little correlation between absorption at 943 cm^{-1} and the Pb concentration.[58] Isolated Pb ions are not expected to absorb at this frequency, but complexes of Pb^{2+} with the divalent anions listed in Table I do absorb. The reason for the negative result of this experiment could be that there were no

uncompensated divalent anions in the samples studied. In crystals containing divalent anions without accompanying divalent cations, the introduction of Pb^{2+} could have a significant effect, particularly in the case of CO_3^{2-}.

Doping KCl crystals with OH^- and CO_3^{2-} was found to have little effect on 943 cm^{-1} absorption when the ions were introduced separately, but a significant increase in β(943 cm^{-1}) was observed when both ions were present.[59] It is possible that in this case the enhanced absorption was due to the formation of HCO_3^- which is much more strongly absorbing at 943 cm^{-1} than either OH^- or CO_3^{2-}.

In internally stressed KCl crystals it was observed that β(943 cm^{-1}) was larger by a factor of two than after the same crystals were annealed.[8] This is difficult to explain on the basis of intrinsic absorption. Although there is little information available regarding the effects of inhomogeneous stresses on molecular impurity absorption, we may speculate that the increased absorption observed in stressed crystals could be due to increased molecular ion line widths and shifts in frequencies.

Discussions with Dr. M. Sparks are gratefully acknowledged.

REFERENCES

*Research supported by the Advanced Research Projects Agency of the Department of Defense, and monitored by the Defense Supply Service, Washington, D.C.

1. M. Sparks, J. Appl. Phys. 42, 5029 (1971); M. Sparks and H. C. Chow, J. Appl. Phys. (to be published).
2. T. F. Deutsch, to be published.
3. For theories of intrinsic multiphonon aborption see M. Sparks and L. J. Sham, Phys. Rev. B 8, 3037 (1973) and references therein.
4. M. Sparks and C. J. Duthler, J. Appl. Phys. 44, 3038 (1973).
5. C. J. Duthler, Appl. Phys. Lett. (to be published).
6. H. W. Morgan and P. A. Staats, J. Appl. Phys. 33, 364 (1962).
7. J. C. Decius, J. L. Jacobson, W. F. Sherman, and G. R. Wilkinson, J. Chem. Phys. 43, 2180 (1965).
8. R. C. Pastor and M. Braunstein, Hughes Research Laboratories Technical Report No. AFWL-TR-72-152, Vol. II, July (1973) (unpublished).
9. T. I. Maksimova, Phys. Stat. Sol. 33, 547 (1969).
10. W. Vedder and D. F. Hornig, J. Chem. Phys. 35, 1560 (1961).
11. A. A. Maradudin in Solid State Physics, Vol. 18, p. 274 and Vol. 19, p. 1, edited by F. Seitz and D. Turnbull; A. A. Maradudin, Phys. Rev. (to be published).
12. See for example J. T. Vallin, G. A. Slack, S. Roberts, and A. E. Hughes, Phys. Rev. B 2, 4313 (1970).
13. V. P. Dem'yanenko and Yu. P. Tsyashchenko, Sov. Phys. - Solid State 11, 3043 (1970).
14. I. I. Kondilenko, Yu. P. Tsyashchenko, and V. A. Pasechnyi, Sov. Phys. - Solid State 12, 2990 (1971).
15. V. Schettino and I. C. Hisatsune, J. Chem. Phys. 52, 9 (1970).
16. M. Tsuboi and I. C. Hisatsune, J. Chem. Phys. 57, 2087 (1972).

17. R. Metselaar and J. van der Elsken, Phys. Rev. 165, 359 (1968).

18. R. Bonn, R. Metselaar, and J. van der Elsken, J. Chem. Phys. 46, 1988 (1967).

19. V. Narayanamurti, W. D. Seward, and R. O. Pohl, Phys. Rev. 148, 481 (1966).

20. W. D. Seward and V. Narayanamurti, Phys. Rev. 148, 463 (1966).

21. G. R. Field and W. F. Sherman, J. Chem. Phys. 47, 2378 (1967).

22. B. Wedding and M. V. Klein, Phys. Rev. 177, 1274 (1969).

23. M. V. Klein, B. Wedding, and M. A. Levine, Phys. Rev. 180, 902 (1969).

24. D. F. Smith, J. Overend, J. C. Decius, and D. J. Gordon, J. Chem. Phys. 58, 1636 (1973).

25. G. K. Pandey and D. K. Shukla, Phys. Rev. B 4, 4598 (1971).

26. A. I. Stekhanov and T. I. Maksimova, Sov. Phys. - Solid State 9, 2900 (1968).

27. C. K. Chau, M. V. Klein, and B. Wedding, Phys. Rev. Lett. 17, 521 (1966).

28. C. K. Chi and E. R. Nixon, J. Phys. Chem. Solids 33, 2101 (1972).

29. I. C. Hisatsune and N. H. Suarez, Inorg. Chem. 3, 168 (1964).

30. J. C. Decius, C. R. Becker, and W. J. Fredericks, J. Chem. Phys. 56, 5189 (1972).

31. K. O. Hartman and I. C. Hisatsune, J. Chem. Phys. 44, 1913 (1966).

32. J. I. Bryant and G. C. Turrell, J. Chem. Phys. 37, 1069 (1962).

33. A. Maki and J. C. Decius, J. Chem. Phys. 31, 772 (1959).

34. R. Kato and J. Rolfe, J. Chem. Phys. 47, 1901 (1967).

35. A. R. Evans and D. B. Fitchen, Phys. Rev. B 2, 1074 (1970).

36. A. Strasheim and K. Buijs, J. Chem. Phys. 34, 691 (1961).

37. J. van der Elsken and S. G. Kroon, J. Chem. Phys. 41, 3451 (1964).

38. V. P. Dem'yanenko, Yu. P. Tsyashchenko, and E. M. Verlan, Sov. Phys. - Solid State 13, 767 (1971).

39. N. G. Politov and B. M. Trakhbrot, Sov. Phys. - Solid State 14, 483 (1972).

40. S. C. Jain, A. V. R. Warrier, and H. K. Sehgal, J. Phys. C 6, 189 (1973).

41. V. P. Dem'yanenko, Yu. P. Tsyashchenko, and E. M. Verlan, Phys. Stat. Sol. 48, 737 (1971).

42. D. L. Bernitt, K. O. Hartman, and I. C. Hisatsune, J. Chem. Phys. 42, 3553 (1965).

43. E. H. Coker and D. E. Hofer, J. Chem. Phys. 48, 2713 (1968).

44. J. C. Decius, E. H. Coker, and G. L. Brenna, Spectrochimica Acta 19, 1281 (1963).

45. E. H. Coker, J. C. Decius, and A. B. Scott, J. Chem. Phys. 35, 745 (1961).

46. D. N. Mirlin and I. I. Reshina, Sov. Phys. - Solid State 10, 895 (1968).

47. V. P. Dem'yanenko, Yu. P. Tsyashchenko, and E. M. Verlan, Sov. Phys. - Solid State 12, 2527 (1971).

48. V. P. Dem'yanenko, Yu. P. Tsyashchenko, and E. M. Verlan, Sov. Phys. - Solid State 12, 417 (1970).

49. S. C. Jain, A. V. R. Warrier, and S. K. Agarwal, J. Phys. Chem. Solids 34, 209 (1973).

50. P. Manzelli and G. Taddei, J. Chem. Phys. 51, 1484 (1969).

51. I. I. Kondilenko, V. A. Pasechny, and Yu. P. Tsyashchenko, Phys. Stat. Sol. 54, 783 (1972).

52. M. Sparks and L. J. Sham, Phys. Rev. Lett. 31, 714 (1973).

53. F. Matossi and O. Bronder, Z. Physik 111, 1 (1938).

54. T. J. Neubert and D. L. Roskelley, J. Phys. Chem. Solids 34, 493 (1973).

55. H. Gründig and C. Rühenbeck, Z. Physik 183, 274 (1965).

56. C. Rühenbeck, Z. Physik 207, 446 (1967).

57. T. F. Deutsch and R. I. Rudko, Raytheon Research Division Final Technical Report, Contract No. DAAH01-72-C-0194 (1973) (unpublished).

58. F. W. Patten, R. M. Garvey, and M. Hass, Mat. Res. Bull. 6, 1321 (1971).

59. H. G. Lipson, J. J. Larkin, B. Bendow, and S. S. Mitra, Third Conference on High Power Infrared Laser Window Materials, Hyannis, Mass., Nov. 12-14, 1973.

D. VERY HIGH-INTENSITY EFFECTS

At the present time, high-power long-focal-length systems, with their requirement for large windows to avoid severe diffraction effects, have low intensities -- possibly up to a few hundred to a few thousand watts/cm^2. Thus, nonlinear optical effects are not expected to be a problem. However, as higher-power and short-pulse lasers become available, the intensity at the window will increase accordingly. At sufficiently high intensities, nonlinear and possibly other high-power effects will become important. Two key questions are: Which high-power effect will first limit the performance of high-power infrared systems? At what intensity and under what conditions will the limit occur? Although the literature abounds with nonlinear effects, these two questions have received little previous attention.

In seeking the answers to these two questions, the following effects were considered:

1. material failure from absorption by macroscopic inclusions,
2. electrical breakdown of air,
3. stimulated scattering processes,
4. electron avalanche breakdown,
5. parametric instabilities of phonons,
6. self focusing,
7. multiphoton absorption, and
8. electrostrictive defocusing.

The first four are shown to be important. Values of intensity as low as $\sim 10^6$, 10^7, 10^8, and 10^{10} W/cm^2, respectively, may cause material failure.

Material failure from absorbing inclusions was considered in the previous technical report[1] and in Refs. 2 and 3. The theoretical results indicate that pulse energy densities of order $1\,J/cm^2$ are sufficient to damage crystals containing macroscopic absorbing inclusions for pulse lengths ranging from picoseconds to microseconds. The corresponding intensities range from $\sim 10^6$-10^{12} W/cm^2. Cone-shaped surface damage pits resulting from inclusions near the surface are discussed in Sec. E.

Although the electrical breakdown of air may not be considered strictly as a window-material failure mode, it should be mentioned that this can be the phenomenon that limits the performance of some systems. The intensity at which air breakdown occurs varies greatly, depending on the condition of the air. For dirty air the breakdown intensity can be as low as ~ 10 MW/cm^2, which is one of the lowest limiting intensities studied.

In the report of stimulated scattering processes to be included in the following Technical Report, it will be shown that there is a threshold intensity I_c having a typical value of 10 GW/cm^2 at 10.6 μm (by scaling from 0.69 to 10.6 μm using $I_c \sim 1/\omega$) above which a large fraction of the laser radiation is converted to Stokes radiation.

Many systems will fail for $I > I_c$. The angular divergence of the Stokes light will be too great for the Stokes radiation to be useful in most long-focal-length systems. Furthermore, the heating of the crystal resulting from the creation of the fundamental phonons in the scattering process will be intolerably great in many applications. For example, if ten percent of the laser radiation at 10.6 μm is converted to Stokes radiation, the intensity absorbed (by the phonons) is

$$l_{abs} \cong (\omega_f / 10\,\omega_L)\, l \qquad (1)$$

where f and L denote the fundamental phonon and laser photon, since one phonon is created for every laser photon annihilated. This result (1) corresponds to an effective βL of

$$(\beta L)_{eff} = \omega_f / 10\,\omega_L = 10^{-3} ,$$

which is not acceptable in many high-power applications.

Electron avalanche breakdown, which has been studied in detail by others, is believed to be an important very high-power effect. Very briefly, the cardinal results are as follows. The electric field of the laser can cause a breakdown, just as a dc electric field does. For 10^{-8} sec pulses in alkali halides, the intensity I_c required is typically of the order of 10^{10} W/cm^2. For shorter pulses, greater intensities are required, with I_c of order 10^{12} W/cm^2 for 1.5×10^{-11} second pulses.[4]

Parametric instabilities of phonons are considered in Sec. F. Self focusing, which has been the subject of numerous previous investigations,[5] is not expected to be a problem in large-diameter windows. The central features of self focusing are, very briefly, as follows. A beam will self focus when the power P exceeds a critical value P_{sf}. Typical values of P_{sf} are tens of kilowatts for materials that are strong self focusers. As the power is increased above P_{sf}, the length z_{sf} of the sample required to obtain self focusing decreases according to the relation

$$z_{sf} = \varkappa D^2 \left(\sqrt{P} - \sqrt{P_{sf}} \right)^{-1} \qquad (2)$$

where D is the beam diameter and $\varkappa$ is a constant. For a strong-self-focusing material such as CS_2, P_{sf} is of the order of 8 kW, and $\varkappa$ is of order 6.9×10^5 $cm^{-1}(kW)^{1/2}$. For $I = 10^{10}$ W/cm^2 and D = 10 cm, (2) gives $z_{sf} = 200$ cm.

It is possible that a shorter distance z_{sf} could result from a self focusing of only part of the beam, having a diameter D_{loc}. For a fixed intensity I, it is convenient to write (2) as

$$z_{loc} = \varkappa D_{loc}^2 \left(D_{loc}\sqrt{I} - \sqrt{P_{sf}} \right)^{-1}$$

which has a minimum of

$$z_{min} = 4\varkappa \sqrt{P_{sf}}/I \qquad (3)$$

at $D_{loc} = 2(P_{sf}/I)^{1/2}$. With the values of P_{sf} and $\varkappa$ from above, and a window thickness $d = z_{min} = 1$ cm, (3) gives $I = 8 \times 10^9$ W/cm^2. Since $\varkappa\sqrt{P_{sf}}$ is much greater in solids than in CS_2, the intensity required for self focusing is much greater than 8×10^9 W/cm^2. Thus, the other high-power effects discussed above are expected to set in at lower powers than that of self focusing.

Multiphoton absorption is clearly negligible. Two-photon absorption is small, and for 10.6 μm (0.12 eV) radiation in a crystal with bandgap $E_g = 5$ eV, 42 photons are required in order to conserve energy.

The following order-of-magnitude estimate indicates that electrostriction is negligible. Since the intensity across the window is not constant in most systems, electrostriction will cause thickness variations. The change in thickness $\Delta\ell$ at the center of a window thickness ℓ is

$$\Delta\ell/\ell = S E^2 \qquad (4)$$

where the electrostriction constant S has a typical value of $10^{-18}\,cm^2/V^2$ for a solid.[6] For a pure thickness effect (refractive index n unchanged), a very strict angle tolerance of 5×10^{-5} radians implies $n\Delta\ell/R \cong 5 \times 10^{-5}$, where R is the window radius. With $R/\ell = 10$ and $n = 1.5$, this gives

$$\Delta\ell/\ell = 3 \times 10^{-4} \quad . \tag{5}$$

Eq. (4) gives this value (5) of $\Delta\ell/\ell$ for $E \cong 2 \times 10^7$ V/cm, which corresponds to $\sim 10^{11}\,W/cm^2$. The actual intensity should be even greater since the reduction in n as the crystal expands was neglected.

A similar negative result is obtained by considering the electrostrictive non-linear index of refraction

$$\Delta n = n_2 E^2 \tag{6}$$

where[7] $n_2 \cong 1.7 \times 10^{-19}\,cm^2/V^2$. With $\ell\Delta n/R = 5 \times 10^{-5}$ and $R/\ell = 10$ from the example above, (6) gives $E \cong 5 \times 10^7$ V/cm.

Discussions with Dr. Y. R. Shen and Dr. M. M. T. Loy on self focusing are gratefully acknowledged. We would like to thank Dr. C. Cason for pointing out that the breakdown in dirty air can occur at quite low intensities.

REFERENCES

1. M. Sparks, "Theoretical Studies of High-Power Infrared Window Materials," Xonics, Inc. First Technical Report, Contract No. DAHC15-73-C-0127, June (1973).
2. M. Sparks and C. J. Duthler, J. Appl. Phys. 44, 3038 (1973); C. J. Duthler and M. Sparks, "Theory of Material Failure in Crystals Containing Infrared Absorbing Inclusions," ASTM 1973 Symposium on Damage in Laser Materials, Boulder, Colorado, May (1973).
3. C. J. Duthler, "Explanation of Laser-Damage Cone-Shaped Surface Pits," Appl. Phys. Lett., in press.
4. D. W. Fradin, N. Bloembergen, and J. P. Letellier, Appl. Phys. Lett. 22, 635 (1973); D. W. Fradin and M. Bass, "Studies of Intrinsic Optical Breakdown," ASTM 1973 Symposium on Damage in Laser Materials, Boulder, Colorado, May (1973).
5. M. T. Loy and Y. R. Shen, IEEE J. Quantum Elec. QE-9, 409 (1973).
6. W. G. Cady, International Critical Tables, 6, p. 207.
7. G. M. Zverev and V. A. Pashkov, Sov. Phys. JETP 30, 616 (1970).

E. EXPLANATION OF LASER-DAMAGE CONE-SHAPED SURFACE PITS

C. J. Duthler
Xonics, Incorporated, Van Nuys, California 91406

An anisotropic, quasi-static stress distribution is found in the material surrounding an absorbing inclusion of a radius a centered a distance d below the surface of a transparent host. Maximum tensile stress greater than the pressure at the inclusion-host interface occurs at the angle $\theta_m = \cos^{-1}(a/d)$ from the line joining the inclusion center to the surface, resulting in cone-shaped fracture.

Recently micron-size cone-shaped damage pits have been observed on the surface of sapphire crystals that have been irradiated with intense 1.06 μm laser pulses.[1] The statistical occurrence of the surface damage sites suggests that the damage is due to absorbing inclusions just below the surface, randomly distributed across the face of the crystal. Due to differing damage thresholds when different polishing compounds are used, it is suspected that polishing grit somehow gets embedded in the surface with subsequent polishing forming surface material over the particle.

Similar damage sites have been observed in multi-layer dielectric films, although in this case the surface pits have a stepped structure due to rupture of the various film layers.[2] Statistical evidence again indicates that the damage is due to absorbing inclusions below the surface which must be formed during the deposition of the films since no polishing compounds are used in this case.

The following model is proposed to explain cone-shaped surface damage: A spherical inclusion a short distance below the surface expands due to heating by laser radiation applying pressure normal to the surface of the cavity in which it is contained. Due to the proximity of the surface, this produces a quasistatic, anisotropic stress distribution in the host material which can result in fracture with a cone-shaped section above the inclusion being ejected intact or in a small number of fragments.

Cross sections for the absorption of laser radiation by inclusions in a transparent host crystal and localized heating effects in the vicinity of the inclusion have been analyzed in a previous paper.[3] The cross section for the absorption of laser energy by a spherical, dielectric inclusion of radius a is approximately given by[3,4]

$$\sigma_{abs} = A \beta_I \pi a^3 \quad , \tag{1}$$

where A is a constant of order unity and β_I is the absorption coefficient for bulk inclusion material. In (1) it has been assumed that $\beta_I a << 1$ as is typically satisfied for micron-sized dielectric inclusions.

The thermal time constant

$$\tau_H = C_H a^2 / 4 K_H \quad , \tag{2}$$

where C_H is the specific heat and K_H is the thermal conductivity of the host, is roughly the time required for heat to diffuse a distance a away from the heated inclusion into the host material.[3,5] For short times $t << \tau_H$, diffusion of heat out of the inclusion is negligible and the temperature of the inclusion increases linearly with time and is given by

$$T = 3\,\sigma_{abs}\,It/4\,\pi\,a^3\,C_I \tag{3}$$

where I is the laser intensity in the host material and C_I is the specific heat of the inclusion. Substitution of (1) into (3) yields

$$T = 3\,A\,\beta_I\,It/4\,C_I \quad . \tag{4}$$

Neglecting the diffusion of heat out of the inclusion, the pressure at the interface with the host is found by equating the volume change of the heated and compressed inclusion to that of the unheated but compressed cavity in the host which yields

$$P = 3\,\alpha_I\,B_{eff}\,T \tag{5}$$

where $B_{eff}^{-1} = B_I^{-1} + B_H^{-1}$. In (5), α_I is the linear thermal expansion coefficient of the inclusion and B_{eff} is an effective bulk modulus obtained from B_I and B_H which are the bulk moduli of the inclusion and host, respectively.

Quasi-static stresses will be produced in the host material for times long compared to the round trip time τ_S for sound to travel from the inclusion to the sample surface. In sapphire the velocity of sound is 1.1×10^6 cm/sec which yields $\tau_S = 9 \times 10^{-11}$ sec for sound to travel one micron. Using $C_H = 3$ J/cm^3 and $K_H = 0.35$ W/cm K for a sapphire host, the thermal diffusion time with $a = 1\,\mu$m is $\tau_H = 3 \times 10^{-8}$ sec. Hence during nanosecond duration laser pulses the conditions $\tau_S < t < \tau_H$ are satisfied and the heated inclusion in the host can be visualized as a spherical cavity within which quasi-static, hydrostatic pressure is applied.

At first glance, the cone-shaped damage sites appear to be similar to the familiar Hopkinson fractures where a hemispherical cap is removed from the face of a large plate opposite the surface on which an impulse force, such as that produced by an explosive charge or projectile, is applied.[6] In Hopkinson fracture, a compressional pulse of short duration diverges from the explosive charge and is reflected from the opposite free surface of the plate. The reflected pulse is one of tension, and failure occurs when the leading edge of the reflected tensile pulse passes the trailing edge of the incident compressional pulse resulting in net longitudinal tensile stress in the material. This mechanism does <u>not</u> apply in laser damage because of the <u>quasi-static</u> nature of the compression. After the termination of the laser pulse, the pressure applied to the host by the heated inclusion will relax at approximately the same rate τ_H as the temperature of the inclusion which is long compared with the time τ_S for sound to travel to the plane surface. As a result, the incident compressional pulse always overlaps the reflected tensile pulse so that there is no net longitudinal tensile stress.

A spherical cavity of radius a at a distance d below the surface of a semi-infinite medium is sketched in Fig. E1. The exact solution for the equilibrium stresses produced in the surrounding material by hydrostatic pressure within the cavity is mathematically intractable, and approximate solutions are very tedious and slowly convergent. Exact solutions to the analogous two-dimensional problem which applies to uniform force normal to a circular hole in a thin plate or a long cylinder in a semi-infinite medium have been obtained by Jeffery[7] and can be used to give insight into the three-dimensional problem.

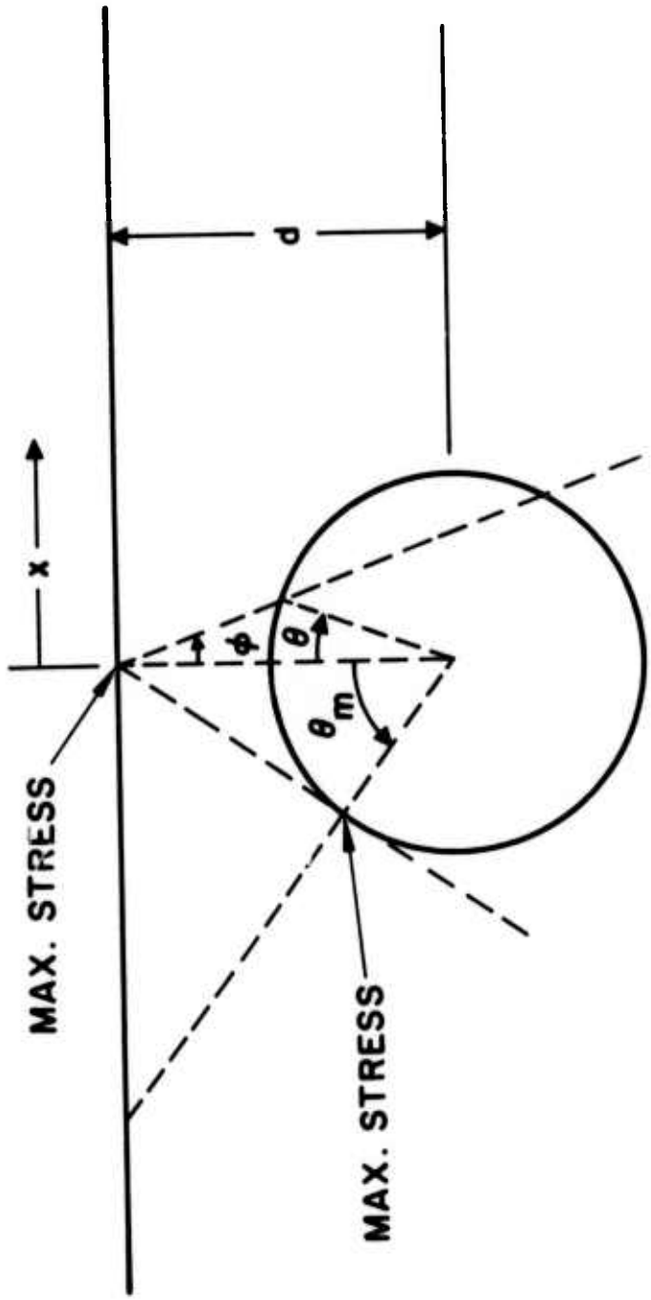

Fig. E1. Sketch of inclusion of radius a at a distance d below the plane surface.

In the two-dimensional case, the tensile stress along the cylindrical surface is given by

$$\sigma_t = P(1 + 2\tan^2\phi) \tag{6}$$

where P is the hydrostatic pressure within the cavity and a point on the surface of the cavity is described by either the angle ϕ or θ as is sketched in Fig. E1, where $\tan\phi = a\sin\theta/(d - a\cos\theta)$. For d/a near unity, the tensile stresses around the cavity are very assymetrical and are much larger than the applied hydrostatic pressure. Maximum stress occurs at the angle $\theta_m = \cos^{-1}(a/d)$ where the dashed line in Fig. 1 from the point on the plane surface directly above the cavity is tangent to the cavity.

Along the plane surface the tensile stress is given by

$$\sigma_x = -4Pa^2(x^2 - d^2 + a^2)/(x^2 + d^2 - a^2)^2 \tag{7}$$

where x is measured along the plane from the point directly above the cavity. Maximum tensile stress in this case occurs at the point $x = 0$ with $\sigma_x(x = 0) > P$ for $d < \sqrt{5}\,a$.

The tensile stresses $\sigma_t(\theta = \theta_m)$ and $\sigma_x(x = 0)$ are plotted as functions of d/a in Fig. E2. For large d, these stresses approach the limiting values $\sigma_t(\theta_m) = P$ and $\sigma_x(0) = 0$ that are appropriate for a two-dimensional cavity in an infinite medium. As d decreases, both $\sigma_t(\theta_m)$ and $\sigma_x(0)$ become larger than P, with $\sigma_x(0) > \sigma_t(\theta_m)$ for $d < \sqrt{3}\,a$.

Solutions for the three-dimensional problem of a spherical cavity are expected to be qualitatively similar to those above. Due to symmetry, maximum

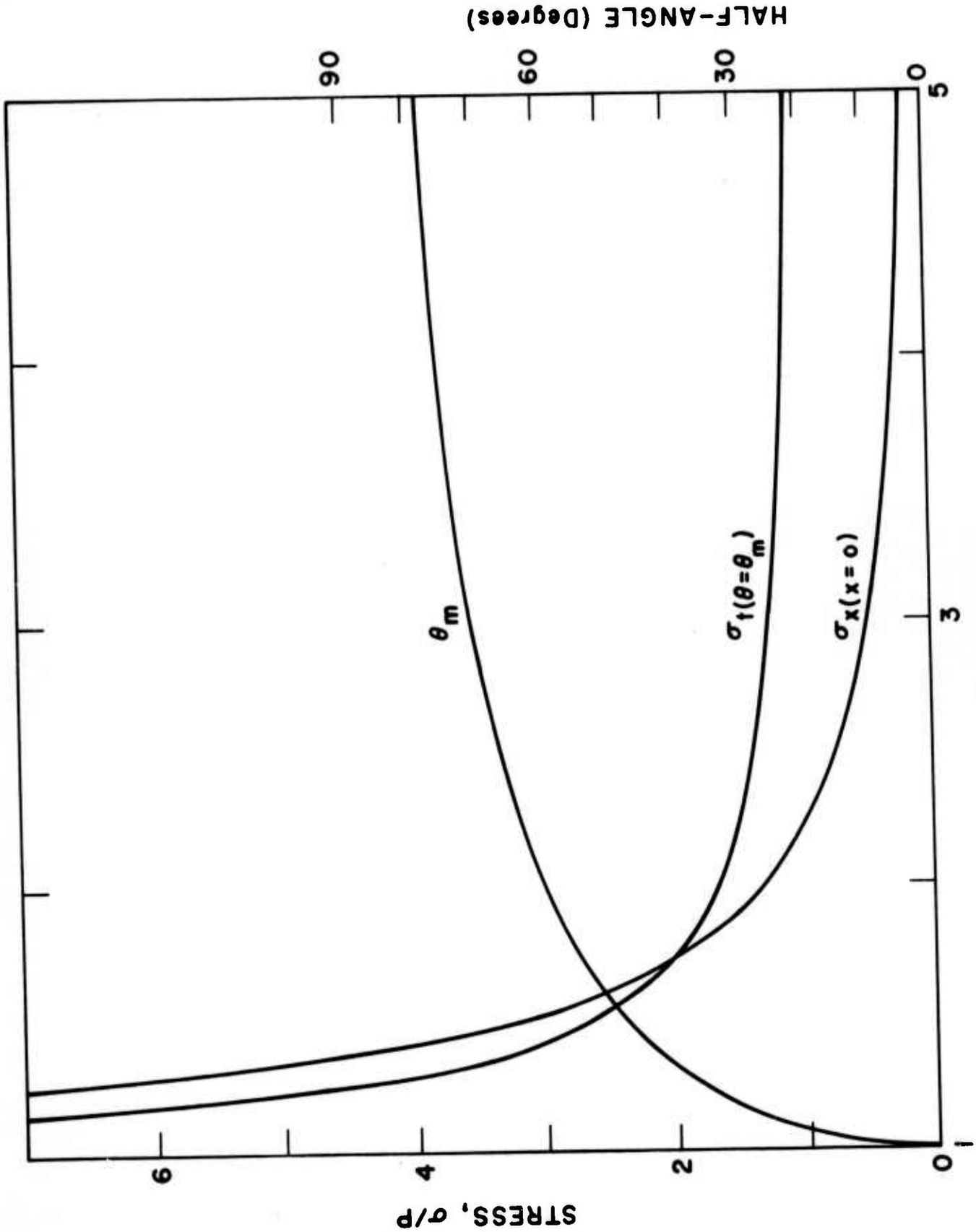

Fig. E2. Tensile stresses and cone half-angle as function of inclusion depth.

tensile stress along the spherical cavity surface is also expected to be a maximum at the angle $\theta = \theta_m$. However, the σ versus d/a curves will be quantitatively different. In the limit of an infinite medium ($d/a \rightarrow \infty$), the tensile stress in the host outside of the cavity will decrease as r^{-3} as compared to r^{-2} in the two-dimensional case and will have the value $P/2$ at the cavity surface.[8] This more rapid decrease of stress with radial distance will cause the σ versus d/a curves to be more strongly peaked near $d/a = 1$ than in Fig. E2.

For homogeneous, isotropic material surrounding the cavity, a crack will nucleate at the point of maximum tensile stress on the boundary and will propagate normal to the boundary with little resistance. When d/a is greater than about $\sqrt{3}$, maximum tensile stress occurs at the angle θ_m on the spherical surface. As is sketched in Fig. E3 A, a crack nucleated at θ_m will propagate normal to the cavity surface toward the plane surface, resulting in a cone-shaped surface pit at half-angle θ_m.

Inclusions very close to the surface ($d/a < \sqrt{3}$) will produce maximum tensile stress at the point $x = 0$ on the plane surface. As is sketched in Fig. 3B, a crack will first propagate from the point $x = 0$ to the cavity surface. Further expansion of the inclusion could result in additional failure near θ_m to produce a cone-shaped damage site.

The following considerations favor fracture first occurring at θ_m as in Fig. E3 A rather than at $x = 0$ as in Fig. E3 B: fracture in bulk materials is strongly dependent on surface cracks and imperfections which have the same size as the inclusion. Similar, but smaller, defects are expected to affect the fracture in the present case. If the inclusion is formed by melting surface

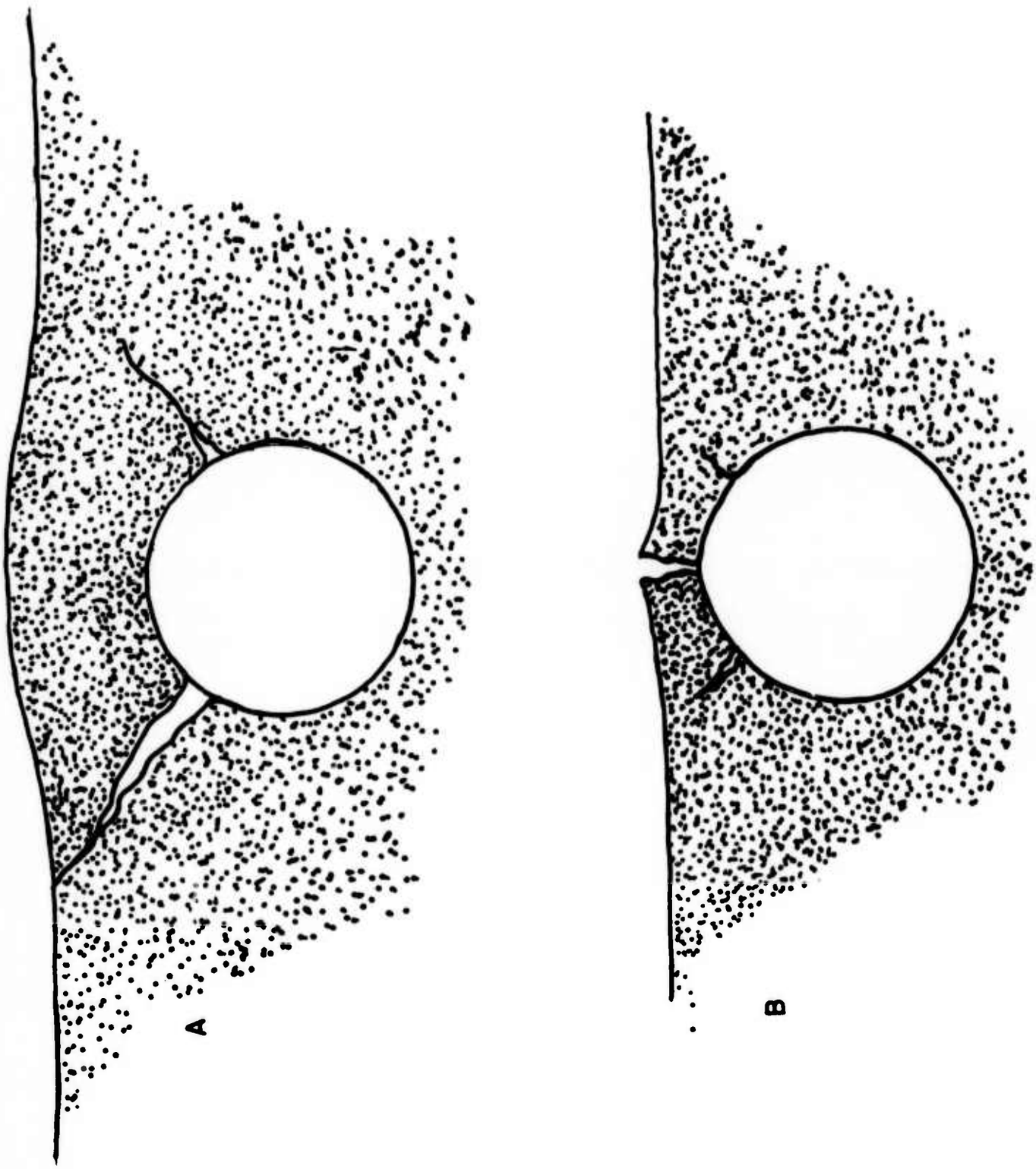

Fig. E3. Cone-producing fracture for crack nucleation at inclusion surface (A) and at plane surface (B).

material over an embedded polishing grit, more defects are expected on the surface of the inclusion than on the highly polished plane surface. In addition, there is much more surface area, hence more probability of finding a defect, along the circumference of the inclusion at the angle θ_m than at the point $x = 0$.

Calculated laser pulse energies It for failure are very imprecise due to large uncertainties in the failure strength σ_f for the material in the vicinity of the inclusion and in the bulk absorption coefficient β_I of the inclusion material. The failure stress for sapphire is estimated to be between the $\sigma_f = 6 \times 10^4$ psi observed in bulk samples and the theoretical strength $\sigma_{theor} = 6 \times 10^6$ psi estimated from $\sigma_{theor} = E/10$ where E is the Young's modulus. Assuming $\sigma_f = 2P$ at the point of failure and using $\sigma_f = 6 \times 10^5$ psi, $B_{eff} = \frac{1}{2} B_{sapphire} = 1.5 \times 10^7$ psi, and $\alpha = 10^{-5}\ K^{-1}$, (5) yields a failure temperature increase of 1000 K. Estimating $\beta_I = 10\ cm^{-1}$ and using $C_I = 3 J/cm^3\ K$ in (4) indicates that failure occurs at approximately $It = 400\ J/cm^2$ accurate to only about two orders-of-magnitude. Pulse energies for damage from 30 to 100 J/cm^2 observed by Boling[1] are well within the range of reasonable theoretical values.

We note that the energy absorbed by a micron-size inclusion at these pulse energies has the same order-of-magnitude as the energy required to disrupt the molecular bonds on the surface of the cone. Hence the removal of the cone material intact or in a small number of fragments is energetically allowed.

For the 30 nsec pulse durations used in many experiments, the assumption of no heat transfer to the host material is not valid. It is reasonable to expect that heating has little effect on the failure strength and that the principal effect

will be to lower the pressure at the inclusion-host interface, hence increase the required energy for damage, due to thermal expansion of the cavity in which the inclusion is contained.[9]

With very short pulses, $t < \tau_S$, damage could be delayed until the time τ_S after the laser pulse. This will occur if the initially formed isotropic stresses are insufficient to cause damage but the quasi-equilibrium, anisotropic stresses, established after the time τ_S for sound to make a round trip to the plane surface, are enhanced sufficiently to cause damage.

Preliminary discussions with Professor R. W. Hellwarth on the comparison of absorbed laser energy to material bond energies which led to the concept of the cone material being removed intact, and his continuing comments are gratefully acknowledged.

REFERENCES

* This research was supported by the Advanced Research Projects Agency of the Department of Defense and was monitored by the Defense Supply Service - Washington, D. C.

1. N. L. Boling and G. Dubé, Appl. Phys. Letters (to be published).
2. D. Milam, R. A. Bradbury, and M. Bass, ASTM Laser Damage Symposium, Boulder, Colorado, May 15-16, 1973.
3. M. Sparks and C. J. Duthler, J. Appl. Phys. 44, 3038 (1973).
4. H. C. Van de Hulst, "Light Scattering by Small Particles" (Wiley, New York, 1971).
5. H. S. Carslaw and J. C. Jaeger, "Conduction of Heat in Solids," 2nd ed. (Clarendon Press, London, 1959).
6. H. Kolsky and D. Rader in "Fracture," Vol. 1, edited by H. Liebowitz (Academic Press, New York, 1968).
7. G. B. Jeffery, Phil. Trans. Roy. Soc. London 221, 265 (1921).
8. S. Timoshenko and J. N. Goodier, "Theory of Elasticity," 2nd ed. (McGraw-Hill, New York, 1951).
9. R. W. Hopper and D. R. Uhlmann, J. Appl. Phys. 41, 4023 (1970).
10. Delayed surface damage on dielectric mirrors in agreement with these predictions has been observed by E. S. Bliss, D. Milam, and R. A. Bradbury, Appl. Opt. 12, 677 (1973).

F. NONLINEAR INFRARED ABSORPTION FROM PARAMETRIC INSTABILITIES OF PHONONS*

M. Sparks
Xonics, Incorporated, Van Nuys, California 91406
and
H. C. Chow
Department of Physics, University of California, Los Angeles, California 90024, and
Xonics, Incorporated, Van Nuys, California 91406

Nonlinear infrared absorption by parametric phonon processes is shown to be negligible in the low-absorption region of exponential frequency dependence of the optical absorption coefficient β, but observable at the Reststrahl resonance and in Raman scattering. At low intensity, the transmission, T, is independent of intensity as usual, but at high intensity the $T(\omega)$ curve broadens and the transmission at resonance increases. This behavior results from the parametric instability in the process in which an intermediate-state Reststrahl phonon is annihilated and a pair of phonons is created. An effective relaxation frequency of the Reststrahl phonon is greater than the low-intensity value as a result of the increase in the amplitudes of the pair phonons above their thermal equilibrium values. The time constant for the approach to the steady state is important since the steady state is not attained in short laser pulses in important cases in which long-lived phonons give rise to low steady-state threshold intensities for anomalous absorption. The threshold for the parametric instability is quite sharp when considered as a

function of the amplitude of the fundamental phonon. In contrast, when considered as a function of the incident laser intensity, the deviation from linear absorption with increasing intensity is quite smooth. Contrary to previously accepted results, even crystals such as NaCl having a center of inversion could have anomalously low thresholds since the threshold is controlled by the phonon (in the pair) having the longer lifetime. Chain instabilities and enhanced relaxation from mutual interaction of excited pair phonons are negligible for the phonon instabilities, in contrast to previous results for plasmas and parallel pumping in ferromagnetic resonance, respectively. The method of calculation, using Boson occupation numbers rather than mode amplitudes, has the simplicity and power to yield more information about parametric instabilities, including effects above the threshold, than has been possible previously.

I. INTRODUCTION

Parametric processes are well known in ferromagnetic resonance,[1-4] plasma physics,[5,6] nonlinear optics, especially stimulated Raman and Brillouin scattering,[7] and many electrical devices.[8] However, apart from Orbach's work showing that it should be possible to create large numbers of long-lifetime phonons on the lowest transverse optical branch by a parametric instability,[9] there apparently have been no studies of phonon instabilities. In particular, the effect of parametric instabilities on optical absorption has not been considered in spite of considerable interest in nonlinear optical effects.

Since the parametric instabilities typically occur at high laser intensities, there are a number of high-intensity effects that could mask the parametric effects. These include absorption by macroscopic inclusions,[10-12] avalanche breakdown,[13,10] self-focusing effects,[14] and differential heating by linear absorption.[15] In previous calculations, the instability threshold for an isolated process, such as annihilation of one Boson and the creation of two other Bosons, has been obtained simply from linearized equations of motion of the mode amplitudes or the mode occupation numbers. More detailed calculations have been severely hampered by the complexity of the nonlinear mode-amplitude equations, especially near and above the threshold, and the difficulty introduced by requiring the amplitudes to relax to their thermal equilibrium values.[1]

In the present paper, the nonlinear absorption of infrared radiation by parametric excitation of phonons is considered and a general method of solving parametric problems is presented. As dicussed in Sec. IIa, an example of a process that has a parametric instability is shown in Fig. F1, where the intermediate phonon f is a

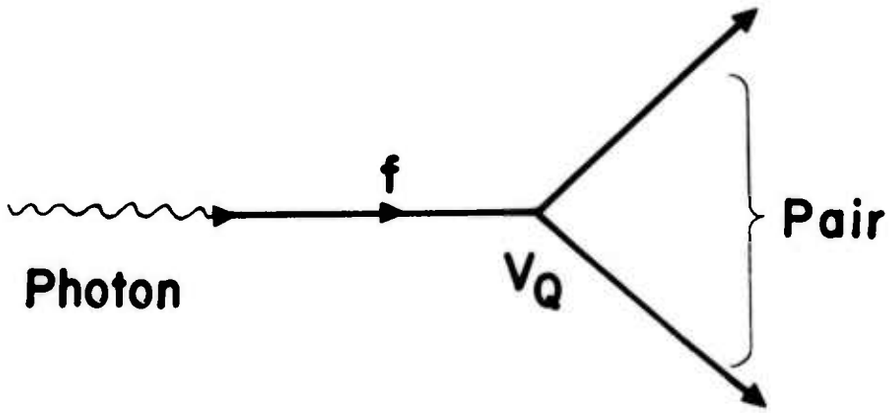

Fig. F1. Two-phonon processes.

fundamental, or Reststrahl phonon (transverse optical mode with wavelength $k \simeq 0$). Special attention is focused on ionic crystals such as NaCl, though the discussion for the most part is quite general. Absorption, as opposed to scattering, processes are emphasized. The results of a similar study on the effect of parametric instabilities on stimulated Raman and Brillouin scattering and on self-focusing of optical beams will be presented elsewhere.

The present treatment differs from previous ones in the following ways: (a) consideration of the nonlinear effects of phonon instabilities on infrared absorption; (b) treatment of transient, as well as steady-state, effects; (c) development of a simple method of calculation which is used even above the threshold; (d) incorporation of effects of sums over potentially unstable modes; (e) analysis of chain parametric processes and enhanced relaxation of output phonons; (f) treatment of the instability in the Lax-Burstein higher-order-dipole-moment process; and (g) consideration of processes in which two fundamental phonons are annihilated.

The following results are obtained: (a) prediction that the thin-film infrared transmission spectrum $T(\omega)$ of crystals is independent of intensity I at low I as usual, but that for $I \gtrsim \frac{1}{2} I_c$, where I_c is the critical intensity for the parametric threshold, the Reststrahl resonance in $T(\omega)$ broadens and the transmission at resonance increases with increasing I; (b) calculation of the value of I_c showing that at the Reststrahl resonance I_c can range from $\sim 10^{-4}$ to 10^{11} W/cm^2; (c) demonstration that the nonlinear parametric-phonon-instability absorption in the infrared region of low multiphonon absorption is negligible with respect to the electron-avalanche breakdown process; (d) indication that transient effects are important, especially in rendering unobservable by present short-pulse lasers the low thresholds resulting from ultralong-lifetime phonons;[9] (e) demonstration that the instability

threshold is sharp when considered as a function of the amplitude n_f of the intermediate (fundamental) phonon, but is a smooth function of the laser intensity I; (f) analysis of effects of many potentially unstable modes which evinces that the value of n_f is considerably less than its threshold value n_c even when $I >> I_c$; (g) calculation of an effective relaxation frequency $\tilde{\Gamma}_f$ for the intermediate mode which shows that $\tilde{\Gamma}_f$ is greater than the usual linear, low-intensity value Γ_f as a result of the increase in the amplitudes n_Q of the output phonons responsible for the damping Γ_f; (h) indication that even crystals (such as NaCl-structure crystals) having a center of inversion could have anomalously low thresholds I_c since the threshold is controlled by the output phonon having the longer lifetime when the two phonons are on different branches; (i) derivation of simple closed-form expressions for transmissivity as a function of I, for $n_f(I)$, for $\tilde{\Gamma}_f(n_f)$, and for $\tilde{\Gamma}_f(I)$; (j) calculation of I_c for n-phonon processes with $n > 2$ which shows that these nonlinear higher-order processes are negligible; (k) analysis of chain parametric-instability processes indicating that these phonon processes are negligible, in contrast to the cases of ferromagnetic resonance and plasma instabilities; and (l) calculation of I_c for the process in which two Reststrahl phonons are annihilated and two other phonons are created, which shows that this process may be important in some cases.

Significant results will be denoted by underscored equation numbers.

II. TWO-PHONON INSTABILITY

a. Physical description. In this section a simple physical description of the two-phonon parametric instability will be given. Consider the two-phonon process in which a photon is annihilated, a fundamental phonon is created, then annihilated, and two other phonons are created, as illustrated in Fig. F1.[16] This process is directly analogous to the Bloch-Bloembergen-Suhl subsidiary-resonance process which occurs at high power levels in ferromagnetic resonance. The fundamental phonon corresponds to the uniform precession magnon (with $\underset{\sim}{k} = 0$) and the pair of created phonons corresponds to a pair of created magnons.[17]

The present section concerns the part of the process in Fig. F1 in which one phonon splits into two phonons, called the pair. The analysis applies to other cases also. For example, the fundamental phonon could be created in the Raman-Stokes process.

The two-phonon process gives rise to ordinary linear absorption at low power levels.[18] In that case, the relaxation of the pair phonons maintains their occupation numbers n_Q at their thermal equilibrium values $\bar{n}_Q$. At higher power levels, n_Q increases above $\bar{n}_Q$. As the intensity I of the radiation increases, the fundamental-mode amplitude n_f increases, and in turn the amplitude of the output pair increases. The balance of power into the pair from the fundamental mode by the power out of the pair by relaxation is the first key to a simple explanation of the parametric instability. The power into the pair increases nonlinearly, that is, the power contains products such as $2n_f n_Q$, since the second vertex in Fig. F1 involves three phonons. On the other hand, the power out of the

pair by relaxation increases linearly as $2\Gamma(n_Q - \bar{n}_Q)$, where Γ is the relaxation frequency of an output phonon. Thus, at a critical value n_c of n_f, the amplitude n_Q becomes very large.

This behavior is analogous to that of a pendulum with a force having frequency $\omega = 2\omega_r$, where ω_r is the resonant frequency of the pendulum, applied along the direction of gravity: For a small angle θ, the loss is linear in θ, while the energy that the force puts into the pendulum (the scalar product of force and distance) is proportional to θ^2 since the projection of the motion along the vertical is proportional to θ^2. The pendulum instability is discussed further in Appendix A. The details of this type of behavior will now be discussed.

b. Instability threshold of a pair. The threshold value n_c of n_f at the parametric-instability threshold and the increase of the pair-mode occupation number n_Q as n_f increases will now be derived, and it will be shown that n_Q increases extremely rapidly as n_f approaches and slightly exceeds n_c, as will be seen in Fig. F2 below.

First consider the power flow from the fundamental mode to the potentially unstable pair in Fig. F1. The Hamiltonian for this process (vertex V_Q in the figure) is[18,19]

$$\mathcal{H} = \sum_{Q_1 Q_2 Q_3} V_{Q_1 Q_2 Q_3} A_{Q_1} A_{Q_2} A_{Q_3} \quad , \tag{2.1}$$

where $Q_i \equiv (\underset{\sim}{k}_i, b_i)$ specifies the phonon mode with wave vector $\underset{\sim}{k}_i$ on branch b_i, $A_{Q_i} \equiv a_{Q_i}^\dagger + a_{-Q_i}$ [with $-Q_i \equiv (-\underset{\sim}{k}_i, b_i)$], and $a^\dagger$ and a are the usual phonon creation and annihilation operators normalized to unit commutators. From the standard second-order perturbation-theory result for the transition probability

between the states of a system, the rate of change of n_f resulting from the coupling to a single pair of phonons Q_1 and Q_2 is[4]

$$\frac{dn_f}{dt} = \frac{2\pi}{\hbar^2} \left\{ \left| \langle n_f + 1, n_{Q_1} - 1, n_{Q_2} - 1 \left| \mathcal{H} \right| n_f, n_{Q_1}, n_{Q_2} \rangle \right|^2 - \left| \langle n_f - 1, n_{Q_1} + 1, n_{Q_2} + 1 \left| \mathcal{H} \right| n_f, n_{Q_1}, n_{Q_2} \rangle \right|^2 \right\} \delta(\tilde{\omega}) , \quad (2.2)$$

where δ is the Dirac delta function and $\tilde{\omega} \equiv \omega - \omega_{Q_1} - \omega_{Q_2}$, with ω the frequency of the photon.

In detailed calculations for specific cases it is important to consider the case of unequal frequencies ω_{Q_1} and ω_{Q_2} since in NaCl-structure crystals a selection rule[20-23] prohibits both phonons of the pair from being on the same branch and a quasiselection rule[24] indicates that the coupling of a fundamental phonon to two acoustical or to two optical phonons is small. However, no essential features of the calculation are lost in the case of equal frequencies and equal relaxation frequencies Γ_Q. The presentation will therefore be simplified by formally using these approximations. The case of $\omega_{Q_1} \neq \omega_{Q_2}$ and $\Gamma_{Q_1} \neq \Gamma_{Q_2}$ is considered in Sec. II d. The occupation numbers n_Q of the two phonons in the pair are equal since $\bar{n}_{Q_1} = \bar{n}_{Q_2}$, where the bar denotes the thermal-equilibrium value as before, the two-phonon process creates the phonons in equal numbers, and $\Gamma_{Q_1} = \Gamma_{Q_2}$.

Substituting (2.1) into (2.2), using the fact that $V_{f Q_1 Q_2}$ vanishes unless $\underset{\sim}{k}_1 = -\underset{\sim}{k}_2$, and using the well known matrix elements of $a^\dagger$ and a gives

$$\left(\frac{dn_Q}{dt}\right)_{\text{pump}} = C \tilde{n} , \quad (2.3)$$

where

$$\tilde{n} = 2n_f n_Q + n_f - n_Q^2, \qquad C = \pi\hbar^{-2} \left| 3!\, V_{f,Q,-Q} \right|^2 \delta(\tilde{\omega}) \ . \tag{2.4}$$

The subscript "pump" in (2.3) denotes the rate of change of n_Q from the coupling to f. The energy-conserving delta function will be eliminated by taking into account the finite lifetime of the pair, as discussed below.

In equilibrium, the net rate of change of n_Q must be zero. Thus, the rate of increase in (2.3) is added to the rate of decrease by relaxation

$$(dn_Q/dt)_{relax} = -\Gamma_Q(n_Q - \bar{n}_Q) \ , \tag{2.4a}$$

and the result is set equal to zero to obtain

$$2n_f n_Q + n_f - n_Q^2 = 2n_c(n_Q - \bar{n}_Q) \ , \qquad n_c \equiv \Gamma_Q/2C \ . \tag{2.5}$$

The solution to (2.5) is

$$n_Q = (n_c - n_f)\left\{ \operatorname{sgn}(n_c - n_f) \left[1 + \frac{2n_c\bar{n}_Q + n_f}{(n_c - n_f)^2} \right]^{1/2} - 1 \right\} \ , \tag{2.6}$$

where $\operatorname{sgn} x \equiv +1$ for $x > 0$ and -1 for $x < 0$. Eq. (2.6) has the limiting values:

$$n_Q \cong \bar{n}_Q \ , \qquad \text{for } n_f \ll n_c \ ; \tag{2.7a}$$

$$n_Q = [n_c(2\bar{n}_Q + 1)]^{1/2} \ , \qquad \text{for } n_f = n_c \ ; \tag{2.7b}$$

and

$$n_Q \cong 2(n_f - n_c) \ , \qquad \text{for } n_f \gg n_c \ , \tag{2.7c}$$

as sketched in Fig. F2. We shall say that the pair has been driven unstable if $n_Q \geq [n_c(2\bar{n}_Q+1)]^{1/2}$, or $n_f \geq n_c$, and the threshold of the instability is defined by $n_f = n_c$. At the critical value n_c of n_f there is a sharp dramatic increase in the value of n_Q. The sharpness is illustrated by considering values of n_Q slightly below and slightly above the threshold. At $n_f = n_c - \epsilon n_c$, where $[(2\bar{n}_Q+1)/n_c]^{1/2} << \epsilon << 1$, (2.6) gives $n_Q \cong (\bar{n}_Q + \frac{1}{2})/\epsilon$, which is of order 10^3 for $\bar{n}_Q \lesssim 1$ and $\epsilon = 10^{-3}$. At $n_f = n_c + \epsilon n_c$, (2.6) gives $n_Q = 2\epsilon n_c$, which is order 10^{19} for $\epsilon = 10^{-3}$ and $n_c = 10^{22}$; i.e., n_Q increases by 16 orders of magnitude for a small change of n_f at $n_f \cong n_c$.

The behavior below the threshold was previously[3,4] approximated for the ferromagnetic-resonance case by linearizing the equation of motion. In the present case, linearizing (2.5) by neglecting the term $-n_Q^2$ gives

$$n_Q = \frac{(\bar{n}_Q + n_f/2n_c)}{1 - (n_f/n_c)} \qquad (2.8)$$

which displays the instability at $n_f = n_c$ vividly, since n_Q goes to infinity there. On a linear scale with $\bar{n}_Q$ visible, a graph of n_Q from (2.6) would have the appearance of (2.8) since n_Q would be off scale at a value of n_f less than n_c according to the discussion in the previous paragraph. It will be shown in Sec. IIIb that the large number of potentially unstable pairs in the present case of phonons restricts n_f to values below $n_f - \epsilon$, so that (2.8) is a good approximation in all cases of interest here.

Next, consider the value of n_c in (2.5). For a crystal with two types of ions with masses $m_>$ and $m_<$ ($m_> > m_<$), the vertex coefficients in (2.1) are[25]

$$V_{Q_1Q_2Q_3} \equiv V_{fQ_1-Q_1} = \frac{\alpha_2 B}{4\rho(1-2\rho)N^{1/2}} \left(\frac{\hbar^3}{2m_r m_<^2 \omega \omega_Q \omega_{-Q}} \right)^{1/2} \qquad (2.9)$$

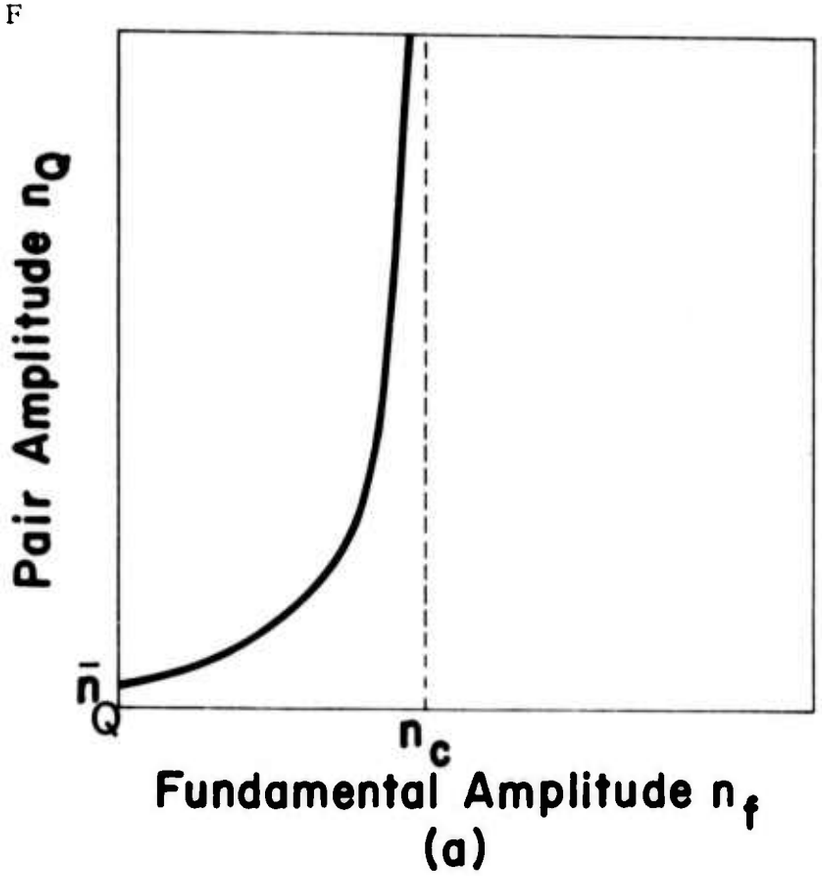

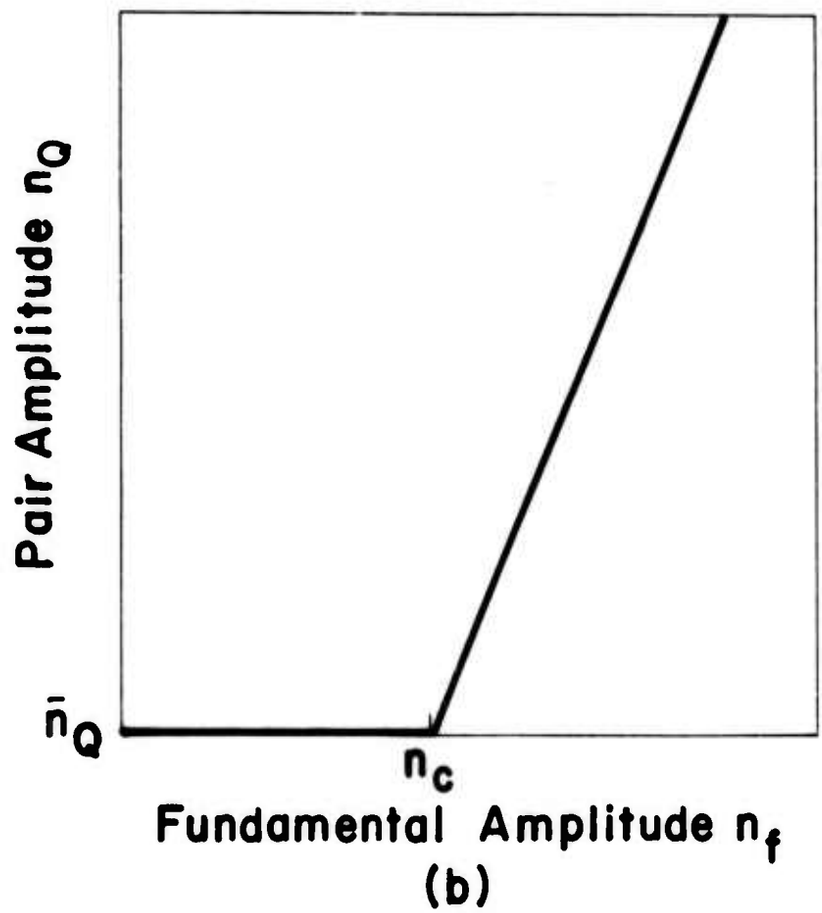

Fig. F2. Increase of the pair amplitude with increasing n_f. (a) The ordinate scale is such that $\bar{n}_Q$ is visible. (b) The ordinate scale is many orders of magnitude smaller than (a).

where B is the bulk modulus, N is the number of unit cells in the crystal, m_r is the reduced mass $m_< m_> / (m_> + m_<)$, ω is the frequency of the electromagnetic field, ρ is the damping-distance parameter in the repulsive potential $V(R) \sim \exp(-R/\rho a)$ between two ions spaced by R and having equilibrium spacing a, and α_2 is an angle factor[25] that is of order unity for allowed transition with large ω_k and is very small for small ω_k (acoustical modes with small $\underset{\sim}{k}$) and for transitions not allowed by selection rules[20-23] ($\alpha_2 = 0$) and quasiselection rules[24] ($\alpha_2 << 0$).

In (2.4), the delta function $\delta(\tilde{\omega})$ is appropriate when a sum (approximated by an integral) is involved. In the present case no sum is involved since the energy into a single pair is of interest. Thus, following Callen[2] and White and Sparks,[3] the delta function will be replaced by a normalized line-shape factor

$$\delta(\omega - 2\omega_Q) \rightarrow \frac{2}{\pi} \frac{\omega(2\omega_Q)(2\Gamma_Q)}{[\omega^2 - (2\omega_Q)^2]^2 + (2\omega_Q)^2 (2\Gamma_Q)^2} \quad . \tag{2.10}$$

On resonance, at $\omega = 2\omega_Q$, (2.10) gives

$$\delta(\omega - 2\omega_Q) = 1/\pi\Gamma_Q \quad . \tag{2.11}$$

Substituting (2.10), (2.9), and (2.4) into (2.5) gives

$$n_c = \frac{\rho^2 (1 - 2\rho)^2 m_r m_<^2 \omega_Q N}{18 \hbar |\alpha_2|^2 B^2} [(\omega^2 - 4\omega_Q^2)^2 + 16 \omega_Q^2 \Gamma_Q^2] \quad . \tag{2.12}$$

The corresponding value of the critical intensity I_c and numerical values of n_c are discussed in the following section.

c. Critical intensity. In order to relate the threshold condition $n_f = n_c$ to the experimentally controllable quantity, which is the intensity I of the incident radiation in this case, the relation between I and n_f is first derived. To do this the energy into the fundamental mode f will be equated to the energy out of f by relaxation. In Sec. III it is shown that near the threshold the increased energy flow from f to the pair has rather important consequences including an increase in the relaxation frequency of the fundamental mode. The usual linear, low-intensity value Γ_f of the relaxation frequency is used in the present section in order to obtain the critical value I_c of the intensity.

Consider radiation incident on an area A of sample. If the intensity just inside the front face is I_0, the intensity at a distance x into a sample with thickness $>> 1/\beta$ is $I = I_0 \exp(-\beta x) \cong I_0 - \beta x I_0$, where β is the absorption coefficient and the approximate equality holds for $\beta x << 1$. The rate of energy absorption in the layer x is $-A(I - I_0) = Ax\beta I$, where $I_0 \cong I$. Equating this rate of energy absorbed by f to the rate of loss by relaxation $\hbar\omega\Gamma_f(n_f - \bar{n}_f)Ax/V \cong \hbar\omega\Gamma_f n_f Ax/V$, where V is the volume of the sample, gives

$$I = \hbar\omega n_f \Gamma_f / V\beta \quad .$$

The well known result for β is[19]

$$\beta = \frac{4\pi Ne^2}{c\, m_r n_r V} \quad \frac{\omega\omega_f\Gamma_f}{(\omega^2 - \omega_f^2)^2 + (\omega_f\Gamma_f)^2} \tag{2.13}$$

where n_r is the index of refraction and N is the number of ion pairs. Substituting this expression for β into that for I gives

$$I_c = \frac{\hbar c m_r n_r}{4\pi N e^2 \omega_f} \left\{ [(\omega^2 - \omega_f^2)^2 + (\omega_f \Gamma_f)^2] n_c \right\}_{min} . \qquad (2.14)$$

The subscript min denotes that the value of the threshold intensity is to be calculated for all possible pairs, and the lowest of these values determines the observed critical field I_c. Recall that the intensities I and I_c are internal to the sample, and reflection at the surfaces must be taken into account to obtain the applied values.

There are two resonance factors in the expression (2.14) for I_c. The first is the laser-resonance factor in the bracket in (2.14), which comes from the resonant denominator in (2.13) for β. The second is the pair-resonance factor in n_c appearing in the bracket in (2.12). The laser-resonance factor is on resonance when the laser frequency ω is tuned to ω_f. The pair-resonance factor is on resonance for the pairs having phonon frequencies $\omega_Q = \frac{1}{2}\omega$. The minimum in (2.14) usually occurs at the pair resonance $\omega_Q = \frac{1}{2}\omega$; it is likely that the pair of modes with the lowest threshold will have $\omega_Q = \frac{1}{2}\omega$ (since the resonance factor has a minimum there) unless there are no phonons having this frequency, or the coupling of the fundamental phonon to this resonant pair is very small ($|\alpha_2|^2$ small), or there are other pairs having small Γ and large coupling.

The threshold usually is lowest at the laser resonance $\omega = \omega_f$. With both factors on resonance, (2.14) and (2.12) give

$$I_c = \frac{\rho^2 (1-2\rho)^2 c m_r^2 m_<^2 n_r \omega^4 \Gamma_f^2}{36\pi e^2 B^2} \left\{ \frac{\Gamma_Q^2}{|\alpha_2|^2} \right\}_{min} . \qquad (2.15)$$

A useful alternate expression is obtained by retaining β in the expressions above:

$$I_c = \frac{\rho^2 (1-2\rho)^2 m_r m_<^2 (N/V) \omega^4 \Gamma_f}{9 B^2 \beta} \left\{ \frac{\Gamma_Q^2}{|\alpha_2|^2} \right\}_{min} . \qquad (2.16)$$

The minimum in (2.16) occurs at small Γ_Q and large $|\alpha_2|$. Physically, the amplitude of a pair is large if less energy relaxes out of the pair and more energy is coupled into it.

In order to obtain numerical values of I_c and n_c, the values of the relaxation frequencies Γ_Q and Γ_f are needed. Since the values of Γ_Q for various phonon modes Q are not well known at present, only rough estimates of the values of I_c and n_c can be obtained: For NaCl at room temperature, $\Gamma_f \cong 2 \times 10^{12}\ \text{sec}^{-1}$.[13] First assuming that $\Gamma_Q = \Gamma_f$ and that the coupling is strong ($|\alpha_2| = 0.25$), and using $\omega = \omega_f = 2\omega_Q = 3 \times 10^{13}\ \text{sec}^{-1}$, $\rho = 1/9$, $m_r = 2.33 \times 10^{-23}$ g, $m_< = 3.84 \times 10^{-23}$ g, $B = 2.4 \times 10^{11}\ \text{dynes/cm}^2$, and $n_r = 7$ (on resonance) in (2.12) and (2.15) gives

$$n_c/N = 0.81 , \qquad I_c = 3.1 \times 10^{10}\ \text{W/cm}^2 . \qquad (2.17)$$

This is a large value of I_c, and in experiments to look for the instability, a small value of I_c is desirable. Thus, smaller values of Γ_f and Γ_Q are needed. For small-k acoustical modes on the lowest-frequency branch at low temperature, Γ_Q is believed to be small.[26,27] A conservative approximation to the lower limit of Γ_Q is $10^9\ \text{sec}^{-1}$, corresponding to a mean free path of order 1μm. At low temperature, Γ_f also will be smaller, say, an order of magnitude smaller than at room

temperature. Thus, according to (2.15), I_c may be eight orders of magnitude smaller than the value in (2.17), or

$$n_c/N = 8.1 \times 10^{-7} , \qquad I_c \cong 310\ W/cm^2 . \tag{2.18}$$

It should be emphasized that the value of I_c is sensitive to the value of Γ_Q, and it may not be possible to achieve such a low threshold.

On the other hand, it has already been pointed out[26,27] that it is conceivable that an anomalously low value of $\Gamma_Q = 10^5\ sec^{-1}$ could be achieved. In this case, the value of I_c would be only $2 \times 10^{-4}\ W/cm^2$. The results of Secs. IIb and V are important in considering such anomalously low values of I_c. In the former, it is shown that the anomalously low values of I_c are not restricted to crystals without a center of inversion,[9] and in the latter it is shown that in the usual case in which lasers with pulse lengths of order 10 nsec are used, the steady state is not attained and the threshold intensity is increased drastically above the previously expected value.

d. Effect of unequal frequencies ($\omega_Q \neq \omega_{-Q}$). In the calculations above it was assumed formally that the fundamental phonon decays into two phonons with equal frequencies. As discussed in Sec. IIb, the threshold may be determined by the decay into two modes having unequal frequencies, especially in NaCl-structure crystals.

The occupation numbers n_1 and n_2, as well as the relaxation frequencies Γ_1 and Γ_2 are now assumed to be unequal in general. The balance of power into the pair of modes from the fundamental against the power out of the pair must be considered separately for the individual modes. Following the reasoning of Sec. IIb, we find

$$C[n_f(n_1+1)(n_2+1) - (n_f+1)n_1 n_2] - \Gamma_1 (n_1 - \bar{n}_1) = 0 \quad ,$$

$$C[n_f(n_1+1)(n_2+1) - (n_f+1)n_1 n_2] - \Gamma_2 (n_2 - \bar{n}_2) = 0 \quad .$$

The coupled algebraic equation can easily be solved by substitution, which gives

$$n_1 = A \left\{ \operatorname{sgn} A [1 + (\Gamma_2 n_f \bar{n}_2 - \Gamma_1 n_f \bar{n}_1 + \Gamma_2 n_f + \Gamma_1 \Gamma_2 \bar{n}_1 C^{-1})/\Gamma_1 A^2]^{1/2} - 1 \right\} \tag{2.19}$$

and

$$n_2 = \bar{n}_2 + (\Gamma_1/\Gamma_2)(n_1 - \bar{n}_1) \tag{2.20}$$

where $A \equiv [-(\Gamma_1 + \Gamma_2) n_f + \Gamma_2 \bar{n}_2 - \Gamma_1 \bar{n}_1 + \Gamma_1 \Gamma_2 C^{-1}]/2\Gamma_1$.

If we now define n_c by

$$n_c = \Gamma_1 \Gamma_2 / (\Gamma_1 + \Gamma_2) C \tag{2.21}$$

it is easily verified that the various limiting behaviors for n_Q found in Sec. IIb are still valid for the present case. In particular, the threshold growth at $n_f = n_c$ remains the same. The threshold value n_c in (2.21) is the same for both modes since n_1 and n_2 are linearly related, as seen in (2.20). The values of n_1 and n_2 at the threshold are different in general, of course. Equation (2.21) reduces to (2.5) if $\Gamma_1 = \Gamma_2$. If one relaxation frequency, $\Gamma_>$, is much greater than the other, $\Gamma_<$, then (2.21) reduces to $n_c = \Gamma_</C$. Thus the equal frequency approximation employed previously introduces no serious error in either qualitative or quantitative description of the threshold behavior if Γ_Q is interpreted as Γ_1 for the case of $\Gamma_1 = \Gamma_2$ or as the lesser of $2\Gamma_1$ and $2\Gamma_2$ for the case of $\Gamma_1 \gg \Gamma_2$ or $\Gamma_2 \gg \Gamma_1$.

This result that the threshold can be low if either mode is long lived (Γ_Q small) is important. In the absence of the analysis above, it might have been guessed incorrectly that the phonon having the shorter lifetime would control the threshold or that one mode might go unstable before the other. The suggestion[26,27] that the phonons on the lowest acoustical branch may have anomalously long lifetimes at low temperature implies that the value of I_c may be anomalously low. Since a selection rule[20-23] prevents both phonons of the pair from being on this lowest branch in crystals with a center of inversion (such as NaCl-structure crystals), it was previously believed that such crystals would not have the anomalously low values of I_c.[9] The present result, that the relaxation frequency Γ_Q that determines the value of I_c is equal to $2\Gamma_<$ when one value $\Gamma_<$ is much less than the other, shows that the lack of a center of inversion is not required.

e. Higher-order two-output-phonon processes. As mentioned in the previous section, the two-phonon processes arising from the cubic anharmonic terms in NaCl-structure materials are subject to rather stringent selection rules[20-23] and quasiselection rules.[24] This is expressed mathematically by the smallness of the angular factor α_2 in the transition matrix element of (2.9). By virtue of (2.15), the critical intensity is increased when α_2 is small, a reasonable result on physical grounds. Since for higher-order processes such as the creation of two phonons from the annihilation of two fundamental phonons (Fig. F3a) or that of one fundamental phonon and one other thermal phonon (Fig. F3b) the selection rules are more relaxed, it is of interest to examine whether these processes lead to parametric excitation and if so, whether the threshold condition is lowered from the previous first-order case.

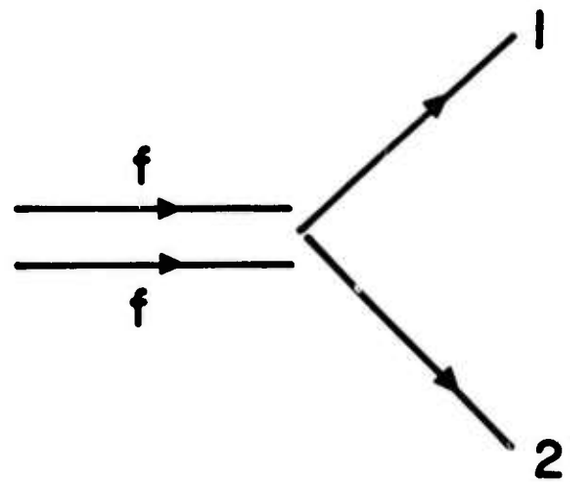

(a)

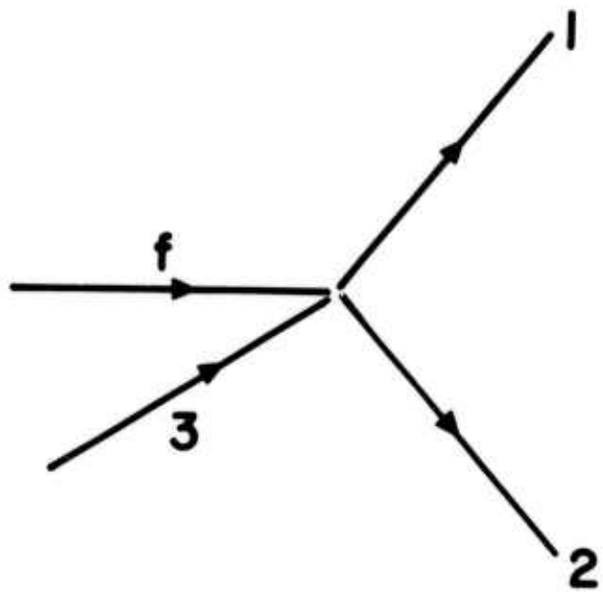

(b)

Fig. F3. High-order two-phonon output processes:
(a) annihilation of two fundamental phonons, and
(b) annihilation of one fundamental phonon and one thermal phonon.

Both processes (a) and (b) arise from the fourth-order term of the anharmonic potential $V_{Q_1Q_2Q_3Q_4}$, which contains a selection-rule-related factor α_3.[25] Process (a) is analogous to the second-order Suhl instability that is responsible for the premature saturation of the main resonance in the ferromagnetic case. The instability condition can be found in exactly the same way as in Sec. II b, and, within the equal frequency approximation, it is

$$I_c = \left\{ \frac{\hbar c m_r n_r [(\omega^2 - \omega_f^2)^2 + (\omega_f \Gamma_f)^2]}{4\pi N e^2 \omega_f} n_c \right\}_{\min} \tag{2.22}$$

with

$$n_c = \hbar \Gamma_{Q'} / |V_{ffQ'-Q'}| \tag{2.23}$$

where the prime distinguishes the relaxation frequency of output phonons in Fig. F3 from that of Fig. F1. One readily obtains the ratio of the critical intensities for second- and first-order instabilities as

$$\frac{I_c(\text{2nd order})}{I_c(\text{1st order})} = \left(\frac{2\Gamma_{Q'}}{\hbar \Gamma_Q^2}\right) \left(\frac{|V_{fQ-Q}|^2}{|V_{ffQ'-Q'}|}\right) . \tag{2.24}$$

The value of the ratio in (2.24) can be estimated with the use of (2.9), and the expression for the fourth order potential term:[25]

$$|V_{ffQ'-Q'}| = \frac{\alpha_3 B}{32 \rho^2 (1 - 2\rho) N} \left(\frac{\hbar^4}{m_r m_<^3 a^2 \omega^2 \omega_{Q'} \omega_{-Q'}} \right)^{1/2} \tag{2.25}$$

where a is the equilibrium nearest-neighbor separation and α_3 is the previously mentioned angular factor related to selection rules. The result of (2.24) can be

resolved into a product of two factors. The first is the ratio $|\alpha_2|^2/|\alpha_3|$, which has to do with the selection rules. The second, $8Ba\,\Gamma_{Q'}/(1-2\rho)\,m_<^{1/2}m_r^{1/2}\omega_f\Gamma_Q^2$, is a dynamical factor and is estimated to be about 1.2×10^3 in NaCl. In obtaining the latter, we have used $\Gamma_Q \cong 1.85\times10^{11}\,\text{sec}^{-1}$ and $\Gamma_{Q'} \cong 5.56\times10^{12}\,\text{sec}^{-1}$. In order for (2.24) to be less than unity, the selection rule factor $|\alpha_2|^2/|\alpha_3|$ must be less than 10^{-3}. It is expected that $|\alpha_3|$ will be of order unity since there is no selection rule and no reason to expect that there are quasiselection rules for this four-phonon vertex. Thus, if the quasiselection rules on α_2 should make $|\alpha_2|^2 < 10^{-3}$ for all potentially unstable pairs, there still would be an instability as a result of the higher-order process.

By proceeding in the same way, one can study the process illustrated in Fig. F3b. It can be easily demonstrated that such a process is characterized by essentially linear increase of final phonon occupation as n_f increases and hence no threshold occurs. In passing, also note that the two-phonon difference process (two phonons annihilated and one created) does not have a parametric instability.

f. Anharmonic interaction vs high-order dipole moment. The process discussed in Secs. IIa-IIe is the absorption of radiation by the fundamental mode (driven off resonance in general), which splits into two phonons as a result of the anharmonic interaction. The same end result, that is the absorption of radiation and the creation of two phonons, can result from the Lax-Burstein interaction involving higher-order dipole moments.[22] In this latter process, the photon splits into two phonons directly, with no intermediate state. The Lax-Burstein mechanism usually is considered to be weaker than the anharmonic-potential mechanism (although there is still debate on this point). Since this implies less energy into

the potentially unstable pair of phonons, it is expected that the threshold is great for the group-four semiconductors, diamond, silicon, and germanium, in which the anharmonic-potential mechanism is inoperative. The following simple estimate indicates that this is indeed the case.

The preceding analysis for instability threshold may be used provided one makes the formal replacements of n_f by the number of photons n_p and $|3!\, V_{f12}|^2$ by the square of the new vertex, $|V_p|^2$. The resulting threshold value of the photon occupation number is

$$n_{pc} = \frac{\hbar^2 \Gamma_Q^2}{2|V_p|^2} \quad . \tag{2.26}$$

The value of $|V_p|^2$ can be estimated from the known values of β as follows. First β is related to the photon relaxation frequency Γ_p, then Γ_p is related to $|V_p|^2$. The time rate of decrease of intensity on passing through a slab of material with absorption coefficient β is

$$\frac{dI}{dt} \simeq -c\beta I/\mathrm{Re}\, n(\omega) = -c^2 \beta \hbar \omega n_p / V [\mathrm{Re}\, n(\omega)]^2 \tag{2.27}$$

where $\mathrm{Re}\, n(\omega)$ is the real part of the refractive index. Differentiating $I = \hbar \omega n_p c / \mathrm{Re}\, n(\omega) V$ directly and assuming linear relaxation gives

$$\frac{dI}{dt} = -c\hbar\omega\Gamma_p n_p / V \mathrm{Re}\, n(\omega) \quad . \tag{2.28}$$

Equating (2.27) and (2.28) gives the simple relation

$$\beta = \mathrm{Re}\, n(\omega)\Gamma_p / c \quad . \tag{2.29}$$

The relaxation frequency Γ_p can be calculated assuming interaction V_p, and is given by

$$\Gamma_p = \frac{\pi}{\hbar^2} \sum_Q |V_p|^2 \delta(\omega - 2\omega_Q)(2\bar{n}_Q + 1)$$

which upon converting into an integral in $\underset{\sim}{k}$-space, neglecting angular dependence of the integral, and assuming a Debye frequency spectrum with maximum frequency ω_{mx} is approximately

$$\Gamma_p \cong 72\pi N |V_p|^2 (2n_{\omega_k} + 1)\omega_k^2/\hbar^2\omega_{mx}^3 \quad . \tag{2.30}$$

Eqs. (2.26), (2.29), and (2.30) lead to

$$\frac{n_{pc}}{N} = \frac{36\pi\omega_k^2\Gamma_Q^2 \operatorname{Re} n(\omega)}{c\beta\omega_{mx}^3}(2\bar{n}_Q + 1) \quad . \tag{2.31}$$

For $\omega_k/\omega_{mx} \cong 1/2$, $\Gamma_Q/\omega_{mx} = 1/50$, $\omega_{mx} \cong 10^{14}\,\mathrm{sec}^{-1}$, $\beta = 10\,\mathrm{cm}^{-1}$, $2\bar{n}_Q + 1 \cong 1$, and $\operatorname{Re} n(\omega_f) = 7$, (2.26) gives $n_c/N \cong 50$ or $I_c = \hbar\omega n_c c/V \operatorname{Re} n(\omega) \cong 10^{19}\,\mathrm{W/cm}^2$, which illustrates the great magnitude of the threshold intensity for the Lax-Burstein mechanism.

III. POWER ABSORPTION AND ENHANCED RELAXATION OF THE FUNDAMENTAL MODE

In the limit of $n_f << n_c$, the steady-state power out of the fundamental mode is simply $\hbar\omega\Gamma_f n_f$ for $n_f >> \bar{n}_f$, where Γ_f is the usual linear (low intensity) relaxation frequency. As the intensity is increased and n_f approaches n_c, this steady-state power increases, becoming many orders of magnitude greater than the linear value $\hbar\omega\Gamma_f n_f$ in the formal limit of $n_f \geq n_c$. This increased absorption is a result of the pair-mode occupation numbers n_Q increasing above their thermal equilibrium values caused by the great power flow into the pairs from the fundamental mode. A convenient measure of the increased power flow is the generalized relaxation frequency $\tilde{\Gamma}_f$ defined by the relation

$$dn_f/dt \cong -\tilde{\Gamma}_f n_f \quad , \tag{3.1}$$

again for $n_f >> \bar{n}_f$. An expression for $\tilde{\Gamma}_f$ will be derived in Sec. III b, and $\tilde{\Gamma}_f$ will be used in the discussion of several effects in Secs. III c, III d, and IVa.

a. Energy flow into a single pair. It will now be shown that the value of the contribution $\tilde{\Gamma}_{f1}$ to $\tilde{\Gamma}_f$ from a single pair, is negligibly small for $n_f \leq n_c$, while $\tilde{\Gamma}_{f1}/\Gamma_f = 1$ for $n_f = 2n_c$. Consider the power into a single pair of modes from the fundamental mode. In equilibrium, this power is equal to the power out of the pair by relaxation:

$$\left(\frac{d\hbar\omega n_Q}{dt}\right)_{\text{pump}} = \hbar\omega\Gamma_Q (n_Q - \bar{n}_Q) \quad . \tag{3.2}$$

The power out of the fundamental mode by linear relaxation is, with $n_f >> \bar{n}_f$,

$$\left(\frac{d\hbar\omega n_f}{dt}\right)_{relax} = \hbar\omega\Gamma_f n_f \quad . \tag{3.3}$$

For $n_f \leq n_c$, $n_Q \leq [n_c(2\bar{n}_Q + 1)]^{1/2}$, and the power (3.2) out of the fundamental mode f to the single pair is much less than the power (3.3) out of f by linear relaxation, since $\Gamma_f \gtrsim \Gamma_Q$ usually is satisfied.

Before considering the effect of the large number of modes into which f is coupled, notice that as n_f is increased above n_c, the value of n_Q in (3.2) increases rapidly: For $n_f > n_c + \epsilon$, (3.3) and (2.7d) give $d\hbar\omega n_Q/dt = \hbar\omega\Gamma_Q(n_f - n_c)$. When $n_f = 2n_c$, the value of n_Q is $2n_c$, and for $\Gamma_f \cong \Gamma_Q$, (3.2) and (3.3) show that the power into the single pair is equal to the total linear-relaxation power out of n_f. This is equivalent to the previous statement $\tilde{\Gamma}_{f1}/\Gamma_f \cong 1$ for $n_f = 2n_c$. Thus, the parametric excitation of many pairs is potentially an extremely strong sink for removing energy from the fundamental mode. This fact is important in the limiting of the value of n_f at a finite value, as discussed in Sec. IVa.

b. Sum over all pairs; dependence of $\tilde{\Gamma}_f$ on n_f. Since there are an enormous number of modes into which the fundamental mode could put energy, it is possible that summing (2.2) over all pairs could give a number greater than the total linear-relaxation values of $\Gamma_f n_f$ even when the single-pair value in (2.2) is negligible. The following calculation, even though highly simplified, clearly illustrates that this is indeed the case. Summing (2.2) over pairs and using (2.1) gives

$$\frac{dn_f}{dt} = -\sum_Q \frac{\pi}{\hbar^2} |3!\, V_{fQ-Q}|^2 \,\delta(\tilde{\omega}) \left[(2n_Q + 1)\, n_f - n_Q^2\right] \quad . \tag{3.4}$$

Setting $n_Q = \bar{n}_Q$ and using $(2\bar{n}_Q + 1)\,\bar{n}_f - \bar{n}_Q^2 = 0$ reduces (3.4) to

$$\frac{dn_f}{dt} = -\Gamma_f (n_f - \bar{n}_f)$$

where

$$\Gamma_f = \sum_Q \frac{\pi}{\hbar^2} \left| 3!\, V_{fQ-Q} \right|^2 \delta(\tilde{\omega})\,(2\bar{n}_Q + 1) \quad . \tag{3.5}$$

At higher power levels the value of n_Q is greater than $\bar{n}_Q$. Then, neglecting n_Q^2 reduces (3.4) to (3.1) with $\tilde{\Gamma}_f$ given by (3.5) with $\bar{n}_Q$ replaced by n_Q. From (2.8)

$$2n_Q + 1 = \frac{2\bar{n}_Q + 1}{1 - n_f/n_c} \quad . \tag{3.5a}$$

From this result with n_c given by (2.5) and (2.4),

$$(2n_Q + 1)\,\delta(\tilde{\omega}) = (2\bar{n}_Q + 1)\,\frac{n_{cm}}{\pi\Gamma_Q}\,\frac{1}{n_c - n_f} \tag{3.6}$$

where n_{cm} is the value of n_c at $\omega = 2\omega_Q$. From (2.4), (2.5), and (2.11),

$$n_{cm} = \hbar^2 \Gamma_Q^2 / 2 \left| 3!\, V_{fQ-Q} \right|^2 \quad . \tag{3.7}$$

It is assumed henceforth that n_{cm} is the minimum of n_c; i.e., that the minimum occurs at $\omega = 2\omega_Q$. From (2.4), (2.5), and (2.10),

$$\frac{1}{n_c - n_f} = \frac{\pi\Gamma_Q}{n_{cm}(1 - n_f/n_{cm})^{1/2}}\,\frac{\omega_Q^2\,\tilde{\Gamma}_Q}{\pi\left[(\omega_Q^2 - \frac{1}{4}\omega^2)^2 + \omega_Q^2\tilde{\Gamma}_Q^2\right]}$$

$$\cong \frac{\pi\Gamma_Q}{2n_{cm}(1 - n_f/n_{cm})^{1/2}}\,\delta(\omega_Q - \tfrac{1}{2}\omega) \tag{3.8}$$

where the delta-function representation was used in the approximate equality and $\tilde{\Gamma}_Q^2 \equiv \Gamma_Q^2 (1 - n_f/n_{cm})$. In the second term in $\tilde{\Gamma}_Q^2$, it was assumed that $\omega \cong 2\omega_Q$. Substituting (3.6) and (3.5a) into (3.4), neglecting n_Q^2, and evaluating the trivial integral gives (3.1) with

$$\frac{\tilde{\Gamma}_f}{\Gamma_f} = \frac{1}{(1 - n_f/n_{cm})^{1/2}} \qquad (3.9)$$

for this case of $n_f < n_{cm} - \epsilon$. The result (3.9), which can also be derived starting with

$$dn_f/dt = -2 \sum_Q \Gamma_Q (n_Q - \bar{n}_Q) \quad , \qquad (3.10)$$

indicates that $\tilde{\Gamma}_f \cong \Gamma_f$ for $n_f << n_{cm}$ and $\tilde{\Gamma}_f$ increases to a value much greater than Γ_f as n_f approaches n_{cm}. A plot of (3.9) is given in Fig. F4.

c. Relation between n_f and I. On the basis of the fact that the relaxation frequency of the fundamental mode is enormously increased at the threshold, one may be tempted to conclude that the power absorption would be increased likewise. This conclusion is erroneous near the laser resonance since enhanced relaxation of the fundamental mode considered in the previous two sections vastly alters the linear dependence of n_f on the incident intensity I, as will now be shown. Physically, the resonance absorption of a harmonic oscillator is inversely proportional to the relaxation frequency. In Sec. III d, the new relation between n_f and I will be used to obtain the behavior of power absorption as a function of I.

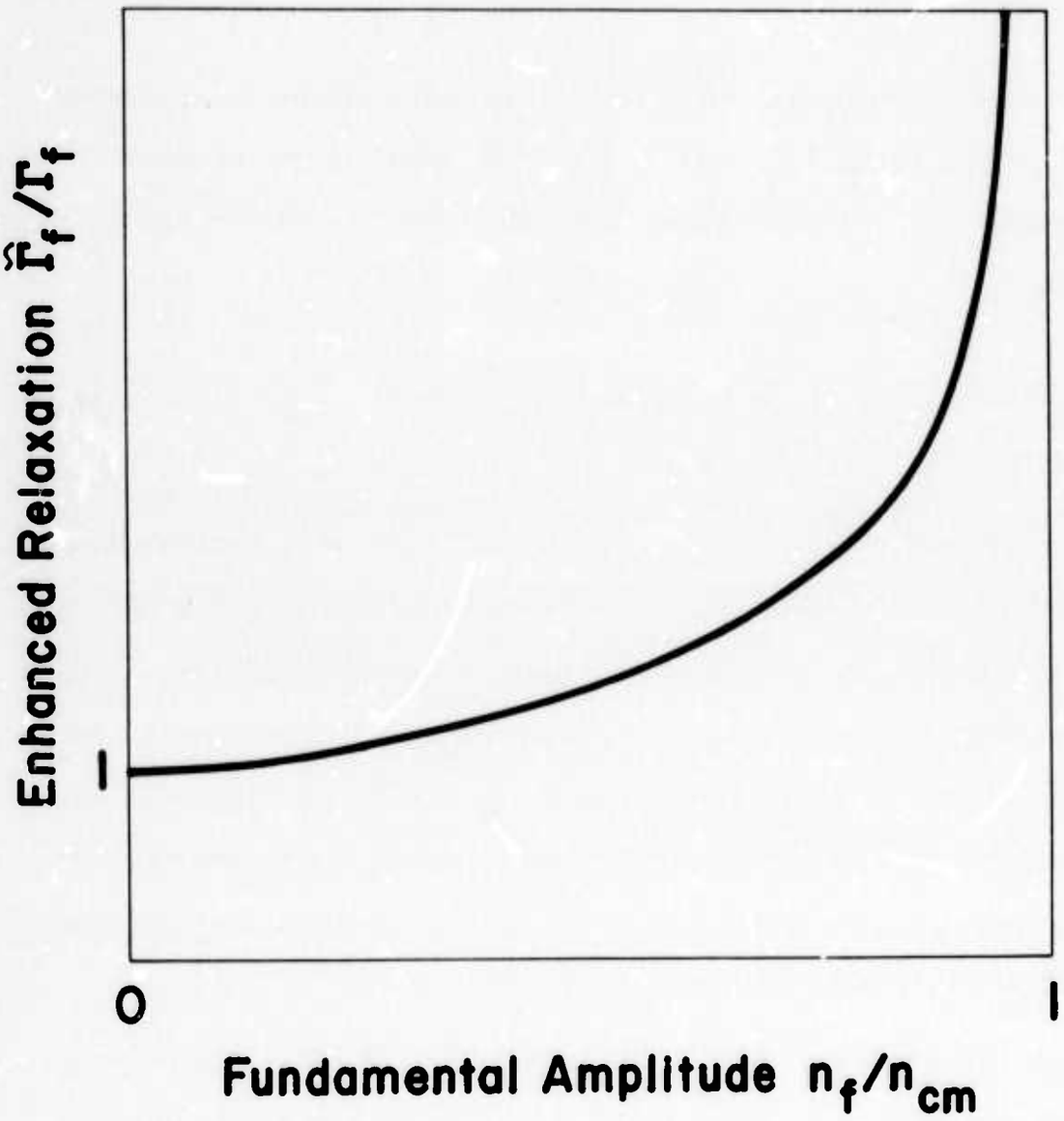

Fig. F4. Enhanced relaxation frequency of the fundamental mode ($n_f < n_{cm}$).

In the steady state, the power absorbed is equal to the power $d\hbar\omega n_f/dt$ out of the fundamental mode. Thus, with (3.1),

$$P_{abs} \cong \hbar\omega\tilde{\Gamma}_f n_f \quad . \tag{3.11}$$

Eq. (3.11) may be equated to $IV\beta$ (Sec. 2c) to yield a relation for n_f in terms of $\tilde{\Gamma}_f$ and I. Using (3.9), (3.11), (2.12), (2.13), and (2.14) for the case of laser resonance ($\omega = \omega_f$) and assuming that the minimum in (2.14) occurs at $n_c = n_{cm}$ gives

$$\frac{n_f}{n_{cm}} = \left(\frac{I}{I_c}\right)\left(\frac{\Gamma_f^2}{\tilde{\Gamma}_f^2}\right) = \frac{I}{I + I_c} \quad . \tag{3.12}$$

For low power levels ($I \ll I_c$), $n_f \cong n_{cm}(I/I_c)$, so that n_f increases linearly with the incident intensity. The linear relation is lost with higher intensity, as is evident from Fig. F5. The region of changeover from $n_f \propto I$ to $n_f \simeq$ constant is not sharp. For n_f to attain a value within a tenth of n_{cm} requires $I = 9I_c$. The value of n_f is limited to values below n_{cm} even for very large values of I. Thus, the simple linearized result (2.8) for n_Q can be used in studying steady-state results. This will not be the case in the time-dependence analysis of Sec. V or in general in other applications.

d. Absorbed power and $\tilde{\Gamma}_f/\Gamma_f$ as functions of I. It will be shown that the power absorption spectrum $P_{abs}(\omega)/I$ is constant for $I \ll I_c$ and decreases in peak amplitude and broadens for I approaching and greater than I_c. First note that (3.9) and (3.12) give

$$\tilde{\Gamma}_f/\Gamma_f = (I/I_c + 1)^{1/2} \tag{3.13}$$

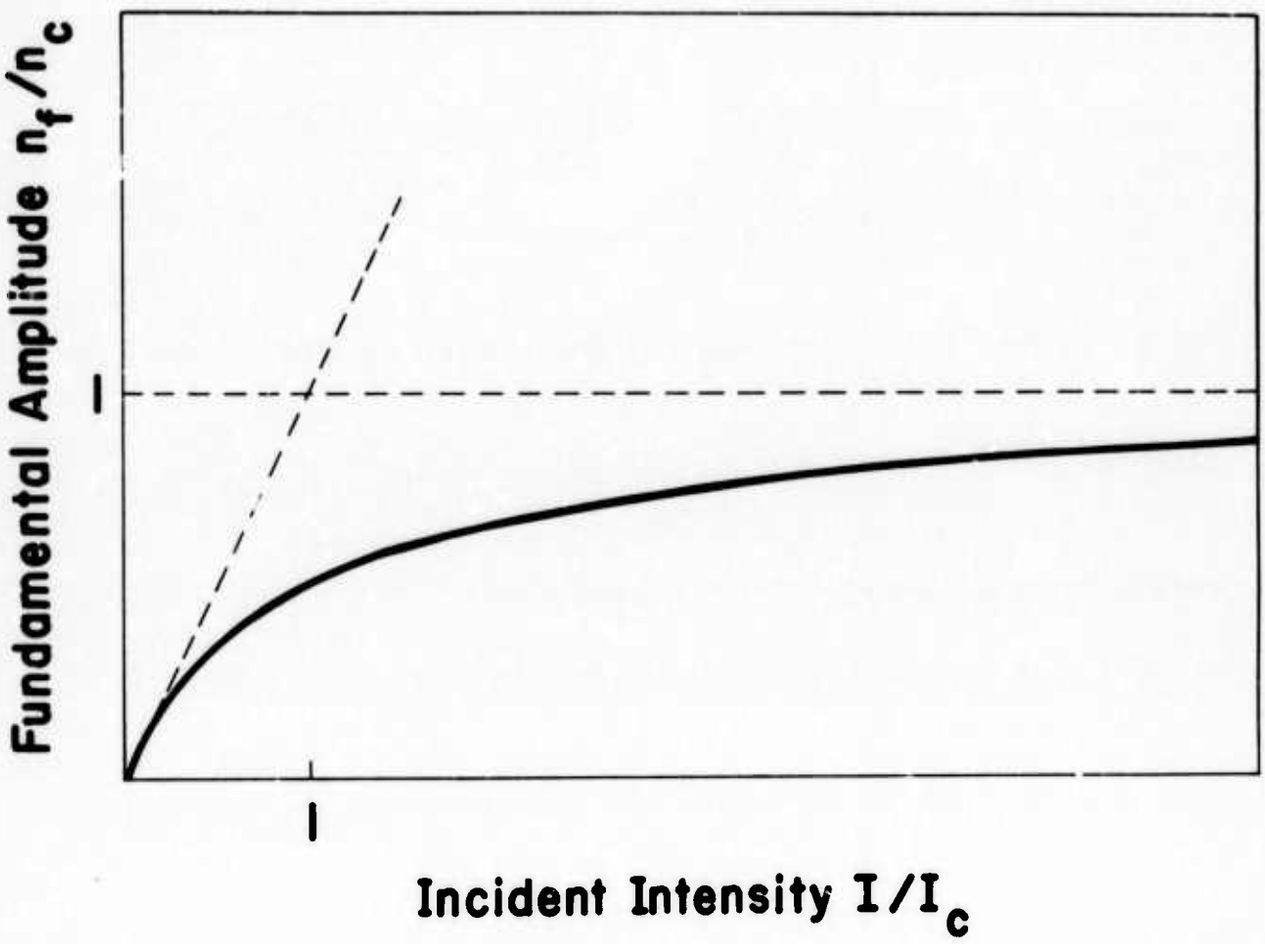

Fig. F5. Dependence of fundamental mode amplitude on incident intensity from (3.12).

which is unity for $I << I_c$ and is equal to $(I/I_c)^{1/2}$ for $I >> I_c$. The transition between the two limiting behaviors is quite gentle, in contrast to the sharp increase in $\tilde{\Gamma}_f/\Gamma_f$ as a function of n_f/n_{cm} at $n_f/n_{cm} = 1$. (See Fig. F4.)

The power absorption at the laser resonance ($\omega = \omega_f$) is obtained by substituting (3.13) and (3.12) into (3,11), which gives

$$P_{abs} = \hbar\omega\Gamma_f n_{cm} \frac{I/I_c}{(1+I/I_c)^{1/2}} \qquad (3.14)$$

From this result (3.14) it is seen that P_{abs} is linear in I for $I << I_c$ and increases only as $I^{1/2}$ for $I >> I_c$. Again, the transition between the two limiting behaviors is smooth. The power-absorption spectrum $P_{abs}(\omega)/I$ decreases at resonance as I approaches and becomes greater than I_c. This result (3.14) is discussed in Sec. VII on experiments.

Since Γ_f, P_{abs}, and T are smoothly varying functions of I, in contrast to the sharp-threshold behavior as functions of n_f, the value of I_c will be referred to as the critical intensity, rather than the threshold intensity.

IV. EFFECTS ABOVE AND NEAR THE THRESHOLD

a. Sticking of n_f. The result, from Sec. III c, that $n_f < n_{cm}$ even for $I >> I_c$, which will be called the sticking of n_f, is analogous to angle sticking in ferromagnetic resonance.[1] The previous explanation of angle sticking was that the energy flow out of the uniform-precession mode u would be so great when $n_u > n_{uc}$, where n_{uc} is the threshold value of the occupation number n_u of the u mode, that n_u would be reduced to the value n_{uc}. This previous explanation is not strictly correct since the analysis of Sec. III c evinces that the strong flow of energy out of u exists for $n_u < n_{uc}$. Thus, n_u sticks at a value somewhat below n_{uc}, just as n_f sticks at a value below n_c as in Fig. F5. In the following section, the previous explanation of the sticking phenomena is considered briefly.

b. Large value of $\tilde{\Gamma}_f/\Gamma_f$ above the threshold. The fact that the power $\hbar\omega\tilde{\Gamma}_f n_f$ out of the fundamental mode would be extremely large if n_f were greater than n_{cm} is the key to the previous explanation of angle sticking, as discussed in Sec. IV a. This result is easily explained intuitively as follows: In Sec. III a it was shown that for $n_f = 2n_{cm}$ and $\Gamma_Q = \Gamma_f$ the energy from n_f to a single pair is equal to the total energy out to all pairs by linear relaxation. Thus, $\tilde{\Gamma}_f/\Gamma_f$ is of the order of the total number N_{pairs} of pairs that are above threshold (i.e., have $n_f > n_c$). Since there are of order 10^{23} potentially unstable pairs, the value of $\tilde{\Gamma}_f/\Gamma_f$ is extremely large.

An order-of-magnitude estimate of the size of $\tilde{\Gamma}_f/\Gamma_f$ for the formal case of $n_f > n_{cm}$ is obtained by extending the analysis of Sec. III b to this case.

For $n_f > n_{cm} + \epsilon$, (2.7) is approximately

$$n_Q - \bar{n}_Q \cong 0 \ , \qquad \text{for } n_f < n_c$$

$$\cong 2(n_f - n_c) \ , \qquad \text{for } n_f > n_c$$

which, with (3.10) gives

$$\frac{dn_f}{dt} = -4 \int_{\omega_-}^{\omega_+} d\omega_Q \, g(\omega_Q) \, \Gamma_Q \, (n_f - n_c) \tag{4.1}$$

where ω_+ and ω_- are the positive roots of $n_f = n_c$. With $n_f - n_c$ given by the top equality in (3.8), (4.1) becomes

$$\frac{dn_f}{dt} = 4 n_{cm} \int_{\omega_-}^{\omega_+} d\omega_Q \, \frac{g(\omega_Q)}{\omega_Q^2 \, \Gamma_Q} \left[\omega_Q^2 \, | \tilde{\Gamma}_Q^2 | - (\omega_Q^2 - \tfrac{1}{4} \omega^2)^2 \right] .$$

When the length $\omega_+ - \omega_- = \Gamma_Q (n_f / n_{cm} - 1)^{1/2}$ of the integration region is short, $g(\omega_Q)/\Gamma_Q$ can be evaluated at $\omega_Q = \frac{1}{2}\omega$. Evaluating the remaining integral gives (3.1) with

$$\frac{\tilde{\Gamma}_f}{\Gamma_f} = \frac{8 n_{cm}^2}{3\pi (\bar{n}_Q + \frac{1}{2}) n_f} \left(\frac{n_f}{n_{cm}} - 1 \right)^{3/2} \tag{4.2}$$

for this case of $n_f > n_{cm} + \epsilon$. Thus, $\tilde{\Gamma}_f / \Gamma_f$ is of order $n_{cm} / (\bar{n}_Q + \frac{1}{2}) >> 1$ for $n_f \cong 2 n_{cm}$.

c. Chain instabilities. In some systems, it is conceivable that the occupation number n_Q of the unstable pair could become so great that the phonons coupled

to the pair could also be driven to their threshold. This chain of unstable pairs could be extended to more and more pairs, as illustrated schematically in Fig. F6.

The method developed for deriving the threshold condition enables us to argue that chain process does not occur in the anharmonic-potential-induced phonon instabilities. For $n_f < n_c$, which is satisfied according to the discussion of amplitude sticking in Sec. IVa, (2.7) gives

$$n_Q < \left[n_c (2 \bar{n}_Q + 1) \right]^{1/2} \quad . \tag{4.3}$$

For these phonons to induce instabilities of other modes, their number n_Q must reach a value of the order of n_c, a requirement that cannot be fulfilled according to (4.3). In other systems, a very small density of states at the frequency of the threshold pair would be required in order to have chain process.

d. Enhanced relaxation of pair modes. In the estimates of critical intensity, we have used the relaxation frequency Γ_Q derived essentially from linear theory. As the instability is approached, the large number of phonons generated interact with one another, leading to further relaxation not accounted for in the linear theory. If this enhanced relaxation were significant, the value of the critical intensity would have to be altered as discussed in Sec. IIc. It will now be shown that this is not the case; i.e., the enhanced relaxation is negligible.

Consider the most extreme case, in which n_Q approaches the right-hand side of (4.3). The dominant mechanism for relaxation is the process in which two of these phonons coalesce to form another phonon under conservation of

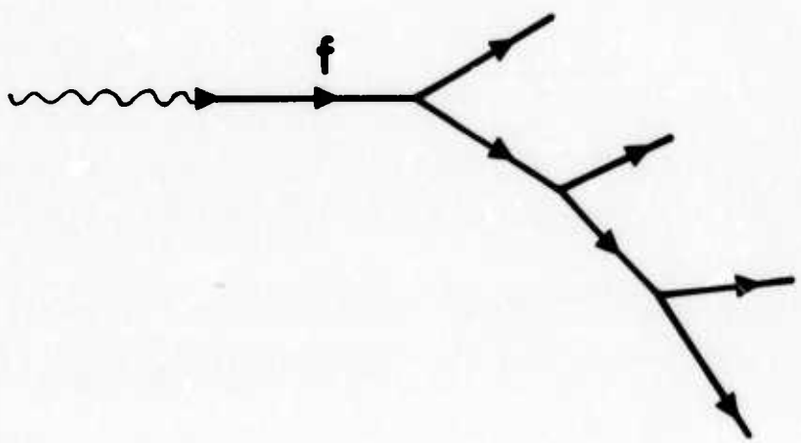

Fig. F6. A chain of parametric processes.

energy and crystal momenta, as illustrated in Fig. F7. Using the standard quantum-mechanical method,[4] the transition probability of this process was calculated and expressed in the form $dn_Q/dt = -\tilde{\Gamma}_Q n_Q$, from which $\tilde{\Gamma}_Q$ is identified as the enhanced relaxation frequency. Here $\tilde{\Gamma}_Q$ is a function of n_Q. Using the steady-state value of (2.7b), $\tilde{\Gamma}_Q$ is found to be 6×10^6 sec^{-1}, much smaller than the value used for evaluating the critical intensity, so that the enhanced relaxation considered here has little effect in altering the critical intensity.

e. Parametric processes without intermediate states. The sticking of n_f, the non-threshold behavior of I, and the absence of chain instabilities and enhanced relaxation all are related to the fact that the physical process (Fig. F1) contains an intermediate state, which is the fundamental phonon state in the present case. Other processes, such as the instability of the phonon created in the stimulated Raman process,[7,28] that have intermediate states are expected to exhibit similar behavior.

By contrast, processes that do not have intermediate states have quite different behavior. For example, in the three-stream plasma instability, no intermediate mode is present and the radiation energy may drive the plasma waves strongly enough to give rise to a chain instability.[29] Similarly, in parallel pumping experiments of ferromagnetic resonance,[4] the rf-field photons convert directly to a pair of magnons without the intervention of uniform precession magnons. In that case the enhanced relaxation of the unstable magnons is indeed significant, and provides a mechanism for additional energy absorption.[30,31]

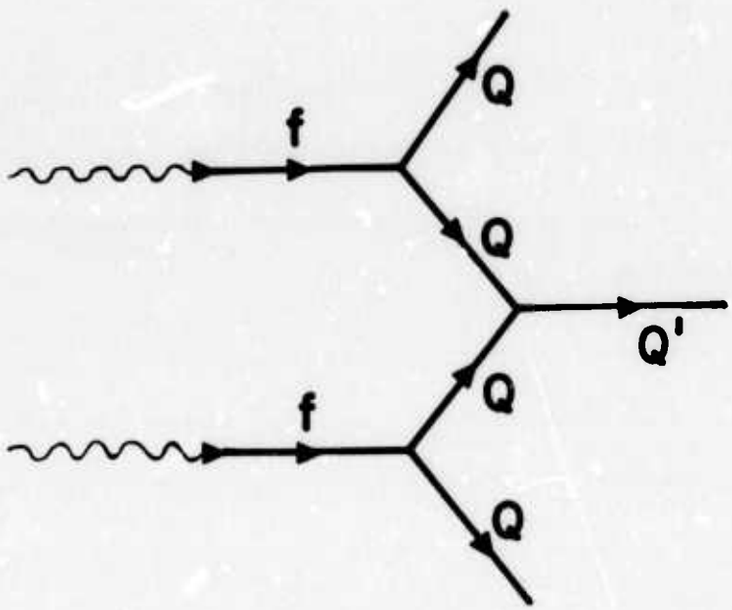

Fig. F7. Enhanced relaxation for phonons Q to phonons Q' when $n_Q >> \bar{n}_Q$.

V. TIME FOR INSTABILITY TO OCCUR

The time τ required for the steady state to be established must be less than the laser pulse length if the steady-state theory is to be applied to experiments using pulsed lasers. It will now be shown that τ is of order Γ_Q, which is sufficiently short under most conditions, but not for ultralong-lifetime phonons ($\Gamma_Q < 10^7$-$10^8\,\mathrm{sec}^{-1}$). For this latter case, pulses longer than the typical value of 10 ns would be required in order to observe the instability.

The total rate of change of $\eta \equiv n_Q + \frac{1}{2}$ is, from (2.3), (2.4), and (2.4a), with $-n_Q^2$ negligible,

$$\frac{d\eta}{dt} = \Gamma_Q \left[\bar{\eta} + \eta \left(\frac{n_f}{n_c} - 1 \right) \right] . \tag{5.1}$$

The time variation of n_f is, for $n_f >> \bar{n}_f$

$$\frac{dn_f}{dt} = R - \tilde{\Gamma}_f n_f \tag{5.2}$$

where $R = V\tilde{\beta} I/\hbar\omega$ is the rate of creation of fundamental phonons by the incident intensity, with $\tilde{\beta}$ given by (2.13) with Γ_f replaced by $\tilde{\Gamma}_f$.

Since $\tilde{\Gamma}_f$ is given as a sum involving the n_Q's, the solution of (5.1) and (5.2) is not trivial. An important practical case is that in which $\Gamma_Q << \Gamma_f$. An approximate solution for this case can be obtained as follows. For $n_Q = \bar{n}_Q$, $\tilde{\Gamma}_f$ is equal to the usual low-intensity, linear value Γ_f. For all η equal to the steady-state values $\bar{\eta}/(1 - n_{fss}/n_c)$ from (3.5a), where n_{fss} is the steady-state value of n_f, $\tilde{\Gamma}_f$ is equal to the steady-state value $\tilde{\Gamma}_{fss} = \Gamma_f/(1 - n_{fss}/n_{cm})^{1/2}$ from (3.9).

If the time constant for the approach of η to its steady-state value is denoted by τ, then $\tilde{\Gamma}_f \cong \Gamma_f$ for $t \ll \tau$, and $\tilde{\Gamma}_f \cong \tilde{\Gamma}_{fss}$ for $t \gg \tau$. For the case under consideration, it will be shown that $\tilde{\Gamma}_f$ in (5.2) is slowly varying; that is, $\tau \gg 1/\Gamma_f$. Thus, with $\tilde{\Gamma}_f$ formally considered to be a constant in (5.2), the solution is

$$n_f \cong \frac{R}{\tilde{\Gamma}_f} \left(1 - e^{-\tilde{\Gamma}_f t}\right) \tag{5.3}$$

which reduces to

$$n_f = R/\tilde{\Gamma}_f = VI\tilde{\beta}/\tilde{\Gamma}_f \hbar\omega \tag{5.4}$$

for $t \gtrsim \left(\tilde{\Gamma}_f\right)^{-1}_{t=0} = \Gamma_f^{-1}$. For still greater times, n_f decreases slowly as $\tilde{\Gamma}_f$ increases, as illustrated schematically in Fig. F8. At the laser resonance ($\omega = \omega_f$), (5.4) gives

$$\frac{n_f}{n_c} = \frac{I}{I_c} \left(\frac{\Gamma_f}{\tilde{\Gamma}_f}\right)^2 \tag{5.5}$$

Now $\tilde{\Gamma}_f$ is a function of a sum over Q's. In the spirit of (3.9) and (3.5a), we formally assume that

$$\left(\Gamma_f/\tilde{\Gamma}_f\right)^2 \cong \bar{\eta}/\eta \tag{5.6}$$

which is correct at $t = 0$ ($\tilde{\Gamma}_f = \Gamma_f$ and $\eta = \bar{\eta}$) and in the steady state [(3.9) and (3.5a)].

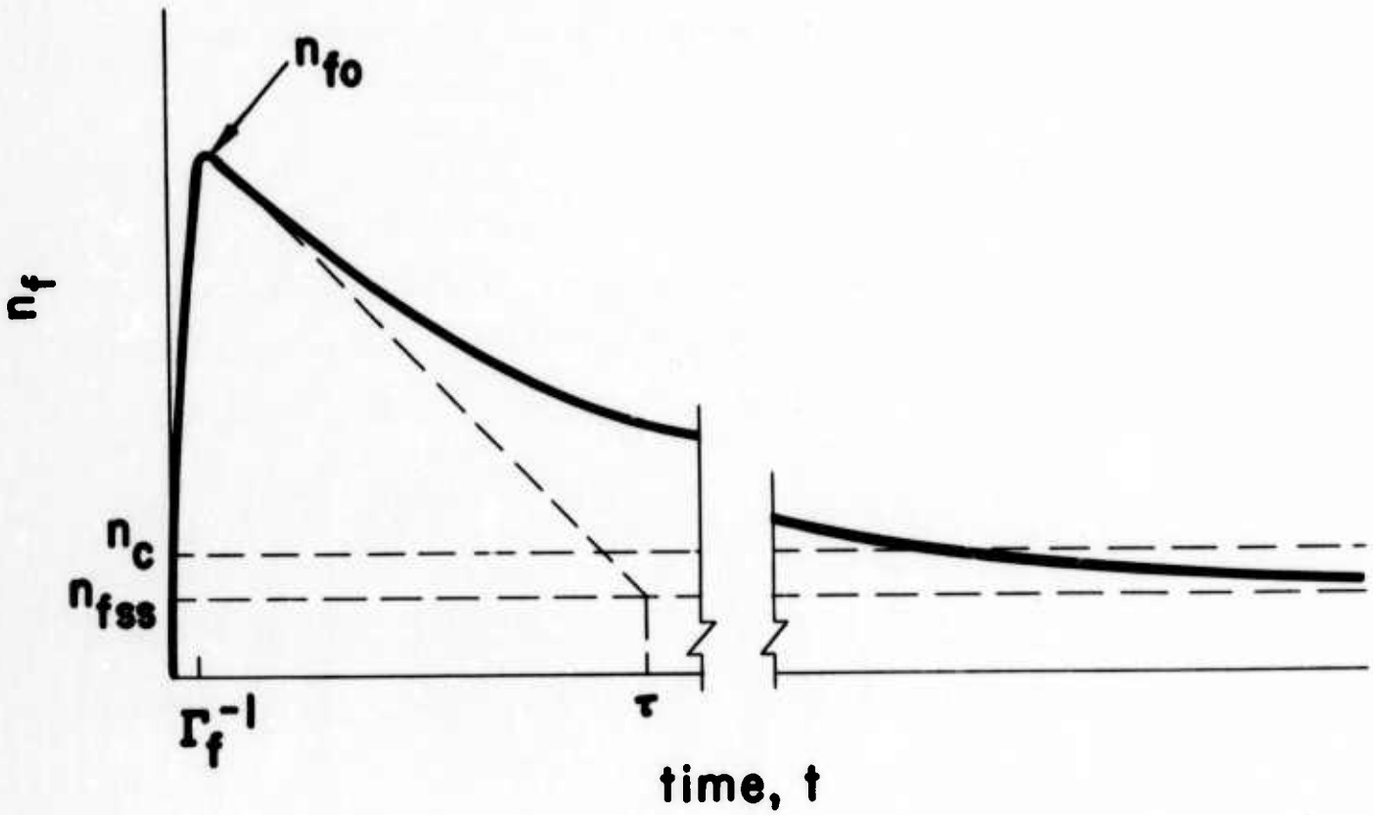

Fig. F8. Schematic illustration of the time dependence of the amplitude n_f of the fundamental mode.

Substituting (5.6) and (5.5) into (5.1) gives

$$\frac{d\eta}{dt} \cong \Gamma_Q \left[\bar{\eta} (1 + I/I_c) - \eta \right] ,$$

which shows that η increases exponentially to the steady-state value $\eta_{ss} = \bar{\eta} (1 + I/I_c)$ [in agreement with (3.5a) and (3.12)] with time constant

$$\tau = 1/\Gamma_Q \quad . \qquad (5.7)$$

In passing, it is mentioned that it can be shown rigorously from (5.1) that $\tau \geq \Gamma_Q^{-1} (I_c/I) \ell n [I/I_c + I_c (I + I_c)^{-1}]$. The proof involves the inequality $d\eta/dt \leq \Gamma_Q (\bar{\eta} + \eta\, n_f/n_c) \leq \Gamma_Q [\bar{\eta} + \eta (n_f/n_c)_{t=0}] = \Gamma_Q (\bar{\eta} + \eta I/I_c)$.

For a typical value of $\Gamma_Q = 10^{12}\ \text{sec}^{-1}$, (5.7) gives $\tau \cong 10^{-12}$ sec., which is short with respect to nanosecond pulses, so that the steady-state solution applies. For $\Gamma_Q^{-1} \gtrsim 10^{-8}$ sec, the steady state is not attained in a 10 nsec pulse. In this case, (5.1) gives $\eta \cong \bar{\eta}$, that is, $n_Q \cong \bar{n}_Q$. Thus $\tilde{\Gamma}_f \cong \Gamma_f$, and the effects of the parametric instability are not observed.

VI. INSTABILITY AT HIGH FREQUENCIES

The effect of phonon instabilities on infrared absorption in the case in which the frequency of the external radiation is high, say, about 3-8 times the reststrahl frequency of the crystal, is of considerable practical interest. Two energy absorption mechanisms, with the fundamental phonon driven off resonance in both cases, will be considered. In the first case, the fundamental phonon decays into two phonons that are off resonance ($\omega_1 + \omega_2 \neq \omega$). In the second case, the fundamental phonon decays into a sufficient number of phonons to allow phonon resonance to occur ($\omega_1 + \omega_2 + \cdots + \omega_m = \omega$).

a. Two-phonon instability off resonance. This can be considered as a special case of the two-phonon instability discussed in Sec. II, in which the delta function in (2.10) is far off resonance. For this case (2.10) is approximated by

$$\delta(\omega - 2\omega_Q) = \frac{2}{\pi} \frac{\omega(2\omega_Q)(2\Gamma_Q)}{[\omega^2 - (2\omega_Q)^2]^2} , \qquad \omega >> \omega_Q . \tag{6.1}$$

Substituting (6.1), (2.9), and (2.4) into (2.5) gives

$$n_c = \frac{\rho^2(1-2\rho)^2 N}{18 |\alpha_2|^2 B^2 \hbar} m_r m_<^2 \omega_Q [\omega^2 - (2\omega_Q)^2]^2 . \tag{6.2}$$

Using (2.14) and (6.2) together with $\omega = 1.78 \times 10^{14}$ sec^{-1} and $\omega_Q = 3.09 \times 10^{13}$ sec^{-1} yields

$$n_c = 1.1 \times 10^5 N , \qquad I_c = 2.2 \times 10^{20} \text{W/cm}^2 \tag{6.3}$$

which is about 10^{10}-10^{17} times as great as the corresponding critical intensity values at resonance and is much greater than the avalanche breakdown value of $\sim 10^{10}$ W/cm^2.[10,13] Thus, the nonlinear absorption by this process is negligible in the high-frequency multiphonon region. This is not surprising since less energy is put into the pair of phonons when they are driven in the wings of their absorption curves than when driven on resonance.

b. m-phonon instabilities. The second mechanism leading to nonlinear energy absorption at high frequency is the multiphonon process in which a fundamental phonon is annihilated and m phonons are created (Fig. F9). It will now be shown that for sufficiently intense external radiation a parametric instability can set in, as in the previous process.

Again using the general relaxation of power balance gives

$$\left(\frac{dn_i}{dt}\right)_{pump} + \left(\frac{dn_i}{dt}\right)_{relax} = 0 , \qquad i = 1, 2, \cdots, m . \tag{6.4}$$

Proceeding as in Sec. IIb yields

$$C^{(m)}[n_f(n_1+1)(n_2+1)\cdots(n_m+1) - (n_f+1)n_1 n_2 \cdots n_m] - \Gamma_i(n_i - \bar{n}_i) = 0 , \tag{6.5}$$

where

$$C^{(m)} = 2\pi\hbar^{-2} |(m+1)!\, V_{f12\cdots m}|^2 \delta(\omega - \omega_1 - \omega_2 - \cdots - \omega_m) . \tag{6.6}$$

In the present general case, the advantages of using the energy balance method over the equation of motion method become even greater than in the case of $m = 2$. The present method yields a single m-order algebraic equation, while

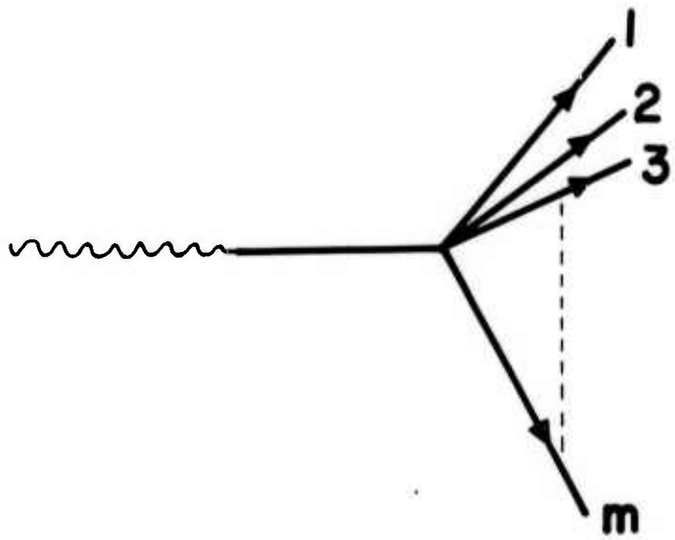

Fig. F9. m-phonon processes.

the equation of motion method leads to m coupled nonlinear differential equations, the solution to which is not easily found.

Since high-order multiphonon processes are subject to much less stringent selection rules than two-phonon processes are, a reasonable first approximation is to assume that the m phonons created have equal frequencies. With this approximation, the set of m equations (6 5) are reduced to the m-order algebraic equation:

$$C^{(m)} [n_f (n_Q + 1)^m - (n_f + 1) n_Q^m] - \Gamma (n_Q - \bar{n}_Q) = 0 \quad . \tag{6.7}$$

Here n_Q and Γ_Q refer to the occupation number and relaxation frequency, respectively, of a final phonon. The delta function in $C^{(m)}$ will subsequently be approximated, at resonance, by

$$\delta(\omega - \omega_1 - \omega_2 - \cdots - \omega_m) \rightarrow 2/m\pi\Gamma_Q \quad . \tag{6.8}$$

It is more expedient to solve for n_f in terms of n_Q than vice versa, which gives

$$n_f = [n^m + \Gamma_Q (n_Q - \bar{n}_Q)/C^{(m)}]/[(n_Q + 1)^m - n_Q^m] \quad .$$

For n_Q slightly greater than $\bar{n}_Q$, n_f is a sharply increasing function of n_Q until it attains its maximum. This local maximum, denoted by n_c, may be obtained approximately by satisfying the dual conditions that (6.7) yields only one root and that n_Q is small. It is found that, for $m > 2$,

$$n_c \cong \Gamma_Q / C^{(m)} (m + b\bar{n}_Q) \quad 1 + [1 + (2b - m^2)/(m + b\bar{n}_Q)]^{1/2} \quad , \tag{6.9}$$

where $b = m(m-1)$. Beyond this maximum, n_f as a function of n_Q decreases until $n_Q^{m-1} \cong \Gamma_Q / C^{(m)}$. It then approaches the asymptotic value $n_f \cong n_Q / m$. These features are exhibited in Fig. F10a.

From Fig. F10a it will be noted that for a given value of $n_f (< n_c)$ the occupation number n_Q in the multiphonon region may be multivalued, corresponding to the different branches in the figure. The actual value of n_Q depends on the stability of the solution on a given branch in the presence of fluctuations in the values of n_Q away from the steady-state solution. It is not difficult to demonstrate that all three branches are stable against even extremely large fluctuations, as long as $n_f < n_c$. For $n_f > n_c$, there is only one solution. This behavior indicates that the final modes remain on the lowest branch until the fundamental mode is excited to a value n_c. For greater values of n_f, n_Q increases to the higher-branch value. The value of n_c can therefore be identified as the threshold for m-phonon parametric instability. The actual growth pattern is shown schematically as the heavy curve in Fig. F10b. The growth from the bottom to the top branch, represented by the heavy dashed vertical line, is not under equilibrium condition since the values in that part of the curve are not steady-state solutions.

Using (2.14) with n_c replaced by (6.9), together with (6.6) and (6.8), we obtain the following numerical estimates:

$$m = 3, \quad n_c = 0.61\, N^2, \quad I_c = 3.9 \times 10^{13}\, N\ W/cm^2$$

$$m = 4, \quad n_c = 14\, N^3, \quad I_c = 6.5 \times 10^{15}\, N^2\, W/cm^2$$

$$m = 5, \quad n_c = 1.3 \times 10^6\, N^4, \quad I_c = 1.4 \times 10^{21}\, N^3\, W/cm^2 .$$

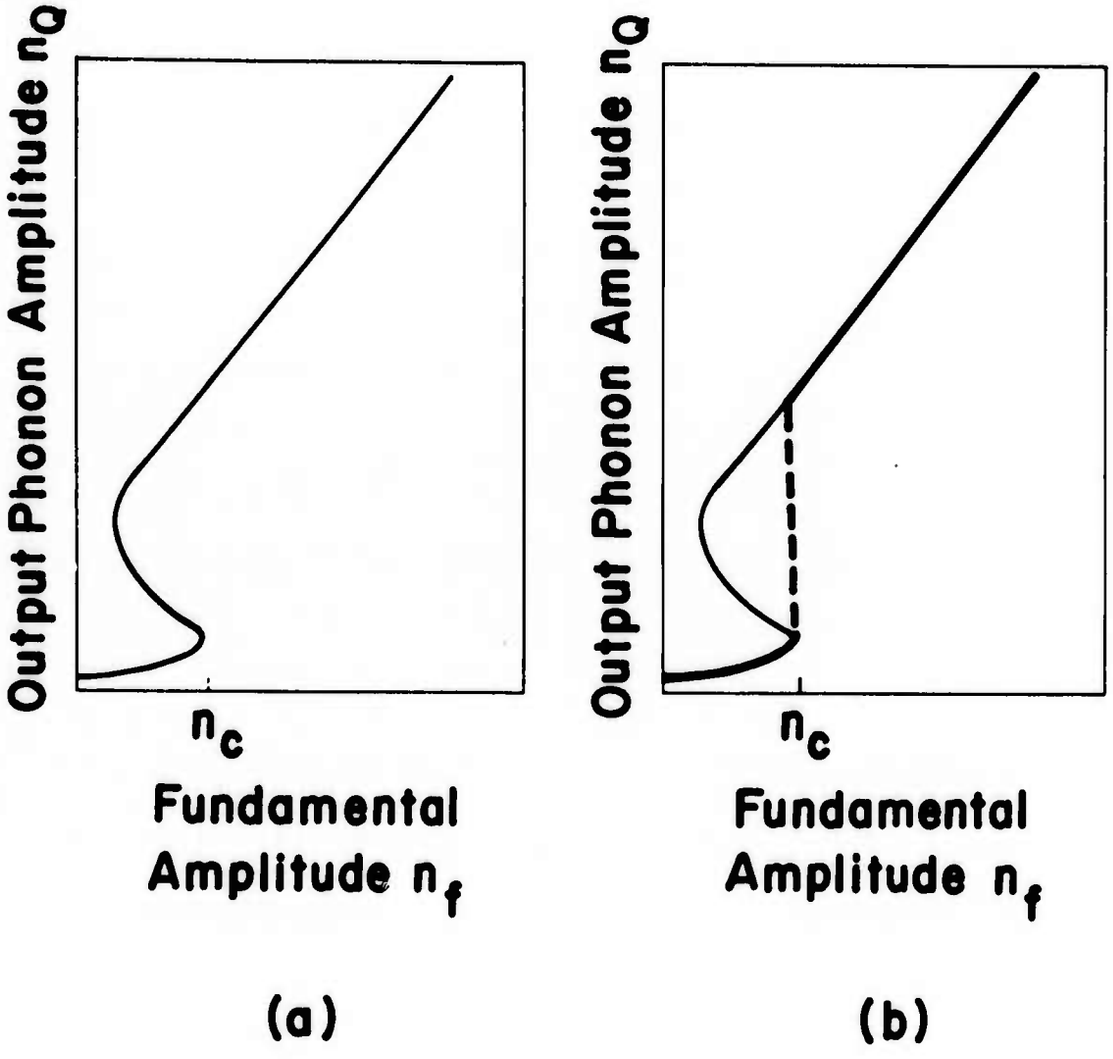

Fig. F10. Parametric excitation of m phonons. (a) Schematic illustration of the approximate steady-state solution to energy balance equation. In (b) the heavy dashed line shows the actual growth path of the final mode as the incident radiation power increases.

In obtaining these estimates, we have not accounted for the limitation due to selection rules so that the actual values are even greater than indicated. For a sample of any reasonable size, the critical intensities in all cases far exceed that required for avalanche breakdown, thus multiphonon instabilities will not be observed.

VII. SUGGESTED EXPERIMENTS

In the preceding section the possibility of parametrically exciting phonons was considered for a wide range of infrared frequencies. The analysis shows that in the higher frequency region, parametric processes, though possible in principle, have large thresholds I_c so that other nonlinear processes, such as avalanche breakdown, would set in first. In the case of two-phonon excitation, however, the parametric instability should be observable. Of all the possible absorption experiments, consider one of the transmission type. It is necessary to use a sample of thickness no greater than a fraction of a micron, this small thickness being necessary to allow some transmission near the laser resonance.

According to (2.18), at least 300 W/cm^2 are required. For NaCl, with $\lambda_f \cong 60\mu m$, and two times diffraction limited spot of $120\mu m$ diameter, the area is $\sim 10^{-4}$ cm^2, corresponding to a power of $\sim 3.1 \times 10^{-2}$ W. In practice, several orders of magnitude greater power may be required. Since tunable sources with this power are not currently available, a fixed frequency laser must be used. For example, H_2S with lines at $60.3\mu m$[32] could be used with NaCl. A low-power spectroscopic measurement of the absorption as a function of ω could be made to determine the position of the NaCl absorption curve with respect to the laser frequencies.

The transmission would be measured as a function of the incident power. A sharp change [increase at resonance -- see (2.13) with $\Gamma_f \rightarrow \tilde{\Gamma}_f$] should occur as I approaches I_c, corresponding to the increase in $\tilde{\Gamma}_f$.

For a thin film of crystal of thickness d, the transmission coefficient T_r is given by[18]

$$T_r \cong 1 - \omega d\, c^{-1}\, \mathrm{Im}\, \epsilon(\omega) , \qquad d \ll \lambda/2\pi \tag{7.1}$$

where $\Im m\, \epsilon(\omega)$ is the imaginary part of the dielectric function $\epsilon(\omega)$. At $\omega = \omega_f$, (7.1) gives

$$1 - T_r \cong \omega_0^2\, d\, c^{-1} (\epsilon_0 - \epsilon_\infty)\, \tilde{\Gamma}_f^{-1} = (1 - T_r)_{lin} (I/I_c + 1)^{-1/2} \quad . \qquad (7.2)$$

In the second equality, the result (3.13) for $\tilde{\Gamma}_f$ was used. The subscript "lin" denotes that $1 - T_r$ is evaluated at $\tilde{\Gamma}_f = \Gamma_f$. By correlating this dependence of $1 - T_r$ on I with the experimental results, parametric processes may be verified. In particular, according to (7.2), the transmission coefficient of a thin film driven parametrically at resonance should increase as I increases, while T_r decreases with increasing I away from resonance. This behavior is analogous to that observed in the premature saturation of the main resonance in the Suhl-Bloch-Bloembergen ferromagnetic instability. Fig. F11 illustrates the change in transmission with increasing intensity.

In principle, the parametric instability could be used to study the relaxation frequencies of various phonon modes as a function of the position of the modes in the Brillouin zone, as has been done for magnons in parallel pumping experiments.[4] However, the results would be more difficult to interpret than in the magnon case since it would be more difficult to determine unambiguously which phonons were going unstable in general. In spite of this difficulty, the parametric instability method does give information that cannot be obtained by any other method.

The effects of the phonon instability on the stimulated Raman process will be discussed in the following technical report.

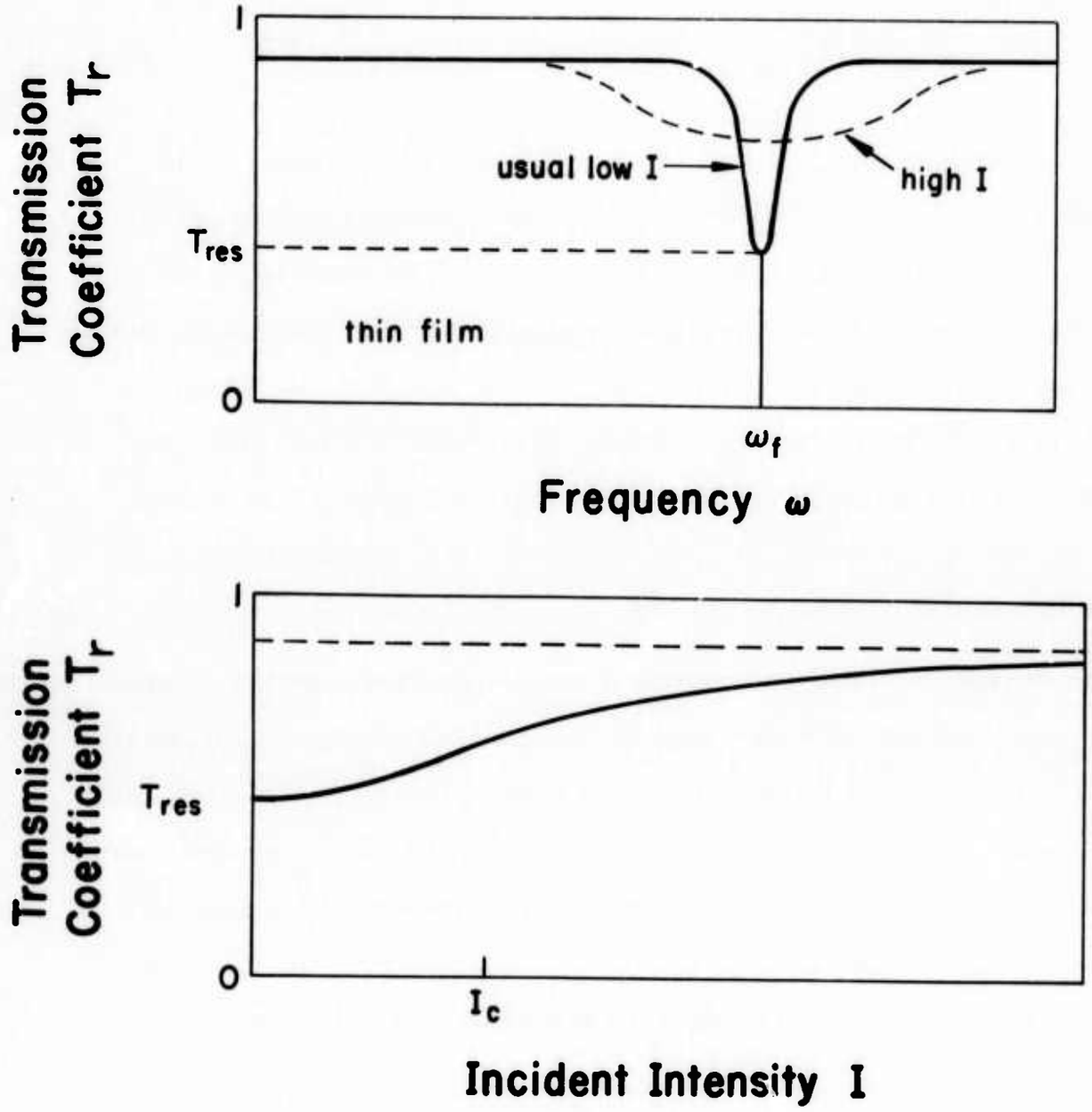

Fig. F11. Spectral transmittance of a thin film schematically illustrating the broadening of the resonance at high values of incident intensity. The bottom curve was sketched using (3.14).

REFERENCES

*Research supported by the Advanced Research Projects Agency of the Department of Defense and monitored by the Defense Supply Service - Washington, D.C.

1. H. Suhl, J. Phys. Chem. Solids 1, 209 (1959).
2. H. B. Callen, Fluctuation, Relaxation and Resonance in Magnetic Systems, Ed. D. ter Haas (Oliver and Boyd, Edinburgh, 1962).
3. R. M. White and M. Sparks, Phys. Rev. 130, 632 (1963).
4. M. Sparks, Ferromagnetic Relaxation Theory (McGraw-Hill, New York, 1964).
5. S. V. Silin, Sov. Phys. JETP 21, 1127 (1965).
6. D. F. DuBois and M. V. Goldman, Phys. Rev. Lett. 14, 544 (1965).
7. N. Bloembergen, Nonlinear Optics (W.A. Benjamin, New York, 1965).
8. W. H. Louisell, Coupled Modes and Parametric Electronics (Wiley and Sons, New York, 1960).
9. R. Orbach, IEEE Trans. Sonics and Ultrasonics 14, 140 (1967).
10. D. W. Fradin, E. Yablonovitch, and M. Bass, Appl. Opt. (to be published).
11. N. Bloembergen, Appl. Opt. 12, 661 (1973).
12. M. Sparks and C. J. Duthler, J. Appl. Phys. 44, 3038 (1973).
13. L. V. Keldysh, Sov. Phys. JETP 20, 1307 (1965); G. M. Zverev, T. N. Mikhailova, V. A. Pashkov, and N. M. Solov'eva, Sov. Phys. JETP 26, 1053 (1968).
14. S. A. Akhmanov, A. P. Sukhorukov, and R. V. Khokhlov, Sov. Phys. - Usp. 91, 609 (1968); M. T. Loy and Y. R. Shen, IEEE J. Quantum Elec. QE-9, 409 (1973).
15. M. Sparks, J. Appl. Phys. 42, 5029 (1971).

16. The processes with the vertex V_Q appearing first and those with the intermediate-state boson being annihilated, then created, must also be considered, of course. Treating these diagrams in second-order perturbation theory and formally replacing $\Gamma_f(\omega^2 - \omega_f^2)^{-2}$ by $\Gamma_f[(\omega^2 - \omega_f^2)^2 + \omega_f^2\Gamma_f^2]^{-1}$ gives the same results as those obtained in the present paper, but affords somewhat less insight into the results.

17. The polariton nature of the intermediate state need not be considered explicitly in either the phonon or magnon case.

18. M. Born and K. Huang, Dynamical Theory of Crystal Lattice (Oxford University Press, Oxford, 1954).

19. R. A. Cowley, Adv. Phys. 12, 421 (1963).

20. E. R. Cowley and R. A. Cowley, Proc. Roy. Soc. (London) A 287, 259 (1965).

21. E. R. Cowley, J. Phys. C 5, 1345 (1970).

22. M. Lax and E. Burstein, Phys. Rev. 97, 39 (1955).

23. R. Loudon, Phys. Rev. 137A, 1784 (1965).

24. C. J. Duthler and M. Sparks, Phys. Rev. (in press).

25. M. Sparks and L. J. Sham, Phys. Rev. B 8, 3037 (1973).

26. L. A. Vredevoe, Phys. Rev. 140, A 930 (1965).

27. R. Orbach and L. A. Vredevoe, Physics 1, 91 (1964).

28. M. Sparks, to be published.

29. H. C. Kim, private communication.

30. P. Gottlieb and H. Suhl, J. Appl. Phys. 33, 1508 (1962).

31. J. J. Green and E. Schlomann, J. Appl. Phys. 33 S, 1358 (1962).

32. J. C. Hassler and P. D. Coleman, Appl. Phys. Lett. 14, 135 (1969).

G. HIGH-POWER 2-6 μm WINDOW-MATERIAL FIGURES OF MERIT WITH EDGE COOLING AND SURFACE ABSORPTION INCLUDED

M. Sparks
Xonics, Incorporated, Van Nuys, California 91406
and
H. C. Chow
Department of Physics, University of California, Los Angeles, California 90024, and
Xonics, Incorporated, Van Nuys, California 91406

Values of the total power $\mathcal{P}$ that a window can transmit under specified conditions are calculated for use as figures of merit for window materials. New features of the figures of merit are: consideration of edge as well as face cooling, treatment of surface as well as bulk absorption, use of $\mathcal{P}$ rather than intensity as the figure of merit, effects of improving materials and calculation for 3.8 and 5.25 μm. New results include the following: For continuous operation, large-diameter windows should be face cooled, but small-diameter windows may be edge cooled, and $\mathcal{P}$ often decreases as the diameter D increases. For pulsed operation, $\mathcal{P}$ increases as D increases, as intuitively expected. Values of the diameter D_{EF}, above which face cooling should be used, are surprisingly large, ranging between 7 and 100 cm, typically. For pulsed operation and for $D > D_{EF}$ in cw operation, $\mathcal{P}$ is independent of thermal conductivity K, while for $D < D_{EF}$ in cw operation, $\mathcal{P} \propto K$. The alkaline-earth fluorides have the greatest figures of merit for large-diameter windows, with $\mathcal{P}$ = 76 MW, ΔT = 50 K, and ℓ = 0.5 cm, for a one-second pulse on a 10 cm-diameter window of BaF_2 at 3.8 μm with a bulk absorption coefficient of 10^{-4} cm^{-1}. For small-diameter windows (1 cm-diameter), Si, BaF_2, and GaAs have the greatest values of $\mathcal{P}$ = 1.8, 0.94, and 0.76 MW, respectively, for cw or 1 sec pulse duration.

I. INTRODUCTION

There have been extensive programs within the last three years to obtain materials for high-power infrared systems at 10.6 μm.[1] Window materials for the 2-6 μm region have received far less attention. However, there is considerable interest in chemical lasers operating in the 2-6 μm range and increasing interest in window materials for this range.

In addition to extending the previous figures of merit[2-4] to 3.8 and 5.25 μm, the following new features are added: (1) Edge cooling, as well as face cooling, is included for continuously operated (cw) systems. (2) As materials are being improved, surface absorption apparently is becoming relatively more important. Surface absorption may also be of interest in field use where contamination is likely. Thus, surface as well as bulk absorption is included. (3) The total power $\mathcal{P}$ that a window can transmit under specified idealized conditions is used as the figure of merit. Use of $\mathcal{P}$, rather than intensity, is more convenient when considering the effect of changing the window diameter. (4) Effects of improving materials, particularly lowering the absorption coefficient β and increasing the strength σ, are included.

In addition to the new ratings for materials, new results include the following: (1) Edge cooling, which is technically much simpler than face cooling, is more effective than previously realized. Before the importance of thermally induced optical distortion and fracture was realized,[3] edge cooling to prevent melting was considered. Subsequently, only face cooling was considered since ΔT must be kept small, and large-diameter windows,

which have large values of ΔT for edge cooling, were contemplated to keep the intensity small and to avoid diffraction in long-focal length systems. It will be shown that edge cooling can be used for surprisingly large diameters D_{EF}, ranging between 7 and 100 cm, typically. In order to obtain the greatest value of θ in a cw system, large-diameter windows ($D > D_{EF}$) should be face cooled, while small-diameter windows ($D < D_{EF}$) may be edge cooled.

(2) For pulsed operation (pulse length of the order of a second, with rapid interpulse cooling), θ increases as D increases as expected intutively, but for continuous operation, θ often decreases as D increases. Thus, for cw systems that can tolerate small-diameter windows (without excessive diffraction, for example), there are the dual advantages of technically easier edge coolings and often greater θ. (3) For small diameters, $D < D_{EF}$, the value of θ_{cw} depends on the thermal conductivity K; whereas for $D > D_{EF}$, θ_{cw} is independent of K. For pulse operation, θ_{pulse} is independent of K.

In considering window materials for high-power infrared lasers, previous theoretical investigations[3,4] have established the effects of temperature gradients and pressure differentials. Briefly, as a result of the spatial inhomogeneity of the intensity of the incident laser beam, a radial temperature gradient is set up, bringing about radial gradients in the thickness and the index of refraction. The resulting optical distortion may cause significant reduction in the target intensity, especially for long-focal length systems. Optical distortion may also be caused by deformation of the window under pressure. In addition, both the temperature gradient and pressure can cause fracture of the window.

Application of these considerations to obtain figures of merit for window materials involves the following three distinct factors:

(a) Pressure-induced optical distortion and fracture are avoided by making the window thickness ℓ greater than a critical value ℓ_{gr}.

(b) Thermally induced optical distortion and fracture are avoided by keeping the temperature difference ΔT between the center and rim of the window below a critical value ΔT_{less}.

(c) The fact that ΔT must be kept below ΔT_{less} limits the total power that a window can transmit to values below a critical value $\mathcal{P}_{pulse}$ for pulse operation or $\mathcal{P}_{cw}$ for cw operation. The relation between $\mathcal{P}$ and ΔT depends on the type of operation (pulse or cw), the thermal properties of the window (heat capacity per unit volume C and thermal conductivity K), the type of heating (bulk or surface), and for cw operation, the type of cooling (edge or face cooling).

Two of the new features of the figures of merit, surface absorption and edge cooling, pertain to the relation (c) between $\mathcal{P}$ and ΔT.

II. FIGURE-OF-MERIT ANALYSIS

The figures of merit are obtained as follows:[3,4] (a) The thickness ℓ_{gr} required to withstand the given pressure P is calculated first. The thicknesses ℓ_f and ℓ_o required to withstand the pressure without fracturing the window and without causing excessive optical distortion are[4,5]

$$\ell_f / D = 0.433 \, (P \, SF / \sigma)^{1/2} , \tag{2.1}$$

$$\ell_o / D = 0.842 \left[(n-1) (P/E)^2 (D/\lambda) \right]^{1/5} , \tag{2.2}$$

respectively, where σ is the window strength, P the pressure, the safety factor SF is taken as SF = 4, n is the refractive index, E the Young's modulus, and λ the optical wavelength. In order to prevent both fracture and excessive optical distortion, the thickness must be greater than both ℓ_f and ℓ_o; that is $\ell > \ell_{gr}$ ≡ greater of ℓ_o and ℓ_f.

(b) Next, the temperature difference ΔT between the center and rim of the window that can be tolerated is calculated as follows. If ΔT exceeds ΔT_f or ΔT_o, defined as

$$\Delta T_f = 2\sigma / \alpha E \, SF, \qquad \Delta T_o = \lambda / 8 \, \ell_{gr} \, | \partial_{nT} | \tag{2.3}$$

with $\partial_{nT} \equiv (\partial n / \partial T)_\sigma + \alpha (1+\nu)(n-1) + S$, in which the derivative is taken at constant stress, α is the linear thermal expansion coefficient, ν is the Poisson ratio, and S is a small stress-optic term,[3] then the window fractures from the excessive thermal gradient or causes excessive thermally induced optical distortion,[3] respectively. In order to prevent both of these system failures,

ΔT must be smaller than both ΔT_f and ΔT_o; that is, $\Delta T < \Delta T_{less}$ $\equiv$ lesser of ΔT_f and ΔT_o.

(c) For pulsed operation in which the heat diffusion and, therefore, the cooling are negligible during the pulse duration t_{pulse}, the temperature rise at every point is determined by the simple expression $CV = \Delta E / \Delta T$, where V is the volume, C is the heat capacity per unit volume, ΔE is the energy added, and ΔT is the temperature rise. From this expression it is easy to show[3] that for intensity $I = I_0 - \frac{2}{3}\left(\rho / \frac{1}{2}D\right)^2 I_0$, where ρ is the radial coordinate, the spatially averaged intensity $\langle I \rangle$ and ΔT are related by the expression $\langle I \rangle_{pulse} = C\,\Delta T / \beta\, t_{pulse}$. The corresponding total power $\mathcal{P}_{pulse}$ that a window can transmit in the pulse mode of operation is

$$\mathcal{P}_{pulse} = \pi \left(\frac{1}{2}D\right)^2 \langle I \rangle_{pulse} = \pi D^2 C\,\Delta T / 4\,\beta\, t_{pulse} \quad . \tag{2.4}$$

A continuously operated system must be cooled, otherwise ΔT goes to infinity as t goes to infinity for fixed $\mathcal{P}_{pulse}$, as seen in (2.4). In this case, (2.4) is valid if t_{pulse} is replaced by τ_{less}, which is the time constant for cooling the window. For edge cooling, τ_{less} is the time constant τ_E for radial heat flow along the radius $\frac{1}{2}D$:

$$\tau_E = C \left(\frac{1}{2}D\right)^2 / 4K \quad . \tag{2.5}$$

The exact value of τ_E has a weak dependence on the radial distribution of the incident intensity. The value given is for a constant intensity. For 1 constant inside the circle of diameter $\frac{1}{2}D$ and zero outside this circle, the factor $\frac{1}{4}$ in τ_E is replaced by 1/2.9.[6] These results are obtained from trivial solutions to the heat-flow equation.

For face cooling, τ_{less} is the sum of the time constant for heat flow across the window thickness ℓ_{gr} plus that for removal of heat at the interface of the window and coolant:[3]

$$\tau_F = \frac{C \ell_{gr}}{h} \left(1 + \frac{h \ell_{gr}}{3K} \right) , \tag{2.6}$$

where h is the heat-transfer coefficient ($W/cm^2 K$) at the interface of the window and coolant.

In calculating the figures of merit, it is assumed that edge cooling is used if $\tau_E < \tau_F$ and that face cooling is used if $\tau_F < \tau_E$, since larger values of θ result. Accordingly, the cw figure of merit that will be used is

$$\theta_{cw} = \pi D^2 C \Delta T_{less} / 4 \beta \tau_{less} , \tag{2.7}$$

where τ_{less} = lesser of τ_E and τ_F.

The critical window diameter D_{EF} that determines whether face or edge cooling is to be used is simply the solution to $\tau_E = \tau_F$. Since the factor $h \ell_{gr} / 3K$ in (2.6) is negligible in all materials considered except TI 1173 glass, this term is neglected, giving $\tau_E = C \ell_{gr} / h$. Solving for D gives

$$D_f = \frac{6.93K}{h} \left(\frac{P SF}{\sigma} \right)^{1/2} , \qquad D_o = \left[\frac{13.47 K P^2 (n-1)}{\lambda^{1/5} h E^2} \right]^{5/4} \tag{2.8}$$

for $\ell_{gr} = \ell_f$ and ℓ_o, respectively. The critical diameter D_{EF} = greater of D_f and D_o.

If the window absorbs the radiation at its surface, rather than throughout the bulk, it is easy to show that β in (2.4) and (2.7) is replaced by f / ℓ_{gr},

where f is the fraction of the incident radiation absorbed by the two surfaces. Then (2.4) and (2.7) are replaced by

$$\mathcal{P}_{pulse} = \pi D^2 \ell_{gr} C \Delta T_{less} / 4 f t_{pulse} \qquad (2.9)$$

and

$$\mathcal{P}_{cw} = \pi D^2 \ell_{gr} C \Delta T_{less} / 4 f \tau_{less} \qquad (2.10)$$

for surface absorption. Since the values of $\mathcal{P}$ for surface absorption are more strongly dependent on the window size (by a factor of ℓ_{gr}) than the corresponding values for bulk absorption, $\mathcal{P}_{cw}$ never decreases with increasing D, and the advantages of using large-diameter windows are greater in the case of surface absorption.

Finally, in strengthening materials there is a critical strength σ_{f-o} that is of interest. If the strength of the material σ is less than σ_{f-o}, then $\ell_{gr} = \ell_f$, and increasing the strength allows the use of thinner windows ($\ell_{gr} \sim \sigma^{-1/2}$). On the other hand, for $\sigma > \sigma_{f-o}$, $\ell_{gr} = \ell_o$. Thus, increasing σ does not allow thinner windows to be used since ℓ_o is independent of σ. The value of σ_{f-o} is obtained by equating ℓ_f and ℓ_o in (2.1) and (2.2) and solving for σ, which gives

$$\sigma_{f-o} = 0.264\ P\ SF \left[\frac{1}{n-1} \left(\frac{E}{P} \right)^2 \frac{\lambda}{D} \right]^{2/5} . \qquad (2.11)$$

III. TABULATION AND DISCUSSION OF RESULTS

Values of θ, ℓ_{gr}, ΔT_{less}, τ_{less}, D_{EF}, and $\sigma_{o\text{-}f}$ are calculated using the results of Sec. 2 and listed in Tables GI-VIII for various materials of interest for $\lambda = 3.8$ and $5.25\,\mu m$ and D = 1, 10, and 100 cm. It is also useful to visualize the results. Thus, Fig. G1 schematically illustrates the D dependence of ℓ_{gr}, ΔT_{less}, and $1/\tau_{less}$. The relative positions of the regions of the three curves change from material to material. The tendency for θ to increase with increasing D caused by the explicit D^2 factor in Eqs. (2.4) and (2.7) tends to be offset by the decreasing factors ΔT_{less} and $1/\tau_{less}$ illustrated in Fig. G1. The resulting dependence of θ and D is plotted in Figs. G2 and G3 for BaF_2, Si, ZnSe, and strengthened KC1 (σ = 4 kpsi). (In the tables, values for unstrengthened KC1, with σ = 330 psi, are given.) Formulae that are useful in scaling and in visualizing the dependence of θ on variables other than D are displayed in Table GVIII.

In the tables and figures all values are computed under the conditions P = 14.7 psi, SF = 4, $h = 10^{-2}$ W/cm^{2}K, $f = 10^{-4}$, and t_{pulse} = 1 sec. The notation f or o designates fracture or optical distortion as the controlling factor, while F or E accompanying τ_{less} signifies face cooling or edge cooling. Values of θ in Table GVII were calculated using the measured values of β, while those of Tables GII-VI were calculated using β equal to the greater of 10^{-4} cm^{-1} and the extrapolated intrinsic value.

This choice of β is dictated by the following considerations. There is very little experimental information on the values of β at 3.8 and $5.25\,\mu m$. With the exception of Al_2O_3, the experimental values for the materials considered here

surely are either extrinsic or characteristic of the experimental calorimetric set up, rather than the material. We have made order-of-magnitude estimates of the intrinsic values of the absorption coefficients by extrapolating from intrinsic values measured at shorter wavelengths. For most materials considered, these intrinsic values are extremely small. As an example, $\beta = 5 \times 10^{-13}\ cm^{-1}$ for BaF_2 at $3.8\mu m$. For such small intrinsic values, the observed values of β will be determined by extrinsic processes. In practice, it is difficult to obtain materials with $\beta = 10^{-4}\ cm^{-1}$. It is even difficult to measure such low values. For references we include the measured absorption coefficients that have been reported: at $2.8\mu m$[7] $\beta = 0.027\ cm^{-1}$ (Ge), $0.018\ cm^{-1}$ (Si), $0.7\ cm^{-1}$ (ZnSe), $0.004\ cm^{-1}$ (CaF_2), $0.001\ cm^{-1}$ (BaF_2), and $0.002\ cm^{-1}$ (TI 1173); at $4.0\mu m$,[1] $\beta = 0.003\ cm^{-1}$ (Ge), $0.009\ cm^{-1}$ (GaAs), $0.002\ cm^{-1}$ (CdTe), $0.043\ cm^{-1}$ (Al_2O_3), and $0.20\ cm^{-1}$ (TI1173); at $5.25\mu m$,[8] $\beta = 0.0018\ cm^{-1}$ (Ge), $0.0059\ cm^{-1}$ (Si), $0.0016\ cm^{-1}$ (ZnSe), $5.0 \times 10^{-4}\ cm^{-1}$ (CaF_2), $4.1 \times 10^{-5}\ cm^{-1}$ (SrF_2), $3.0 \times 10^{-5}\ cm^{-1}$ (BaF_2), and $1.5 \times 10^{-5}\ cm^{-1}$ (KC1); and at $2.8\mu m$,[9] $\beta = 3 \times 10^{-4}\ cm^{-1}$ (BaF_2). From these considerations it is clear that figures of merit based on the estimated intrinsic values of β would be misleading at the present state of the art. In addition to the difficulties in using the experimental values of β already mentioned, the experimental values surely will be decreased as better crystals and better measurements become available, as has been the case at $10.6\mu m$.

In small-diameter windows, $\tau_{less}\ (= \tau_E)$ is often less than t_{pulse}, as seen in Table GIV and Figs. G2 and G3, and the radial heat flow reduces the value of ΔT. Thus, the value of θ is not increased by using the pulse mode of operation in small-diameter windows. This is indicated in Fig. G2 by the dashed

portions of the curves, for which $t_{pulse} > \tau_{cw}$ (so that $\theta_{pulse} < \theta_{cw}$ formally). In Table GIV, for D = 1 cm, only the values of θ_{cw} are given since τ_{cw} is less than or only slightly greater than t_{pulse} = 1 sec for all materials except TI 1173 glass.

The dependence of θ on the thermal conductivity K is of interest. For pulse operation, thermal diffusion is assumed negligible. Thus, θ_{pulse} is independent of K, as also seen in (2.4). For cw operation of small-diameter windows ($D < D_{EF}$), the thermal time constant τ_{less} is equal to $\tau_E \sim 1/K$, from (2.5). Thus, $\theta_{cw} \sim K$, according to (2.7). For cw operation of large-diameter windows ($D > D_{EF}$), $\tau_{less} = \tau_F$. The value of τ_F usually is controlled by the heat transfer at the window face, rather than by the heat diffusion across the window thickness. In other words, the factor $h \ell_{gr}/3K$ in (2.6) is much less than unity, one exception being TI 1173 glass in large-diameter windows. For example, for BaF_2 with D = 10 cm and $h = 10^{-2}$ W/cm^2 K, $h \ell_{gr}/3K = 1.47 \times 10^{-2}$. Thus, θ_{cw} is independent of K for $D > D_{EF}$.

It should be emphasized that the figures of merit θ are not the actual powers that windows in real systems can transmit. In this connection, two factors must be stressed. First, the figures of merit apply to specific and idealized conditions.[4] In spite of this qualification, it is convenient to use θ as the figure of merit since it does give a rough idea of the power expected and the relative values of θ for different materials are at least as useful as previous figures of merit. Second, the figures of merit are proportional to $1/\beta$ (or to 1/f for surface absorption), and an arbitrary choice of the values of β must be made, as discussed above.

IV. CHOICE OF MATERIALS

Some materials that have too great an optical absorption at 10.6 μm are expected to have sufficiently small absorption for use in the 2-6 μm. This is important since some of these materials, such as Si, Ge, and the alkaline-earth fluorides, have better physical and thermal properties than most 10.6 μm materials, such as KBr and KCl.

A study of the tables indicates that of the candidate materials analyzed, the alkaline-earth fluorides have the greatest values of the figures of merit at 3.8 and 5.25 μm and 10-100 cm diameters. For diameter D = 10 cm the value of ΔT is controlled by the effect of optical distortion for most materials, but for the alkaline-earth fluorides, which have large values of ΔT, it is controlled by fracture. For D = 100 cm, it is the optical distortion effect, rather than fracture, which limits this temperature difference, with only one exception (BaF_2 at 3.8 μm). For alkaline-earth fluorides, the effects of the temperature dependence of the refractive index and of thermal expansion are opposite and nearly cancel each other [first two terms in ∂_{nT} defined under (2.3)], with the result that the optical distortion is smaller than that for other materials. The value of ΔT for BaF_2 with D = 10 cm is 50 K, compared with ~1 K for the other materials, excluding the oxides and the other fluorides.

In the case of edge-cooled small-diameter windows at 3.8 μm (Table GIV), the alkaline-earth fluorides are again relatively good materials because they can tolerate large temperature gradients without fracturing. However, in small-diameter windows, radial heat flow is far more important. Specifically, (2.7) with $\tau_{less} = \tau_D \sim 1/K$ shows a linear dependence of θ_{cw} on the thermal

conductivity K. Since silicon has by far the largest value of K, it has the greatest figure of merit for small D.

It has been suggested privately by several investigators that it may be possible to fabricate a mixed alkaline-earth fluoride with $\partial_{nT} \cong 0$, thereby making θ approach infinity. Unfortunately, for a 10 cm-diameter window the value of θ already is limited by fracture (or nearly so for BaF_2 at 3.8 μm); thus no improvement would result from lowering the value of ∂_{nT} unless the crystals were strengthened also. Furthermore, the increase in θ by decreasing ∂_{nT} is a result of increasing the value of ΔT, which already has a value of 50 K in the case of BaF_2. In addition, the temperature dependence of ∂_{nT} would prevent $\partial_{nT} \cong 0$ over the whole window for large values of ΔT.

Based on the fact that the multiphonon absorption decreases rapidly with decreasing wavelength λ for λ less than the wavelength λ_f at which the lattice absorption is maximum, it is sometimes stated that a material that is acceptable for 10.6 μm use will be even better at lower wavelengths. This is not true in general for several reasons. Diamond, with $\lambda_f < 10.6\,\mu$m, may be useful for small windows at 10.6 μm, but the absorption is too great in the shorter-wavelength region. In other materials, impurities, interband transitions, and possibly deep-gap-level transitions, can give rise to absorption in the 2-6 μm region. Since extrinsic processes of unknown origin determine the values of β for most materials of interest, the smaller intrinsic values at the shorter wavelengths have little direct consequence.

Finally, factors other than the figures of merit obviously must be considered in choosing a material for a given application. For example, if programs to obtain

improvements in materials are undertaken, the expected difficulty in purifying or otherwise improving a crystal is obviously of interest, and factors such as ease of fabrication, resistance to moisture, hardness, and antireflection and protective coating must be considered. The value of ℓ_{gr} could be so great that the weight of the window could be unacceptably large, or the value of ΔT_{less} could be unacceptably high.

V. ACKNOWLEDGMENTS

Appreciation is expressed to Dr. C. M. Stickley for suggesting this investigation and to Dr. J. A. Harrington for suggesting improvements of the manuscript.

REFERENCES

* This research was supported by the Advanced Research Projects Agency of the Department of Defense and was monitored by the Defense Supply Service - Washington, D. C.

1. See, for example, Conference on High Power Infrared Laser Window Materials, Oct. 30, 31 and November 1, 1972, C. A. Pitha, editor, AFCRL-TR-73-0372, Vols. I and II, 19 June 1973.
2. F. A. Horrigan and R. I. Rudko, Raytheon Research Division Final Technical Report on Contract No. DAAH01-69-C-0038, 1969 (unpublished); F. A. Horrigan, C. Klein, R. Rudko, and D. Wilson, Microwaves 68 (1969); F. A. Horrigan and T. F. Deutsch, Raytheon Research Division Final Technical Report on Contract No. DAAH01-70-C-1251, 1971 (unpublished); T. F. Deutsch and R. I. Rudko, Raytheon Research Division Final Technical Report on Contract No. DAAH01-72-C-0194, 1973 (unpublished).
3. M. Sparks, J. Appl. Phys. 42, 5029 (1971).
4. M. Sparks and M. Cottis, J. Appl. Phys. 44, 787 (1973).
5. Mechanical Engineers Handbook, 4th ed., edited by Lionel S. Marks (McGraw-Hill, New York, 1941), pp. 447-480.
6. M. Sparks, "Temperature and Stress Analysis for Bulk- and Surface-Heated Slabs," Parke Mathematical Laboratories, Inc. TM-2 (1971).
7. T. F. Deutsch (private communication).
8. T. F. Deutsch, Raytheon Research Division Semi-Annual Report, Contract No. DAAH01-72-C-0194, August 1973 (unpublished).
9. J. Loomis, S. Aikens, L. Marrers, and G. Thompson, Laser Digest, Air Force Weapons Laboratory, Technical Report No. AFWL-TR-73-131, Spring 1973 (unpublished).

Figure Captions

Figure G1. Schematic illustration of the diameter dependence of thickness, temperature difference, and thermal time constant.

Figure G2. Diameter dependence of figures of merit θ_{pulse} at $\lambda = 3.8\,\mu m$. Symbols such as (f, o) in this figure and (f, o, E) in Fig. G3 denote the controlling factors for ℓ_{gr}, ΔT_{less}, and τ_{less}, respectively: o - optical distortion; f - fracture; E - edge cooling; and F - face cooling. Quantities used to obtain the curves are those used for Tables GI-IV except KC1 (σ = 4,000 psi for curves; σ = 330 psi for circled numbers). The dashed line indicates that $\tau_{pulse} > \tau_{less}$; thus θ approaches cw value of Fig. G3.

Figure G3. Diameter dependence of figures of merit θ_{cw} at $\lambda = 3.8\,\mu m$. See caption of Fig. G2.

Thickness, Temperature, and Thermal Time Constant

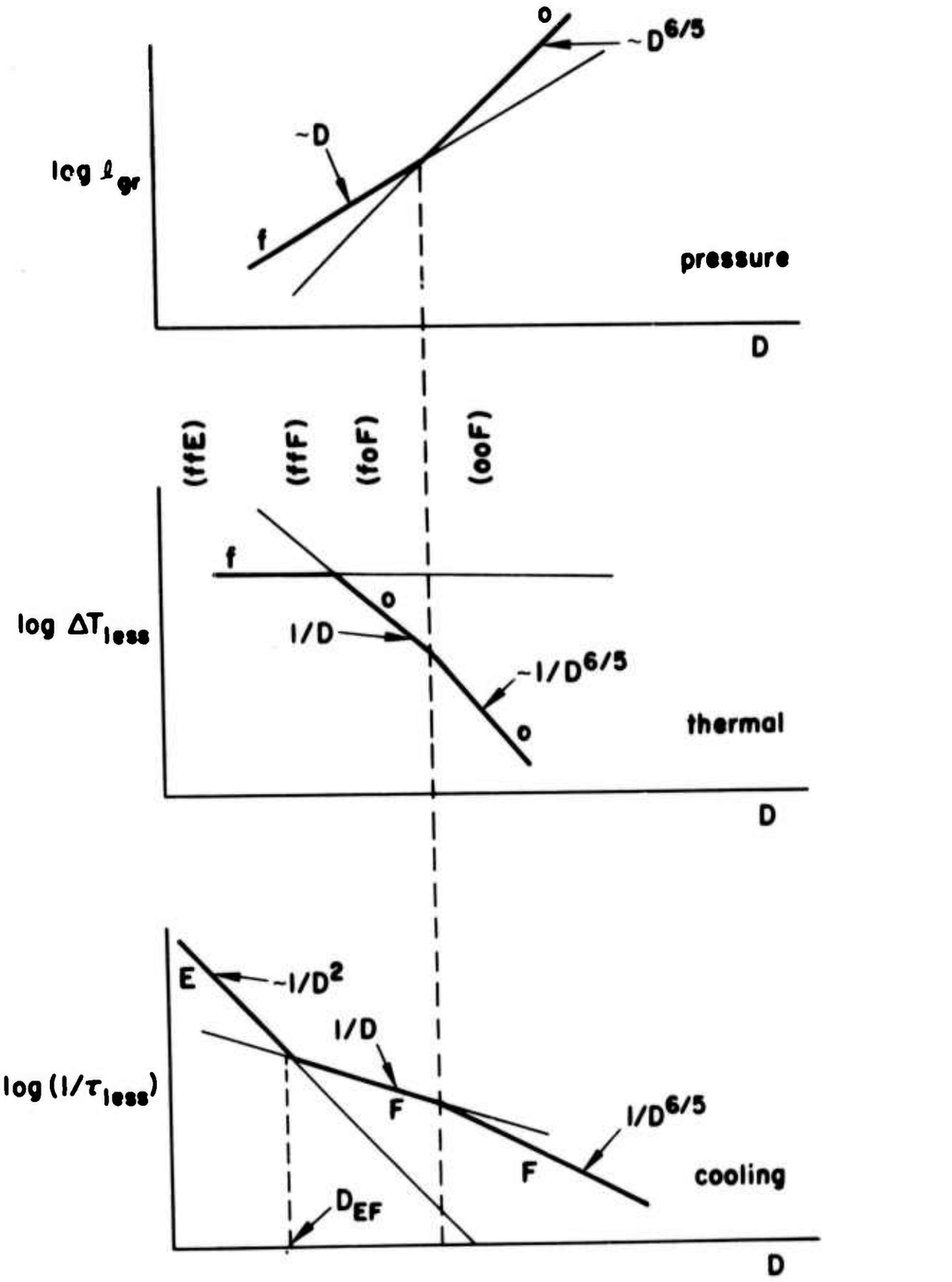

$$P_{cw} = \frac{\pi}{4} D^2 \frac{C\Delta T_{less}}{\beta \tau_{less}} \quad , \qquad \tau_{less} \rightarrow t_{pulse}$$

pulse

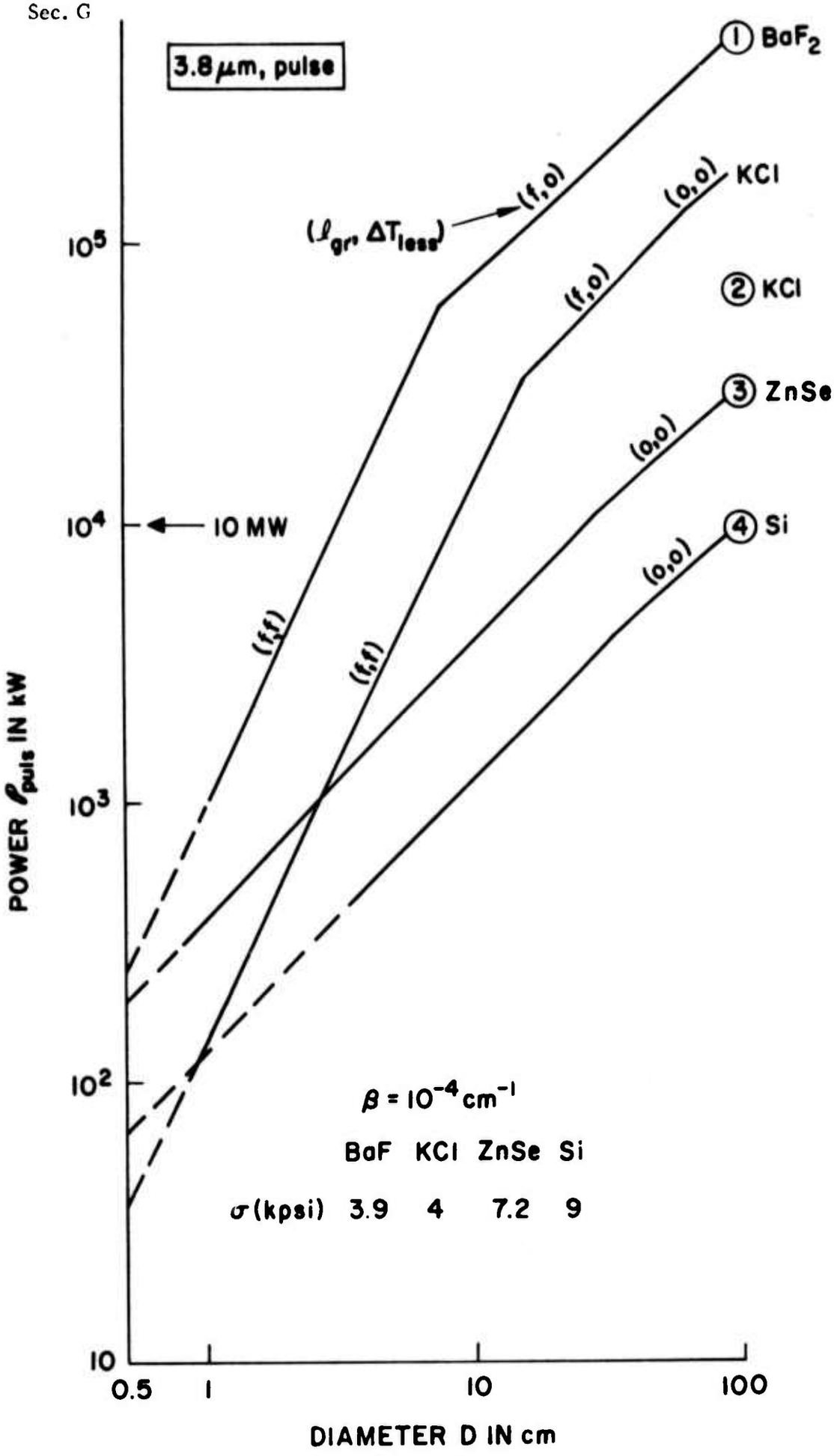
3.8 μm, pulse
① BaF2
② KCl
③ ZnSe
④ Si
(f,o)
(o,o)
(f,o)
(o,o)
(o,o)
(f,f)
(f,f)
(lgr, ΔTless)
10 MW
10^5
10^4
10^3
10^2
10
POWER Ppuls IN kW
β = 10^-4 cm^-1
BaF KCl ZnSe Si
σ (kpsi) 3.9 4 7.2 9
0.5
1
10
100
DIAMETER D IN cm

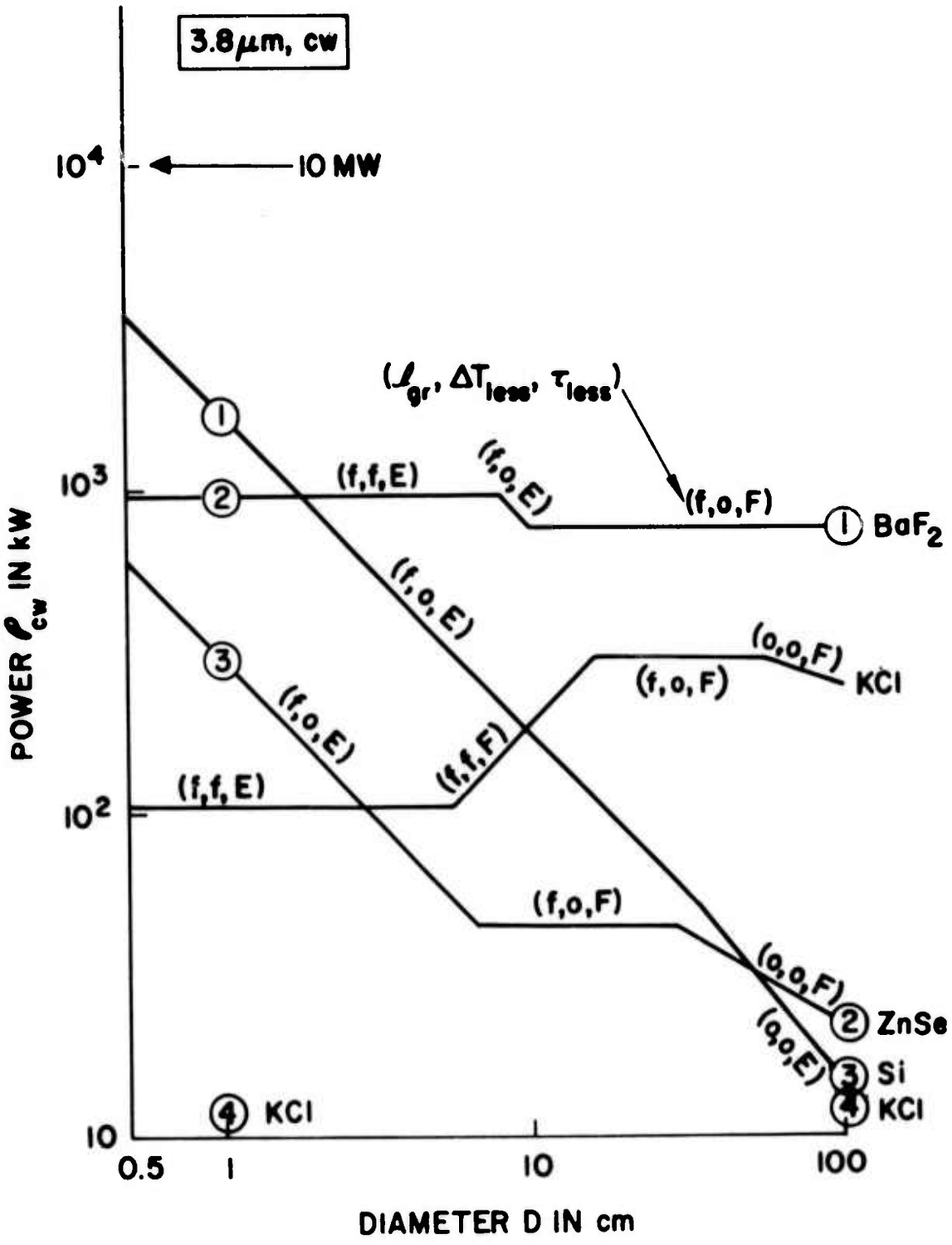
3.8μm, cw
10⁴
10 MW
10³
10²
10
POWER P_{cw} IN kW
0.5
1
10
100
DIAMETER D IN cm
$(\ell_{gr}, \Delta T_{less}, \tau_{less})$
(f,f,E)
(f,o,E)
(f,o,F)
(f,o,E)
(f,o,E)
(f,f,E)
(f,f,F)
(f,o,F)
(o,o,F)
(f,o,F)
(o,o,F)
(o,o,E)
1 BaF2
KCl
2 ZnSe
3 Si
4 KCl
4 KCl

Table Captions

Table GI. Values of material parameters used in calculating figures of merit and values of critical window diameter D_{EF}. The use of symbols, calculation schemes, and the meaning of superscripts accompanying numerical values in this and the following tables are explained in Secs. II and III. The values of the parameters are from Refs. 1-3 unless otherwise stated.

a. Values of n at $\lambda = 4\,\mu m$ are used in all calculations with the exception of TI 1173, for which the $10.6\,\mu m$ value is used.

b. In calculating ∂_{nT}, the values of $(\partial n/\partial T)_\sigma$ at $\lambda = 4\,\mu m$ are used except for MgF_2 (at $\lambda = 0.7\,\mu m$).

c. Ref. 3.

d. P. Miles, private communication.

e. Estimate.

Table GII. Figures of merit, values of thermal time constant τ_{less}, critical thickness ℓ_{gr}, temperature difference ΔT_{less}, and fracture-to-optical distortion crossover strength $\sigma_{f\text{-}o}$ for the case $\lambda = 3.8\,\mu m$ and $D = 100\,cm$. In Tables II-VI, the choice of $\beta = 10^{-4}\,cm^{-1}$ for all materials except MgO ($\beta = 8\times10^{-4}$) and Al_2O_3 ($\beta = 2\times10^{-2}\,cm^{-1}$) is explained in Sec. III.

Table GIII. Figures of merit, values of thermal time constant τ_{less}, critical thickness ℓ_{gr}, temperature difference ΔT_{less}, and fracture-to-optical distortion crossover strength $\sigma_{f\text{-}o}$ for the case $\lambda = 3.8\,\mu m$ and $D = 10\,cm$.

Table GIV. Figures of merit and related information for small-diameter ($D = 1\,cm$) windows at $\lambda = 3.8\,\mu m$.

Table Captions (Continued)

Table GV. Figures of merit, values of thermal time constant τ_{less}, critical thickness ℓ_{gr}, temperature difference ΔT_{less}, and fracture-to-optical distortion crossover strength $\sigma_{f\text{-}o}$ for the case $\lambda = 5.25\,\mu m$ and D = 100 cm.

Table GVI. Figures of merit, values of thermal time constant τ_{less}, critical thickness ℓ_{gr}, temperature difference ΔT_{less}, and fracture-to-optical distortion crossover strength $\sigma_{f\text{-}o}$ for the case $\lambda = 5.25\,\mu m$ and D = 10 cm.

Table GVII. Figures of merit calculated from the measured values of absorption coefficient β.

Table GVIII. Formulae useful for scaling θ to parameters other than D.

Table GI.

Material	n [a]	C ($J/cm^3 K$)	K (W/cm K)	σ (10^3 psi)	E (10^6 psi)	α (10^{-6}/K)	$\lvert \partial_{nT} \rvert$ [b] (10^{-6}/K)	D_{EF} (3.8 μm) (cm)	D_{EF} (5.25 μm) (cm)
Ge	4.02	1.65	0.59	13.5	14.9	5.7	320	40 (o)	37 (o)
Si	3.43	1.63	1.48	9.0	19.0	2.3	140	105 (o)	97 (o)
GaAs	3.30	1.42	0.48	20.0	12.3	5.7	160	31 (o)	29 (o)
CdTe	2.69	1.3	0.06	0.85	5.3	5.9	120	11 (f)	11 (f)
ZnSe	2.44	2.6 [c]	0.13	7.2 [d]	10.3	7.0	64	8.1 (f)	8.1 (f)
MgF_2	1.38	3.14	0.1-0.3	7.6	24.5	13.7	10	12 (f)	12 (f)
CaF_2	1.41	2.71	0.09	5.3	11.0	19.7	3.1	6.6 (f)	6.6 (f)
SrF_2	1.44	2.37	0.1 [e]	6.1	14.7	15.8	1.0	6.8 (f)	6.8 (f)
BaF_2	1.45	1.96	0.12	3.9	7.7	20.3	1.8	10 (f)	10 (f)
NaCl	1.52	1.84	0.065	0.35	5.8	44	0.66	19 (f)	19 (f)
KCl	1.47	1.35	0.065	0.33	4.3	36	4.6	19 (f)	19 (f)
MgO	1.67	3.13	0.6	20	36.1	10.5	26	23 (f)	23 (f)
Al_2O_3	1.67	3.0	0.45	65	50	5.5	16	11 (o)	9.7 (o)
TI 1173 glass	2.60	1.25 [c]	0.003	6.3	3.1	15.0	120	0.2 (f)	0.2 (f)

Table GII.

Material	τ_{less} (sec)	ℓ_{gr} (cm)	ΔT_{less} (K)	$\sigma_{f\text{-}o}$ (10^3 psi)	Bulk Absorption		Surface Absorption	
					θ_{pulse} (kW)	θ_{cw} (kW)	θ_{pulse} (kW)	θ_{cw} (kW)
Ge	860 (F)	5.0 (o)	0.030 (o)	4.3	3.8×10^3	4.5	2.0×10^4	23
Si	690 (E)	4.4 (o)	0.077 (o)	5.7	1.0×10^4	14	4.3×10^4	62
GaAs	760 (F)	5.2 (o)	0.058 (o)	4.1	6.4×10^3	8.6	3.3×10^4	44
CdTe	2,400 (F)	11 (f)	0.039 (o)	2.4	3.9×10^3	16	3.9×10^4	16
ZnSe	1,500 (F)	5.0 (o)	0.15 (o)	4.3	3.0×10^4	20	1.5×10^5	1.0×10^2
MgF_2	1,300 (F)	3.8 (f)	1.2 (o)	15	3.0×10^5	24	1.2×10^6	94
CaF_2	1,400 (F)	4.6 (f)	3.4 (o)	7.6	7.1×10^5	4.9×10^2	3.3×10^6	2.3×10^3
SrF_2	1,200 (F)	4.3 (f)	11 (o)	11	2.0×10^6	1.8×10^3	8.6×10^6	7.7×10^3
BaF_2	1,100 (F)	5.3 (f)	4.9 (o)	5.5	7.6×10^5	7.2×10^2	4.1×10^6	3.8×10^3
NaCl	6,200 (F)	18 (f)	0.69 (f)	4.1	1.0×10^5	16	1.7×10^6	2.8×10^2
KCl	4,800 (F)	18 (f)	0.57 (o)	3.4	6.0×10^4	13	1.1×10^6	2.3×10^2
MgO	830 (F)	2.6 (o)	0.70 (o)	16.0	2.2×10^4	26	4.6×10^5	5.4×10^2
Al_2O_3	700 (F)	2.3 (o)	1.3 (o)	21	1.5×10^3	2.1	6.9×10^5	1.0×10^3
TI 1173 glass	10,000 (F)	8.3 (o)	0.050 (o)	1.6	4.9×10^3	0.46	4.1×10^4	3.8

Table GIII.

Material	τ_{less} (sec)	ℓ_{gr} (cm)	ΔT_{less} (K)	$\sigma_{f\text{-}o}$ (10^3 psi)	Bulk Absorption		Surface Absorption	
					θ_{pulse} (kW)	θ_{cw} (kW)	θ_{pulse} (kW)	θ_{cw} (kW)
Ge	17 (E)	0.32 (o)	0.47 (o)	11	6.0×10^2	37	2.0×10^2	12
Si	6.9 (E)	0.35 (f)	0.96 (o)	14	1.3×10^3	1.8×10^2	4.3×10^2	62
GaAs	18 (E)	0.33 (o)	0.91 (o)	10	1.0×10^3	56	3.3×10^2	18
CdTe	140 (E)	1.1 (f)	0.34 (o)	6.0	3.5×10^2	2.5	3.9×10^2	2.9
ZnSe	100 (F)	0.39 (f)	1.9 (o)	11	3.8×10^3	38	1.5×10^3	15
MgF_2	98 (E)	0.38 (f)	11 (f)	37	2.8×10^4	2.9×10^2	1.1×10^4	1.0×10^2
CaF_2	130 (F)	0.46 (f)	12 (f)	19	2.6×10^4	2.0×10^2	1.2×10^4	94
SrF_2	100 (F)	0.43 (f)	38 (f)	23	7.0×10^4	6.8×10^2	3.0×10^4	2.9×10^2
BaF_2	100 (E)	0.53 (f)	50 (o)	14	7.6×10^4	7.9×10^2	4.1×10^4	4.2×10^2
NaCl	180 (E)	1.8 (f)	0.69 (f)	10	1.0×10^3	5.5	1.8×10^3	10
KCl	130 (E)	1.8 (f)	1.1 (f)	8.4	1.1×10^3	8.6	2.0×10^3	16
MgO	33 (E)	0.23 (f)	7.9 (o)	40	2.4×10^3	74	4.6×10^3	1.4×10^2
Al_2O_3	42 (E)	0.15 (o)	21 (o)	52	2.4×10^2	5.8	7.1×10^3	1.6×10^2
TI 1173 glass	100 (F)	0.53 (o)	0.78 (o)	40	7.7×10^2	7.4	4.1×10^2	39

Table GIV.

Material	τ_D (sec)	ℓ_{gr} (cm)	ΔT_{less} (K)	θ_{cw} bulk absorption (kW)	θ_{cw} surface absorption (kW)
Ge	0.17	0.029 (f)	5.2 (o)	3.1×10^2	11
Si	0.069	0.035 (f)	9.6 (o)	1.8×10^3	63
GaAs	0.18	0.023 (f)	13 (o)	7.6×10^2	18
CdTe	1.4	0.11 (f)	3.4 (o)	26	2.9
ZnSe	1.3	0.039 (f)	19 (o)	3.1×10^2	12
MgF_2	0.98	0.038 (f)	11 (f)	2.8×10^2	11
CaF_2	1.8	0.045 (f)	12 (f)	1.4×10^2	6.4
SrF_2	1.5	0.043 (f)	38 (f)	4.7×10^2	20
BaF_2	1.0	0.053 (f)	65 (f)	9.4×10^2	52
NaCl	1.8	0.18 (f)	0.69 (f)	5.6	1.0
KCl	1.3	0.18 (f)	1.1 (f)	8.6	1.6
MgO	0.33	0.023 (f)	26 (f)	2.5×10^2	46
Al_2O_3	0.42	0.013 (f)	120 (f)	34	86
TI 1173 glass	26	0.042 (f)	9.9 (o)	3.7	0.16

Table GV.

Material	τ_{less} (sec)	ℓ_{gr} (cm)	ΔT_{less} (K)	$\sigma_{f\text{-}o}$ (10^3 psi)	Bulk Absorption		Surface Absorption	
					θ_{pulse} (kW)	θ_{cw} (kW)	θ_{pulse} (kW)	θ_{cw} (kW)
Ge	780 (F)	4.7 (o)	0.04 (o)	4.9	5.3×10^3	6.6	2.6×10^4	31
Si	680 (F)	4.1 (o)	0.11 (o)	6.5	1.4×10^4	21	6.0×10^4	86
GaAs	710 (F)	4.8 (o)	0.08 (o)	4.7	2.4×10^3	13	4.6×10^4	64
CdTe	2,400 (F)	11 (f)	0.047 (o)	2.7	4.8×10^3	2.0	5.4×10^4	23
ZnSe	1,400 (F)	4.7 (o)	0.22 (o)	4.9	4.4×10^4	32	2.0×10^5	1.5×10^2
MgF_2	1,300 (F)	3.8 (f)	1.7 (o)	17	6.0×10^3	4.7	1.6×10^6	1.3×10^3
CaF_2	1,400 (F)	4.6 (f)	4.6 (o)	8.7	1.0×10^6	6.8×10^2	4.6×10^6	3.2×10^3
SrF_2	1,200 (F)	4.3 (f)	15 (o)	11	2.9×10^6	2.5×10^3	1.3×10^7	1.1×10^4
BaF_2	1,100 (F)	5.3 (f)	6.9 (o)	6.2	1.0×10^6	1.0×10^3	5.6×10^6	5.2×10^3
NaCl	6,200 (F)	18 (f)	0.69 (f)	4.7	1.0×10^5	16	1.7×10^6	2.7×10^2
KCl	4,800 (F)	18 (f)	0.79 (o)	3.8	8.6×10^4	17	1.5×10^6	3.2×10^2
MgO	780 (F)	2.5 (o)	1.0 (o)	18	1.7×10^3	2.2	6.3×10^5	7.9×10^2
Al_2O_3	660 (F)	2.2 (o)	1.9 (o)	24	35	5.3×10^{-2}	9.4×10^5	1.5×10^3
TI 1173 glass	9,500 (F)	7.8 (o)	0.073 (o)	1.8	7.1×10^3	0.75	5.6×10^4	5.9

Table GVI.

Material	τ_{less} (sec)	ℓ_{gr} (cm)	ΔT_{less} (K)	$\sigma_{f\text{-}o}$ (10^3 psi)	Bulk Absorption		Surface Absorption	
					θ_{pulse} (kW)	θ_{cw} (kW)	θ_{pulse} (kW)	θ_{cw} (kW)
Ge	17 (E)	0.29 (o)	0.69 (o)	12	8.6×10^2	53	2.7×10^2	16
Si	6.9 (E)	0.35 (f)	1.3 (o)	16	1.6×10^3	2.4×10^2	6.0×10^2	86
GaAs	18 (E)	0.31 (f)	1.3 (o)	12	1.5×10^3	86	4.6×10^2	24
CdTe	140 (E)	1.1 (f)	0.47 (o)	6.8	4.8×10^2	3.4	5.4×10^2	3.8
ZnSe	100 (F)	0.39 (f)	2.6 (o)	12	5.3×10^3	52	2.0×10^3	20
MgF_2	98 (E)	0.38 (f)	11 (f)	42	4.0×10^2	4.0	1.1×10^4	1.0×10^2
CaF_2	130 (F)	0.46 (f)	12 (f)	22	2.6×10^4	2.0×10^2	1.2×10^4	94
SrF_2	100 (F)	0.43 (f)	38 (f)	26	7.0×10^4	6.8×10^2	3.0×10^4	2.9×10^2
BaF_2	100 (E)	0.53 (f)	65 (f)	16	1.0×10^5	1.0×10^3	5.3×10^4	5.5×10^2
NaCl	180 (E)	1.8 (f)	0.69 (f)	12	1.0×10^3	5.5	1.7×10^3	10
KCl	130 (E)	1.8 (f)	1.1 (f)	9.6	1.1×10^3	8.6	2.0×10^3	16
MgO	33 (E)	0.23 (f)	11 (o)	46	1.8×10^3	5.5	6.3×10^3	2.0×10^2
Al_2O_3	41 (F)	0.14 (o)	30 (o)	59	5.5	0.18	9.4×10^3	2.4×10^2
TI 1173 glass	95 (F)	0.49 (o)	1.2 (o)	4.5	1.1×10^3	1.2×10^2	5.6×10^2	5.9

Table GVII.

Material	λ (μm)	Measured β (cm^{-1})	D = 10 cm		D = 100 cm	
			θ_{pulse} (kW)	θ_{cw} (kW)	θ_{pulse} (kW)	θ_{cw} (kW)
Ge	4	3.0×10^{-3}	20	0.38	1.3×10^{2}	0.15
Ge	5.25	1.8×10^{-3}	50	1.0	3.1×10^{2}	0.41
Si	5.25	5.9×10^{-3}	29	0.5	2.4×10^{2}	0.36
GaAs	4	9.0×10^{-3}	11	0.24	71	9.4×10^{-2}
CdTe	4	2.0×10^{-3}	17	0.11	2.0×10^{2}	7.8×10^{-2}
ZnSe	5.25	1.6×10^{-3}	3.3×10^{2}	3.2	2.7×10^{3}	2.0
CaF_2	5.25	5.0×10^{-4}	5.2×10^{3}	42	2.0×10^{5}	1.4×10^{2}
SrF_2	5.25	4.1×10^{-5}	1.7×10^{4}	1.6×10^{3}	7.0×10^{6}	6.1×10^{3}
BaF_2	5.25	$<3.0 \times 10^{-5}$	3.3×10^{5}	3.1×10^{3}	3.5×10^{6}	3.3×10^{2}
KCl	5.25	1.5×10^{-5}	7.5×10^{3}	28	5.6×10^{5}	1.2×10^{2}
Al_2O_3	4	4.3×10^{-2}	1.1×10^{2}	0.26	7.0×10^{2}	1.0
TI 1173 glass	4	0.20	0.38	3.7×10^{-3}	24	2.3×10^{-5}

Table GVIII.

θ \ ΔT_{less}	ΔT_f	ΔT_o	
θ_{pulse}	$\frac{\pi D^2 C \sigma}{2\beta t_{pulse} \alpha E SF}$	$\frac{\pi D^2 C \lambda}{32\beta t_{pulse} \lvert \partial_{nT} \rvert \ell_{gr}}$ (a)	
θ_{cw}	$\frac{8\pi K\sigma}{\beta \alpha E SF}$	$\frac{\pi K \lambda}{2\beta \lvert \partial_{nT} \rvert \ell_{gr}}$ (a)	$\tau_{less} = \tau_E$
	$\frac{\pi D^2 h \sigma}{2\beta \alpha E SF \ell_{gr}}$ (a)	$\frac{\pi D^2 h \lambda}{32\beta \lvert \partial_{nT} \rvert \ell_{gr}^2}$ (a)	$\tau_{less} = \tau_F$

(a) ℓ_{gr} is the greater of ℓ_f and ℓ_o; $\ell_f = 0.433 D \left(\frac{P SF}{\sigma} \right)^{1/2}$;

$\ell_o = 0.842 D \left[(n-1) \left(\frac{P}{E} \right)^2 \left(\frac{D}{\lambda} \right) \right]^{1/5}$.

H. HIGH-POWER 10.6 μm WINDOW-MATERIAL FIGURES OF MERIT WITH EDGE COOLING AND SURFACE ABSORPTION INCLUDED*

M. Sparks
Xonics, Incorporated, Van Nuys, California 91406
and
H. C. Chow
Department of Physics, University of California, Los Angeles, California 90024, and
Xonics, Incorporated, Van Nuys, California 91406

Values of the total power θ that a window can transmit under specified conditions are calculated for use as figures of merit for window materials. New features of the figures of merit are: consideration of edge as well as face cooling, treatment of surface as well as bulk absorption, use of θ rather than intensity as the figure of merit, and effects of improving materials. New results include the following: For continuous operation, large-diameter windows should be face cooled, but small-diameter windows may be edge cooled, and θ often decreases as the diameter D increases. For pulsed operation, θ increases as D increases, as intuitively expected. Values of the diameter D_{EF}, above which face cooling should be used, are surprisingly large, ranging between 7 and 20 cm, typically. For pulsed operation and for $D > D_{EF}$ in cw operation, θ is independent of thermal conductivity K, while for $D < D_{EF}$ in cw operation, $\theta \propto K$. For continuous operation with bulk absorption, a diamond window with D = 1 cm has the greatest value (θ = 0.57 MW) of the existing materials and values of D considered. If the materials are improved (absorption coefficient β reduced for ZnSe, strength σ increased for KCl, and both improvements for CdTe and KBr), 1-cm-diameter windows of ZnSe, KCl, KBr, and CdTe will transmit 0.74, 0.58, 0.51, and 0.24 MW, respectively. For one-second pulse duration, a 100-cm-diameter window of KCl transmits 67 MW for σ = 330 psi or 260 MW for σ improved to 5,100 psi.

I. INTRODUCTION

There have been extensive programs within the last three years to obtain materials for high-power infrared systems at 10.6 μm.[1] In rating window materials, previous figures of merit[2-4] have proved useful. However, studies of window materials in the 2-6 μm range[5] have revealed some new features which may be of practical importance. In the present paper these new features are incorporated to obtain figures of merit for a number of candidate materials at 10.6 μm. The new features include the following: (1) Edge cooling, as well as face cooling, is included for continuously operated (cw) systems. (2) As materials are being improved, surface absorption apparently is becoming relatively more important. Surface absorption may also be of interest in field use where contamination is likely. Thus, surface as well as bulk absorption is included. (3) The total power θ that a window can transmit under specified idealized conditions is used as the figure of merit. Use of θ, rather than intensity, is more convenient when considering the effect of changing the window diameter. (4) Effects of improving materials, particularly lowering the absorption coefficient β and increasing the strength σ, are included.

In addition to the new ratings for materials, new results include the following: (1) Edge cooling, which is technically much simpler than face cooling, is more effective than previously realized. Before the importance of thermally induced optical distortion and fracture was realized,[3] edge cooling to prevent melting was considered. Subsequently, only face cooling was considered since the temperature difference ΔT between the center and rim of a window must be kept small, and large-diameter windows, which have large values of ΔT for edge cooling, were contemplated to keep the intensity small and to avoid diffraction in long-focal

length systems. It will be shown that edge cooling can be used for surprisingly large diameters D_{EF}, ranging between 7 and 20 cm, typically. In order to obtain the greatest value of θ in a cw system, large-diameter windows ($D > D_{EF}$) should be face cooled, while small-diameter windows ($D < D_{EF}$) may be edge cooled.

(2) For pulsed operation (pulse length of the order of a second, with rapid interpulse cooling), θ increases as D increases as expected intuitively, but for continuous operation, θ often decreases as D increases. Thus, for cw systems that can tolerate small-diameter windows (without excessive diffraction, for example), there are the dual advantages of technically easier edge cooling and often greater θ. (3) For small diameters, $D < D_{EF}$, the value of θ_{cw} depends on the thermal conductivity K; whereas for $D > D_{EF}$, θ_{cw} is independent of K. (For pulse operation, θ_{pulse} is independent of K.)

In considering window materials for high-power infrared lasers, previous theoretical investigations[3,4] have established the effects of temperature gradients and pressure differentials. Briefly, as a result of the spatial inhomogeneity of the intensity of the incident laser beam, a radial temperature gradient is set up, bringing about radial gradients in the thickness and the index of refraction. The resulting optical distortion may cause significant reduction in the target intensity, especially for long-focal length systems. Optical distortion may also be caused by deformation of the window under pressure. In addition, both the temperature gradient and pressure can cause fracture of the window.

Application of these considerations to obtain figures of merit for window materials involves the following three distinct factors:

(a) Pressure-induced optical distortion and fracture are avoided by making the window thickness ℓ greater than a critical value ℓ_{gr}.

(b) Thermally induced optical distortion and fracture are avoided by keeping the temperature difference ΔT between the center and rim of the window below a critical value ΔT_{less}.

(c) The fact that ΔT must be kept below ΔT_{less} limits the total power that a window can transmit to values below a critical value $\mathcal{P}_{pulse}$ for pulse operation or $\mathcal{P}_{cw}$ for cw operation. The relation between $\mathcal{P}$ and ΔT depends on the type of operation (pulse or cw), the thermal properties of the window (heat capacity per unit volume C and thermal conductivity K), the type of heating (bulk or surface), and for cw operation, the type of cooling (edge or face cooling).

Two of the new features of the figures of merit, surface absorption and edge cooling, pertain to the relation (c) between $\mathcal{P}$ and ΔT.

II. FIGURE-OF-MERIT ANALYSIS

The figures of merit are obtained as follows:[3,4] (a) The thickness ℓ_{gr} required to withstand the given pressure P is calculated first. The thicknesses ℓ_f and ℓ_o required to withstand the pressure without fracturing the window and without causing excessive optical distortion are[4,6]

$$\ell_f/D = 0.433\ (P\,SF/\sigma)^{1/2}\ , \tag{2.1}$$

$$\ell_o/D = 0.842\ \left[(n-1)(P/E)^2(D/\lambda)\right]^{1/5}\ , \tag{2.2}$$

respectively, where σ is the window strength, P the pressure, the safety factor SF is taken as SF = 4, n is the refractive index, E the Young's modulus, and λ the optical wavelength. In order to prevent both fracture and excessive optical distortion, the thickness ℓ must be greater than both ℓ_f and ℓ_o; that is, $\ell > \ell_{gr} \equiv$ greater of ℓ_o and ℓ_f.

(b) Next, the temperature difference ΔT between the center and rim of the window that can be tolerated is calculated as follows. If ΔT exceeds ΔT_f or ΔT_o, defined as

$$\Delta T_f = 2\sigma/\alpha E\ SF\ , \qquad \Delta T_o = \lambda/8\,\ell_{gr}\,|\,\partial_{nT}\,| \tag{2.3}$$

with $\partial_{nT} \equiv (\partial n/\partial T)_\sigma + \alpha(1+\nu)(n-1) + S$, in which the derivative is taken at constant stress, α is the linear thermal expansion coefficient, ν is the Poisson ratio, and S is a small stress-optic term,[3] then the window fractures from the excessive thermal gradient or causes excessive thermally induced optical distortion,[3]

respectively. In order to prevent both of these system failures, ΔT must be smaller than both ΔT_f and ΔT_o; that is, $\Delta T < \Delta T_{less} \equiv$ lesser of ΔT_f and ΔT_o.

(c) For pulsed operation in which the heat diffusion and, therefore, the cooling are negligible during the pulse duration t_{pulse}, the temperature rise at every point is determined by the simple expression $CV = \Delta E / \Delta T$, where V is the volume, C is the heat capacity per unit volume, ΔE is the energy added, and ΔT is the temperature rise. From this expression it is easy to show[3] that for intensity $I = I_0 - \frac{2}{3}\left(\rho / \frac{1}{2} D\right)^2 I_0$, where ρ is the radial coordinate, the spatially averaged intensity $\langle I \rangle$ and ΔT are related by the expression $\langle I \rangle_{pulse} = C \Delta T / \beta t_{pulse}$. The corresponding total power $\mathcal{P}_{pulse}$ that a window can transmit in the pulse mode of operation is

$$\mathcal{P}_{pulse} = \pi \left(\frac{1}{2} D\right)^2 \langle I \rangle_{pulse} = \pi D^2 C \Delta T / 4 \beta t_{pulse} \quad . \tag{2.4}$$

A continuously operated system must be cooled, otherwise ΔT goes to infinity as t goes to infinity for fixed $\mathcal{P}_{pulse}$, as seen in (2.4). In this case, (2.4) is valid if t_{pulse} is replaced by τ_{less}, which is the time constant for cooling the window. For edge cooling, τ_{less} is the time constant τ_E for radial heat flow along the radius $\frac{1}{2} D$:

$$\tau_E = C \left(\frac{1}{2} D\right)^2 / 4 K \quad . \tag{2.5}$$

The exact value of τ_E has a weak dependence on the radial distribution of the incident intensity. The value given is for a constant intensity. For I constant

inside the circle of diameter $\frac{1}{2}$ D and zero outside this circle, the factor $\frac{1}{4}$ in τ_E is replaced by 1/2.9.[7] These results are obtained from trivial solutions to the heat-flow equation.

For face cooling, τ_{less} is the sum of the time constant for heat flow across the window thickness ℓ_{gr} plus that for removal of heat at the interface of the window and coolant:[3]

$$\tau_F = \frac{C \ell_{gr}}{h} \left(1 + \frac{h \ell_{gr}}{3K} \right) , \tag{2.6}$$

where h is the heat-transfer coefficient ($W/cm^2 K$) at the interface of the window and coolant.

In calculating the figures of merit, it is assumed that edge cooling is used if $\tau_E < \tau_F$ and that face cooling is used if $\tau_F < \tau_E$, since larger values of θ result. Accordingly, the cw figure of merit that will be used is

$$\theta_{cw} = \pi D^2 C \Delta T_{less} / 4 \beta \tau_{less} , \tag{2.7}$$

where τ_{less} = lesser of τ_E and τ_F.

The critical diameter D_{EF} that determines whether face or edge cooling is to be used is simply the solution to $\tau_E = \tau_F$. Since the factor $h \ell_{gr} / 3K$ in (2.6) is negligible in all materials considered except TI 1173 glass, this term is neglected, giving $\tau_E = C \ell_{gr} / h$. Solving for D gives

$$D_f = \frac{6.93K}{h} \left(\frac{P SF}{\sigma} \right)^{1/2} , \qquad D_o = \left[\frac{13.47 K P^2 (n-1)}{\lambda^{1/5} h E^2} \right]^{5/4} \tag{2.8}$$

for $\ell_{gr} = \ell_f$ and ℓ_o, respectively. The critical diameter D_{EF} = greater of D_f and D_o.

If the window absorbs the radiation at its surface, rather than throughout the bulk, it is easy to show that β in (2.4) and (2.7) is replaced by f/ℓ_{gr}, where f is the fraction of the incident radiation absorbed by the two surfaces. Then (2.4) and (2.7) are replaced by

$$\theta_{pulse} = \pi D^2 \ell_{gr} C \Delta T_{less} / 4 f t_{pulse} \tag{2.9}$$

and

$$\theta_{cw} = \pi D^2 \ell_{gr} C \Delta T_{less} / 4 f \tau_{less} \tag{2.10}$$

for surface absorption. Since the values of θ for surface absorption are more strongly dependent on the window size (by a factor of ℓ_{gr}) than the corresponding values for bulk absorption, θ_{cw} never decreases with increasing D, and the advantages of using large-diameter windows are greater in the case of surface absorption.

Finally, in strengthening materials there is a critical strength σ_{f-o} that is of interest. If the strength of the material σ is less than σ_{f-o}, then $\ell_{gr} = \ell_f$, and increasing the strength allows the use of thinner windows ($\ell_{gr} \sim \sigma^{-1/2}$). On the other hand, for $\sigma > \sigma_{f-o}$, $\ell_{gr} = \ell_o$. Thus, increasing σ does not allow thinner windows to be used since ℓ_o is independent of σ. The value of σ_{f-o} is obtained by equating ℓ_f and ℓ_o in (2.1) and (2.2) and solving for σ, which gives

$$\sigma_{f-o} = 0.264\ P\ SF \left[\frac{1}{n-1} \left(\frac{E}{P} \right)^2 \frac{\lambda}{D} \right]^{2/5} . \tag{2.11}$$

The principal assumptions[3,4] made in deriving (2.1)-(2.11) are now summarized: The optical system is diffraction limited before the beam is distorted

by the window, and the window distortion halves the intensity at the target. The intensity and temperature distributions across the window are radially symmetric and parabolic in the radial coordinate ρ with the edge intensity equal to one-third the center intensity. The optical calculations were made by assuming an untruncated Gaussian distribution. It is assumed that the beam is not refocused to minimize optical distortion. In practice, it is conceivable that an order of magnitude increase in intensity could be gained by refocusing.[3]

Other assumptions and approximations include the following: The window is thin (in the sense that thickness << diameter) and is made of elastically and optically isotropic material. The window diameter is taken to be equal to the diameter of the aperture of the optical system, which is focused on a distant target when the window is undistorted. In all the calculations the window is assumed to be clamped; the stress produced by window mounting and the optical distortion resulting from the static deformation of the window under its own weight are both neglected.

III. TABULATION AND DISCUSSION OF RESULTS

Values of $\mathcal{G}$, ℓ_{gr}, ΔT_{less}, τ_{less}, D_{EF}, and $\sigma_{f\text{-}o}$ are calculated using the results of Sec. 2 and listed in Tables I - IV for various materials of interest for $\lambda = 10.6\,\mu m$ and D = 1, 10, and 100 cm. Results are given for strengthened CdTe, KCl, and KBr with β lowered to $10^{-4}\,cm^{-1}$. Formulae that are useful in scaling and in visualizing the dependence of $\mathcal{G}$ on variables other than D are displayed in Table V.

It is also useful to visualize the results. Thus, Fig. H1 schematically illustrates the D dependence of ℓ_{gr}, ΔT_{less}, and $1/\tau_{less}$. The relative positions of the regions of the three curves change from material to material. The tendency for $\mathcal{G}$ to increase with increasing D caused by the explicit D^2 factor in Eqs. (2.4) and (2.7) for $\mathcal{G}$ tends to be offset by the decreasing factors ΔT_{less} and $1/\tau_{less}$ illustrated in Fig. H1. The resulting dependence of $\mathcal{G}$ and D is plotted in Figs. H2 and H3 for diamond, ZnSe, strengthened KBr, and strengthened KCl (σ = 4 k psi in both cases).

It should be emphasized that the figures of merit $\mathcal{G}$ are not the actual powers that windows in real systems can transmit. In this connection, two factors must be stressed. First, the figures of merit apply to specific and idealized conditions as summarized in Sec. 2. In spite of this qualification, it is convenient to use $\mathcal{G}$ as the figure of merit since it does give a rough idea of the power expected and the relative values of $\mathcal{G}$ for different materials are at least as useful as previous figures of merit. Second, the figures of merit are proportional to $1/\beta$ (or to $1/f$ for surface absorption). The values of $\mathcal{G}$ based on experimentally determined absorption coefficients can be drastically altered as better crystals and better measurements

become available. For this reason the values of θ for a number of materials are calculated both with the measured values of β and with $\beta = 10^{-4}\,cm^{-1}$. The latter choice is made because it is difficult to obtain materials with β less than $10^{-4}\,cm^{-1}$; it is even difficult to measure such low values. For surface absorption we use $f = 10^{-4}$. Despite the arbitrariness inherent in this set of choices, the values of θ given in Tables II-IV are useful since they can be easily scaled to any specific β (or f) by noting that $\theta \sim 1/\beta$ (or $\theta \sim 1/f$).

In the tables and figures all values are computed under the conditions $P = 14.7$ psi, $SF = 4$, $h = 10^{-2}\,W/cm^2K$, $f = 10^{-4}$, and $t_{pulse} = 1$ sec. The notation f or o designates fracture or optical distortion as the controlling factor, while F or E accompanying τ_{less} signifies face cooling or edge cooling. Values of θ in Tables II-IV were calculated using the choice of β as explained above. For figures, $\beta = 10^{-4}\,cm^{-1}$ is used for all materials except KCl ($\beta = 1.5 \times 10^{-4}\,cm^{-1}$).

In small-diameter windows, $\tau_{less}\,(=\tau_E)$ is often less than t_{pulse}, as seen in Table IV and Figs. H2 and H3, and the radial heat flow reduces the value of ΔT. Thus, the value of θ is not increased by using the pulse mode of operation in small-diameter windows. This is indicated in Fig. H2 by the dashed portions of the curves, for which $t_{pulse} > \tau_{cw}$ (so that $\theta_{pulse} < \theta_{cw}$ formally).

The dependence of θ on the thermal conductivity K is of interest. For pulse operation, thermal diffusion is assumed negligible. Thus, θ_{pulse} is independent of K, as also seen in (2.4). For cw operation of small-diameter windows ($D < D_{EF}$), the thermal time constant τ_{less} is equal to $\tau_E \sim 1/K$, from (2.5).

Thus, $\theta_{cw} \sim K$, according to (2.7). For cw operation of large-diameter windows ($D > D_{EF}$), $\tau_{less} = \tau_F$. The value of τ_F usually is controlled by the heat transfer at the window face, rather than by the heat diffusion across the window thickness. In other words, the factor $h\ell_{gr}/3K$ in (2.6) is generally less than unity, one exception being TI 1173 glass in large-diameter windows. For example, for KCl with $D = 10$ cm and $h = 10^{-2}$ W/cm^2 K, $h\ell_{gr}/3K = 9.23 \times 10^{-2}$. Thus, θ_{cw} is nearly independent of K.

Table I. Values of material parameters used in calculating figures of merit and values of critical window diameter D_{EF}. The use of symbols, calculation schemes, and the meaning of superscripts accompanying numerical values in this and the following tables are explained in Secs. 2 and 3. The values of the parameters are from Refs. 2-4 unless otherwise stated.

Material	β^{a}_{meas} (cm^{-1})	n	C (J/cm^3K)	K (W/cm K)	σ^{b} (10^3 psi)	E (10^6 psi)	$\lvert \partial_{nT} \rvert$ ($10^{-5} K^{-1}$)	α (10^{-6} K)	D_{EF} (cm)
ZnSe	2×10^{-3}	2.43	2.65	0.13	7.2 [c]	10.3 [d]	6.23	7.7	8.1 (f)
CdTe	6×10^{-4}	2.67	1.23	0.041	0.85	5.3	12.7	4.5	7.5 (f)
GaAs	5×10^{-3}	3.3	1.42	0.37	20	12.3	19.8	5.7	18 (o)
KCl	1.5×10^{-4}	1.46	1.36	0.066	0.33 [e]	4.3	0.77	36	19 (f)
KBr	9×10^{-4}	1.52	1.2	0.048	0.16 [e]	3.9	0.57	43	20 (f)
TI 1173 glass	7×10^{-3}	2.6	1.25	0.003	3 [f]	4	11.3	15	0.29 (f)
Diamond	0.05	2.42	1.56	20	1000	100	1.17	1.1	800 (o)

a. Values of β_{meas} are from E. Kuhl, Air Force Materials Lab, Wright Patterson Air Force Base, Ohio (private communication).

b. Values of σ are from F. A. Horrigan and R. I. Rudko, Raytheon Research Division, Final Report on Contract DAAH01-69-C-0038, 1969 (unpublished). The values of σ are known to vary from sample to sample and from one method of measurement to another and can be increased by over an order of magnitude in some cases by sample processing.

c. P. Miles, Raytheon Research Division (private communication).

d. Irtran-4 polycrystalline value.

e. Elastic limit.

f. Modulus of rupture (annealed); 7000 psi for tempered.

Table II. Figures of merit, values of thermal time constant τ_{less}, critical thickness ℓ_{gr}, temperature difference ΔT_{less}, and fracture-to-optical distortion crossover strength $\sigma_{f\text{-}o}$ for the case $\lambda = 10.6\,\mu m$ and $D = 100$ cm. The choice of β in Tables II-IV is explained in Sec. 3. ‖ Not generally realizable in practice for the following reasons: (a) $\Delta T = 1{,}700$ K too great; (b) bulk absorption greater than surface absorption for $f = 10^{-4}$; (c) such large D for diamond unlikely; ( ) β decreased to 10^{-4} cm^{-1}. [ ] σ increased to $\sigma_{f\text{-}o}$.

Material	β (cm^{-1})	σ (10^3 psi)	$\sigma_{f\text{-}o}$ (10^3 psi)	τ_{less} (sec)	ℓ_{gr} (cm)	ΔT_{less} (K)	Bulk Absorption $\mathcal{P}_{pulse}$ (kW)	Bulk Absorption $\mathcal{P}_{cw}$ (kW)	Surface Absorption $\mathcal{P}_{pulse}$ (kW)	Surface Absorption $\mathcal{P}_{cw}$ (kW)
ZnSe	2×10^{-3}	7.2	6.5	1.2×10^{-2} (F)	4.1 (o)	0.52 (o)	5.4×10^{3}	4.5	$\{4.4\times10^{5}\}$ b	$\{370\}$ b
ZnSe	(10^{-4})	7.2	6.5	1.2×10^{3} (F)	4.1 (o)	0.52 (o)	(1.1×10^{5})	(90)	(4.4×10^{5})	(370)
CdTe	6×10^{-4}	0.85	3.6	2.7×10^{3} (F)	11 (f)	0.092 (o)	1.5×10^{3}	0.55	1.0×10^{5}	37
CdTe	(10^{-4})	0.85	3.6	2.7×10^{3} (F)	11 (f)	0.092 (o)	(8.8×10^{3})	(3.3)	(1.0×10^{5})	(37)
CdTe	(10^{-4})	[3.6]	3.6	980 (F)	5.5 (o,f)	0.19 (o)	[(1.8×10^{4})]	[(19)]	[(1.0×10^{5})]	[(100)]
GaAs	5×10^{-3}	20	6.2	620 (F)	4.2 (o)	0.16 (o)	360	0.57	$\{7.5\times10^{4}\}$ b	$\{120\}$ b
KCl	1.5×10^{-4}	0.33	5.1	4.8×10^{3} (F)	18 (f)	0.94 (o)	6.7×10^{4}	14	1.8×10^{6}	380
KCl	1.5×10^{-4}	[5.1]	5.1	780 (F)	4.6 (o,f)	3.7 (o)	[2.6×10^{5}]	[340]	[1.8×10^{6}]	[2.3×10^{3}]
KBr	9×10^{-4}	0.16	4.5	8.9×10^{3} (F)	26 (f)	0.48 (f)	5.0×10^{3}	0.56	1.2×10^{6}	130
KBr	(10^{-4})	0.16	4.5	8.9×10^{3} (F)	26 (f)	0.48 (f)	(5.0×10^{4})	(5.1)	(1.2×10^{6})	(130)
KBr	(10^{-4})	[4.5]	4.5	800 (F)	4.9 (o,f)	4.7 (o)	[(4.4×10^{5})]	[(560)]	[(2.2×10^{6})]	[(2.7×10^{3})]
TI 1173 glass	7×10^{-3}	3	2.9	6×10^{3} (F)	6.1 (o)	0.19 (o)	2.7×10^{2}	4.5×10^{-2}	$\{1.2\times10^{5}\}$ b	$\{19\}$ b
Diamond	5×10^{-2}	10^{3}	40	49 (E)	1.7 (o)	6.9 (o)	1.7×10^{3}	34	$\{1.4\times10^{6}\}$ b,c	$\{2.8\times10^{4}\}$ b,c

Table III. Figures of merit, values of thermal time constant τ_{less}, critical thickness ℓ_{gr}, temperature difference ΔT_{less}, and fracture-to-optical distortion crossover strength $\sigma_{f\text{-}o}$ for the case $\lambda = 10.6\,\mu m$ and $D = 10\,cm$. For symbols, also see caption of Table II.

Material	β (cm^{-1})	σ (10^3 psi)	$\sigma_{f\text{-}o}$ (10^3 psi)	τ_{less} (sec)	ℓ_{gr} (cm)	ΔT_{less} (K)	Bulk Absorption $\mathcal{E}_{pulse}$ (kW)	Bulk Absorption $\mathcal{E}_{cw}$ (kW)	Surface Absorption $\mathcal{E}_{pulse}$ (kW)	Surface Absorption $\mathcal{E}_{cw}$ (kW)
ZnSe	2×10^{-3}	7.2	16	100 (F)	0.39 (f)	5.4 (o)	570	5.4	$\{4.4\times10^3\}$ [b]	$\{42\}$ [b]
ZnSe	(10^{-4})	7.2	16	100 (F)	0.39 (f)	5.4 (o)	(1.1×10^4)	(110)	(4.4×10^3)	(42)
CdTe	6×10^{-4}	0.85	9.1	150 (F)	1.1 (f)	0.92 (o)	150	0.96	$\{1.0\times10^3\}$ [b]	$\{6.6\}$ [b]
CdTe	(10^{-4})	0.85	9.1	150 (F)	1.1 (f)	0.92 (o)	(890)	(5.8)	(1.0×10^3)	(6.6)
CdTe	(10^{-4})	[9.1]	9.1	44 (F)	0.35 (f, o)	3.0 (o)	$[(2.9\times10^3)]$	[(66)]	$[(1.0\times10^3)]$	[(23)]
GaAs	5×10^{-3}	20	16	24 (E)	0.27 (o)	2.5 (o)	56	2.3	$\{750\}$ [b]	$\{31\}$ [b]
KCl	1.5×10^{-4}	0.33	13	130 (E)	1.8 (f)	1.1 (f)	760	5.9	$\{2.1\times10^3\}$ [b]	$\{16\}$ [b]
KCl	1.5×10^{-4}	[13]	13	40 (F)	0.29 (f, o)	42 (f)	$[3.0\times10^4]$	[730]	$[1.3\times10^4]$	[320]
KBr	9×10^{-4}	0.16	11	160 (E)	2.6 (f)	0.48 (f)	50	0.32	$\{1.2\times10^3\}$ [b]	$\{7.6\}$ [b]
KBr	(10^{-4})	0.16	11	160 (E)	2.6 (f)	0.48 (f)	(450)	(2.9)	(1.2×10^3)	(7.6)
KBr	(10^{-4})	[11]	11	38 (F)	0.31 (f, o)	34 (f)	$[(3.2\times10^4)]$	[(830)]	$[(9.9\times10^3)]$	[(260)]
TI1173 glass	7×10^{-3}	3	7.4	130 (F)	0.61 (f)	1.9 (o)	27	0.21	$\{1.2\times10^3\}$ [b]	$\{9.1\}$ [b]
Diamond	0.05	1000	100	0.49 (E)	0.10 (o)	110 (o)	$\{550\}$ [c]	$\{550\}$ [c]	$\{1.4\times10^4\}$ [b, c]	$\{2.8\times10^4\}$ [b, c]

Table IV. Figures of merit, values of thermal time constant τ_{less}, critical thickness ℓ_{gr}, temperature difference ΔT_{less}, and fracture-to-optical distortion crossover strength $\sigma_{f\text{-}o}$ for the case $\lambda = 10.6\,\mu m$ and D = 1 cm. For symbols, also see caption of Table II.

							Bulk Absorption		Surface Absorption	
Material	β (cm^{-1})	σ (10^3 psi)	$\sigma_{f\text{-}o}$ (10^3 psi)	τ_{less} (sec)	ℓ_{gr} (cm)	ΔT_{less} (K)	$\mathcal{P}_{pulse}$ (kW)	$\mathcal{P}_{cw}$ (kW)	$\mathcal{P}_{pulse}$ (kW)	$\mathcal{P}_{cw}$ (kW)
ZnSe	2×10^{-3}	7.2	41	1.3 (E)	0.039 (f)	45 (f)	47	37	37	29
ZnSe	(10^{-4})	7.2	41	1.3 (E)	0.039 (f)	45 (f)	(950)	(740)	(37)	(29)
CdTe	6×10^{-4}	0.85	23	1.9 (E)	0.11 (f)	9.2 (o)	15	7.9	10	5.4
CdTe	(10^{-4})	0.85	23	1.9 (E)	0.11 (f)	9.2 (o)	(88)	(47)	(10)	(5.4)
CdTe	(10^{-4})	[23]	23	1.9 (E)	0.022 (f,o)	47 (o)	[(460)]	[(240)]	[(10)]	[(5.4)]
GaAs	5×10^{-3}	20	39	0.24 (E)	0.023 (f)	29 (o)	27	27	{31} b	{31} b
KCl	1.5×10^{-4}	0.33	32	1.3 (E)	0.18 (f)	1.1 (f)	7.6	5.9	2.1	1.6
KCl	1.5×10^{-4}	[32]	32	1.3 (E)	0.018 (f,o)	100 (f)	[740]	[580]	[21]	[16]
KBr	9×10^{-4}	0.16	28	1.6 (E)	0.26 (f)	0.48 (f)	0.50	0.32	{1.2} b	{0.76} b
KBr	(10^{-4})	0.16	28	1.6 (E)	0.26 (f)	0.48 (f)	(4.5)	(2.9)	(1.2)	(0.76)
KBr	(10^{-4})	[28]	28	1.6 (E)	0.020 (f,o)	85 (f)	[(800)]	[(510)]	[(16)]	[(10)]
Ti 1173 glass	7×10^{-2}	3	19	8.1 (F)	0.061 (f)	19 (o)	2.7	0.33	{12} b	{1.4} b
Diamond	0.05	1000	250	4.9×10^{-3} (E)	6.6×10^{-3} (o)	1.7×10^{3} (o)	{8.7×10^{3}} a	{8.7×10^{3}} a	{2.9×10^{4}} a,b	{2.9×10^{4}} a,b
Diamond	0.05	1000	250	4.9×10^{-3} (E)	0.1 (f,o)	110 (o)	570	570	{2.9×10^{4}} b	{2.9×10^{4}} b

Table V. Formulae useful for scaling θ to parameters other than D.

θ \ ΔT_{less}	ΔT_f	ΔT_o	
θ_{pulse}	$\frac{\pi D^2 C \sigma}{2\beta t_{pulse} \alpha E SF}$	(a) $\frac{\pi D^2 C \lambda}{32\beta t_{pulse} \lvert \partial_{nT} \rvert \ell_{gr}}$	
θ_{cw}	$\frac{8\pi K \sigma}{\beta \alpha E SF}$	(a) $\frac{\pi K \lambda}{2\beta \lvert \partial_{nT} \rvert \ell_{gr}}$	$\tau_{less} = \tau_E$
	(a) $\frac{\pi D^2 h \sigma}{2\beta \alpha E SF \ell_{gr}}$	(a) $\frac{\pi D^2 h \lambda}{32\beta \lvert \partial_{nT} \rvert \ell_{gr}^2}$	$\tau_{less} = \tau_F$

(a) ℓ_{gr} is the greater of ℓ_f and ℓ_o; $\ell_f = 0.433 D \left(\frac{P SF}{\sigma}\right)^{1/2}$;

$\ell_o = 0.842 D \left[(n-1)\left(\frac{P}{E}\right)^2 \left(\frac{D}{\lambda}\right)\right]^{1/5}$.

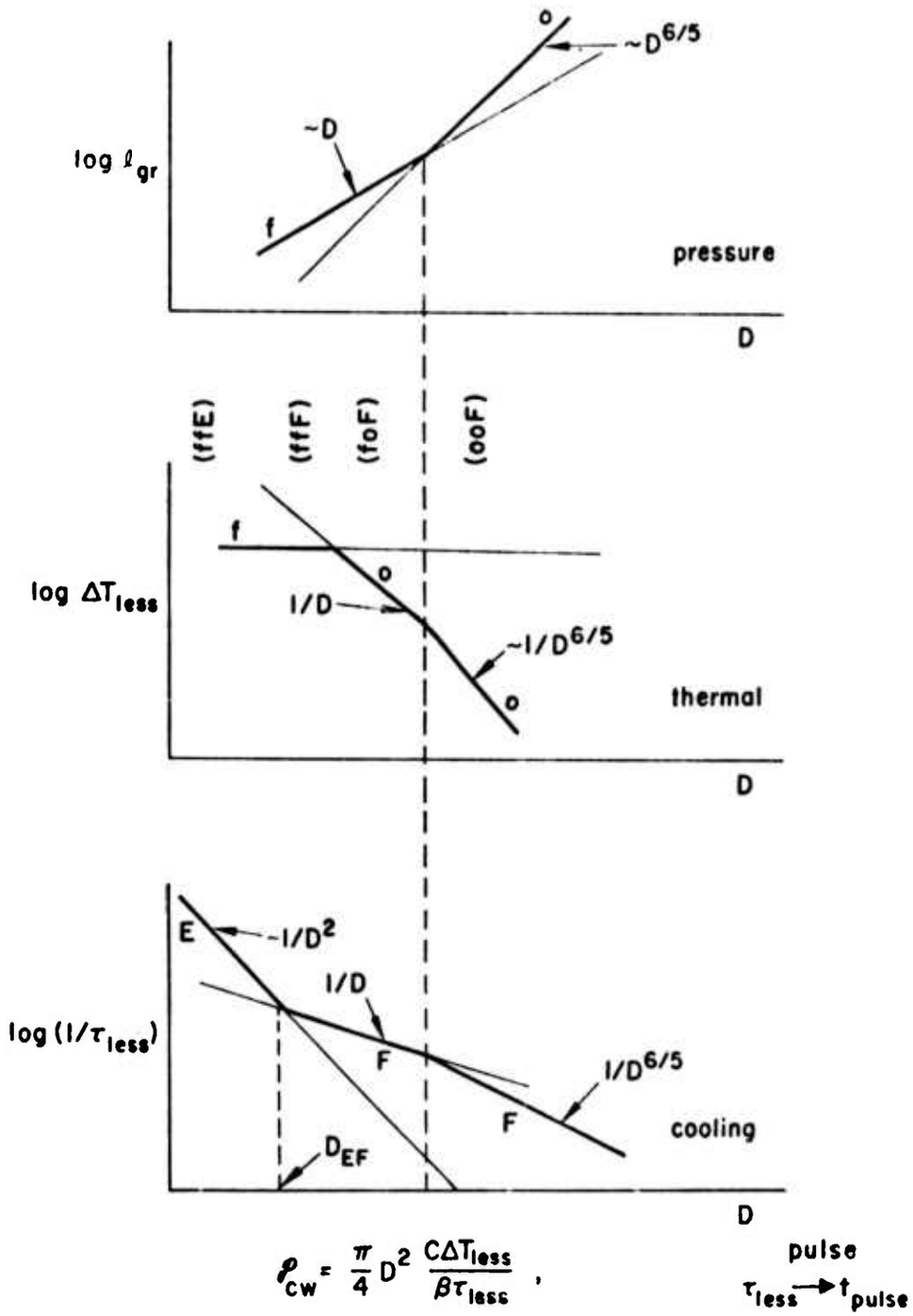

Fig. H1. Schematic illustration of the diameter dependence of thickness, temperature difference, and thermal time constant.

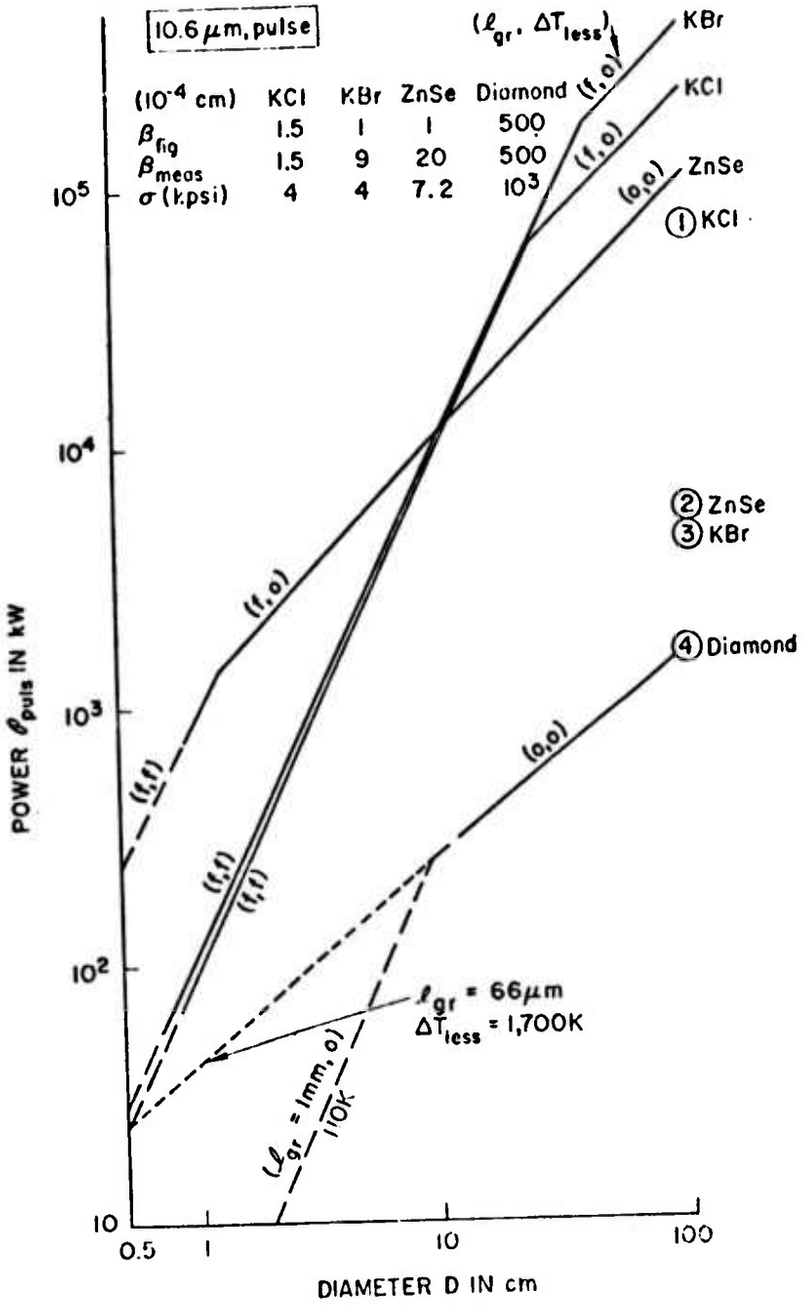

(10^{-4} cm)	KCl	KBr	ZnSe	Diamond
β_{fig}	1.5	1	1	500
β_{meas}	1.5	9	20	500
σ (kpsi)	4	4	7.2	10^3

Fig. H2. Diameter dependence of figures of merit θ_{pulse} at $\lambda = 10.6\,\mu m$. Symbols such as (f, o) in this figure and (f, o, E) in Fig. H3 denote the controlling factors for ℓ_{gr}, ΔT_{less}, and τ_{less}, respectively: o - optical distortion; f - fracture; E - edge cooling; and Γ - face cooling. Curves are for improved materials [σ = 4 kpsi for KCl and KBr, and $\beta = 10^{-4}$ cm^{-1} for all materials except KCl ($\beta = 1.5 \times 10^{-4}$ cm^{-1})], and circled numbers are for existing materials. The dashed line indicates that $\tau_{pulse} > \tau_{less}$; thus θ approaches cw value of Fig. H3.

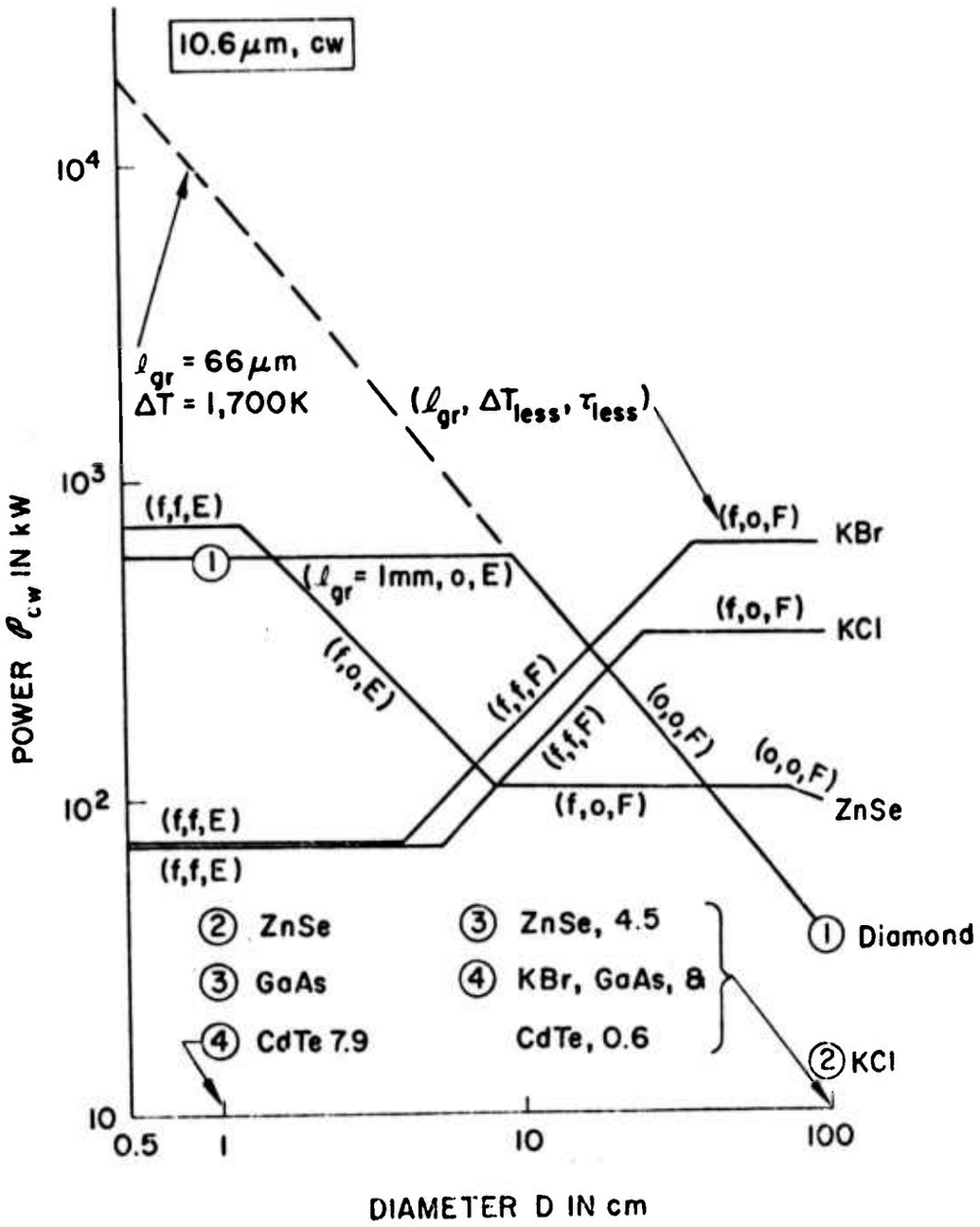

Fig. H3. Diameter dependence of figures of merit θ_{cw} at $\lambda = 10.6\,\mu m$. See caption of Fig. H2.

IV. CHOICE OF MATERIALS

Figures H2 and H3 are useful in selecting the materials with the greatest values of transmittable intensity θ. The curves are for improved materials, as indicated in the figure captions. The values of θ for currently available materials are indicated by the circled number on the figures for D = 1 and 100 cm. For example, for both cw and pulse operation with D = 100 cm, KBr and KCl are the best (highest θ) improved and available materials, while for D = 1 cm, ZnSe and diamond are the best improved and current materials. Note that diamond has a higher value of θ_{cw} than does KCl at D = 100 cm, but the cost of even a mosaic 100 cm-diameter diamond window usually is prohibitive.

The values of θ for diamond are surprisingly high in view of the large absorption, $\beta = 0.05\ cm^{-1}$, the reason being the exceptional strength ($\sigma = 10^6$ psi) and thermal conductivity (20 W/cm K). Diamonds were previously ruled out for consideration as windows because of prohibitive cost, inclusion-free requirement, difficulties associated with mosaic windows, and other reasons. However, Mr. Russell Seitz has recently emphasized that diamond windows may afford practical solutions to some window problems.[8] Apparently, 1/2 cm-diameter, inclusion-free, synthetic diamonds are available and may be useful for systems that can tolerate a small-diameter window.

The value of θ_{cw} for diamond with D = 1 cm is very large, θ = 8. MW. However, the values of ΔT_{less} = 1,700 K and ℓ_{gr} = 66 μm are unreasonable for many applications. Thus the value of θ_{cw} was recalculated for use with small-diameter windows for the case of ℓ_{gr} = 0.1 mm, which gives ΔT_{less} = 110 K, as an arbitrary reasonable choice. The values used above for D = 1 cm

are for this choice. For high-power use, removing the heat at the small edge of the window may be a problem.

Factors other than the figures of merit obviously must be considered in choosing a material for a given application. For example, if programs to obtain improvements in materials are undertaken, the expected difficulty in purifying or otherwise improving a crystal is obviously of interest, and factors such as ease of fabrication, resistance to moisture, hardness, and antireflection and protective coating must be considered. The value of ℓ_{gr} could be so great that the weight of the window could be unacceptably large, or the value of ΔT_{less} could be unacceptably high.

REFERENCES

*Research supported by Advanced Research Projects Agency of the Department of Defense and monitored by Defense Supply Service - Washington, D. C. under Contract No. DAHC15-73-C-0127.

1. See, for example, Conference on High Power Infrared Laser Window Materials, Oct. 30, 31 and November 1, 1972, C. A. Pitha, editor, AFCRL-TR-73-0372, Vols. I and II (1973).
2. F. A. Horrigan and R. I. Rudko, Raytheon Research Division Final Technical Report, Contract No. DAAH01-69-C-0038 (1969); F. A. Horrigan, C. Klein, R. Rudko, and D. Wilson, Microwaves 68 (1969); F. A. Horrigan and T. F. Deutsch, Raytheon Research Division Final Technical Report, Contract No. DAAH01-70-C-1251 (1971); T. F. Deutsch and R. I. Rudko, Raytheon Research Division Final Technical Report, Contract No. DAAH01-72-C-0194 (1973).
3. M. Sparks, J. Appl. Phys. 42, 5029 (1971).
4. M. Sparks and M. Cottis, J. Appl. Phys. 44, 787 (1973).
5. M. Sparks and H. C. Chow, J. Appl. Phys., in press.
6. Mechanical Engineers Handbook, 4th ed., edited by Lionel S. Marks (McGraw-Hill, New York, 1941), pp. 447-480.
7. M. Sparks, "Temperature and Stress Analysis for Bulk- and Surface-Heated Slabs," Parke Mathematical Laboratories TM-2 (1971) (unpublished).
8. Russell Seitz, private communication.

I. EXPLICIT EXPONENTIAL FREQUENCY DEPENDENCE OF MULTIPHONON INFRARED ABSORPTION

L. J. Sham
University of California, San Diego, La Jolla, California 92037, and
Xonics, Incorporated, Van Nuys, California 91406
and
M. Sparks
Xonics, Incorporated, Van Nuys, California 91406

The nearly exponential frequency dependence of the infrared absorption coefficient β observed by Rupprecht, Deutsch, and others has been explained previously by evaluating the individual n-phonon contributions to β, summing the results, and noting that the sum was nearly exponential over a fairly wide range of frequencies. A new derivation of the multiphonon absorption coefficient yields $\beta \sim \exp(-\omega\tau)$ directly, rather than as a sum on n, and provides a prescription for estimating the range of ω over which the nearly exponential behavior extends.

The nearly exponential frequency dependence of the infrared absorption coefficient β observed[1] in LiF, NaF, NaCl, KCl, KBr, MgF_2, CaF_2, BaF_2, SrF_2, MgO, Al_2O_3, SiO_2, TiO_2, $BaTiO_2$, and $SrTiO_2$ has been explained by a theory of multiphonon absorption in which the individual n-phonon processes were calculated, summed, and the sum observed to be a nearly exponentially decaying function of frequency ω. Since this frequency dependence of β has attracted wide attention, a derivation of the exponential dependence in closed form, rather than as a sum over the individual n-phonon contributions, is of interest. A brief description of the results was presented elsewhere[2] in connection with the temperature dependence of β.

This derivation is accomplished as follows: First, our previous approximation[3,4] of using the central-limit theorem to reduce the multiple sum over phonon coordinates to a Gaussian is not made. Rather, using a well known integral representation of the energy-conserving delta function reduces the previous expression for β to a time integral of a sum over n. This infinite sum on n is expressed as a sum of a few simple functions, which are easily integrated to give the closed-form exponential. The details are as follows.

The previous formal expression for β is[3,4] $\beta = \sum_{n=2}^{\infty} \beta_n$ with

$$\beta_n = \text{con. } f(\omega)\,\omega^{-4}\,(\Lambda_n^2/n!) \sum_{Q_1}\cdots\sum_{Q_n} \delta\Big(\omega - \sum_{j=1}^{n} \omega_{Q_j}\Big) \prod_{\ell=1}^{n} \sigma_{Q_\ell} \qquad (1)$$

where $f(\omega) = [1 - \exp(-\omega/\omega_T)]$ is very nearly independent of the laser frequency ω for most cases of interest, $\omega_T = k_B T/\hbar$, $\sigma_{Q_\ell} = W_{Q_\ell}(n_{Q_\ell}+1)\,N\,\omega_\rho/\omega_{Q_\ell}$, $\omega_\rho = \hbar/2\rho_K^2 m$, m is the reduced mass, ρ_K is the damping length in the Born-Mayer potential, W_{Q_ℓ} is a dimensionless constant that is of order unity for large ω_{Q_ℓ} and is very small for small ω_{Q_ℓ}, n_{Q_ℓ} are phonon occupation numbers, $2N$ is the number of ions in the crystal, and the higher-order terms in the perturbation expansion give rise to the vertex-correction factors

$$\Lambda_n = 1 + A_n \xi + \theta(\xi^2)\,, \qquad A_n = \sum_{m=2}^{n-1} \binom{n}{m} m^{-2} \qquad (2)$$

where $A_4 = 1.94$, $A_5 = 3.93$, $A_6 = 7.15$, $A_7 = 12.36$, and $\xi \cong 9B_0 a_0/5(1-2\rho_0)\,m\,\omega_m^2$. Here B is the bulk modulus, $\rho \equiv \rho_K/a$, the subscript 0 denotes $T = 0$, and ω_m is a frequency near the top of the phonon spectrum. Eq. (1) can be written down immediately from the well known expression[5,3,4] for β with $\omega^2 >>$ (reststrahl frequency, $\omega_f)^2$ and standard perturbation-theory results, apart from the details of Λ_n and W_{Q_ℓ} which are not needed here. In the previous calculation,[3,4] the central-limit approximation

was used to reduce the n-fold multiple sum over $Q_1 \cdots Q_n$ in (1) to a Gaussian whose position, height, and width are given by single sums over phonon coordinates. The sum of these Gaussians then gave a nearly exponential frequency dependence of β.

Representing $\delta(\omega - \Sigma \omega_{Q_j})$ by $(2\pi)^{-1} \int dt \exp(i\omega t) \Pi_j \exp(-i\omega_{Q_j} t)$ and using the approximation

$$\Lambda_n^2 / n^4 n! \cong D^n \tag{3}$$

reduces (1) to

$$\beta = [f(\omega)/2\pi\omega^4] \int_{-\infty}^{\infty} dt e^{i\omega t} \sum_{n=2}^{\infty} n^4 [g(t)]^n \tag{4}$$

where $g(t) = D \sum_Q \sigma_Q \exp(-i\omega_Q t)$. The value of D and the range of n over which (3) is valid are obtained by plotting $\ell n(\Lambda_n^2 / n^2 n!)$ as a function of n as discussed below.

In order to illustrate the central features of the calculation as simply as possible, we first approximate ω^4 by $n^4 \bar{\omega}^4$, where $\bar{\omega}$ is an average frequency having a typical value $\bar{\omega} \cong \omega_f$. Physically, the phonon driven at frequency ω decays into n phonons whose average frequency is $\bar{\omega}$. The resulting sum in (4) can be written as $\sum_{n=2}^{\infty} g^n = (1-g)^{-1} - 1 - g$. When this expression is substituted into (4), the term $(2\pi)^{-1} \int dt \exp(i\omega t)(1+g) = \delta(\omega) + N^{-1} \sum_Q W_Q (n_Q + 1) n_Q^{-1} \delta(\omega_Q - \omega)$ vanishes for $\omega > \omega_g$, where ω_g is the greatest phonon frequency. Evaluating the remaining integral $\int dt \exp(i\omega t)(1-g)^{-1}$, which has a simple pole at $t = i\tau$, where τ is the solution to $1 - g(i\tau) = 0$, gives

$$\beta = \beta_0 e^{-\tau\omega}, \qquad \beta_0 = \text{con.}\, f(\omega) [\bar{\omega}^4 \, dg(i\tau)/d\tau]^{-1}. \tag{5}$$

The equation for τ,

$$1 - D\omega_\rho N^{-1} \sum_Q W_Q (n_Q + 1) \omega_Q^{-1} \exp(\omega_Q T) = 0 \quad , \tag{6}$$

is easily solved numerically for specific cases.[6] The following approximate solution illustrates the general dependence of τ on T, Λ_n, etc., although it is too crude to afford accurate values of τ. Neglecting the angle dependence of W_Q and using the Einstein approximation $\delta(\omega - \omega_E)$ to the density of states gives

$$\tau \cong -\omega_E^{-1} \ln [6D\omega_\rho W_E (n_E + 1)/\omega_E] \quad , \tag{7}$$

$dg(i\tau)/d\tau = \omega_E$. Making these approximations to determine the value of τ is more reasonable than making the same approximation in (1). The latter gives β as a sum of delta functions. For NaCl at 300 K with $\omega_E = \omega_f$, (7) gives $\omega_f \tau = 3.4$, in fortuitously good agreement with the experimental value of 3.2 in view of the crudeness of the approximate solution (7). Other simple approximate solutions to (6) can be obtained. For example, neglecting the angle dependence of W_Q, using the truncated Debye approximation $\theta(\omega - \frac{1}{2}\omega_D)\theta(\omega_D - \omega) 3\omega_Q^2/\omega_D^3$ to the density of states (where the truncation at $\frac{1}{2}\omega_D$ accounts for the fact that W_Q is small for small ω_Q[3,4]), making the high-temperature approximation $n_Q + 1 \cong \hbar\omega_Q/k_B T$, and reinserting $\hbar\omega_D/k_B T \cong n_{\omega_D} + 1$ after integration gives

$$\tau \cong -\omega_D^{-1} \ln [6D\omega_\rho W_b (n_{\omega_D} + 1)/\omega_D] + \omega_D^{-1} \ln (\omega_D \tau/3) \tag{8}$$

which is quite similar to (7), since the last term in (8) is small, the value of $\omega_D\tau$ being approximately equal to 3 for typical cases.

It is not necessary to make the approximation $\omega = n\bar{\omega}$. The sum in (4) can be written as

$$\sum_{n=0}^{\infty} n^4 g^n = \left(g \frac{\partial}{\partial g}\right)^4 \frac{1}{1-g} = \frac{4!}{(1-g)^5} - \frac{10(3!)}{(1-g)^4} + \frac{25(2!)}{(1-g)^3} - \frac{15}{(1-g)^2} + \frac{1}{1-g} . \quad (9)$$

Each integral is evaluated by residues, which gives (5) as the leading term, with the same value of τ as before, but with

$$\beta_0 = \text{con.}\, f(\omega)[dg(i\tau)/d\tau]^{-5} . \quad (10)$$

For the Einstein approximation above, the new value of β_0 is $\text{con.}\, f(\omega)/\omega_E^5$, which is quite similar to the previous value $\beta_0 = \text{con.}\, f(\omega)/\bar{\omega}^4 \omega_E$. (If the Einstein approximation is made in evaluating $\bar{\omega}$ also, then $\bar{\omega} = \omega_E$, and the two results are identical.) The small correction terms to (10), which vanish in the limit of the single-frequency approximation discussed above, can be obtained simply in terms of cumulent moments by carrying out the straightforward details of the calculation outlined above. In this calculation, the results (9) and

$$n^4 = [(n+4)! - 10(n+3)! + 25(n+2)! - 15(n+1)! + n!]/n!$$

are useful.

It was clear from our previous analysis[3,4] that the nearly exponential dependence of β would be valid only over a limited range of frequency. The present results make it even simpler to study this range of validity. Two features of the exponential are of interest -- the overall near exponential decay, which could show local structure such as multiphonon peaks superimposed on the decay, and the smoothness (presence or lack of multiphonon peaks) of the $\beta(\omega)$ curves. The latter has been discussed previously.[3,4] Briefly, the smoothness of the phonon density of states, the phonon lifetimes, the broadening of any structure with each convolution involved in going from β_n to β_{n+1}, and the ratio of the width to

the spacing of the Gaussians obtained in applying the central-limit theorem are important in determining the smoothness of $\beta(\omega)$.

An overall exponential behavior is obtained when: (a) $\Lambda_n^2/n^4 n!$ is an exponential function of n, that is, (3) is satisfied; and (b) $f(\omega)$ is essentially independent of ω. The second condition is satisfied for most cases of interest. For example, $\omega_T = 208\,\mathrm{cm}^{-1}$ at 300 K, and $\omega_f = 164\,\mathrm{cm}^{-1}$ for NaCl at 300 K; thus $f(\omega) \cong 1 - \exp(-164n/208) \cong 1$ for $\omega = n\omega_f$ with $n \gtrsim 2$. However, for small ω and high T, $f(\omega)$ does become a nonconstant function of ω. Concerning (a), the function $\ell n(1/n^4 n!)$ is nearly linear in n over a large range of values for n, while $\ell n(\Lambda_n^2/n^4 n!)$ has a positive curvature as seen in Fig. 11. Over a limited range of n, which often includes the experimental values, $\Lambda_n^2/n^4 n!$ is nearly exponential in n; consequently β is nearly exponential in ω. For example, in Fig. 11, $\ell n(\Lambda_n^2/n^4 n!)$ is well approximated by the straight line D^n with $D = 0.130$ for $n = 3$ to 5, which is the experiment range over which the nearly exponential frequency dependence was observed.

The vertex-correction factor Λ_n^2 causes $\Lambda_n^2/n^4 n!$ to deviate above the exponential as n increases. (The corresponding increase of β above the exponential as ω is increased is not as drastic as that of $\Lambda_n^2/n^4 n!$ since β contains an explicit exponential dependence in addition to the nearly exponential term $\Lambda_n^2/n^4 n!$.) Thus, larger values of ξ give greater deviation from the exponential. The oversimplified model of Ref. 7 takes $\xi = 1$, which greatly overestimates the vertex correction and gives noticeable deviations of β from the exponential even over the small range of experimental values of n. Our estimate of $\xi = 0.18$ may even be too large.[3,8]

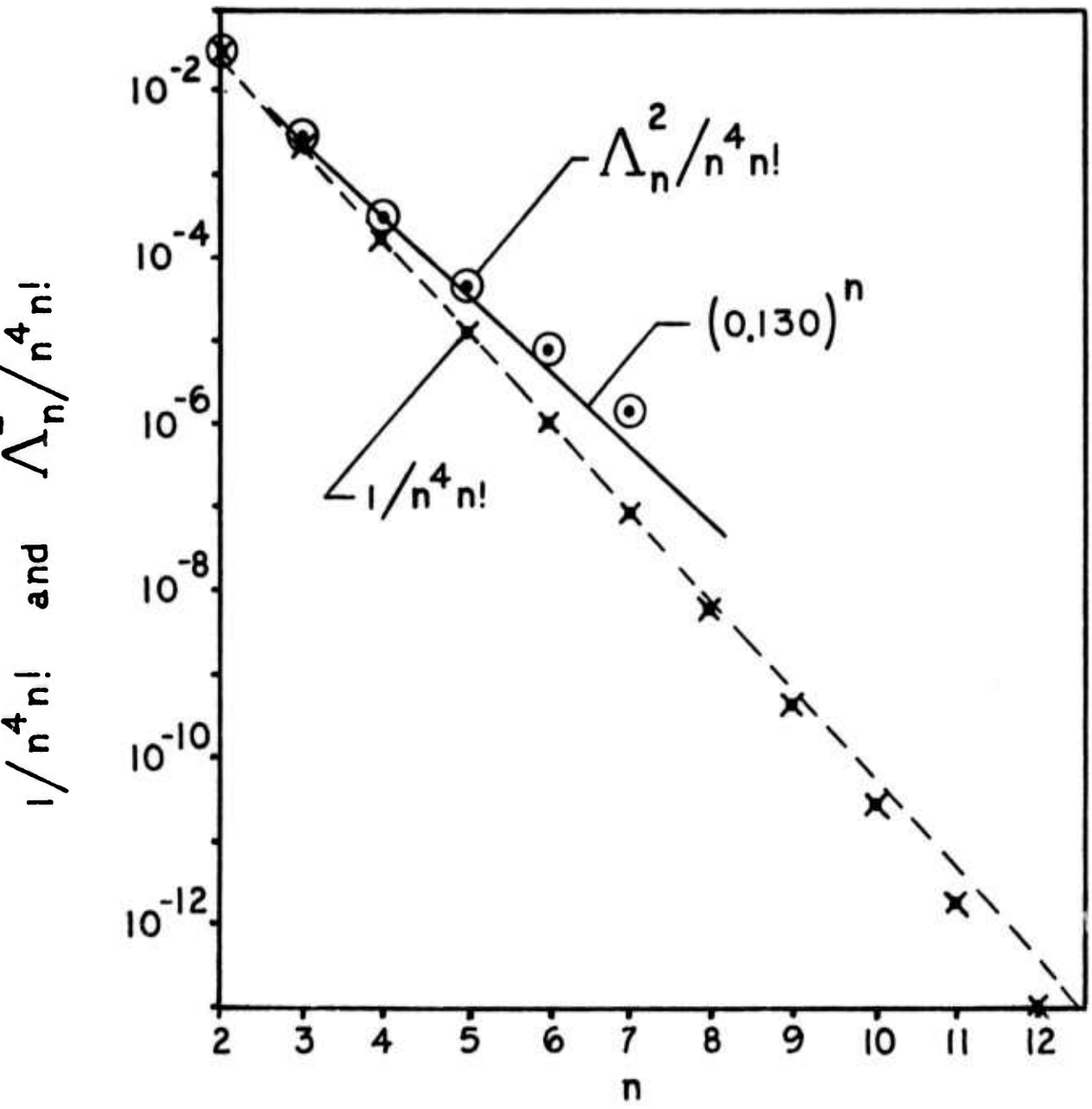

Fig. I 1. Values of $1/n^4 n!$ and $\Lambda_n^2/n^4 n!$ used in determining the range over which β decays exponentially with increasing frequency. The values of Λ_n^2 are for NaCl at 300 K, for which $\xi = 0.18$. The straight line is fit to the $1/n^4 n!$ points at small n.

The recently observed[8] deviation of the T dependence of β from the previously expected results has been explained[2] by including the T dependence of the phonon frequencies and lattice constants in our previous theory. The present result displays the temperature dependence in a much simpler form, the T dependence being contained in the two parameters β_0 and τ.

REFERENCES

*This research was supported by the Advanced Research Projects Agency of the Department of Defense and was monitored by the Defense Supply Service - Washington, D.C. under Contract No. DAHC15-73-C-0127.

1. G. Rupprecht, Phys. Rev. Letters 12, 580 (1964); T. Deutsch, to be published; American Institute of Physics Handbook, 3rd ed., Ed. D. E. Gray (McGraw-Hill, New York, 1972).

2. M. Sparks and L. J. Sham, Phys. Rev. Letters, in press.

3. M. Sparks and L. J. Sham, Solid State Commun. 11, 1451 (1972); M. Sparks and L. J. Sham, "Theory of Multiphonon Infrared Absorption," Conference on High Power Infrared Laser Window Materials, Hyannis, Massachusetts, Oct. 30-Nov. 1, 1972 (proceedings to be published by Air Force Cambridge Research Laboratories, Cambridge, Massachusetts); M. Sparks, "Recent Developments in High-Power Infrared Window Research," 4th ASTM Damage in Laser Materials Symposium, Boulder, Colorado, June 14-15, 1972; M. Sparks, "Theoretical Studies of High-Power Infrared Window Materials," Xonics, Inc. Technical Progress Reports, March and June (1972), and Final Report, December (1972), Contract No. DAHC15-72-C-0129.

4. M. Sparks and L. J. Sham, Phys. Rev., in press. This paper contains references to later studies of multiphonon absorption.

5. R. A. Cowley, Adv. in Phys. 12, 421 (1963); E. R. Cowley and R. A. Cowley, Proc. Roy. Soc. (London) A 287, 259 (1965); E. R. Cowley, J. Phys. C 5, 1345 (1970).

6. A. Karo, M. Sparks, and L. J. Sham, to be published.

7. T. C. McGill, R. W. Hellwarth, M. Mangir, and H. V. Winston, private communication.

8. J. A. Harrington and M. Hass, to be published.

J. QUASISELECTION RULE FOR INFRARED ABSORPTION BY NACL-STRUCTURE CRYSTALS*

C. J. Duthler and M. Sparks
Xonics, Incorporated, Van Nuys, California 91406

A selection rule forbids splitting of a reststrahl phonon into two phonons on the same branch. We propose that the interaction (summation or difference) of a reststrahl phonon with two acoustical or two optical phonons is much weaker than the interaction with one acoustical and one optical phonon. This quasi-selection rule is useful in explaining several multiphonon absorption results including the small number of two-phonon peaks observed in NaCl-structure crystals.

In recent theories[1-9] of the absorption of infrared radiation by alkali-halide crystals, an infrared photon is absorbed by the virtual excitation of the fundamental reststrahl mode (transverse optical phonon with $\underset{\sim}{q} \cong 0$) which decays by emitting n final-state phonons. For crystals with centers of inversion, the fundamental phonon cannot split into two final-state phonons on the same branch according to a well-known selection rule[10, 11] (matrix element identically zero). In addition, we propose the quasi-selection rule (matrix element small) that splitting (or confluence) of a fundamental phonon into two final-state phonons on the same type of branch (both optical or both acoustical) is a weak process. Relaxation of the fundamental mode by processes involving one optical and one acoustical phonon is a much stronger process.

The quasi-selection rule has a number of important consequences: (a) A distinguishing feature of absorption by NaCl-structure crystals is the small number (typically four) of secondary maxima, as opposed to zincblende-structure crystals where many distinct maxima are observed. This can be understood by considering the widely used model of the density of states with four peaks (TA, LA, TO, LO) which results in four quasi-allowed combinations. A more realistic model is discussed below. (b) The temperature dependence of the lifetime of a fundamental phonon on resonance is strongly affected by the quasi-selection rule. Decay of the fundamental mode on resonance by splitting into two acoustical phonons is weak, and the major contribution to the relaxation of this mode at room temperature is from difference processes. As the temperature is lowered below room temperature, the contributions to the relaxation from difference processes vanishes, and the temperature dependence of the fundamental-mode lifetime will be stronger than for the summation process alone. (c) The quasi-selection rule is also useful in calculating vertex corrections to n-phonon processes ($n \geq 3$) where one of the intermediate state phonons that splits from the fundamental phonon also splits into two or more phonons. In this more general case (where the initial phonon need not be a $\underset{\sim}{q} = 0$, TO phonon), the vertex is relatively large only if one of the three phonons is from an acoustical branch and the other two from optical branches. This weakens the effect of the higher-order processes and gives improved agreement between experiment and theory at high frequency.

When analyzing experimental absorption results, it has been noted that it is necessary to actually calculate the transition matrix elements rather than using the two-phonon density of states, because the transition matrix elements are

small for many regions in the Brillouin zone. Very satisfactory agreement has been achieved by detailed computer calculations of the absorption near the fundamental mode (2 phonon region).[1-5] Sparks and Sham[6] and others[7-9] have explained the exponential dependence of the absorption coefficient β on frequency ω in the multiphonon region where two or more final-state phonons are emitted.

Using the notation and results of Sparks and Sham,[6] dielectric properties as a function of frequency can be obtained from the imaginary part of the Green's function of the fundamental mode which yields the complex dielectric constant[5]

$$\epsilon = \epsilon_\infty + (\epsilon_0 - \epsilon_\infty) \frac{\omega_f^2}{\omega_f^2 - \omega^2 - i\omega_f \Gamma(\omega)} \quad , \tag{1}$$

where ϵ_0 is the static dielectric constant, ϵ_∞ is the electronic dielectric constant, ω_f is the frequency of the fundamental mode, and $\Gamma(\omega)$ is the relaxation frequency of the fundamental mode. The absorption coefficient β is obtained from ϵ using $\beta = k_0 \epsilon_\jmath / n_R$, where k_0 is the wave vector in vacuum, $\epsilon_\jmath$ is the imaginary part of ϵ, and n_R is the real part of the index of refraction $n = \epsilon^{1/2}$. Peaks in the absorption coefficient off resonance result from maxima in $\Gamma(\omega)$. Contributions to $\Gamma(\omega)$ from two-phonon summation (splitting, Γ_S) or difference processes (confluence, Γ_D) can be calculated using standard perturbation theory[12] which yields

$$\Gamma_S(\omega) = \frac{36\pi}{\hbar^2} \sum_{Q_1 Q_2} \left| \mathcal{V}_{f Q_1 Q_2} \right|^2 \Delta(q_1 + q_2)\, \delta(\omega - \omega_{Q_1} - \omega_{Q_2})\, (n_{Q_1} + n_{Q_2} + 1) \tag{2a}$$

and

$$\Gamma_D(\omega) = \frac{72\pi}{\hbar^2} \sum_{Q_1 Q_2} \left| \mathcal{V}_{f Q_1 Q_2} \right|^2 \Delta(\underset{\sim}{q}_1 - \underset{\sim}{q}_2)\, \delta(\omega + \omega_{Q_1} - \omega_{Q_2})\, (n_{Q_1} - n_{Q_2}) \tag{2b}$$

where Q_j represents the phonon mode with wavevector $\underset{\sim}{q}_j$ and branch b_j, Δ is the modified Kronecker delta which is unity when the argument is zero or a reciprocal lattice vector and zero otherwise, $\mathcal{V}_{fQ_1Q_2}$ is the transition matrix element from the interaction Hamiltonian, and n_{Q_j} is the Bose-Einstein occupation number of the mode Q_j.

Assuming nearest neighbor central forces and neglecting terms involving the second derivative of the potential energy to simplify the equations presented below (quasi-selection rule still valid including these terms), the matrix element becomes

$$\mathcal{V}_{fQ_1Q_2} = \frac{V^{(3)}}{3!} \left(\frac{\hbar}{2Nm_<} \right)^{3/2} \left(\frac{m_<}{m_r} \right)^{1/2} \alpha \quad , \tag{3a}$$

where

$$\alpha = \sum_{\gamma=1}^{6} (\hat{x} \cdot \hat{w}_f)\, U_\gamma(Q_1)\, U_\gamma(Q_2) \quad , \tag{3b}$$

with

$$U_\gamma = \hat{x}_\gamma \cdot \left[\underset{\sim}{w}_{<Q_j} - (m_</m_>)^{1/2}\, \underset{\sim}{w}_{>Q_j}\, e^{i \underset{\sim}{q}_j \cdot \underset{\sim}{x}_\gamma} \right] \quad . \tag{3c}$$

In (3), $\underset{\sim}{x}_\gamma$ is a vector from a light ion to a nearest neighbor heavy ion, $V^{(3)} = d^3V/dx_\gamma^3$ evaluated at the equilibrium lattice spacing $x_\gamma = a_{nn}$ (see Ref. 2 for details), $m_<$, $m_>$, and m_r denote the smaller, larger, and reduced ionic masses respectively; $\underset{\sim}{w}_{\tau Q}$ is a polarization vector with τ denoting smaller or larger ionic masses, and carets are used to denote unit vectors.

Because each ion in a NaCl-structure crystal occupies a site of inversion, α, hence Γ and β, are independent of the direction of $\hat{w}_f$. Choosing $\hat{w}_f = \hat{x}$ (unit vector in x direction) yields

$$\alpha = 2i\,(m_< / m_>)^{1/2} \left(w_{<qb_1x}\, w_{>qb_2x} - w_{>qb_1x}\, w_{<qb_2x} \right) \sin(q_x a_{nn}). \quad (4)$$

There are several cases where α, hence Γ and β, are small. First, for both phonons on the same branch, α is identically zero as is obvious from (4) and as has been established by group theory. Next, at the zone center and at the symmetry point X, the sine factors in α are always zero. Also at the symmetry point L, depending on the branch, either the displacement of the light or heavy ion is zero, which causes α to be zero.

To gain insight into the proposed selection rule, consider $\underset{\sim}{q}$ near the zone center. Here the polarization vectors are model independent, and the polarization vectors

$$\underset{\sim}{w}_{\tau qb} = (-1)^{\tau} \left(\frac{m_r}{m_\tau} \right)^{1/2} \hat{w}_{qb} \qquad \text{(optical)} \qquad (5a)$$

and

$$\underset{\sim}{w}_{\tau qb} = \left(\frac{m_\tau}{m_< + m_>} \right)^{1/2} \hat{w}_{qb} \qquad \text{(acoustical)} \qquad (5b)$$

can be used as a lowest order approximation.[13] When (5) is substituted into (4), α and Γ are non-zero, apart from the sine factor, only for an optical phonon plus an acoustical phonon. Two optical or two acoustical final-state phonons give zero.

Away from the center of Brillouin zone, a more realistic model must be used for the polarization vectors which forces us to consider a particular case due to the algebraic complexity of these models. To this end, published polarization vectors at 300 K obtained from the deformable dipole model of Karo and Hardy[14] were used, including the Coulomb part and second derivative terms in the potential. The particular crystal, NaI, was chosen because the various phonon branches are easily identified due to relatively large separation of the frequency dispersion curves.

In general, with the other alkali halides, branch identification is more difficult due to dispersion curve crossings, although in this case the branches can be defined in order of increasing frequency (TA-LA-TO-LA).[15] Longitudinal or transverse character and relative phase of light and heavy ions cannot be used for branch identification away from the zone center even in the case of NaI.

Relaxation frequencies in (2) were evaluated at 1000 points in the Brillouin zone keeping the contributions to Γ_S and Γ_D from the various branches distinct. Frequency delta functions in Γ were spread out into a histogram, preserving the area under the curve. The results of this calculation are shown in Fig. J1, where summation or difference processes are indicated by a plus or minus sign between the branch symbols, respectively. Above ω_f, the major contribution to Γ results from the splitting of the fundamental mode into an optical plus an acoustical phonon in agreement with the proposed selection rule. The two large maxima near 3×10^{13} sec^{-1} and 4×10^{13} sec^{-1} are from splitting into a transverse optical (TO) plus an acoustical phonon and into a longitudinal optical (LO) plus an acoustical phonon, respectively. Below ω_f, the major contributions are due to confluence processes again involving an acoustical and an optical phonon. Frequency regions where unallowed processes (two optical or two acoustical phonons) occur are denoted at the top of Fig. J1. Contributions to Γ from unallowed processes that are non-zero on the scale of the figure are denoted by double cross hatching, with two acoustical phonons making small contributions near 2×10^{13} sec^{-1} and $\omega < 0.6\times 10^{13}$ sec^{-1} in summation and difference, respectively. The fact that the unallowed processes are either unobserved on the scale of Fig. J1 or are small illustrates the validity of the quasi-selection rule.

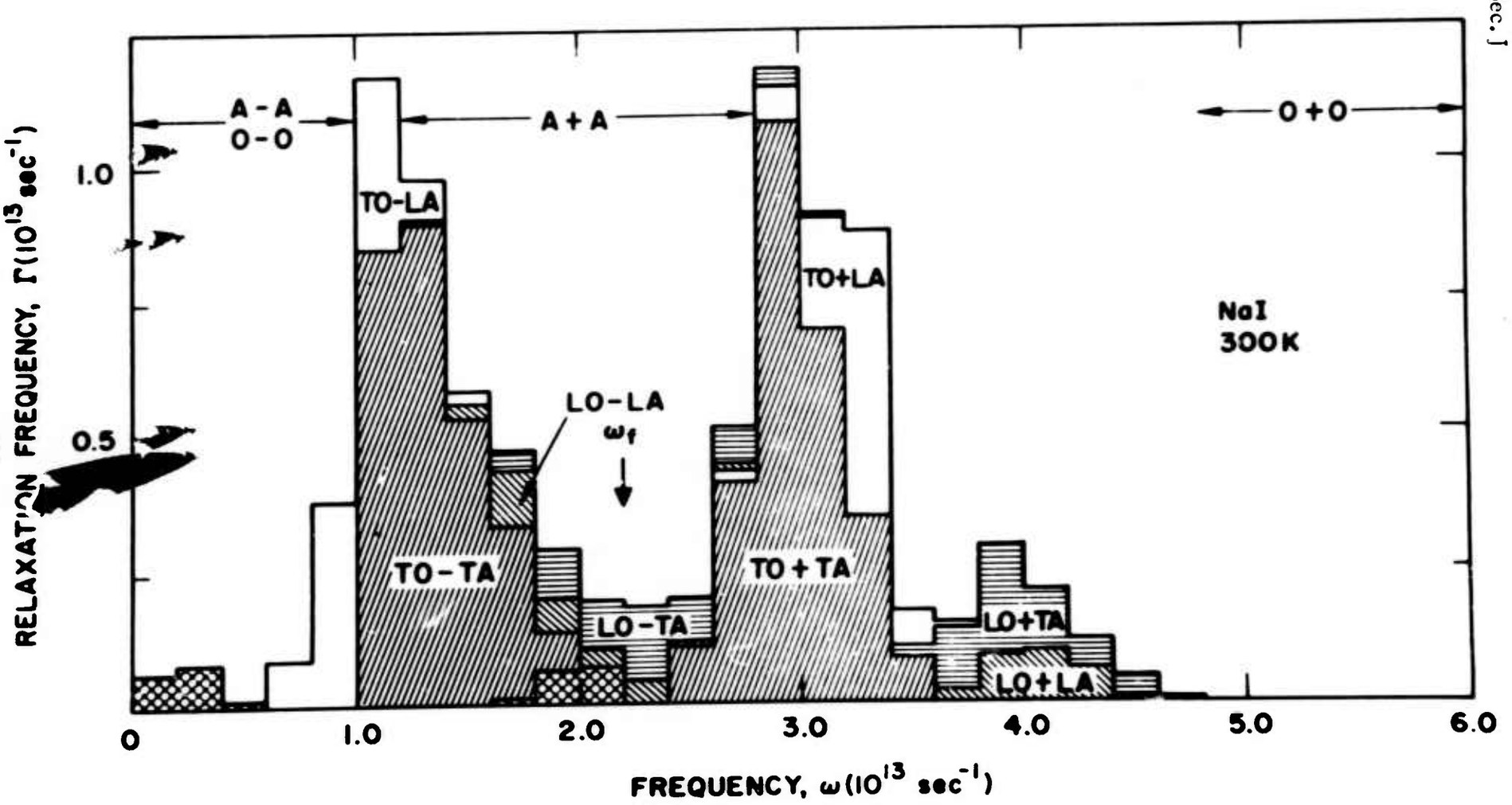

Fig. J1. Relaxation frequency of the reststrahl mode as a function of frequency. Contributions that violate the quasiselection rule are doubly cross-hatched.

The overall relaxation frequency presented in Fig. J1 is in qualitative agreement with the detailed calculations of others, establishing the essential validity of our model.[1-5] A previous, empirical selection rule that two longitudinal or two transverse phonons do not combine has been proposed on the basis of experimental results at low frequencies where only difference processes between two optical or two acoustical branches occur.[16] This is in agreement with our results at low frequency but is a misstatement of the general quasi-selection rule that is valid for the entire two-phonon region.

REFERENCES

* This research was supported by the Advanced Research Projects Agency of the Department of Defense and was monitored by the Defense Supply Service - Washington, D. C. under Contract No. DAHC15-73-C-0127.

1. J. E. Eldridge, Phys. Rev. B 6, 1510 (1972).
2. J. E. Eldridge and R. Howard, Phys. Rev. B 7, 4652 (1973).
3. A. D. Bruce, J. Phys. C 6, 174 (1973).
4. E. R. Cowley, J. Phys. C 5, 1345 (1972).
5. R. A. Cowley, Adv. Phys. 12, 421 (1963).
6. M. Sparks and L. J. Sham, Phys. Rev., in press, September 1973; Solid State Commun. 11, 1451 (1972).
7. T. McGill, R. Hellwarth, M. Mangir, and H. Winston, J. Phys. Chem. Solids, in press.
8. D. L. Mills and A. A. Maradudin, Phys. Rev., in press.
9. B. Bendow, S. C. Ying, and S. P. Yukon, Phys. Rev., in press, August 1973.
10. M. Lax and E. Burstein, Phys. Rev. 97, 39 (1955).
11. R. Loudon, Phys. Rev. 137A, 1784 (1965).
12. M. Sparks, Ferromagnetic-Relaxation Theory (McGraw-Hill, New York, 1964).
13. M. Born and K. Huang, Dynamical Theory of Crystal Lattices (Oxford, London, 1954).
14. A. M. Karo and J. R. Hardy, Phys. Rev. 129, 2024 (1963).
15. J. C. Phillips, Phys. Rev. 104, 1263 (1956).
16. R. Stolen and K. Dransfeld, Phys. Rev. 139, 1295 (1965).

K. THE ABSORPTION COEFFICIENT OF ALKALI HALIDES IN THE MULTIPHONON REGIME: EFFECTS OF NONLINEAR DIPOLE MOMENTS †

D. L. Mills and A. A. Maradudin

Department of Physics

University of California

Irvine, California 92664

and

Xonics Corporation

Van Nuys, California 91406

† This research supported by the Advanced Research Projects Agency of the Department of Defense and monitored by the Defense Supply Service, Washington, D.C. under Contract No. DAHC 15-73-C-0127.

ABSTRACT

The theory of the absorption coefficient for a model of alkali halide crystals in the multiphonon regime developed earlier by the authors is extended to incorporate the effects of a nonlinear dipole moment. The resulting expression for the absorption coefficient is evaluated for several different interatomic potential functions and choices for the nonlinear dipole moment. We suggest that the relative sign of the contributions to the absorption coefficient from crystalline anharmonicity and the nonlinear variation of the electric dipole moment with interatomic separation is such that these contributions interfere constructively in the alkali halides.

I. Introduction

In two recent papers [1,2] by the authors, a very simple model of a diatomic crystal, e.g. an alkali-halide crystal, was employed in the calculation of the frequency and temperature dependence of the absorption coefficient of such a crystal at frequencies several times (up to 7 times) its maximum vibrational frequency. In this frequency region, the principal contribution to the absorption coefficient of a pure crystal presumably is from multiphonon processes, in which the number of phonons involved is quite large.

The model employed in our work replaced the diatomic crystal consisting of N unit cells by an array of N non-interacting electric dipole active, anharmonic oscillators. By employing several potential functions for which the classical equations of motion can be solved exactly, in closed form, simple analytic expressions for the absorption coefficient could be obtained by the methods of classical physics. The results obtained for absorption by a Morse potential oscillator $\left(V(x) = D\left[1 - \exp\left(-a[x-x_o]\right)\right]^2 \right)$, and by a second potential which possesses a hard core and admits an harmonic approximation $(V(x) = (a/x^2) + b\,x^2)$, are in good qualitative and quantitative agreement with experimental data for the absorption coefficients of several alkali-halide crystals in the multiphonon regime, at elevated temperatures.[3,4]

In the crystal model just described, the electric dipole moment of each anharmonic oscillator was approximated by a linear function of the relative coordinate of the two atoms comprising it, $M(x) = qx$, where q is an effective charge. However, it is well known [5] that crystals in general, and alkali halide crystals in particular, possess contributions to their electric dipole moment which are nonlinear in the displacements of the constituent atoms or ions from their equilibrium positions. The physical origin of these nonlinear contributions is the deformation of the electronic charge density about each nucleus as it moves relative to its neighbors, when the nuclei are displaced from their equilibrium positions.[6]

In this paper, we generalize the results of our earlier work [1,2] to include the effects of the nonlinear contributions to the dipole moment of the anharmonic oscillators which form the basic elements in one simple model. For the Morse potential oscillator, when the nonlinear contribution to the electric dipole moment varies exponentially with interatomic separation, we shall see that once again we can obtain closed, exact analytic expressions for the absorption coefficient at high temperatures, where the methods of classical statistical mechanics may be used.

Earlier work has suggested [6] that in the region where the dominant contribution to the absorption coefficient comes from two phonon processes, in a number of alkali-halides, and semiconductors of the zinc blende structure, the contribution

from the presence of the nonlinear variation of the electric dipole moment interferes destructively with the part from anharmonicity in the crystal potential. We find a similar behavior for a certain choice of parameters, and since we treat both the anharmonic and the nonlinear electric dipole moment contributions to the absorption coefficient exactly for our model, we can explore the effect of this interference on the absorption coefficient for frequencies beyond the two phonon regime. We shall see that the interference between these two contributions to the absorption coefficient can have a dramatic effect on its frequency dependence in the multiphonon regime, although its temperature dependence is not affected to any appreciable extent. However, we shall argue on physical grounds that a certain parameter which enters the expression for the nonlinear electric moment should have a sign which favors constructive interference between the two contributions to the absorption coefficient.

The outline of this paper is as follows: In Section II, we obtain a general expression for the absorption coefficient for the oscillator array, in the simultaneous presence of vibrational and electrical anharmonicity, by the methods of classical statistical mechanics. In Section III, we apply this expression to the case of an oscillator described by a Morse potential. In Section IV, we present a set of numerical calculations of the absorption coefficient in the presence of the nonlinear electric dipole moment, and we discuss the results of these calculations.

II. General Theory

In this section we obtain an expression for the time and thermodynamically averaged rate at which energy is absorbed from an external ac electric field by an anharmonic diatomic molecule possessing a nonlinear dipole moment.

Our starting point is the general expression for this quantity derived in ref. 1,

$$\langle\langle \frac{d\mathcal{E}}{dt} \rangle\rangle = \frac{\beta E_o^2}{4} \int_{-\infty}^{\infty} \langle \dot{M}(o)\dot{M}(t) \rangle_o \cos\omega t \; e^{-\eta|t|} dt \; . \qquad (2.1)$$

In this equation $\beta = (k_B T)^{-1}$, where k_B is Boltzmann's constant and T the absolute temperature, E_o is the amplitude of the external electric field, which is given by $E(t) = E_o \cos \omega t$, so that ω is its frequency, and $M(t) \equiv M(x(t))$, where $M(x)$ is the dipole moment of the molecule as a function of the relative separation x of the two atoms comprising it. The limit $\eta \to o+$ is to be taken at the end of the calculation. The angular brackets in Eq. (2.1) are defined by

$$\langle A \rangle_o = \frac{1}{Z} \int_{-\infty}^{\infty} dp \int_{-\infty}^{\infty} dx \; e^{-\beta H_o} A(x,p,t) \qquad (2.2)$$

for any function A (x,p,t), where H_o is the Hamiltonian describing the relative motion of the two atoms comprising the molecule

$$H_o = \frac{p^2}{2m} + V(x) \; . \qquad (2.3)$$

Here p is the momentum conjugate to the coordinate x, and m is the reduced mass of the molecule. The partition function Z is defined by

$$Z = \int_{-\infty}^{\infty} dp \int_{-\infty}^{\infty} dx\, e^{-\beta H_o} \quad . \tag{2.4}$$

We can write the time derivative of the dipole moment as

$$\dot{M}(t) = \frac{dM(x)}{dx} \frac{dx}{dt} = \frac{1}{m} q(x(t))\, p(t), \tag{2.5}$$

where

$$q(x) \equiv \frac{dM(x)}{dx} \tag{2.6}$$

can be regarded as a position dependent effective charge.

When we substitute Eq. (2.5) into Eq. (2.1), we obtain

$$\langle\langle \frac{d\mathcal{E}}{dt} \rangle\rangle = \frac{\beta E_o^2}{4m^2} \int_{-\infty}^{\infty} \langle q(x(o))\, p(o)\, q(x(t))\, p(t) \rangle_o \times$$

$$\times \cos\omega t\, e^{-\eta|t|}\, dt \quad . \tag{2.7}$$

In refs. 1 and 2 q(x) was treated as a constant independent of x. Our task here is to rewrite Eq. (2.7) in a form well suited for its evaluation when q(x) is a nonconstant function of x.

The autocorrelation function $\langle q(x(o))\, p\,(o)\, q\,(x(t))\, p\,(t) \rangle_o$ can be written explicitly in the form

$$\langle q\ (x(o))\ p(o)q(x(t))\ p(t)\rangle_o$$

$$= \frac{1}{Z} \int_{-\infty}^{\infty} dp \int_{-\infty}^{\infty} dx\ e^{-\beta \left| \frac{p^2}{2m} + V(x) \right|_{q(x)\ p\ q\ (x(t))\ p(t)}} \quad . \tag{2.8}$$

Because the Hamiltonian is time independent, we have expressed it in terms of the values of p and x at time t = o in Eq. (2.8). Thus, here and in what follows p and x denote p(o) and x(o), respectively. In addition, as integration of the equations of motion shows, the values of the momentum and position at time t are functions of the initial values x and p, and we indicate this explicitly by writing p(t) and x(t) as p(x,p,t) and x(x,p,t), respectively.

We now rewrite Eq. (2.8) as

$$\langle q(x(o))p(o)q\ (x(t))\ p(t)\rangle_o$$

$$= \frac{1}{Z} \int_{-\infty}^{\infty} dE e^{-\beta E} \int_{-\infty}^{\infty} dp \int_{-\infty}^{\infty} dx\ \delta(E - V(x) - \frac{p^2}{2m})q(x)p \times$$

$$\times\ q(x(x,p,t))\ p(x,p,t)$$

$$= \frac{m}{Z} \int_{E_{min}}^{\infty} dE e^{-\beta E} \int_{x_1(E)}^{x_2(E)} dx \int_{-\infty}^{\infty} dp\ \frac{\delta(p - p_E) + \delta(p + p_E)}{p_E} \times$$

$$\times\ q(x)pq(x(x,p,t))p(x,p,t) \tag{2.9}$$

where

$$p_E = \left[2m\ (E - V(x))\right]^{\frac{1}{2}} \tag{2.10}$$

and $x_1(E)$ and $x_2(E)$ (with $x_1(E) \leq x_2(E)$) are the classical turning points for motion in the potential V(x), i.e., they are the solutions of

$$E = V(x) \quad . \tag{2.11}$$

We assume that the potential V(x) possesses two classical turning points for energies $E \geq E_{min}$, where E_{min} is the minimum value of V(x). The physical interpretation of p_E is that it is the momentum at t = o at the point x in a motion corresponding to the total energy E.

The integration over p in Eq.(2.9) can be carried out directly with the result that

$$\langle q(x(o))\ p(o)q(x(t))\ p(t)\rangle_o = \frac{m}{Z}\int_{E_{min}}^{\infty} dE e^{-\beta E} \times$$

$$\times\Big\{\int_{x_1(E)}^{x_2(E)} dx\ q(x)q(x(x,p_E,t))p(x,p_E,t) +$$

$$+\int_{x_2(E)}^{x_1(E)} dx\ q(x)q(x(x,-p_E,t))p(x,-p_E,t)\Big\} \quad . \tag{2.12}$$

Since the momentum at t = o for x in the interval $(x_2(E), x_1(E))$ is the negative of that at the same point in the interval $(x_1(E), x_2(E))$, because the motion reverses itself at each turning point, the expression in braces is the integral over one period of the motion beginning at $x_1(E)$, and returning to $x_1(E)$ after one period. Consequently we can rewrite Eq.(2.12) in the form

$$\langle q(x(o))p(o)q(x(t))p(t)\rangle_o = \frac{m}{Z}\int_{E_{min}}^{\infty} dE\ e^{-\beta E} \quad x$$

$$x \oint dx\ q(x)q(x(x,p_E,t))p(x,p_E t) \quad . \qquad (2.13)$$

The one-dimensional motion of a particle in a region bounded by two turning points is a periodic function of time with a period T(E) given by [7]

$$T(E) = \sqrt{2m}\int_{x_1(E)}^{x_2(E)} \frac{dx}{\sqrt{E-V(x)}} \quad . \qquad (2.14)$$

This result holds for any initial position x and momentum p_E in a motion corresponding to total energy E. Consequently $x(x,p_E,t)$ and $p(x,p_E,t)$ are periodic functions of time with period T(E), and so, therefore, is $q\ (x(x,p_E,t))$. The integral over a period in Eq.(2.13) is thus a periodic function of time with the same period, and we expand it in a Fourier series

$$\oint dx q(x)q(x(x,p_E,t))p(x,p_E,t)$$

$$= \sum_{n=-\infty}^{\infty} f_n(E)e^{-in\omega(E)t} \qquad (2.15)$$

where

$$f_n(E) = \frac{1}{T(E)}\int_o^{T(E)} dt \oint dx\ q(x)q(x(x,p_E,t))p(x,p_E,t) \quad x$$

$$xe^{in\omega(E)t} \quad , \qquad (2.16)$$

and we have defined

$$\omega(E) = \frac{2\pi}{T(E)} \quad . \tag{2.17}$$

The solution of the equation of motion for a particle moving in a one-dimensional potential is given implicitly by [7]

$$t - t_o = \left(\frac{m}{2}\right)^{\frac{1}{2}} \int_{x_1(E)}^{x} \frac{dx'}{\sqrt{E-V(x')}} \qquad x_1(E) \leq x \leq x_2(E) \tag{2.18}$$

if we measure time from the instant t_o at which the particle is at the left hand turning point $x_1(E)$. The solution of Eq. (2.18) can be written in the form

$$x_E(t) = x_1(E) + f_E(t-t_o) \quad , \tag{2.19}$$

where $f_E(t)$ is periodic in t with period T(E), is an even function of t, is even about $t = T(E)/2$, and vanishes as $t \to o$ [1]. The momentum $p_E(t)$ for the orbit of energy E is

$$p_E(t) = m \frac{d}{dt} f_E(t-t_o) = m g_E(t-t_o) \quad , \tag{2.20}$$

where $g_E(t)$ is periodic in t with period T(E), is an odd function of t, and is odd about $t = T(E)/2$.

Using these results we can rewrite Eq. (2.16) for $f_n(E)$ in the form

$$f_n(E) = \frac{1}{T(E)} \oint dx\, q(x)\, e^{in\omega(E)t_o} \times$$

$$\times \int_o^{T(E)} dt\, e^{in\omega(E)(t-t_o)}\, q\,(x_1(E) + f_E(t-t_o)) \times$$

$$\times\, m g_E(t-t_o) \quad . \tag{2.21}$$

Since $f_E(t)$ and $g_E(t)$ are periodic with period $T(E)$, and the integral on t is over a complete period, this expression becomes

$$f_n(E) = \frac{i}{T(E)} \oint dx\, q(x)\, e^{in\omega(E)t_o} \int_o^{T(E)} dt\, q(x_E(t))\, p_E(t) \quad x$$

$$x \quad \sin(n\omega(E)t), \qquad (2.22)$$

where we have used the fact that $f_E(t)$ is even and $g_E(t)$ is odd about $t = T(E)/2$. Moreover, because the integral on t is over a complete period of the motion, it is independent of the coordinate of the initial point, x.

We now convert the first integral from an integral on x into an integral on t_o

$$f_n(E) = \frac{i}{T(E)} \int_o^{-T(E)} dt_o \quad \frac{dx}{dt_o} \quad e^{in\omega(E)t_o} \int_o^{T(E)} dt\, q\, (x_E(t)) \quad x$$

$$x\, p_E(t)\, \sin\, (n\omega(E)t) \quad , \qquad (2.23)$$

where x is obtained as a function of t_o by setting $t = o$ in Eq. (2.18). If we now make the change of variable $t_o = - t$, and use the fact that $f_E(t)$ in Eq. (2.19) is an even function of t, and that $f_E(t)$ and $g_E(t)$ are even and odd, respectively, about $t = T(E)/2$, we find finally that

$$mf_n(E) = \frac{1}{T(E)}\, Q_n^2\, (E) \quad , \qquad (2.24)$$

where

$$Q_n(E) = \int_0^{T(E)} dt\; q(x_E(t))\; p_E(t)\; \sin(n\omega(E)t) \quad . \tag{2.25}$$

It should be kept in mind that the coordinate $x_E(t)$ and the momentum $p_E(t)$ appearing in Eq. (2.25) are obtained from Eq. (2.18) by setting $t_o = 0$.

If we now substitute Eqs. (2.13), (2.15), and (2.24) into Eq. (2.7), we obtain for the average rate of energy absorption by a diatomic molecule

$$\left\langle\left\langle \frac{d\mathcal{E}}{dt} \right\rangle\right\rangle = \frac{\omega\beta E_o^2}{4m^2 Z} \sum_{n=1}^{\infty} \frac{1}{n} \int_{E_{min}}^{\infty} dE\; e^{-\beta E}\; Q_n^2(E)\; \delta(\omega - n\omega(E)) \quad . \tag{2.26}$$

A quantity more closely related to experiment is obtained by multiplying Eq. (2.26) by N, the number of primitive unit cells in the crystal, dividing the result by the time averaged energy stored in the electromagnetic field, $(\epsilon_\infty V E_o^2/8\pi$, where ϵ_∞ is the optical frequency dielectric constant of the crystal and V is the crystal volume), and finally multiplying the answer by $\epsilon_\infty^{\frac{1}{2}}/c$, to obtain 1/L, where L is the absorption length, the distance over which the energy density of the incident electromagnetic wave decays to 1/e of its initial value. One obtains

$$\frac{1}{L} = \frac{2\pi\omega\hat{\rho}}{m^2 v_a\, \epsilon_\infty^{\frac{1}{2}} c}\; \frac{1}{Z} \sum_{n=1}^{\infty} \frac{1}{n} \int_{E_{min}}^{\infty} dE\; e^{-\beta E} Q_n^2\; (E)\; \delta(\omega - n\omega(E)), \tag{2.27}$$

where v_a is the volume of a primitive unit cell of the crystal. This result is the desired generalization of the results of Ref. 1, to which it reduces when $q(x) = q$, a constant.

III. Application to the Study of Multiphonon Absorption for the Case of a Morse Potential:

In order to apply the result given by Eq. (2.27) to a particular example, we have to choose not only the potential function V(x) but the functional form of the dipole moment function M(x) as well. In this paper, we will choose for V(x) the Morse potential

$$V(x) = D\left[1-\exp\left(-a[x-x_o]\right)\right]^2 \quad , \qquad (3.1)$$

because predictions based on its use have been found to be in good agreement with experiment in our earlier work.[2]

To motivate the choice of the form for M(x), we consider contributions with two distinct physical origins. The first of these is the dipole moment generated by the displacement of the two charged ions, regarded as point charges of fixed strength, from their equilibrium positions. If we consider only the part of M(x) which depends on the displacement of the ions from their equilibrium position, then this contribution to M(x) may be written

$$m_1(x) = q\ (x - x_o) \quad , \qquad (3\text{-}2)$$

where x is the separation between the ions, and x_o is the equilibrium separation.

The second contribution to the dipole moment arises from the deformation of the election charge distributions of the two

atoms as they move with respect to each other. As a result of this, the center of negative charge on each atom can be displaced with respect to its nucleus, giving rise to a dipole moment on each atom, which in the lowest approximation is linear in the relative displacement of the two atoms. It is physically reasonable to presume this contribution varies with interatomic separation in a manner similar to the repulsive term in the interatomic potential, as Szigeti has suggested. [6] (Strictly speaking, it should vary in a manner similar to the short range part of the potential which arises from overlap of the atomic cores.) With this thought in mind, the contribution to the dipole moment which results from deformation of the electron cloud will be written in the form

$$m_2(x) = qx_o m_o \left\{ e^{-sa(x-x_o)} - 1 \right\} . \qquad (3.3)$$

The parameter m_o is a measure of the strength of the nonlinear contribution to the dipole moment, and s is a measure of its spatial range. If we choose s=2, then the spatial variation of $m_2(x)$ is the same as that exhibited by the repulsive contribution to the Morse potential. We shall regard s and m_o as parameters which can vary over a considerable range.

Thus, the total dipole moment M(x) assumes the form

$$M(x) = q \left[(x-x_o) + m_o x_o \left\{ e^{-sa(x-x_o)} - 1 \right\} \right] \qquad (3.4)$$

for our model. For small values of $(x-x_o)$, M(x) may be approximated by the form

$$M(x) \simeq q\,[1-sam_o x_o]\,(x-x_o) \quad . \tag{3.5}$$

We may rewrite this result in the form

$$M(x) = e_s^*\,(x-x_o) \quad , \tag{3.6}$$

where the quantity

$$e_s^* = q\,[1 - sam_o x_o] \tag{3.7}$$

is identified as the Szigeti effective charge of the ion pair.

If we accept the preceding interpretation of the pieces $m_1(x)$ and $m_2(x)$ of the total dipole moment function $M(x)$ literally, then the charge q must be interpreted as the magnitude of the static, or valence charge on each member of the ion pair. While the quantity e_s^* defined in Eq. (3.6) is quite clearly the Szigeti effective charge by definition, we wish at this point to relax our physical interpretation of the two distinct pieces of $M(x)$, and focus our attention only on the properties of the complete function. The reason is that if we retain this interpretation, then for the simple alkali halides $q > e_s^*$, so the parameter m_o is positive. In Section IV, we shall argue that the form for $M(x)$ obtained by this means (used also in the earlier work of Szigeti) is unphysical in one sense. A physically reasonable form for $M(x)$ is obtained by choosing m_o negative; we shall see that this choice of m_o also leads to results for the frequency dependence of the absorption coefficient in the multiphonon regime consistent with the existing data. These points will be discussed in detail in Section IV. For the moment, we regard q, s and m_o as free parameters constrained in value by Eq. (3.7).

It must also be recognized that M(x) is not the electric dipole moment which couples to the macroscopic field E_o which enters in the calculation of the absorption coefficient. Rather it is the dipole moment acted upon by the local field, which differs from the macroscopic field by the addition of the Lorentz field. We can correct approximately for the neglect of the Lorentz field by noting that the relation between the Szigeti effective charge and the transverse effective charge e_T^* (which is the charge which couples to the macroscopic field) is [6]

$$e_T^* = \left(\frac{\epsilon_\infty+2}{3}\right) e_s^* \quad , \tag{3.8}$$

where ϵ_∞ is the high frequency dielectric constant. (This relation assumes the Lorentz field is $\frac{4\pi}{3}\vec{P}$, where $\vec{P}$ is the macroscopic polarization in the crystal.) Thus, if we replace M(x) by

$$M(x) = \frac{\epsilon_\infty+2}{3}\left[m_1(x) + m_2(x)\right] \quad , \tag{3.9}$$

we obtain an approximate expression for the electric dipole moment which couples to the macroscopic electric field.

The position dependent effective charge which enters the expressions in Section II is defined by

$$q(x) = \frac{dM}{dx} \tag{3.10}$$

so we have

$$q(x) = \frac{\epsilon_\infty+2}{3}\, q\left[1-sm_o a x_o e^{-sa(x-x_o)}\right] \tag{3.11a}$$

$$\equiv q_1 - q_2 \exp\left[-sa(x-x_o)\right] \quad . \tag{3.11b}$$

Note that q_1 and q_2 are related to the transverse effective charge e_T^* in a simple manner:

$$q_1 - q_2 = e_T^* \tag{3.12a}$$

We shall see shortly that the dimensionless parameter which controls the strength of the contribution to the absorption coefficient from the nonlinear electric moment relative to that from anharmonicity alone is the quantity

$$R = \frac{q_2}{e_T^*} \quad . \tag{3.12b}$$

We now turn to the derivation of the form of the absorption coefficient for the model described in the preceding paragraphs.

The solution of the equation of motion for a particle moving in a bound orbit of energy E of the Morse potential, with the particle at a classical turning point at t = o has been shown to be [1]

$$x_E(t) = x_o + \frac{1}{a} \ln \frac{D}{D-E} + \frac{1}{a} \ln \left[1 - \left(\frac{E}{D}\right)^{\frac{1}{2}} \cos\omega(E)\, t \right] \tag{3.13}$$

for $0 \le E \le D$, where

$$\omega(E) = \omega_o \left(1 - \frac{E}{D}\right)^{\frac{1}{2}} \tag{3.14}$$

and

$$\omega_o = \left(\frac{2a^2 D}{m} \right)^{\frac{1}{2}} \quad . \tag{3.15}$$

It follows that the momentum $P_E(t)$ is given by

$$p_E(t) = \frac{m}{a}\left(\frac{E}{D}\right)^{\frac{1}{2}} \omega(E)\,\frac{\sin\omega(E)t}{1 - (E/D)^{\frac{1}{2}}\cos\omega(E)t} \quad . \tag{3.16}$$

When we substitute Eq. (3.13) into Eq. (3.11), we find that the effective charge $q\ (x_E(t))$ is given by

$$q\ (x_E(t)) = q_1 - q_2\left(\frac{D-E}{D}\right)^s \frac{1}{[1-(E/D)^{\frac{1}{2}}\cos\omega(E)t]^s} \quad . \tag{3.17}$$

We turn now to the expression for the inverse absorption length given by Eq. (2.27). For the Morse potential $E_{min} = 0$. Then if we use the approximation [2]

$$Z = \frac{2\pi}{\omega_o\beta} \quad , \tag{3.18}$$

and make the change of variable

$$\xi = \frac{E}{D} \quad , \tag{3.19}$$

we obtain

$$\frac{1}{L} = \frac{\omega\omega_o\beta^2 D}{m^2 v_a \zeta_\infty^2 c}\sum_{n=1}^{\infty}\frac{1}{n}\int_o^{\infty} d\xi\ e^{-\beta D\xi}\ Q_n^2\ (D\xi)\,\delta(\omega - n\omega(D\xi)) \quad . \tag{3.20}$$

Combining Eqs. (3.14) and (3.19) we find that

$$\delta(\omega - n\omega(D\xi)) = \frac{2\omega}{n^2\omega_o^2}\,\delta(\xi - \xi_o) \quad , \tag{3.21}$$

where

$$\xi_o = 1 - \frac{\omega^2}{n^2\omega_o^2} \quad . \tag{3.22}$$

It follows that

$$\frac{1}{L} = \frac{2}{m^2}\,\frac{\omega^2}{\omega_o}\,\frac{\beta^2 D}{\epsilon_a^{\frac{1}{2}}\epsilon_\infty^{\frac{1}{2}} c}\sum_{n=\left[\frac{\omega}{\omega_o}\right]+1}^{\infty}\frac{1}{n^3}\,e^{-\beta D\xi_o}\,Q_n^2\,(D\xi_o)\,. \tag{3.23}$$

In writing this expression we have used the notation that [x] is the largest integer contained in x. The restriction on the summation in Eq. (3.23) stems from the condition that the total energy of the vibrational motion E be less than the dissociation energy D of the molecule. According to Eq. (3.19) this requires that ξ_o defined by Eq. (3.22) satisfy the condition $0 \le \xi_o < 1$.

The function $Q_n(E)$ is now obtained by substituting Eqs. (3.16) and (3.17) into Eq. (2.25):

$$Q_n(E) = \frac{mq_1}{a}\left(\frac{E}{D}\right)^{\frac{1}{2}}\omega(E)\int_o^{2\pi/\omega(E)} dt\,\frac{\sin\omega(E)t\,\sin n\omega(E)t}{1-\left(\frac{E}{D}\right)^{\frac{1}{2}}\cos\omega(E)t} -$$

$$-\frac{mq_2}{a}\left(\frac{E}{D}\right)^{\frac{1}{2}}\left(\frac{D-E}{D}\right)^{s}\omega(E)\int_o^{2\pi/\omega(E)} dt\,\frac{\sin\omega(E)t\,\sin n\omega(E)t}{\left[1-\left(\frac{E}{D}\right)^{\frac{1}{2}}\cos\omega(E)t\right]^{s+1}}\,. \tag{3.24}$$

Thus we can write $Q_n(D\xi)$ in the form

$$Q_n(D\xi) = \frac{mq_1}{a}\,\xi^{\frac{1}{2}}\,I_n(\xi) - \frac{mq_2}{a}\,\xi^{\frac{1}{2}}\,(1-\xi)^s\,J_n(\xi) \tag{3.25}$$

where

$$I_n(\xi) = \int_o^{2\pi} dx\,\frac{\sin x \sin nx}{1-\xi^{\frac{1}{2}}\cos x} \tag{3.26a}$$

$$J_n(\xi) = \int_0^{2\pi} dx \, \frac{\sin x \sin nx}{[1-\xi^{\frac{1}{2}}\cos x]^{s+1}} \quad . \tag{3.26b}$$

The inverse absorption length can then be put in the form

$$\frac{1}{L} = \frac{2}{a^2} \, \frac{\omega^2}{\omega_o} \cdot \frac{\xi^2 D}{v_a \epsilon_\infty^{\frac{1}{2}} c} \sum_{(n=[\frac{\omega}{\omega_o}]+1)}^{\infty} \frac{1}{n^3} \, e^{-\beta D \xi_o} \, \xi_o I_n^2(\xi_o) \quad \times$$

$$\times \left\{ e_T^* + q_2 \left[1 - (1-\xi_o)^s \frac{J_n(\xi_o)}{I_n(\xi_o)} \right] \right\}^2 , \tag{3.27}$$

where we have used Eq. (3.12). The second term in braces describes the effects of the nonlinear dipole moment.

The integral $I_n(\xi)$ has already been evaluated [1], with the result that

$$I_n(\xi) = \frac{2\pi}{\xi^{\frac{1}{2}}} \left[\frac{1 - \sqrt{1-\xi}}{\xi^{\frac{1}{2}}} \right]^n \quad . \tag{3.28}$$

To evaluate $J_n(\xi)$, we first integrate by parts to obtain

$$J_n(\xi) = \frac{2n}{s\xi^{\frac{1}{2}}} \int_0^{\pi} dx \, \frac{\cos nx}{[1 - \xi^{\frac{1}{2}}\cos x]^s}$$

$$= \frac{2n}{s\xi^{\frac{1}{2}}} \, \frac{1}{\Gamma(s)} \int_0^{\pi} dx \cos nx \int_0^{\infty} dt \, t^{s-1} \, e^{-t(1-\xi^{\frac{1}{2}}\cos x)}$$

$$= \frac{2n}{s\xi^{\frac{1}{2}}} \, \frac{\pi}{\Gamma(s)} \int_0^{\infty} dt \, t^{s-1} \, e^{-t} \, I_n(\xi^{\frac{1}{2}} t) \quad , \tag{3.29}$$

where $I_n(x)$ is a modified Bessel function of the first kind. Thus we obtain finally that [8]

$$J_n(\xi) = 2n\pi \frac{\Gamma(s+n)}{\Gamma(s+1)} \frac{1}{\xi^{\frac{1}{2}}(1-\xi)^{\frac{1}{2}s}} P_{s-1}^{-n}\left(\frac{1}{\sqrt{1-\xi}}\right) , \tag{3.30}$$

where $P_\nu^\mu(z)$ is an associated Legendre function of the first kind. Since n is an integer, we have the relation (9)

$$P_\nu^{-n}(z) = \frac{\Gamma(\nu-n+1)}{\Gamma(\nu+n+1)} P_\nu^n(z) , \tag{3.31}$$

which enables us to rewrite Eq. (3.30) in the alternative form

$$J_n(\xi) = 2n\pi \frac{\Gamma(s-n)}{\Gamma(s+1)} \frac{1}{\xi^{\frac{1}{2}}(1-\xi)^{\frac{1}{2}s}} P_{s-1}^{n}\left(\frac{1}{\sqrt{1-\xi}}\right) \tag{3.32}$$

which may be more convenient in certain contexts.

If we substitute Eqs. (3.28) and (3.30) into Eq. (3.27), and use the definition, Eq. (3.22), we obtain

$$\frac{1}{L} = \frac{8\pi^2}{a^2} \frac{\omega^2}{\omega_o} \frac{\beta^2 D}{v_a \epsilon_\infty^{\frac{1}{2}} c} \sum_{n=[\frac{\omega}{\omega_o}]+1} \frac{1}{n^3} e^{-\frac{D}{k_B T}\left(1-\frac{\omega^2}{n^2\omega_o^2}\right)} \times$$

$$\times \left(\frac{n\omega_o-\omega}{n\omega_o+\omega}\right)^n \left\{e_T^* + q_2\left[1 - \frac{n\Gamma(s+n)}{\Gamma(s+1)} \times\right.\right.$$

$$\left.\left. \times\left(\frac{\omega}{n\omega_o}\right)^s \left(\frac{n\omega_o+\omega}{n\omega_o-\omega}\right)^{n/2} P_{s-1}^{-n}\left(\frac{n\omega_o}{\omega}\right)\right]\right\}^2 . \tag{3.32}$$

In the present context a convenient representation for $P_{s-1}^{-n}(n\omega_o/\omega)$ is (10) .

$$P^{-n}_{s-1}\left(\frac{n\omega_o}{\omega}\right) = \frac{1}{\Gamma(n+1)}\left(\frac{n\omega_o-\omega}{n\omega_o+\omega}\right)^{\frac{n}{2}}\left(\frac{n\omega_o+\omega}{2\omega}\right)^{s-1} \times$$

$$\times F\left(1-s,\ n+1-s;\ n+1;\ \frac{1-\frac{\omega}{n\omega_o}}{1+\frac{\omega}{n\omega_o}}\right) , \qquad (3.33)$$

where F (a,b;c;x) is Gauss' hypergeometric function. With the aid of this result we obtain finally

$$\frac{1}{L} = \frac{8\pi^2}{a^2}\frac{\omega^2}{\omega_o}\frac{\beta^2 D}{\nu_a \epsilon_\infty^{\frac{1}{2}} c}\sum_{n=\left[\frac{\omega}{\omega_o}\right]+1}^{\infty}\frac{1}{n^3}\, e^{-\frac{D}{k_B T}\left(1-\frac{\omega^2}{n^2\omega_o^2}\right)} \times$$

$$\times \left(\frac{n\omega_o-\omega}{n\omega_o+\omega}\right)^{n}\left\{ e_T^* + q_2\left[1-\frac{\Gamma(s+n)}{\Gamma(s+1)\Gamma(n+1)}\left(\frac{\omega}{\omega_o}\right)\times\right.\right.$$

$$\left.\left.\times\left(\frac{n\omega_o+\omega}{2n\omega_o}\right)^{s-1} F\left(1-s,n+1-s;n+1;\ \frac{n\omega o-\omega}{n\omega o+\omega}\right)\right]\right\}^2 . \qquad (3.34)$$

When s vanishes,

$$F\left(1,n+1;n+1;\ \frac{n\omega_o-\omega}{n\omega_o+\omega}\right) = \frac{1}{2}\left(1+\frac{n\omega_o}{\omega}\right) ; \qquad (3.35)$$

when s is a positive integer, F(1-s, n+1-s; n+1;z) is a polynomial in z of degree s-1; when s is half an odd integer F(1,n+1-s;n+1;z) can be expressed in terms of complete elliptic integrals of the first and second kinds.

In terms of the parameter $R = q_2/e_T^*$ introduced earlier in Eq. (3.12b), Eq. (3.34) may be written in the form

$$\frac{1}{L} = \frac{8\pi^2}{a^2}\ \frac{\omega^2}{\omega_o}\ \frac{\beta^2 D}{v_a \epsilon_\infty^{\frac{1}{2}} C}\ e_T^{*\,2} \sum_{n=[\frac{\omega}{\omega_o}]+1}^{\infty} \frac{\exp\left[-\beta D\left(1 - \frac{\omega^2}{n^2\omega_o^2}\right)\right]}{n^3}$$

$$\times \left(\frac{n\omega_o - \omega}{n\omega_o + \omega}\right)^n \left\{1 + R\left[1 - \frac{\Gamma(s+n)}{\Gamma(s+1)\Gamma(n+1)}\left(\frac{\omega}{\omega_o}\right) \times\right.\right.$$

$$\left.\left. \times \left(\frac{n\omega_o + \omega}{2n\omega_o}\right)^{s-1} F\left(1-s, n+1-s; n+1; \frac{n\omega_o - \omega}{n\omega_o + \omega}\right)\right]\right\}^2 . \qquad (3.36)$$

In the limit R→0, the expression in Eq. (3.36) reduces to that employed in our earlier work [2]. Upon utilizing the form of the hypergeometric function valid for s=o given in Eq. (3.35), one sees that as s→o, we also recover our former result, as physical considerations demand.

IV. Results and Discussion

We have carried out a series of numerical calculations of the frequency and temperature dependence of the absorption coefficient in the presence of the nonlinear electric dipole moment. In these calculations, we evaluate the expression for the absorption length given in Eq. (3.36) through the use of a series representation for the hypergeometric function. In this section, we present these results, and we discuss their relationship to earlier work in the field.

In all of the calculations, we have chosen the Reststrahl frequency ω_o, and the Morse potential parameters, appropriate to NaCl. The parameters D, a, and x. for NaCl are tabulated in our first paper [1]. We are then left with the dimensionless parameters s and R. It is reasonable to presume that s does not differ greatly from unity, and the parameter R is less than unity. For NaCl , if we presume the parameter q in Eq. (3.2) equals the electron charge e, and note that the Szigeti effective charge e_s^* in NaCl is ≈ 0.75, then we find $R = +0.35$. The first series of calculations described below employ this value of R.

In Fig. 1 we present calculations of the effect of the nonlinear electric dipole moment on the absorption coefficient for NaCl at 900^oK, for several values of s, and $R = +0.35$. Recall from the remarks at the end of Section III that when s=o, there is no effect of the nonlinear electric dipole moment in our model, since the effective charge function q(x) of Eq. (3.11) becomes independent of x. Thus, the curve s = o in Fig. 1

is the same one that appears in one of our earlier papers,[2] which assumed R = 0.

We see from Fig.1 that for this value of R the presence of the nonlinear electric moment has a dramatic and qualitative effect on the frequency dependence of the absorption coefficient. The large dip occurs because when R is positive, the contribution to the absorption coefficient from the nonlinear electric dipole moment interferes destructively with that from anharmonicity in the potential. In the two phonon regime, this interference effect reduces the magnitude of the absorption coefficient compared to the value appropriate to the case R = 0, as Szigeti pointed out previously. In essence, within the framework of our simple model, we are able to extend Szigeti's calculation outside the phonon region, and we see the remarkable interference dip that results.

For a fixed value of R, as the range parameter s increases, the position of the interference dip moves to lower and lower frequencies. For $s = \frac{1}{2}$, the minimum occurs for a value of ω greater than $7\omega_o$, and thus is not exhibited explicitly in Fig.1.

This interference dip in the absorption coefficient is a very remarkable feature, particularly when one notes that in Fig.1 we plot the logarithm of the absorption coefficient as a function of frequency. One may ask whether the absorption coefficient vanishes identically right at the minimum, or whether it is simply very small there. For general values of s, we have been unable to answer this question by analytic means, although for certain particular values of s, one may see that the answer is

that the absorption coefficient vanishes identically for the model, at the minimum. The reason is that for integral values of s, the hypergeometric function F which appears in Eq. (3.36) is represented by simple analytic expressions. For example, for s = 1 and s = 2, we have

$$F(o,n;n+1;z) = 1 \qquad (s=1) \tag{4.1a}$$

$$F(-1,n-1;n+1;z) = 1 - \left(\frac{n-1}{n+1}\right) z \quad (s=2) \; . \tag{4.1b}$$

If these results are inserted into the expression for the inverse absorption length L, then we find the simple results for s = 1 and s = 2:

s = 1:

$$\frac{1}{L} = \left[1 + R\left(1 - \frac{\omega}{\omega_o}\right)\right]^2 \frac{1}{L_o} \; ; \tag{4.2a}$$

s = 2:

$$\frac{1}{L} = \left[1 + R\left(1 - \tfrac{1}{2}\frac{\omega}{\omega_o} - \tfrac{1}{2}\frac{\omega^2}{\omega_o^2}\right)\right]^2 \frac{1}{L_o} \; . \tag{4.2b}$$

In Eqs. (4.2), the quantity L_o is the absorption length calculated in the absence of the non-linear electric dipole moment, i.e. this quantity is given by Eq. (3.36) with R=0.

Thus, for these two special values of s, the effect of the nonlinear electric dipole moment may be represented by multiplying the expression for the absorption coefficient for R=0 by a frequency dependent factor. It is clear that for R>0, the absorption coefficient vanishes identically at the minimum. Furthermore, for a given value of R, one sees that the zero in the absorption coefficient occurs for a larger frequency when s = 1 than it does for s = 2.

In Figs. 2 and 3 we present results of calculations of the frequency dependence of the absorption coefficient for NaCl at room temperature, again for R = +0.35, and the values of s used in Fig.1. As before, the curve s=0 is the same result that appeared in our earlier work. Once again the dramatic interference dip is the most prominent feature in the curves. Within graphical accuracy, the position of the interference dip is independent of temperature in each case. The analytic results displayed in Eqs.(4.2) show that for s = 1 and s = 2, the position of the zero in the absorption coefficient is rigorously independent of temperature, and the numerical calculations indicate that this is so also for other values of s, to a very good approximation.

We have explored the effect of the nonlinear dipole moment on the temperature dependence of the absorption coefficient for our model of NaCl at 10.6 μm, which corresponds to a frequency of 5.8 ω_o for this material. When R = + 0.35, and for the values of s used in Figs. 1 - 3, we find that to within graphical accuracy the temperature dependence of the absorption coefficient is left

unaltered by the finite value of R. In Fig.4 we present a plot of the temperature dependence of the absorption coefficient for NaCl at 10.6 μm, with the absorption coefficient normalized to its value at room temperature. As discussed in one of our previous papers,[2] this curve provides an excellent fit to the data of Harrington and Hass,[4] from room temperature up to the melting temperature of the crystal.

As we indicated in the preceding discussion, the most prominent feature of the curves which describe the frequency dependence of the absorption coefficient of the model is the very large, sharp dip produced by the destructive interference between the contribution to the absorption coefficient from the nonlinear electric dipole moment and that from the anharmonicity in the potential function V(x). This feature is present in all of the curves, with its precise location controlled in any particular case by the numerical values of R and s. This interference minimum occurs only when R is positive; for R negative, no such dip occurs, and the absorption coefficient exhibits the well known monotonic, quasi-exponential falloff in frequency. To illustrate this, for s = 1, in Fig. 5 we have plotted the frequency dependence of the absorption coefficient for several values of R between +0.35 and -0.35. For R = +0.1, there is a sharp dip in the frequency dependence of the absorption constant, but it lies at frequencies higher than the value $7\omega_o$, the highest frequency on the graph. For negative values of R, the shape of the curve which describes the variation of the absorption coefficient with frequency is remarkably similar to the curve at R = 0, save

for an upward shift which arises from the constructive interference between the contribution from the electrical and the mechanical anharmonicity.

We next turn to a discussion of work closely related to ours, and also to an examination of the form of M(x) used here and by previous authors, to decide on physical grounds which sign of the parameter R is most reasonable.

The only paper to examine quantitatively the effect of the nonlinear variation of the electric dipole moment with interatomic spacing on the absorption coefficient in the multiphonon regime (i.e. for frequencies beyond that dominated by two phonon processes) is a recent work by McGill, Hellwarth, Mangir and Winston.[11] These authors also consider the theory of infrared absorption by an anharmonic Morse potential oscillator. However, they approach the problem quantum mechanically, and assume the effect of anharmonicity is sufficiently weak that the energy levels of the oscillator can be regarded as equally spaced. This approach, which is the quantum mechanical analogue of the quasi-harmonic approximation employed in our first paper,[1] leads to a line absorption spectrum which consists of a sequence of sharp lines centered at the frequencies $n\omega_o$, where ω_o is the frequency of the oscillator computed in the harmonic approximation. These authors examine the effect of nonlinear contributions to the electric dipole moment by assuming for M(x) the form

$$M(x) = e_s^* [x - x_o] \left(1 + S \frac{\left[x-x_o\right]}{x_o}\right) \quad , \qquad (4.3)$$

where S is a dimensionless parameter chosen to be positive in sign, with a value between 0.1 and 0.5.

We can see that, in a certain sense, the assumption made by McGill et al. that their parameter S is positive corresponds to the choice R > 0 for our case. If our expression for M(x) is expanded as a power series in $(x-x_o)$, and terms higher order than $(x-x_o)^2$ are discarded, we have

$$M(x) = e_s^* [x-x_o] \left(1 + \frac{R}{2} \, a x_o s \left[\frac{x-x_o}{x_o}\right] + \ldots\right) \qquad .(4.4)$$

Thus, if we choose R > 0, we find that the curvature of M(x) at the origin, considered as a function of $(x-x_o)$, is positive, as McGill et al. assume.

McGill and coworkers state that they find little effect of S on the temperature dependence of their computed values of the absorption coefficient, as we do. However, they find that the nonlinear variation of the moment has only a very small quantitative effect on the frequency dependence of the absorption coefficient. This is a result quite in contrast with the results of our analysis, and also in contrast with that of Szigeti's earlier study.[6] We have no clear understanding of why this is so, since in all three papers the nonlinear part of M(x) is presumed to be of comparable magnitude to that used here.

The first theoretical study of the interference between the contribution to the absorption coefficient from the nonlinear part of M(x) and the anharmonicity in the crystal potential is the paper of Szigeti cited earlier.[6] Szigeti confined his attention

to the frequency region where the absorption coefficient is dominated by the contribution from two phonon processes. He writes down a general expression for the contribution to the absorption coefficient, examines its general structure, and by estimating the magnitude and sign of a certain parameter φ_{ij} which enters his theory, he concludes that destructive interference between the two contributions occurs. Indeed, his estimate of the parameter φ_{ij} shows this quantity is large enough that an interference minimum similar to that we obtain for $R > 0$ occurs near or within the high frequency end of the two phonon absorption bands. Szigeti then argues that φ_{ij} must be smaller in magnitude than the value deduced from the simple model he introduces to make this estimate.

Our model for M(x) is in fact patterned after the one Szigeti introduced to provide the estimate of the parameter φ_{ij} which appears in his theory. He considers a diatomic linear chain, with positively charged ions in the even numbered sites, and negatively charged ions in the odd numbered sites. For the electric dipole moment M he writes

$$M = e \sum_n (x_{2n}-x_{2n-1}) + B \sum_n \left\{ \exp\left[-\epsilon(x_{2n}-x_{2n-1})\right] - \exp\left[-\epsilon(x_{2n+1}-x_{2n})\right] \right\}, \tag{4.5}$$

where B is a parameter, presumed positive, with the dimension of charge, and x_r is the displacement of the r^{th} ion from its equilibrium position. From Eq. (4.5) one sees that the electric dipole moment

associated with the bond between the ion at the site 2n and that at site 2n-1 is

$$\bar{M}_{2n} = e\,(x_{2n} - x_{2n-1}) + B\left\{\exp\left[-\epsilon(x_{2n} - x_{2n-1})\right] - 1\right\} \quad . \tag{4.6}$$

We have chosen our function M(x) to have precisely the same functional dependence on relative displacement of the ions as Szigeti's form. In fact, he chooses B > 0, the sign which corresponds to R > 0, in our notation. Our work and his thus agree that when R > 0, destructive interference between the two contributionsto the absorption coefficient occurs, and that this effect is surely quantitatively significant even in the two phonon regime, for physically reasonable values of R.

We next turn in our discussion to consideration of a very simple physical argument which suggests that one should expect R to be negative, and not positive, as Szigeti and McGill et al. have presumed.

Consider a diatomic molecule constructed from inequivalent atoms, so one bears a negative static charge and the other bears a positive charge, when the nuclei are at rest. Now, increase the internuclear separation, and consider the change in electric dipole moment. If the election charge follows the nuclei rigidly without "flowing" from one atom to another, the change in dipole moment is just $e_v(x-x_o)$, where e_v is the charge on each ion when the nuclei are at rest. We know when the ions are very far apart,

we have two electrically neutral atoms, and the electric dipole moment must vanish identically at large separations. Thus, we see that as the internuclear separation is increased, electrons must "flow" from to the negative ion to the positive ion at a rate which insures the ions become elecrically neutral at large separations. Clearly the dipole moment varies linearly with $(x-x_o)$ for small values of $(x-x_o)$, so we can always write $M(x) = e_s(x-x_o)$, where e_s is a phenomenological parameter (the Szigeti effective charge). The physical argument suggests $e_s < e_v$, as a consequence of the electron counterflow.

These arguments are well known. What we wish to focus our attention on here is the fact that necessarily M(x) must approach zero at large separations. This suggests that if M(x) varies smoothly with $(x-x_o)$, the second derivative of M(x) in an expansion of this function in powers of $(x-x_o)$ should be <u>negative</u>, since M(x) should begin to turn down and drop below the linear law $e_s(x-x_o)$, as $(x-x_o)$ increases. This argument is not rigorous, of course, but we feel it suggests that on physical grounds the sign of the quadratic turn in the expansion should be opposite that of the linear term. To support this view, we note that a recent careful analysis of oscillator strengths associated with the HCl and the CO molecules by Toth, Hunt and Plyler[12] has shown that for both molecules the quadratic terms in the expansion of M(x) have negative coefficients, as our argument suggests.

With this thought in mind, upon examining Eq. (4.4), we conclude that the physical considerations in the preceding

paragraph require that we choose a model with a negative sign for R, and not the positive sign assumed by earlier authors, which produces the dramatic interference minima evident in Figs.1-3 of the present paper. In fact, there is no experimental evidence for such an interference minimum in the frequency dependence of the absorption coefficient in the multiphonon regime in any crystal examined experimentally so far.[13]

Furthermore, in the alkali halides, in our earlier work,[1],[2] we saw that the simple theory with R = 0 provided an excellent account of the frequency and temperature dependence of the absorption coefficient. From Fig.4 we see that for R < 0 there is little change in the shape of the curve which describes the frequency dependence. The effect of the nonlinear variation of the electric dipole moment with internuclear separation is principally to increase the magnitude of the absorption coefficient, leaving the shape of the curve relatively unchanged in the multiphonon regime. It is interesting to note that in our second paper we used our theory with R = 0 to make a quantitative estimate of the magnitude of the absorption coefficient at 10.6μ in NaCl and NaF, at high temperatures. In both cases, the theory produced a value for the absorption coefficient that was too small by a factor of roughly 2.5 in the case of NaCl, and a factor of 4 for NaF. If we presume R < 0, then the presence of the nonlinear contribution to M(x) with interatomic separation provides a reasonable explanation of this discrepancy.

Thus, we conclude that a considerable body of evidence, from physical arguments, molecular data, and the absence of an

interference minimum in the frequency dependence of the absorption coefficient in the multiphonon regime in alkali halides, supports the suggestion that the curvature of the function M(x) for small $(x-x_o)$ should be negative; for our model this requires $R < 0$.

If we accept this, and use the functional form for M(x) employed here and in Szigeti's paper, then we must abandon the physical interpretation placed on the two pieces $m_1(x)$ and $m_2(x)$ which led to the final form of M(x). If we retain this interpretation, then we must choose q equal to the static charge on each ion, and through Eq. (3.7) we shall find $R > 0$, since the Szigeti effective charge e_s^* is less than the static charge on each ion, for the simple alkali halides. It is quite reasonable to use the form of M(x) in Eq. (3.4) to describe the variation of the electric dipole moment with interatomic separation, and to assume that q, R and s are to be determined from experimental data and the constraint in Eq. (3.7). This functional form is qualitatively reasonable, and has the virtue that in one simple limit $(R \to 0)$ it reduces to a function with a linear dependence on $(x-x_o)$. It does have one defect. In the limit $(x-x_o) \to \infty$, the physical requirement $M(x) \to 0$ is not satisfied. This should not be a serious limitation of the empirical form for M(x) for our purposes, since in solid state applications one is always involved with the regime where the mean square vibration amplitudes are a small fraction of the inter-nuclear separation, so the behavior of M(x) at values of $(x-x_o)$ that are large is of little consequence.

We conclude by noting that we have not yet discussed the paper by Flytzanis.[14] This paper examines the relative magnitude and sign of the contribution to a nonlinear susceptibility from anharmonicity and the nonlinear variation of the electric dipole moment for some crystals of the zinc blende and wurtzite structures, and its relation to the absorption coefficient in the two phonon regime. We are concerned here with the alkali halides primarily, so there is little direct overlap between our analysis and his. In fact, a key step in Flytzanis' analysis is the replacement of a certain quantity $\Theta_{\sigma\sigma'}$ (which depends on the wave vector of each phonon created in the two phonon absorption process) by its value at the Brillouin zone center $\vec{k} = 0$. The resulting quantity, denoted by $\Theta_{ss'}$ by Flytzanis, vanishes identically in the alkali halides, and any crystal which possesses a center of inversion. Thus, the analysis of Flytzanis cannot be extended to the alkali halides. Furthermore, we are somewhat concerned by this one approximation, since $\Theta_{\sigma\sigma'}$ evaluated at finite $\vec{k}$ and the quantity $\Theta_{ss'}$ Flytzanis replaces it by have very different symmetry properties, and it is not clear to us that this replacement gives one a reliable measure of whether the two contributions to the absorption coefficient interfere constructively or destructively. For example, in both zinc blende and wurtzite, $\Theta_{ss'}$ is non-zero only by virtue of the lack of an inversion center, while for general values of the wave vector $\Theta_{\sigma\sigma'}$ is non-vanishing even in the presence of an inversion center. Thus, on the microscopic level, these two quantities may depend on different physical parameters of the crystal.

References

1. D. L. Mills and A. A. Maradudin, Phys. Rev. B8, 1617(1973).
2. A. A. Maradudin and D. L. Mills, Phys. Rev. Letters 31, 718(1973).
3. T. F. Deutsch (to be published). See also F. A. Horrigan and T. F. Deutsch, Quarterly Technical Report No.2, Raytheon Corp., Waltham, Mass., April 1972.
4. J. A. Harrington and M. Hass, Phys. Rev. Letters 31, 710(1973).
5. See, for example, M. Born and K. Huang, Dynamical Theory of Crystal Lattices (Oxford University Press, New York, 1954).
6. B. Szigeti, page 397 of Lattice Dynamics, edited by R. F. Wallis. (Pergamon Press, New York, 1965).
7. L. D. Landau and E. M. Lifshitz, Mechanics (Pergamon Press, Oxford, 1969).
8. This identity follows from identity 6.628.4 on page 716 of I. S. Gradshteyn and I. M. Ryzhik, Table of Integrals Series and Products (Academic Press, New York, 1965).
9. This follows from identity 8.736.1 on p.1006 of reference (8) upon noting that n in our Eq. (3.31) is an integer.
10. Reference 8, p. 1010, formula 8.772.3. It should be noted that the equation as given in this reference contains a misprint, and should read

$$P_\nu^\mu(z) = \frac{1}{\Gamma(1-\mu)} \left(\frac{z-1}{z+1}\right)^{-\frac{\mu}{2}} \left(\frac{z+1}{2}\right)^{\nu} F\left(-\nu,-\nu-\mu;1-\mu;\frac{z-1}{z+1}\right) .$$

11. T. C. McGill, R. W. Hellwarth, M. Mangir and H. V. Winston, (to be published).

12. Robert A. Toth, Robert H. Hunt and Earle K. Plyler, J. Mol. Spectroscopy 32, 85 (1969) and 35, 110 (1970).

13. For a convenient tabulation of a large quantity of absorption data in the multiphonon regime, see M. Sparks, Theoretical Studies of High Power Laser Window Materials, Final Technical Report for Contract No. DAHC 15-72-C-0129, Advanced Research Projects Agency (December, 1972).

14. C. Flytzanis, Phys. Rev. Letters 29, 772(1972).

Figure Captions

Figure 1: The effect of the nonlinear electric dipole moment on the absorption coefficient at 900°K for several values of s, and R = +0.35. The remaining parameters have been chosen to characterize NaCl.

Figure 2: The effect of the nonlinear electric dipole moment on the absorption coefficient at 300°K for several values of s, and R = +0.35. The remaining parameters have been chosen to represent NaCl.

Figure 3: The effect of the nonlinear electric dipole moment on the absorption coefficient at 300°K for several values of s, and R = +0.35. The remaining parameters have been chosen to represent NaCl. The dot-dash line shows a portion of the curve for s = 0, for reference purposes.

Figure 4: The temperature dependence of the absorption coefficient at 10.6μ in the model of NaCl. We find that the temperature dependence is unaffected by the presence of the nonlinear electric dipole moment.

Figure 5: Frequency dependence of the absorption coefficient for NaCl at 900°K, for s = 1 and several values of R.

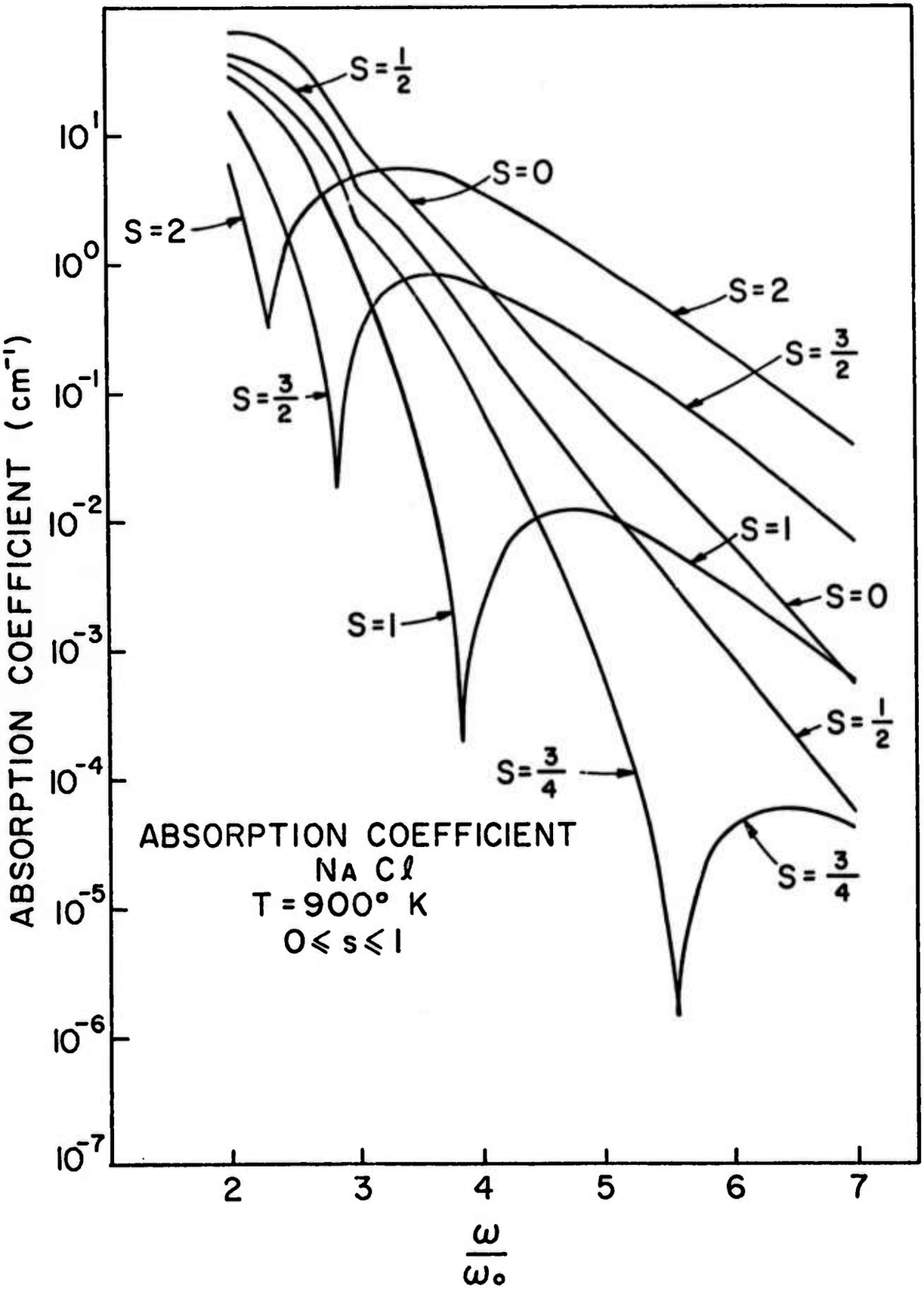
ABSORPTION COEFFICIENT (cm⁻¹)
10¹
10⁰
10⁻¹
10⁻²
10⁻³
10⁻⁴
10⁻⁵
10⁻⁶
10⁻⁷
2
3
4
5
6
7
ω/ω₀
S=1/2
S=0
S=2
S=3/2
S=3/2
S=2
S=1
S=0
S=1
S=1/2
S=3/4
S=3/4
ABSORPTION COEFFICIENT
NA Cl
T=900° K
0≤s≤1

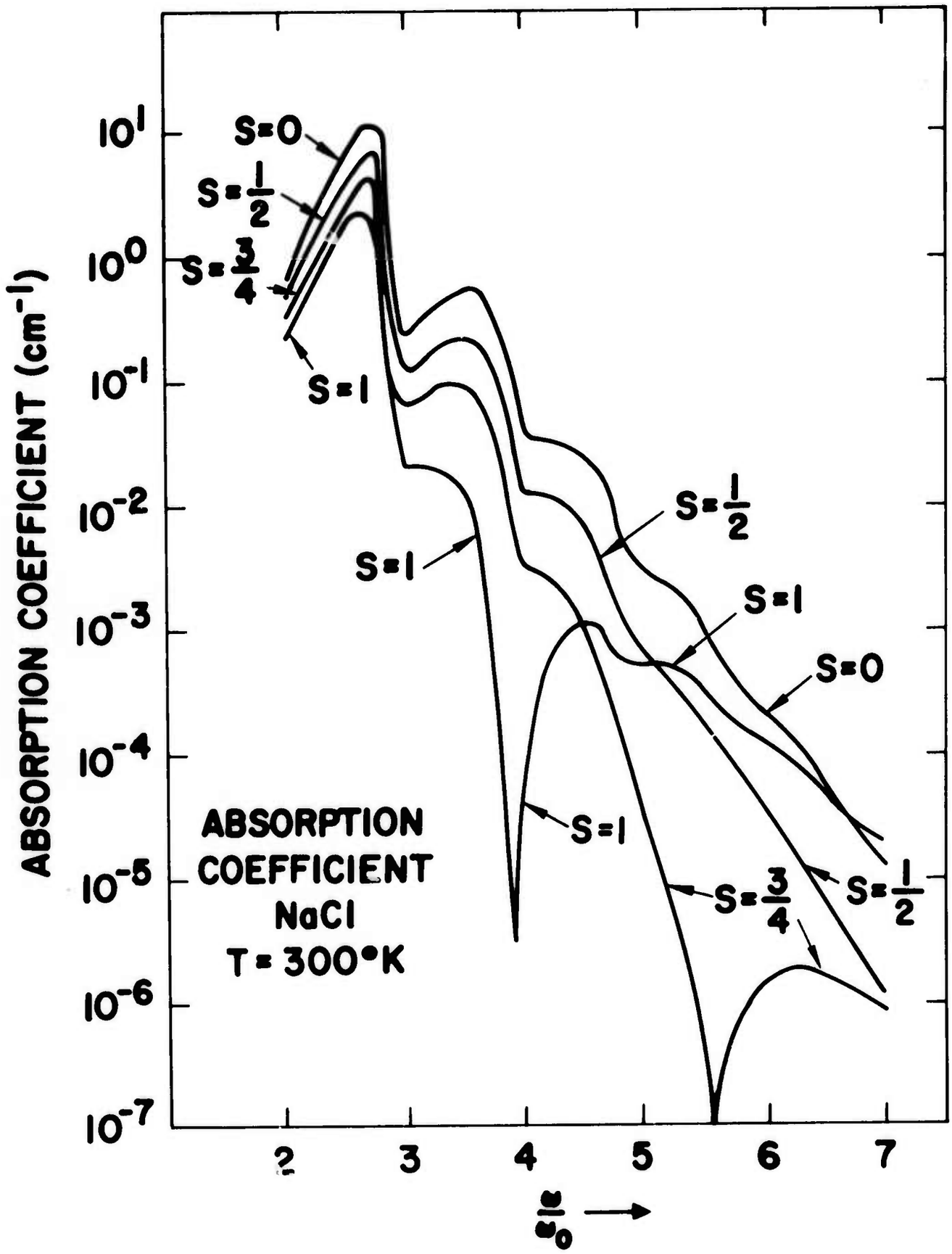
ABSORPTION COEFFICIENT (cm⁻¹)
10¹
10⁰
10⁻¹
10⁻²
10⁻³
10⁻⁴
10⁻⁵
10⁻⁶
10⁻⁷
S=0
S=1/2
S=3/4
S=1
S=1/2
S=1
S=1
S=0
S=1
S=3/4
S=1/2
ABSORPTION
COEFFICIENT
NaCl
T=300°K
2
3
4
5
6
7
ħω/ε₀

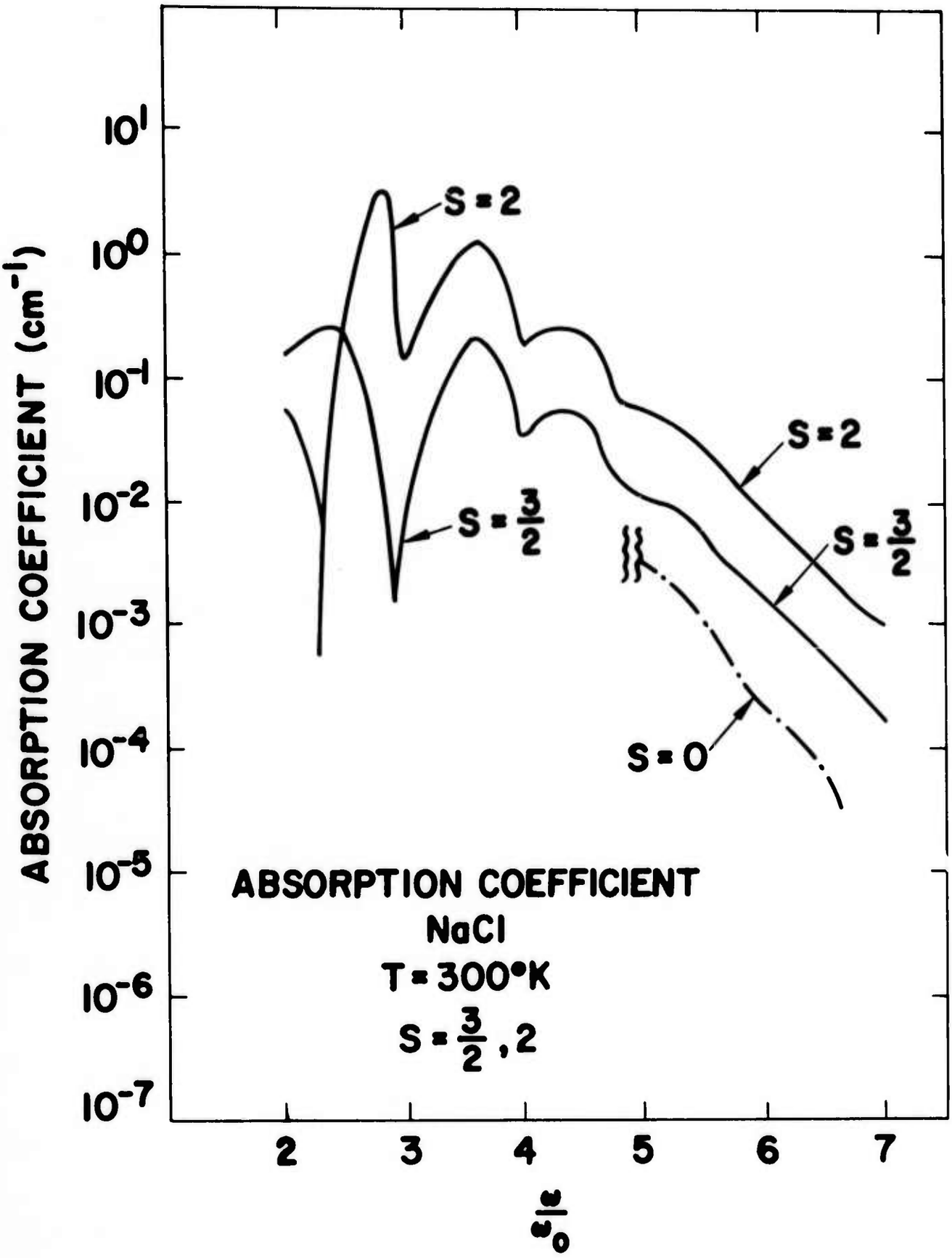
ABSORPTION COEFFICIENT (cm⁻¹)
10¹
10⁰
10⁻¹
10⁻²
10⁻³
10⁻⁴
10⁻⁵
10⁻⁶
10⁻⁷
S = 2
S = 3/2
S = 2
S = 3/2
S = 0
ABSORPTION COEFFICIENT
NaCl
T = 300°K
S = 3/2, 2
2
3
4
5
6
7
ω/ω₀

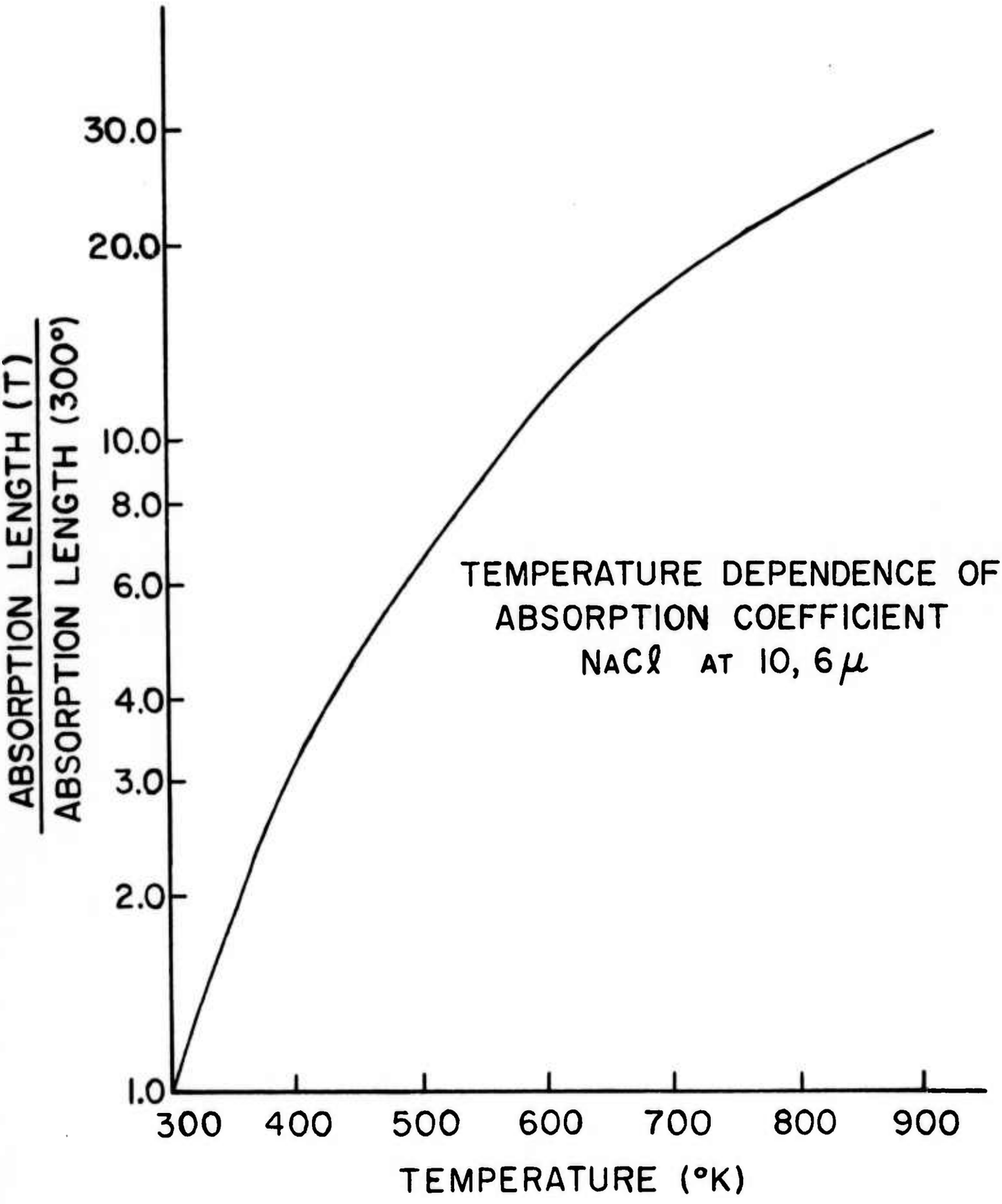
ABSORPTION LENGTH (T) / ABSORPTION LENGTH (300°)
30.0
20.0
10.0
8.0
6.0
4.0
3.0
2.0
1.0
300
400
500
600
700
800
900
TEMPERATURE (°K)
TEMPERATURE DEPENDENCE OF
ABSORPTION COEFFICIENT
NaCl AT 10, 6 μ

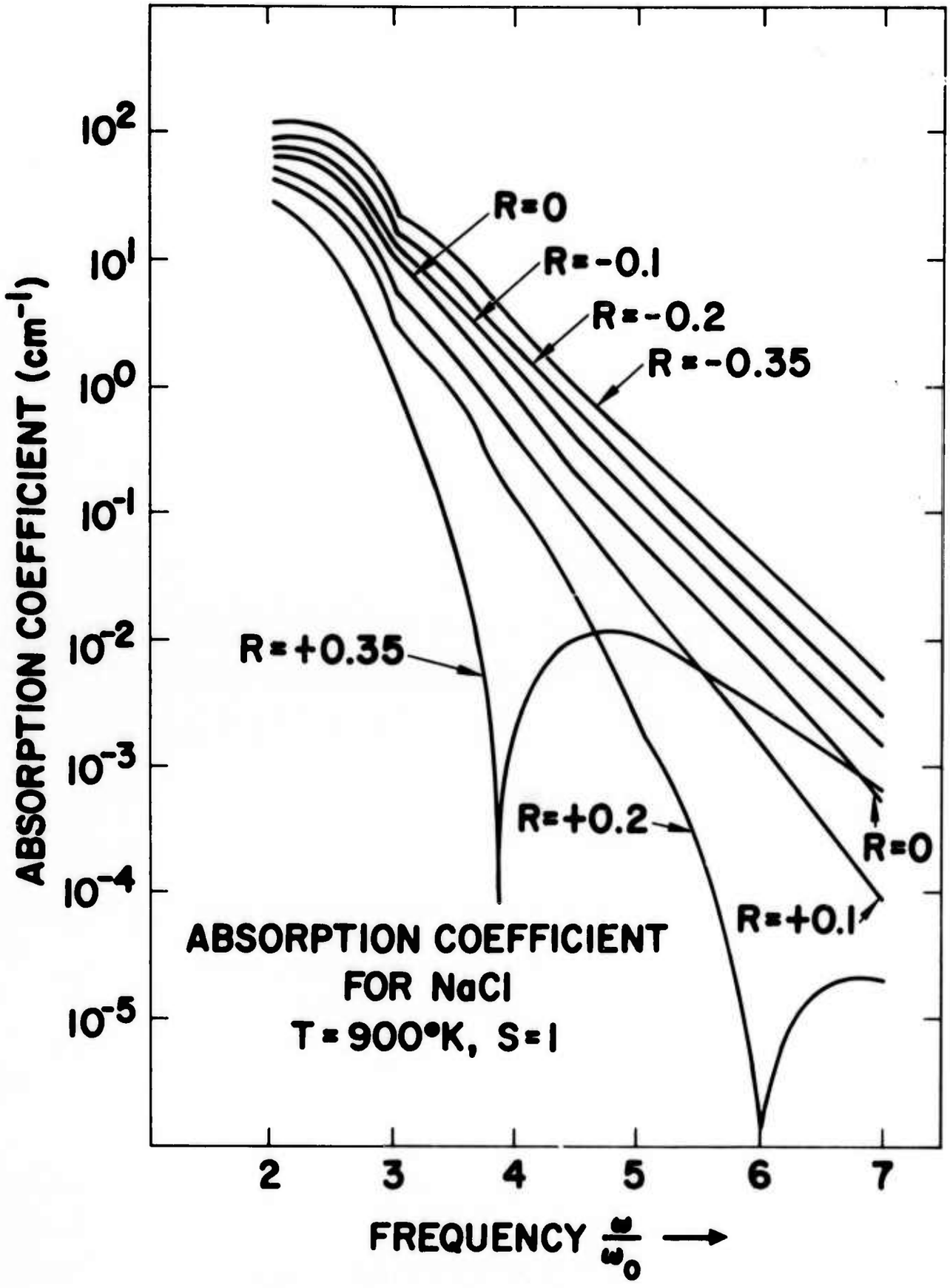
ABSORPTION COEFFICIENT (cm⁻¹)
10²
10¹
10⁰
10⁻¹
10⁻²
10⁻³
10⁻⁴
10⁻⁵
R=0
R=-0.1
R=-0.2
R=-0.35
R=+0.35
R=+0.2
R=0
R=+0.1
ABSORPTION COEFFICIENT
FOR NaCl
T=900°K, S=1
2
3
4
5
6
7
FREQUENCY ω/ω₀ →

L. VERTEX CORRECTIONS FOR MULTIPHONON ABSORPTION

In the previous technical report,[1] vertex correction factors Λ_n were calculated for all processes through $n = 6$, where n is the number of final phonons created in the absorption process. In numerical calculation progress, the value of Λ_n was needed. Thus, this seventh-order vertex has been calculated.

From the previous technical report or Ref. 2,

$$\Lambda_7 = \sum_{m=0}^{5} S_7^{(m)} \xi^m \quad .$$

The absorption vertices for $S_7^{(1)}$ are shown in Fig. L1. Adding the five contributions from the figure gives $S_7^{(1)} = 12.360$. The absorption vertices for the other $S_7^{(m)}$ are straightforward but cumbersome, there being almost one hundred diagrams, which will be supplied on request. The results are

$$\Lambda_7 = 1 + 12.360\,\xi + 27.2088\,\xi^2 + 17.88235\,\xi^3 + 4.06695\,\xi^4 + 0.2274\,\xi^5 \quad . \tag{1}$$

For $\xi = 0.18$,

$$|\Lambda_7|^2 = 17.766 \quad . \tag{2}$$

For the Einstein model, $\xi = 1$, and (1) gives $|\Lambda_7|^2 = 3.812 \times 10^3$. It is clear that the value of the vertex correction is sensitive to the model, and that the Einstein model grossly overestimates the value of the vertex corrections.

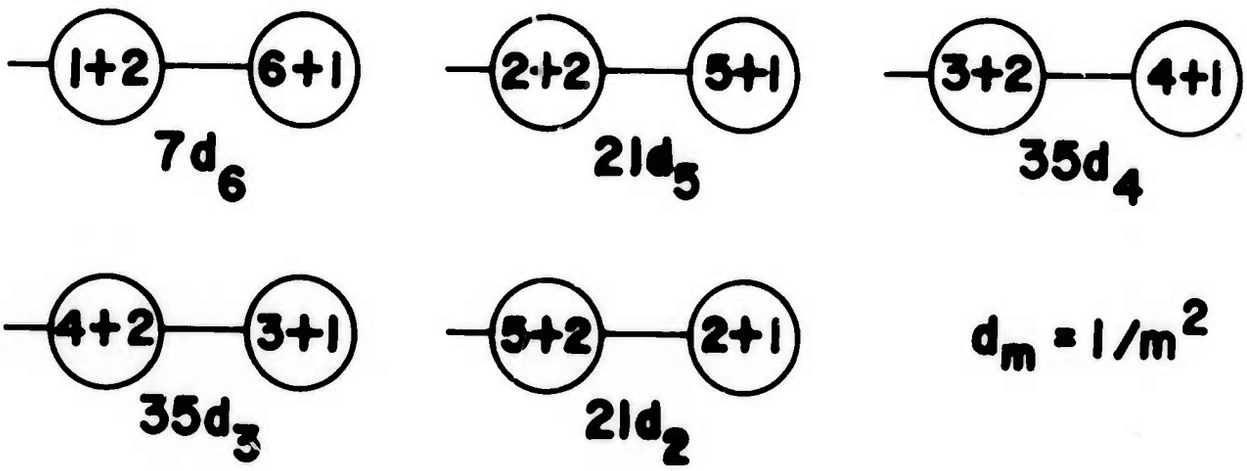

Figure L1. Absorption vertices for $S_7^{(1)}$.

REFERENCES

1. M. Sparks, "Theoretical Studies of High-Power Infrared Window Materials," Xonics Inc. First Technical Report, Contract No. DAHC15-73-C-0127, June (1973).

2. M. Sparks and L. J. Sham, Phys. Rev. B 8, 3037 (1973).

M. NEGLIGIBLE INTRINSIC-ABSORPTION PROCESSES

There are many effects in addition to those considered in the present and previous reports that give rise to infrared absorption, but whose strengths are too small to be observable. Simple order-of-magnitude calculations indicate that ultraviolet-induced infrared absorption and low-intensity inelastic scattering including Raman, Brillouin, and ionic Raman and Brillouin scattering, are in this category. These are discussed only very briefly in view of the negative results.

Ultraviolet-Induced Infrared Absorption. One possible, but unlikely, source of absorption at 10.6 μm is absorption due to free carriers produced by ultraviolet radiation present in CO_2 laser environments. In an experiment at the Air Force Cambridge Research Laboratories, the 10.6 μm absorption coefficients of several laser-window materials, including GaAs and CdTe, simultaneously illuminated by 3.6 milliwatts of 325 nm laser radiation and 10.6 μm laser radiation were measured.[1] Potassium chloride also was studied, but the results are less meaningful since the band gap $E_g > \hbar\omega_{uv}$. The experiments yielded a negative result as the following order-of-magnitude calculation shows should be the case.

Consider a 1 cm^3 sample, 1 cm on a side. Assume that all of the 325 nm radiation is absorbed uniformly throughout the sample with each photon producing an electron-hole pair. Hence the rate of pair creation is

$$\text{rate of pair creation} = I/\hbar\omega , \tag{1}$$

where ω is the ultraviolet laser frequency. The created pairs will recombine, with a characteristic lifetime τ_R:

$$\text{rate of recombination} = n_p / \tau_R , \tag{2}$$

where n_p is the number of pairs present. In equilibrium, $dn_p/dt = 0$, and we can equate the rates of creation and recombination, which yields

$$n_p = I \tau_R / \hbar\omega . \tag{3}$$

Using $I_{uv} = 4 \times 10^{-3}$ W/cm^2 and underestimating the recombination rate with $\tau_R = 10^{-4}$ sec which overestimates the free carrier concentration and infrared absorption, (3) yields $n_p = 7 \times 10^{11}$ cm^{-3}.

To calculate β we first use the Drude formula for the complex dielectric constant[2]

$$\epsilon = \epsilon_\infty - \frac{\omega_p^2}{\omega^2 + i\omega/\tau_c} \tag{4}$$

where τ_c is the electron relaxation time and

$$\omega_p^2 = 4\pi n e^2 / m . \tag{5}$$

In (4) and (5), ϵ_∞ is taken to be unity, ω is the frequency of interest, ω_p is the plasma frequency determined by the number of free carriers, $n = 2 n_p$, and m and e are effective mass and effective charge of the free carriers which are approximated by the electronic mass and charge, respectively. The collisional relaxation time τ_c usually falls in the range 10^{-13} sec to 10^{-15} sec.[3] With these values, (5) yields $\omega_p = 7 \times 10^{10}$ sec^{-1}. Substitution into (4) yields the imaginary part of the dielectric constant

$$\epsilon_\vartheta \cong \omega_p^2 / \omega^3 \tau_c = \omega_p^2 / \omega^3 \tau_c = 9 \times 10^{-12} \text{ to } 9 \times 10^{-10} .$$

Using $\beta \cong 2\pi \epsilon_2 / \lambda$ yields $\beta(10.6\,\mu m) = 5 \times 10^{-7}\ cm^{-1}$ to $5 \times 10^{-5}\ cm^{-1}$, which is completely negligible.[4] Hence under the conditions of the experiment, there should be no coupling of the infrared and ultraviolet absorption, and the heating should simply be a sum of the two sources separately. Similarly, in the CO_2 laser systems there should be no coupling unless there is nearly $1\ W/cm^2$ of ultraviolet radiation present.

Low-Intensity Inelastic Scattering. A slight amendment to the estimate in Sec. D of the effect of Raman scattering at high intensities shows that inelastic scattering is negligible at low intensities, that is, for $I \lesssim 0.9\, I_c$. As the intensity decreases through the threshold value I_c, the Stokes intensity decreases almost discontinuously by seven orders of magnitude, typically. The value of $(\beta L)_{eff}$ is reduced from $\sim 10^{-3}$ in the high-intensity case to $\sim 10^{-10}$ in the low-intensity case. The ionic Raman and Brillouin processes are known to be weaker than the usual electronic ones.[5]

A number of other effects are shown to be negligible in Sec. D on nonlinear effects and Sec. B on imperfection absorption.

REFERENCES

1. AFCRL-72-0559, "High Power Infrared Laser Window Materials (LQ-10 Program)," Quarterly Progress Report No. 6, September (1972).

2. C. Kittel, Introduction to Solid State Physics, 3rd edition (Wiley and Sons, New York, 1967), p. 227.

3. Ref. 2, p. 318.

4. This form for β derived in Xonics, Inc. Final Report, Contract DAHC15-72-C-0129, December (1972).

5. L. B. Humphreys and A. A. Maradudin, Phys. Rev. B6, 3868 (1972); L. B. Humphreys, A. A. Maradudin, and R. F. Wallis, Physics of Impurity Centres in Crystals (Academy of Sciences of Estonian SSR) Tallin (1972).

N. SUMMARY OF PUBLICATIONS AND RESULTS

PUBLICATIONS

All publications of this program and the previous programs are included in the following list:

1. M. Sparks, "Immediate Needs of the High Power Infrared Window Program and Methods of Reducing Thermally Induced Optical Distortion," Rand Corporation Report WN-7243-PR, June 1971.

2. M. Sparks, "Stress and Temperature Analysis for Surface Cooling or Heating of Laser Window Materials," Parke Mathematical Laboratories TM-1, July 1971.

3. M. Sparks, "Physical Principles, Materials Guidelines, and Materials List for High-Power 10.6 μ Windows," Rand Corporation Report R-863-PR, August 1971.

4. M. Sparks, "Temperature and Stress Analysis for Bulk- and Surface-Heated Slabs," Parke Mathematical Laboratories TM-2, August 1971.

5. M. Sparks, "Optical Distortion by Heated Windows in High-Power Laser Systems," Rand Corporation Report R-545-PR, September 1971.

6. M. Sparks, "Calculated Temperature Distributions in Slabs Heated in a Thin Surface Layer," Parke Mathematical Laboratories TM-3, September 1971.

7. M. Sparks, "Optical Distortion by Heated Windows in High-Power Laser Systems," J. Appl. Phys. 42, 5029 (1971).

8. M. Sparks, "Introduction to the High-Power Infrared Window Material Problem," AFCRL Conference on High-Power IR Laser Window Materials, December 1971.

9. M. Sparks, "Engineering Approaches to High Power Infrared Window Problems," AFCRL Conference on High-Power IR Laser Window Materials, December 1971.

10. M. Sparks and T. Azzarelli, "Theoretical Studies of High-Power Infrared Window Materials," Xonics Quarterly Technical Progress Report No. 1, Contract DAHC15-72-C-0129, March 1972.

11. M. Sparks, "Recent Developments in High-Power Infrared Window Research," 4th ASTM Damage in Laser Materials Symposium, Boulder, Colo., June 1972.

12. M. Sparks and T. Azzarelli, "Theoretical Studies of High-Power Infrared Window Materials," Xonics Quarterly Technical Progress Report No. 2, Contract DAHC15-72-C-0129, June 1972.

13. M. Sparks and L. J. Sham, "Theory of Multiphonon Infrared Absorption," AFCRL Conference on High Power IR Laser Window Materials, Hyannis, Mass., Oct. 30-Nov. 1, 1972.

14. M. Sparks and M. Cottis, "Pressure-Induced Optical Distortion in Infrared Windows," AFCRL Conference on High Power Infrared Laser Window Materials, Hyannis, Mass., Oct. 30-Nov. 1, 1972.

15. M. Sparks and L. J. Sham, "Exponential Frequency Dependence of Multiphonon Summation Infrared Absorption," Solid State Commun. 11, 1451 (1972).

16. M. Sparks, "Theoretical Studies of High-Power Infrared Window Materials," Xonics Final Report, Contract DAHC15-72-C-0129, December 1972.

17. M. Sparks and M. Cottis, "Pressure-Induced Optical Distortion in Laser Windows," J. Appl. Phys. 44, 787 (1973).

18. M. Sparks, "Stress and Temperature Analysis for Surface Cooling or Heating of Laser Window Materials," J. Appl. Phys. 44, 4137 (1973).

19. M. Sparks, "Temperature and Stress Calculations for Face-Cooled High-Power Laser Optical Materials," to be published.

20. M. Sparks and C. J. Duthler, "Theory of Infrared Absorption and Material Failure in Crystals Containing Inclusions," J. Appl. Phys. 44, 3038 (1973).

21. M. Sparks and L. J. Sham, "Theory of Multiphonon Absorption in Insulating Crystals," Phys. Rev. B 8, 3037 (1973).

22. M. Sparks, "Short-Pulse Operation of Infrared Windows without Thermal Defocusing," Appl. Opt. 12, 2033 (1973).

23. M. Sparks and L. J. Sham, "Temperature Dependence of Multiphonon Infrared Absorption," Phys. Rev. Lett. 31, 714 (1973).

24. C. J. Duthler and M. Sparks, "Theory of Material Failure in Crystals Containing Infrared Absorbing Inclusions," ASTM 1973 Symposium on Damage in Laser Materials, Boulder, Colo., May 15-16, 1973.

25. M. Sparks, "Temperature and Frequency Dependence of Infrared Absorption as a Diagnostic Tool," Appl. Phys. Lett. 23, 368 (1973).

26. L. J. Sham and M. Sparks, "Explicit Exponential Frequency Dependence of Multiphonon Infrared Absorption," Phys. Rev., in press.

27. C. J. Duthler and M. Sparks, "Quasiselection Rule for Infrared Absorption by NaCl-Structure Crystals," Phys. Rev., in press.

28. M. Sparks and H. C. Chow, "Nonlinear Infrared Absorption from Parametric Instabilities of Phonons," in preparation.

29. D. L. Mills and A. A. Maradudin, "Theory of Infrared Absorption by Crystals in the High Frequency Wing of Their Fundamental Lattice Absorption," Phys. Rev. B 8, 1617 (1973).

30. A. A. Maradudin and D. L. Mills, "Temperature Dependence of the Absorption Coefficient of Alkali Halides in the Multiphonon Regime," Phys. Rev. Lett. 31, 718 (1973).

31. A. Karo, M. Sparks, and L. J. Sham, "Infrared Multiphonon Absorption Calculations," in preparation.

32. C. J. Duthler, "Explanation of Laser-Damage Cone-Shaped Surface Pits," Appl. Phys. Lett., in press.

33. M. Sparks and H. C. Chow, "High-Power 2-6 μm Window-Material Figures of Merit with Edge Cooling and Surface Absorption Included," J. Appl. Phys., in press.

34. M. Sparks, C. J. Duthler, H. C. Chow, L. J. Sham, A. A. Maradudin, and D. L. Mills, "Theoretical Studies of High-Power Infrared Window Materials," AFCRL Conference on High Power Infrared Laser Window Materials, Hyannis, Mass., Nov. 12-14, 1973.

35. M. Sparks and H. C. Chow, "High-Power 10.6 μm Window Material Figures of Merit with Edge Cooling and Surface Absorption Included," AFCRL Conference on High Power Infrared Laser Window Materials, Hyannis, Mass., Nov. 12-14, 1973.

36. M. Sparks, "Stimulated Raman and Brillouin Scattering: Parametric Instability Explanation of Anomalies," to be published.

37. D. L. Mills and A. A. Maradudin, "The Absorption Coefficient of Alkali Halides in the Multiphonon Regime: Effects of Nonlinear Dipole Moments," to be published.

PRESENTATIONS AT INFORMAL MEETINGS:

- "Materials and Engineering Approaches for High-Power Infrared Windows," Air Force Materials Laboratory Conference on High-Power Laser Windows, Dayton, Ohio, July 1970.
- "Theory of Infrared Absorption," ARPA Materials Research Council, Falmouth, Mass., July 1971.
- NMAB Ad Hoc High Power Infrared Laser Windows Committee Meeting, Washington, D.C., September 16, 1971.
- Dr. Edward Teller Review Meeting, Rand Corporation, November 9, 1971.
- Naval Research Laboratories, Washington, D.C., January 12, 1972.
- NMAB Ad Hoc High Power Infrared Laser Windows Committee Meeting, Washington, D.C., February 24, 1972.
- USAF Scientific Advisory Board Ad Hoc Committee on Laser Technology Meeting, Albuquerque, New Mexico, February 29, 1973.
- IRIS 20th National Infrared Information Symposium, Gaithersburg, Maryland, May 16-18, 1972.

- AFCRL-NYU Multiphonon Absorption Conference, New York University, New York, February 7-8, 1973.
- "Figures of Merit for High-Power Infrared Windows," University of Southern California Physics Department, March 2, 1973.
- Review of ARPA-Supported Laser Window Research, ARPA, Arlington, Virginia, April 25-26, 1973.
- ARPA Materials Research Council Summer Meeting on Materials Problems Related to Reflection and Transmission of High-Power Ultraviolet Radiation, La Jolla, Calif., July 19-20, 1973.
- Redstone Arsenal, Huntsville, Alabama, September 28, 1973.
- Combat Surveillance and Target Acquisition Laboratory, Fort Monmouth, New Jersey, November 8, 1973.
- Avco Everett Research Laboratories, Boston, Massachusetts, November 15, 1973.

OUTLINE OF RESULTS

This outline-form summary includes all results of this program and the previous programs, rather than being restricted to the present report period as are the other sections. A summary of results of the present report period is included at the beginning of the report. A brief overview of the results can be obtained by reading IA, IB, etc., and skipping the subentries 1, 2, etc.

I. Intrinsic Multiphonon Absorption

A. The observed exponential frequency dependence of the optical absorption coefficient β was explained qualitatively and quantitatively with no adjustable parameters in terms of multiphonon absorption.

1. Phonon dispersion was included.
2. The central-limit theorem was used to reduce multiple sums to easily evaluate single sums.
3. A reasonable model with no adjustable parameters was employed.
4. The approximations used were shown to be reasonable.
5. It was demonstrated that confluence processes, in which some thermally excited phonons are annihilated, are negligible in the exponential region.

6. The vertex corrections through $n = 7$ for a reasonable lattice model were calculated, and it was shown that the Einstein model overestimates the importance of vertex corrections.

B. The exponential frequency dependence $\beta \sim \exp(-\omega\tau)$ was derived directly, rather than as a sum of n-phonon terms.

1. The range over which the exponential law is valid was determined.

2. An equation for τ in terms of a single-phonon sum was derived.

C. The anomalous temperature dependence of β observed in the exponential frequency region was explained by including the temperature dependence of the phonon frequencies and lattice constant in the theory, and good agreement with experiment with no adjustable parameters was obtained.

D. A quasiselection rule that the decay of a fundamental phonon into two acoustical or two optical modes is weak in NaCl-structure materials was proposed and used to explain a number of observed features of these materials.

E. An explanation involving finite phonon lifetimes was proposed to explain the fact that the alkali halides show less structure in the β-ω curves than do the semiconductor crystals.

F. A one-dimensional model was developed as the simplest model which gives nonzero higher-order dipole moments (Lax-Burstein effect).

1. It was emphasized that relative importance of the Lax-Burstein anharmonic-potential mechanism is strongly model dependent.

2. It was shown that the simplest model suggests that the Lax-Burstein mechanism is not negligible in NaCl-structure crystals, but that this result is not conclusive in view of (1) above.

G. An exactly solvable isolated-molecule classical model of a lattice of noninteracting anharmonic diatomic molecules was developed and the results were applied to a number of potentials without making the approximations that previously gave β as a sum of delta functions to obtain $\beta(\omega, T)$ in satisfactory agreement with experiment at high temperature.

1. Four potentials were used: a Morse potential, a potential of the form $V(x) = (a/x^2) + bx^2$, an infinite square well potential, and a triangular-well potential.

2. The absorption coefficient for large frequencies associated with potentials which admit an harmonic approximation decreases nearly exponentially over the frequency region covered by recent experiments, in agreement with the results of previous theories.

3. For the square and triangular well potentials, the absorption decreases like ω^{-2} for frequencies large compared to a characteristic frequency.

H. The isolated-molecule classical model was used to calculate $\beta(\omega)$ with both anharmonic-potential and Lax-Burstein mechanisms included.

I. Ultraviolet-induced electrical-carrier infrared absorption was shown to be negligible.

J. Four inelastic scattering processes (Raman and Brillouin, both electronic and ionic) were shown to be negligible at current low intensities ($\sim$kW/cm^2).

II. Extrinsic Absorption Processes

A. It was shown that very low concentrations of absorbing macroscopic inclusions (volume fractions as low as 10^{-8}) can give rise to $\beta \sim 10^{-4}$ cm^{-1}, and the temperature and frequency dependence of β was calculated.

1. The frequency dependence of β ranges from increasing as ω^2, to independent of ω, to exponentially decreasing with ω.

2. The temperature dependence ranges from independent of T to increasing as T^p in the high-temperature limit, where $p \simeq 2$-4 typically.

3. Correct cross sections were included.

4. Effects of different types of inclusions were analyzed.

5. Material failure from localized heating also was considered. See III A.

B. It was demonstrated that very low concentrations (as low as parts per billion) of a number of molecules that go into anion sites can give rise to $\beta = 10^{-4}\,cm^{-1}$ at $10.6\,\mu m$.

1. There are many molecules that fit into anion sites in alkali halides and retain their free molecule character to a large extent.

2. The frequency line widths are small, with $\Delta\omega/\omega \approx 5 \times 10^{-3}$ typically, compared with 8×10^{-2} typically for the fundamental resonance.

3. The molecules most likely to give rise to absorption at $10.6\,\mu m$ are NO_2^-, HCO_3^-, SO_4^{2-}, and CrO_4^{2-}, all of which are estimated to give $\beta = 10^{-4}\,cm^{-1}$ for less than 0.1 ppm.

C. It was pointed out that the U center is the only known impurity in alkali halides that have localized vibrational modes sufficiently close to $10.6\,\mu m$ to cause noticeable absorption.

1. Absorption in the far high-frequency wing ($\omega >> \omega_{res}$) of the impurity-absorption resonance, in addition to absorption near resonance, may be important, in contrast to previous beliefs.

2. The high-frequency side of resonance is more important because the intrinsic absorption decreases rapidly with increasing frequency, making the extrinsic absorption relatively more important.

3. Gap-mode and resonance-mode absorption were shown theoretically to be negligible at $10.6\,\mu m$.

4. Impurity-induced infrared activity of phonon modes was estimated to be negligible.

D. Analyses and estimates of surface absorption indicated that surface absorption can give rise to an equivalent absorption of $\beta = 10^{-4}\,cm^{-1}$.

1. Molecular absorption (see II B) and inclusion absorption (see II A) are two sources of surface absorption.

2. Electronic states in the band gap in both semiconductor and alkali-halide crystals are potentially important absorption centers. See II E.

3. Absorption by pure surface vibrational modes is believed to be negligible.

E. Absorption by electrical carrier and electronic absorption is important.

1. Free-carrier absorption and thermal runaway were already known to be important in conducting materials.

2. The conditions necessary to avoid free-carrier absorption were discussed.

3. The importance of inter-valence band transitions that were previously observed to give rise to strong absorption in a broad band (β = 0.3 cm^{-1} on 2-6 μm, for example) was pointed out.

4. Electronic levels with small spacing had already been observed to give rise to infrared absorption (near 2μm for Cr in zincblende-structure crystals).

5. Electronic levels in the gap of semiconductors and possibly alkali halides can cause measurable absorption.

6. Shallow levels that can be emptied thermally can give rise to absorption with β decreasing with increasing temperature.

7. Electronic absorption across the gap is negligible at 10.6 μm.

8. Strain-induced absorption was shown theoretically to be negligible.

F. The negative experimental results of no correlation between Pb^{2+} concentration and 10.6 μm absorption in alkali halides was explained in terms of the absence of resonances near 10.6 μm.

G. It was shown theoretically that adding divalent ions such as Mg^{2+}, Ca^{2+}, Ba^{2+}, Sr^{2+}, and Pb^{2+} to strengthen alkali halides should not give rise to measurable ($\beta > 10^{-4}$ cm^{-1}) absorption.

H. It was emphasized that measurements of $\beta(\omega, T)$ on intentionally doped samples would be extremely useful.

I. A classification scheme for impurity absorption was proposed.

III. Very High-Intensity Effects

A. The intensity at which a material fails as a result of local heating of absorbing macroscopic inclusions was calculated.

1. Energy densities of order $1\,J/cm^2$ were shown to be sufficient to damage crystals containing inclusions.

2. Correct cross sections of inclusions were included.

3. The damage thresholds as functions of particle size and laser pulse lengths were considered.

4. Effects of different types of absorbing inclusions were analyzed.

5. The heat flow into the host material was properly treated.

6. The increase in β (average absorption) also was considered. See II A.

B. Laser-damage micron-size cone-shaped surface pits were explained in terms of absorption by inclusions near the sample surface.

1. The correct order of magnitude of intensity damage threshold was calculated.

2. A time-delay effect for damage to occur was predicted.

C. A new instability in the stimulated Raman process was discovered, analyzed, and shown to have important consequences.

1. Anomalous results such as the nearly discontinuous increase in Stokes intensity as a function of laser intensity in materials with no self focusing were explained.

2. It was shown that the instability is one of the limiting very high-intensity effects.

3. The laser threshold intensity I_c for the instability was calculated and it was shown that $I_c \sim 10^9\ W/cm^2$ for a number of gases, liquids, and solids.

D. It was emphasized that the well known phenomena of air breakdown and electron avalanche breakdown could limit the performance of some systems.

E. Estimates were made of the effects of electrostriction showing that this effect should be negligible with respect to other very high-intensity effects.

F. A new method of solving parametric-instability problems was developed, and the method was applied to the calculation of nonlinear infrared absorption by parametric processes.

1. It was shown that absorption resulting from the phonon instabilities is negligible in the exponential-frequency multiphonon absorption region.

2. Calculations were performed showing that the transmissivity of films thinner than a wavelength changes near the fundamental resonance, the film becoming more transparent at resonance at high intensity.

3. The time constant for the approach to the steady state was shown to be important since the steady state is not attained in short laser pulses in important cases in which long lived phonons give rise to low steady-state threshold intensities.

4. An explanation was given that the effective relaxation frequency of the Reststrahl phonon is greater than the low-intensity value as a result of the increase in the amplitudes of the pair phonons above their thermal equilibrium values.

5. It was demonstrated that the threshold for the parametric instability is quite sharp when considered as a function of the amplitude n_f of the fundamental phonon. In contrast, when considered as a function of the incident laser intensity, the deviation from linear absorption with increasing intensity is quite smooth.

6. In contrast to a previously accepted result, it was demonstrated that crystals, such as NaCl, having a center of inversion could have anomalously low thresholds since the threshold is controlled by the phonon (in the pair) having the longer lifetime.

7. The method of calculation, using Boson occupation numbers rather than mode amplitudes, had the simplicity and power to yield us to obtain more information about parametric instabilities, including effects above the threshold, than has been possible previously.

8. Chain instabilities and enhanced relaxation from mutual interaction of excited pair phonons were proven negligible for the phonon instabilities, in contrast to previous results for plasmas and parallel pumping in ferromagnetic resonance, respectively.

IV. Optical Distortion and Figures of Merit

A. It was demonstrated that thermally induced optical distortion, rather than thermal fracture, would limit the performance of many systems.

1. Calculations were made on the distortion, including the effects of mechanical expansion, dn/dT, and strain optic effects.

2. It was explained that the temperature between the center and rim of the window must be small (< 1 K in some cases).

3. Refocusing was suggested and analyzed as a method of partially correcting for the thermally induced optical distortion.

4. Experiments to study optical distortion were proposed.

B. The effects of pressure-induced optical distortion were calculated, and these effects were shown to be important in general.

1. It was determined that pressure-induced optical distortion limits the window thickness in general.

2. Static deformation of a window under its own weight was shown to be negligible.

3. It was calculated that the strength of a material above which further increase in strength does not improve system performance because pressure-induced optical distortion, rather than fracture, limits the performance.

C. Figures of merit for material were developed, calculated, and tabulated for a number of materials for operation at 10.6, 5.25, and 3.8 μm.

1. Edge cooling, as well as face cooling, was included for continuously operated (cw) systems.

2. Surface as well as bulk absorption was included.

3. The total power θ that a window can transmit under specified idealized conditions was used as the figure of merit.

4. Effects of improving materials, particularly lowering the absorption coefficient β and increasing the strength σ, were included.

5. In order to obtain the greatest value of θ in a cw system, it was determined that large-diameter windows ($D > D_{EF}$) should be face cooled, while small-diameter windows ($D < D_{EF}$) may be edge cooled.

6. It was shown that for pulsed operation (pulse length of the order of a second, with rapid interpulse cooling), θ increases as D increases as expected intuitively, but for continuous operation, θ often decreases as D increases.

7. It was established that for pulse operation, θ_{pulse} is independent of K.

8. For small diameters, $D < D_{EF}$, it was explained that the value of θ_{cw} depends on the thermal conductivity K; whereas for $D > D_{EF}$, θ_{cw} is independent of K.

V. Engineering Considerations

A. A number of engineering solutions to the window problem were proposed and analyzed.

1. A pulse mode of operation, with pulse duration of the order of 1 sec and rapid interpulse cooling was suggested and analyzed to show that two to three orders of magnitude increase in average transmitted power can be gained over cw operation.

2. Relative motion of the beam and window was shown to be very effective in increasing the transmitted power, but the implementation of the method is extremely cumbersome.

3. A suggestion was made that refocusing the optics can reduce the effect of thermally induced optical distortion.

4. Many other possibilities include:

   a. differential cooling schemes

   b. truncating the beam at a relatively great intensity and redirecting the truncated energy to the low-intensity areas of the window

   c. using two compensating windows

   d. spatially tailoring surface or bulk absorption coefficients

   e. controlling the pressure on the window to reduce the strength requirements.

B. It was shown that in optimized continuously operated systems, edge cooling, which is technically easier than face cooling, can be used for small-diameter windows, while face cooling must be used for large-diameter windows. See IV. C. 5.

1. The values of D_{EF} at which the crossover from edge to face cooling occurs are surprisingly large, with typical values from 7 to 100 cm, and some even greater.

C. A number of problems concerning heating and cooling of windows, absorbing materials, and metals were analyzed.

1. The heat flow equation was solved for model problems representing absorption of heat near the surface of a material, and limiting cases were discussed and explained intuitively.

   a. The results are used for absorption by metals, by a thin antireflection or protective coating, by strongly absorbing materials (with $\beta^{-1} \ll$ thickness), and by painted surfaces.

2. The stress and temperature distribution in a material that is surface cooled or surface heated were analyzed.

   a. Three thermal time constants determine the thermal behavior of the material.

   b. The maximum reduction in the average temperature $b^{-1}\int dz\, T$ of a slab of thickness b which can be obtained by face cooling in a given time, typically ~ 1 s, without fracturing the slab, was calculated.

   c. The results indicated that $Ge_{28}Sb_{12}Se_{60}$ glass can be cooled rapidly enough for use at relatively high power levels (possibly $\sim 400\ W/cm^2$ at the center of the disk) in the pulse mode of operation.

   d. For a GaAs disk originally at room temperature, a coolant of 0° K can be used without fracturing the disk.

D. The possibility of transmitting short infrared pulses through materials with little thermally induced optical distortion was shown to exist.

   1. For sufficiently short pulses, of the order of $10^{-8} - 10^{-9}$ sec, the absorbed energy does not have time to thermalize, thus avoiding heating effects until after the pulse has been transmitted.

VI. Miscellaneous

A. The need for measurements of β over a wide range of ω and T that present transmission and calorimetric techniques cannot measure, and the fact that emissivity measurements should give the required values, were pointed out.

B. It was shown that it may be possible to transmit short pulses through materials without thermally induced optical distortion. See V. D.

C. Data from literature on β was collected and all data was reduced to overlayable curves of $\ell n\beta$ vs ω/ω_f, where ω_f is the fundamental mode frequency.

D. Guidelines were proposed for selecting materials, and materials from which to choose those to study in detail were suggested.

APPENDIX: SIMPLE PENDULUM INSTABILITY

The instability in a pendulum driven with a time-dependent force along the direction of gravity will be considered briefly in order to illustrate several features of parametric instabilities, using the simplest possible model. The cases of a single pendulum and of a pendulum in thermal equilibrium with its surroundings at temperature T will be considered. The linearized equation of motion of the amplitude of oscillation will be solved in the former, and energy flow considerations will be used in the latter.

For the single pendulum, the linearized equation of motion is

$$\frac{d^2\theta}{dt^2} + \omega_0^2\,\theta + \Gamma\frac{d\theta}{dt} = F\theta \qquad \text{(A1)}$$

where θ is the angle of the pendulum from the vertical z axis, ω_0 is the resonant frequency for small oscillations, Γ is the frictional-damping constant, and $m\ell F$ is the time-dependent force applied along the vertical z axis, with m the point mass on a massless rod of length ℓ. For the more common case of a force applied perpendicular to z, rather than along z, the force, rather than the force times θ, would appear on the right-hand side of (A1). The term $F\theta$ just cancels the effect of the damping term $\Gamma\, d\theta/dt$ for a certain critical value of F. For larger values of F, θ grows exponentially in time.

This behavior is easily demonstrated by substituting the trial solution

$$\theta = \theta_0 \sin\omega_0 t \exp(\gamma t) \qquad \text{(A2)}$$

into (A1) with

$$F = F_0 \sin 2\omega_0 t$$

and dropping the small terms of order $\gamma/\omega_0 \sim \Gamma/\omega_0 \sim F_0/\omega_0$ and the off-resonance terms in the product

$$F\theta = \frac{1}{2} F_0 \theta_0 \cos \omega_0 t + \text{off-resonance terms} .$$

This gives the time factor $\cos \omega_0 t$ for all three leading terms. Cancelling this common factor gives

$$\gamma = \frac{1}{2} \Gamma (F_0/F_c - 1)$$

with $F_c = 2\omega_0 \Gamma$. For $F_0 < F_c$, γ is negative and θ is exponentially damped according to (A2). For $F_0 > F_c$, γ is positive, and θ grows exponentially in time. For the case of the force perpendicular to z, the solution to (A1) with θ deleted on the right-hand side has the well known harmonic oscillator solution, which does not increase exponentially in time.

Notice that the frequency of F was chosen as twice the resonant frequency ω_0 and that the choice of the phase of the solution (A2) is critical. Physically, the force puts energy into the pendulum if the force is positive (upward) when the pendulum is traveling upward and negative when traveling downward, thus the importance of the phase. Since this z velocity of the pendulum has twice the frequency of θ, the force must have frequency $2\omega_0$ in order to drive θ at ω_0.

Next consider a pendulum in contact with an infinite heat bath of temperature T. The effect of the bath on the equation of motion of θ is complicated to treat correctly. Thus, the balance of energy into the pendulum from the applied force by the energy transferred to the bath in relaxing toward the thermal-equilibrium value will be considered.

The time average of the energy into the pendulum is

$$\left(\frac{d\mathcal{E}}{dt}\right)_{\text{from F}} = \int_{\text{one cycle}} f\, dz / T_\omega \qquad \text{(A3)}$$

where T_ω is the period of oscillation, $f = m\ell F$, and $\underset{\sim}{f} \cdot \underset{\sim}{dr} = f\, dz$. Substituting $f = f_0 \sin \omega_0 t$, $dz = d\left(\frac{1}{2}\ell\theta^2\right) = \ell\theta\, d\theta$, and $d\theta = \omega_0 \theta_0 \cos \omega_0 t\, dt$ into (A3) and evaluating the simple integral gives

$$\left(\frac{d\mathcal{E}}{dt}\right)_{\text{from F}} = \frac{\mathcal{E} F_0}{2\omega_0} \quad . \qquad \text{(A4)}$$

The energy out of the pendulum by relaxation is

$$\left(\frac{d\mathcal{E}}{dt}\right)_{\text{relax}} = -\Gamma(\mathcal{E} - \bar{\mathcal{E}}) \qquad \text{(A5)}$$

where $\bar{\mathcal{E}}$ is the thermal equilibrium value of $\mathcal{E}$. In equilibrium, the net rate of change of $\mathcal{E}$ is zero. Adding the right-hand sides of (A4) and (A5), setting the result equal to zero, and solving for $\mathcal{E}$ gives

$$\mathcal{E} = \frac{\bar{\mathcal{E}}}{1 - F_0/F_c} \qquad \text{(A6)}$$

where $F_c = 2\omega_0 \Gamma$, as for the single oscillator. This result (A6) indicates that as the strength of the force is increased, the relaxation to the bath maintains $\mathcal{E}$ at a finite value until F reaches the critical value F_c, at which value $\mathcal{E}$ becomes infinite, for this linearized case. Including the nonlinear terms in either treatment above removes the infinity, of course.

REFERENCES

References are listed by sections.